Reflection Anisotropy Spectroscopy as a Potential New Tool for Linking Macromolecular Conformation to Biological Function

Thesis submitted in accordance with the requirements of the University of Liverpool for the degree of Doctor in Philosophy by

James Hugh Convery

Department of Physics

August 2012

Abstract

The results reported in this thesis were obtained in a research programme that employed the surface sensitive optical probe reflection anisotropy spectroscopy (RAS) and related techniques to investigate conformational change associated with electron transfer processes in the protein cytochrome P450 reductase (CPR) adsorbed onto the Au(110)/electrode interface.

It was found that controlling the adsorption of an ordered layer of CPR on the Au(110) surface is difficult and far more complex than first expected. In order to understand the adsorption process further an extensive investigation using quartz crystal microbalance with dissipation (QCM-D) was carried out. The results of the QCM-D experiments established that the conditions necessary for the adsorption of a monolayer of CPR are extremely sensitive to protein concentration and buffer pH. This was a crucial step in the research which allowed the preparation of adsorbed ordered monolayers of CPR on Au(110)/electrode interfaces.

The RA spectral signatures of a monolayer and bilayer of CPR adsorbed on the Au(110) surface have been identified and are reported in this thesis. Using azimuthal dependent reflection anisotropy spectroscopy (ADRAS) it was shown that a monolayer of adsorbed CPR aligns along one of the principle axis of the Au(110) surface.

RAS investigations of the effect of inducing electron transfer processes in an adsorbed monolayer of CPR by stepping the applied electrode potential reveal changes in RA spectral shape and intensity which may be associated with conformational events in the adsorbed CPR. The RA spectra produced as a function of applied potential show that the adsorption of a monolayer of CPR impedes the Au(110) surface reconstruction from a (1×3) to the anion induced (1×1) structures.

Acknowledgments

I would like to thank Peter Weightman for his constant support, enthusiasm and for sharing his knowledge and wisdom over the last four years which made even the most difficult times of this research enjoyable. It has been an honour to work amongst such a well respected and professional research group for which I am extremely grateful. I would also like to thank the other members of the research group, Caroline Smith, Paul Harrison, Trevor Farrell, Gareth Holder, Andrew Bowfield, Chris Mansley and Liz Barritt for their support, friendship and the many interesting and amusing tea break conversations.

I would also like to thank Nigel Scrutton and Basile Khara from the University of Manchester for sharing their biological expertise and providing the protein samples without which this thesis would not have been possible.

Acronyms

ACF	Autocorrelation Function
ADRAS	Azimuth Dependent Reflection Anisotropy Spectroscopy
AFM	Atomic Force Microscopy
BZ	Brillouin Zone
CD	Circular Dichroism
CPR	Cytochrome P450 Reductase
DNA	Deoxyribonucleic Acid
ds-DNA	Double Stranded Deoxyribonucleic Acid
DTT	Dithiothreitol
DVM	Digital Voltmeter
ELDOR	Electron-electron Double Resonance
ERS	Electroreflectance Spectroscopy
FAD	Flavin Adenine Dinucleotide
FCC	Face Centred Cubic
FFT	Fast Fourier Transform
FMN	Flavin Mononucleotide
FWHM	Full Width at Half Maximum
IHP	Inner Helmholtz Plane
IR	Infra-Red
LEED	Low Energy Electron Diffraction
MIB	Manchester Institute of Biotechnology
NADPH	Nicotinamide Adenine Dinucleotide Phosphate (oxidised form)
$NADP^+$	Nicotinamide Adenine Dinucleotide Phosphate (reduced form)
OHP	Outer Helmholtz Plane
PEM	Photoelastic Modulator
PMT	Photomultiplier Tube
PZC	Potential of Zero Charge
QCM	Quartz Crystal Microbalance

QCM-D	Quartz Crystal Microbalance with Dissipation
RAS	Reflection Anisotropy Spectroscopy
RDS	Reflection Difference Spectroscopy
SARIS	Scattering and Recoil Imaging Spectroscopy
SAXS	Small angle X-ray Scattering
SBZ	Surface Brillouin Zone
SCE	Standard Calomel Electrode
SDA	Surface Dielectric Anisotropy
SE	Spectroscopic Ellipsometry
SERS	Surface Enhanced Raman Spectroscopy
SLFE	Surface Local Field Effect
SPR	Surface Plasmon Resonance
ss-DNA	Single Stranded Deoxyribonucleic Acid
STM	Scanning Tunnelling Microscopy
SXRD	Surface X-ray Diffraction
SXS	Surface X-ray Scattering
UHV	Ultra High Vacuum
UPD	Underpotential Deposition
UV	Ultra Violet
UV-VIS	Ultra Violet - Visible
XPS	X-Ray Photoelectron Spectroscopy

Contents

Chapter 1

Introduction

1.1 Introduction 2

1.2 Thesis Structure 7

1.3 References 10

Chapter 2

Experimental Apparatus and Theory

2.1 Reflection Anisotropy Spectroscopy 13

2.1.1 RA Spectrometer and its Components 14

2.2 The Propagation of Light through the System 18

2.2.1 The Jones Matrix Formalism 22

2.2.2 Errors 30

2.2.3 Rapid RAS 30

2.3 Electrochemistry 31

2.3.1 Measuring Electrode Potential 34

2.3.2 The Electrochemical Cell 36

2.4 Crystal Preparation 37

2.5 Quartz Crystal Microbalance with Dissipation Monitoring (QCM-D) 37

2.6 Atomic Force Microscopy (AFM) 43

2.7 References 47

Chapter 3

The Au(110) Surface

3.1 The Need for a Substrate 51

3.2 Surface Phase Transitions 52

3.3 The Physical Structure of the Au(110) Surface 53

3.3.1 Au(110) in the UHV Environment 53
3.3.2 Au(110) in the Electrochemical Environment 58
3.4 The Electronic Structure of the Au(110) Surface 61
3.5 RAS of the Au(110) Surface 63
3.6 The Three Phase Model 70
3.6.1 The Dielectric Function 71
3.6.2 The Lorentzian Transition Model 72
3.7 Spectral Signatures of the Surface Reconstructions of Au(110)/electrolyte Interfaces 74
3.7.1 RA Spectral Signatures in 0.1 M NaH_2PO_4/K_2HPO_4 82
3.8 Monitoring the Adsorption of Molecules at the Au(110)/Electrolyte Interface using RAS. 83
3.9 Summary. 89
3.10 References 91

Chapter 4

Preliminary Studies of Protein Adsorbed at the Au(110)/Electrolyte Interface

4.1 Introduction 96
4.2 RAS of the Au(110) Surface in 0.1 M NaH_2PO_4/K_2HPO_4 101
4.2.1 .....The Adsorption of P499C Full Length CPR onto the Au(110) Surface 104
4.2.2 The Adsorption of Isolated P499C FAD Variant onto the Au(110) Surface 115
4.2.3 Summary of the Adsorption of Variant CPR onto the Au(110) Surface 120
4.3 Preliminary Investigation of the Effect of Switching the Applied Potential on the RAS of Adsorbed Protein 121
4.4 The Effect of Repeated Potential Steps on the RAS of Au(110) + Protein 130
4.5 Summary of the Preliminary Data 133
4.6 References 135

Chapter 5

Controlling the Formation of a Monolayer of Cytochrome P450 Reductase onto the Au(110) Surface

5.1 The Adsorption of Variant CPR onto Au Substrate Monitored Using QCM-D 138

5.2 Experimental 139

5.2.1 Preliminary Experiment 140

5.2.2 Controlled Experiments 141

5.3 QCM-D Results for Adsorption of Full Length CPR 142

5.3.1 The Effect of pH and Concentration on the Formation of a Bilayer and Monolayer of P499C Full Length CPR 145

5.4 QCM-D Results for the Adsorption of the Isolated P499C FAD Variant of CPR 150

5.5 QCM-D Monitoring the Adsorption of Wild Type CPR 152

5.6 AFM Measurements of a Monolayer and Bilayer of Variant CPR Molecules 154

5.7 QCM-D Measurements of the Adsorption of Variant CPR Molecules under Potential Control 156

5.8 Summary 157

5.9 References 159

Chapter 6

RA Spectra of Monolayer and Bilayer Adsorption of P499C Truncated FAD and Full Length CPR Molecules

6.1 Introduction 161

6.2 RA Signature of Monolayer and Bilayer Coverage of P499C Full Length CPR on the Au(110) Surface 161

6.3 RA Spectral Signature of a Monolayer and Bilayer of P499C FAD 176

6.4 Comparison of RAS of a Monolayer P499C FAD and Full Length CPR 179

6.5 Summary 181

6. 6 References 183

Chapter 7

Monitoring the Effect of Changing the Applied Potential on the RAS of a Monolayer of P499C Full Length CPR on the Au(110) Surface

7.1 Introduction 186

7.2 The Effect of Electron Transfer in a Monolayer of Adsorbed P499C Full Length CPR 187

7.2.1 Monitoring the RAS Intensity of Au(110) + P499C Full Length CPR During Repeated Potential Steps Between -0.652 V and -0.465 V 190

7.2.2 Monitoring the RAS Intensity of Clean Au(110) During Repeated Potential Steps Between -0.652 V and -0.465 V 194

7.2.3 Monitoring the RAS Intensity of Clean Au(110) and After the Adsorption of a Monolayer of Full Length CPR as a Function of Applied Potential Using the Rapid RAS Instrument 196

7.3 Summary 203

7.4 References 205

Chapter 8

Further Investigation and Analysis of Protein Adsorbed at the Au(110)/Electrolyte Interface

8.1 Introduction 208

8.2 Does the Adsorption of P499C Full Length CPR Prevent the Au(110) Surface from Reconstructing? 208

8.2.1 Simulation of RA Spectra of Au(110) + P499C Full Length CPR 212

8.2.2 Adsorption of CPR Impedes the Potential Induced (1×3) to (1×1) Reconstruction of Au(110) 216

8.2.3 Interaction Between CPR and the Anion Induced (1×1) Reconstruction of Au(110) 223

8.3 P499C Full Length CPR Adsorbed onto the Roughened Au(110) Surface 226

8.3.1 Preliminary Investigation of the Oxidation of Full Length CPR with $NADP^+$ 230

8.4 Summary 237

8.5 References 239

Chapter 9

Conclusions

9.1 Conclusions 242

9.2 Future Work 243

Publications 246

Chapter 1

Introduction

This chapter describes the aims of this thesis and the importance of the work presented. It also introduces the reader to the biological importance of Cytochrome P450 reductase (CPR). The chapter also gives an outline of the content of this thesis.

1.1 Introduction

Our knowledge and understanding of the world around us, is driven by mankind's desire to find the answer to the question, how? Although potentially such a simple question the answers are often remarkably complex and extremely difficult to uncover.

Over the last century advancements in science have not only improved our understanding of the universe but have lead directly to developments in technology that have revolutionised our way of life. Nuclear fission provides reliable energy for millions, whilst improvements in diagnostics and treatments of diseases mean we are living longer healthier lives. The development of semiconductor materials which, gave rise to computer chip, played a crucial role in the continued relentless pace at which new technologies are being developed. The recent observation of the elusive Higgs boson at CERN highlights the extraordinary developments in physical sciences over the last hundred years or so.

Despite the huge advancements in our understanding of many aspects of the universe, the complexity and reproducibility with which biological systems function is far from being fully understood. Surface science techniques which were originally developed to probe the physics and chemistry of surfaces have become particularly useful to biologists as they seek to understand biological interactions on molecular length scales. Interest in experimental surface science took off after the development of Ultra High Vacuum (UHV) techniques which enabled techniques such as X-Ray Photoelectron Spectroscopy (XPS), Low Energy Electron Diffraction (LEED) and Scanning Tunnelling Microscopy (STM) to provide information on the properties of surfaces by exploiting the short mean free path of electrons [1]. Optical probes such as Reflection Anisotropy Spectroscopy (RAS) have been used to study biological molecules in UHV environments [2-4]. However it is desirable to study biological molecules in a liquid environment, in order to observe their natural functional activity. RAS is also capable of operation in ambient and electrochemical environments which has lead to RAS investigations of the adsorption of biological molecules at the Au(110)/liquid interface [5-16]. The work in this thesis is directed

at exploiting the sensitivity of the RAS technique to monitor conformational events in the protein NADPH-cytochrome P450 reductase (CPR) adsorbed at the metal/liquid interface.

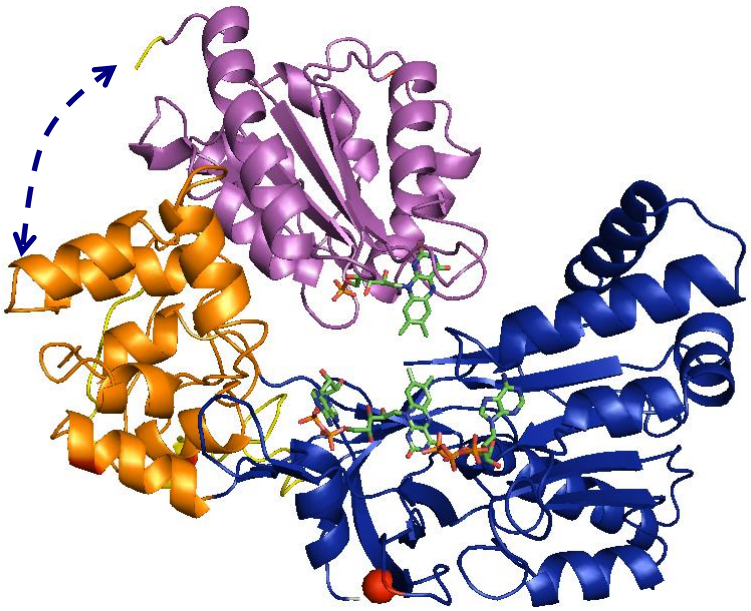

Figure 1.1: Molecular graphics ribbon diagram representation for the structure of the 78 kDa enzyme cytochrome P450 reductase. The Pro-499 residue that was targeted by site directed mutangenisis to produce the P499C variant is shown by the red sphere. The FMN-binding domain is shown in purple, the connecting domain in orange, and the FAD/NADP-domain in blue. The FAD and FMN cofactors are shown as green sticks. The position of the 'hinge' connecting the FMN-binding domain to the rest of the structure, which is not shown in the diagram, is represented by the dashed blue arrow.

CPR is an important mammalian enzyme which catalyzes electron transfer between, the two electron donor Nicotinamide adenine dinucleotide phosphate (NADPH) and cytochrome P450 enzymes [17] (figure 1.1). Cytochrome P450 are part of a superfamily of enzymes that play an important role in the metabolism of endogenous compounds including fatty acids, steroids and postaglandins, which are fundamental in drug metabolism and xenobiotics [18]. As a result of this importance in drug metabolism research in CPR function has closely paralleled that of drug

metabolism and development [19]. CPR plays a vital role in the electron transfer chain and research into the electron transfer process from NADPH to these heme containing enzymes is of great interest and importance.

CPR facilitates the transfer of electrons from NADPH via its two flavin cofactors, flavin mononucleotide (FMN) and flavin adenine dinucleotide (FAD), which are oxidised and reduced as part of the natural catalytic cycle [18]. The isoalloxazine ring is a tricyclic heteronuclear organic ring (figure 1.2) found in each flavin cofactor and it facilitates the redox activity of the flavins [20]. Each flavin cofactor possesses three oxidation states: oxidised quinine, 1-electron reduced semi-quinone and 2-electron reduced hydroquinone. Consequently CPR possesses redox states as shown in table 1.1.

Oxidised	$1e^-$ reduced	$2e^-$ reduced	$3e^-$ reduced	$4e^-$ reduced
FMN FAD	FMN FADH•	FMNH• FADH•	FMNH• $FADH_2$	$FMNH_2$ $FADH_2$
	FMNH• FAD	FMN $FADH_2$	$FMNH_2$ FADH•	
		$FMNH_2$ FAD		

Table 1.1: Shows the different possible redox states of the mutant P499C full length CPR and the possible sites for the electron, denoted by; •.

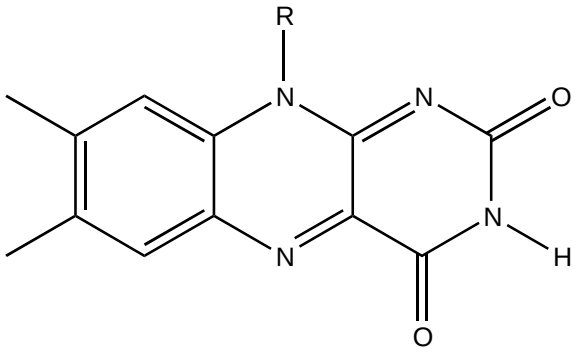

Figure 1.2: Diagram showing the structure of the isoalloxazine ring.

CPR is modular in construction comprising two distinct domains, the FMN and the FAD/NADP-domain, with the two domains joined by a linker region, the purpose of which is expected to be predominantly structural. Each domain is bound to one of the flavin cofactors, with CPR being one of only four mammalian proteins known to contain both FMN and FAD in a single polypeptide chain [17]. The two domains appear ideally located in close proximity to allow interflavin electron transfer, although this conformation is far less suitable for the subsequent electron transfer to large cytochrome P450 proteins. Therefore the crystallographic structure of CPR suggests that the enzyme is dynamic and that domain motion is crucial to the electron transfer process. The FMN domain is joined to the rest of the protein via a 'hinge' like structure of 13 residues which is expected to be flexible, further implying that CPR is a dynamic molecule [21].

There has been extensive analysis of electron transfer in CPR with interflavin electron transfer monitored using stopped-flow techniques where oxidised CPR was reduced by anaerobically mixing with excess NADPH whilst monitoring changes in the absorbance spectrum at 450 nm and 600 nm. These wavelengths are indicative of flavin reduction and the presence of the blue di-semiquinone species respectively [18]. Further experimental evidence supporting the importance of domain motion in CPR function was observed in temperature-jump relaxation experiments where, after the viscosity of the solution was increased by the addition of high concentrations of glycerol, the rate of interflavin electron transfer was drastically reduced [22]. A significant decrease in the electron transfer rate was also observed after the deletion of several amino acids in the flexible 'hinge' that connects the FMN-binding domain to the rest of the protein in a further study [23]. Other techniques such as small-angle X-ray scattering (SAXS) and pulsed electron-electron double resonance (ELDOR) [21,24] spectroscopy have also been used to study CPR. SAXS studies revealed that reduced and oxidised CPR have different overall shapes [21]. Whilst ELDOR spectroscopy of two-electron reduced CPR was used to measure distances between the FAD and FMN centres, which identified multiple conformations of CPR, suggesting a rugged energy landscape for domain motion [24].

Despite the strong evidence for domain motion coupled to CPR function, direct observation of domain motion and its timescale is challenging, and there are a wide range of timescales from picoseconds to seconds depending on the mass of the molecule and the environment. The aim of this thesis is to utilise the sensitivity and accuracy of the RAS technique to monitor dynamic properties of engineered CPR molecules adsorbed in a monolayer coverage at the Au(110)/electrolyte interface. The RAS technique has the potential to measure real time conformational change in CPR associated with electron transfer processes. In order to allow controlled adsorption of CPR molecules onto the Au(110) surface mutant CPR molecules were engineered which contained a surface exposed cysteine residue in the location shown in figure 1.1. Cysteine is known to form a strong covalent bond between the thiol group and the Au(110) surface [5,14,25]. The position of the cysteine residue was selected, after studying the crystallographic structure of CPR, to optimise the potential of observing domain motion with RAS after studying the crystallographic structure of CPR. Two forms of CPR have been investigated: full length CPR as shown in figure 1.1 and a truncated form of CPR containing the isolated FAD domain only as shown in figure 1.3.

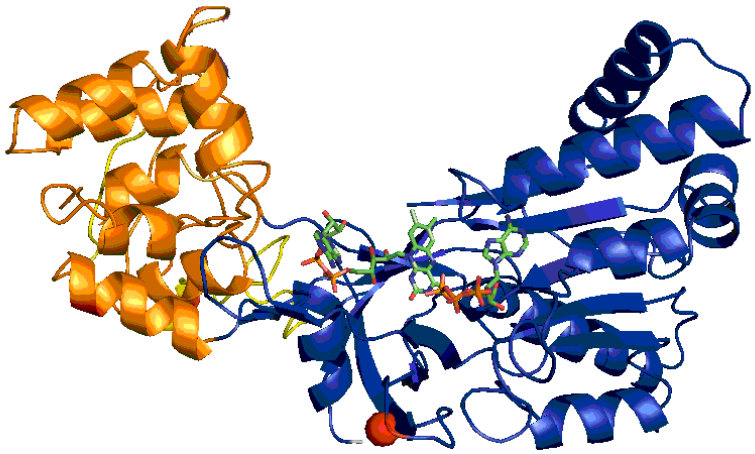

Figure 1.3: Molecular graphics ribbon diagram representation for the structure of isolated FAD domain(purple) and the connecting domain (yellow). Diagram also shows the Pro-499 residue that was targeted by site directed mutagenesis to produce the P499C variant (red sphere).

1.2 Thesis Structure

There now follows a brief description of the thesis structure with a breakdown of what is discussed in each chapter of the thesis.

Chapter 2: Experimental Apparatus and Theory

The RAS technique is introduced along with a detailed description of each of the instrument components and its layout. This is followed by a theoretical analysis of the passage of light through the system. The newly developed rapid RAS instrument is also introduced which uses a 32 channel enhanced photodiode array to collect spectra in parallel. The electrochemical cell and the solid/liquid interface at electrode surfaces is also described.

The quartz crystal microbalance with dissipation (QCM-D) technique is introduced along with a detailed description of its development from the quartz crystal microbalance (QCM) instrument and a review of previous QCM-D experiments on biological molecules.

Chapter 3: The Au(110) Surface

The Au(110) surface has been used as the substrate in all RAS and rapid RAS experiments reported in this thesis. Therefore this chapter provides a summary of previous work on this surface including a detailed discussion of the tendency of the Au(110) surface to adopt a (1×1), (1×2) or (1×3) surface structures depending on it's environment. Previous work which established the RA spectral signatures of all three reconstructions and explored the behaviour of the Au(110) surface under and electrochemical environment is also described. This chapter concludes with a detailed review of previous RAS studies of molecules adsorbed onto the Au(110) surface.

Chapter 4: Preliminary Studies of Protein Adsorption at the Au(110)/Electrolyte Interface

RAS has been used to monitor the adsorption of several biological molecules on the Au(110) surface in previous work. In this chapter the same techniques of adsorption are used in an attempt to adsorb a monolayer of CPR onto the Au(110) surface. This chapter discusses changes in the RA spectrum of Au(110) as a result of the adsorption of CPR, and also establishes a technique to monitor the RAS intensity as a function of repeated electron transfer processes.

Chapter 5: Controlling the Formation of a Monolayer of Cytochrome P450 Reductase onto the Au(110) Surface

QCM-D is used to study the adsorption of CPR onto polycrystalline Au coated quartz crystals. The effect of protein concentration and solution pH on adsorbed coverage and layer thickness is investigated and the conditions for both monolayer and bilayer adsorption of P499C CPR and truncated isolated FAD are established. A supplementary investigation of layer thickness and the order and structure of the adsorbed CPR molecules was carried out using Atomic Force Microscopy (AFM). Autocorrelation analysis of both monolayer and bilayer coverage of P499C CPR on polycrystalline Au surface has also been discussed.

Chapter 6: RA Spectra of Monolayer and Bilayer Adsorption of P499C Truncated FAD and Full Length CPR Molecules

The condition for monolayer and bilayer adsorption of both CPR and isolated FAD established in chapter 5 were replicated in RAS experiments. The RA spectral signatures of a monolayer and bilayer coverage of P499C full length CPR and isolated FAD are established. Rapid RAS data produced during the adsorption of full length CPR is discussed and information on the orientation of the adsorbed CPR molecules is produced after monitoring the RAS intensity as a function of angular variation.

Chapter 7: Measuring Conformational Change in a Monolayer of P499C Full Length CPR Adsorbed on the Au(110) surface

In this chapter the RAS intensity at key energies is monitored as the applied electrode potential is stepped between redox potentials of mutant full length CPR. The changes in RAS intensity as a function of the applied potential is expected to reveal evidence of conformational events in CPR as a function of electron transfer processes.

Chapter 8: Further Investigation and Analysis of CPR Adsorbed at the Au(110)/Electrolyte Interface

After the investigation of the effect of applied potential on RAS intensity in chapter 7, this chapter utilises a variety of different techniques to induce conformational events in CPR, whilst attempting to minimise the RAS contribution from the Au(110) substrate. RAS data was compared to ultra violet-visible (UV-Vis) absorbance spectra produced from oxidised and reduced CPR in solution, and RA spectra are simulated to try and establish the RA contribution from the adsorbed CPR molecules as a function of redox potential.

1.3 References

[1] *Introduction to Surface Physics*, M Prutton (oxford University Press 1998)

[2] G. Goletti, G. Bussetti, P. Chiaradia, R. Paolesse, C. Di Natale, E. Mazzone and A. D'Amico, *Phys. Status Solidi* A **188**, 1339 (2001)

[3] D. R. T. Zahn, S. D. Silaghi, C. Cobet, M. Friedrich and N. Esser, *Phys. Status Solidi* B **242**, 2671 (2005)

[4] R. Forker and T. Fritz, *Phys. Chem. Chem. Phys.* **11**, 2142 (2009)

[5] R. LeParc, C. I. Smith, M. C. Cuquerella, R. L. Williams, D. G. Fernig, C. Edwards, D. S. Martin and P. Weighman. *Langmuir* **22**, 3413 (2006)

[6] P. Weightman, G. J. Dolan, C. I. Smith, M. C. Cuquerella, N. J. Almond, T. Farrell, D. G. Fernig, C. Edwards and D. S. Martin, *Phys. Rev. Lett.* **96**, 086102 (2006)

[7] M. C. Cuquerella, C. I. Smith, D. G. Fernig, C. Edwards and P. Weightman. *Langmuir* **23**, 2078 (2007)

[8] C. P. Mansley, C. I. Smith, M. C. Cuquerella, T. Farrell, D. G. Fernig, C. Edwards and P. Weightman, *Phys. Status Solidi C* **5**, 2582 (2008)

[9] H. L. Messiha, C. I. Smith, N. S. Scrutton and P. Weightman, *Euro. Phys. Lett*. **83**, 18004 (2004)

[10] C. I. Smith, A. Bowfield, G. J. Dolan, M. C. Cuquerella, C. P. Mansley, D. G. Fernig, C. Edwards and P. Weightman, *J. Chem. Phys* **130**, 044702 (2009)

[11] A. Bowfield, C. I. Smith, G. J. Dolan, M. C. Cuquerella, C. P. Mansley and P. Weightman, *e-J. Surf. Sci. Nanotech*. **7**, 225 (2009)

[12] A. Bowfield, C. I. Smith, C. P. Mansley and P. Weightman. *Phys. Status Solidi* B **247**, 1937 (2010)

[13] C. P. Mansley, C. I. Smith, A. Bowfield, D. G. Fernig, C. Edwards and P. Weightman, *J. Chem. Phys*. **132**, 214708 (2010)

[14] B. Morozzo della Rocca, C. I. Smith, C. Teasuro, A. Desideri and P. Weightman,. *Surf. Sci.* **604**, 2170 (2010)

[15] A. L. Schofield, C. I. Smith, V. R. Kearns, D. S. Martin, T. Farrell, P. Weightman and R. L. Williams, *J. Phys. D: Appl. Phys*. **44**, 335302 (2011)

[16] J. H. Convery, C. I. Smith, B. Khara, N. S. Scrutton, P. Harrison, T. Farrell, D. S. Martin and P. Weightman, *Phys. Rev. E* **86**, 011903 (2012)

[17] A. Gutierrez, A. Grunau, M. Paine, A. W. Munro, C. R. Wolf, G. C. K. Roberts and N. S. Scrutton, *Biochem. Soc. T.* **31**, 497 (2003)

[18] A. Gutierrez, L. Y. Lian, C. R. Wolf, N. S. Scrutton, and G. C. K. Roberts. *Biochemistry* **40**, 1964 (2001)

[19] *Guide to Cytochromes P450, Structure and Function*, F. F. V. Lewis (Taylor & Francis 2001)

[20] T. Climent, R. Gonzalez-Lugue, M. Merchán and L. Serrano-Andrés. *J. Phys. Chem. A.* **110**, 13584 (2006)

[21] J. Ellis, A. Gutierrez, I. L. Barsukov, W. C. Huang, J. G. Grossmann, and G. C. Roberts, *J. Biol. Chem*. **284**, 36628 (2010)

[22] A. Gutierrez, M. Paine, C. R. Wolf , N. S. Scrutton, and G. C. Roberts. *Biochemistry* **41**, 4626 (2002)

[23] A. Grunau, K. Geraki, J. G. Grossmann, and A. Gutierrez, *Biochemistry* **46**, 8244 (2007)

[24] S. Hay, S. Brenner, B. Khara, A. M. Quinn, S. E. Rigby, and N. S. Scrutton, *J. Am. Chem. Soc.* **132**, 9738 (2010)

[25] A. Bowfield, C. I. Smith, M. C. Cuquerella, T. Farrell, D. G. Fernig, C. Edwards and P. Weightman, *Phys. Status Solidi* C **5**, 2600 (2008)

Chapter 2

Experimental Apparatus and Theory

The objective of this chapter is to describe the experimental apparatus and theory that has been used during this research to the reader.

2.1 Reflection Anisotropy Spectroscopy

Reflection Anisotropy Spectroscopy (RAS) is an optical probe of surfaces developed from the similar technique Spectroscopic Ellipsometry (SE) [1,2]. RAS is a non-destructive technique which can be used to probe the surfaces of many bulk crystals in a range of environments. The surface sensitivity of the RAS technique is achieved by measuring the difference in reflectance (Δr) of normal incidence plane polarised light between two orthogonal directions in the surface plane (x, y) normalised to the mean reflectance (r):

$$\frac{\Delta r}{r} = \frac{2\left(r_x - r_y\right)}{r_x + r_y} \tag{2.1}$$

where r_x and r_y are complex Fresnel reflection amplitudes in the two surface plane directions x and y, respectively.

The response from the bulk crystal usually dominates the response of optical techniques due to the probe light being able to penetrate many atomic layers, however the RAS signal arising from the isotropic bulk of a crystal structure at normal incidence cancels due to symmetry, leaving the reflected signal solely arising from the anisotropic surface structure.

The majority of surface sensitive techniques gain surface sensitivity by exploiting the short mean free path of electrons and this also restricts these techniques to an ultra high vacuum (UHV) environment. The development of the RAS technique highlights an advantage of using optical probe techniques as they are able to operate in environments consisting of any optically transparent medium. This advantage has enabled RAS to bridge the gap between UHV and non-UHV techniques and has also opened up the solid/liquid interface for investigation specifically under electrochemical conditions.

RAS is highly sensitive to surface structure and has been successfully used to monitor changes in the surface structure. Originally developed from SE and Circular Dichroism (CD) the first RAS kits were used to monitor semiconductor growth by

Aspnes *et al.* [3]. The ability of RAS to work in both UHV and ambient conditions has facilitated many studies in the last three decades.

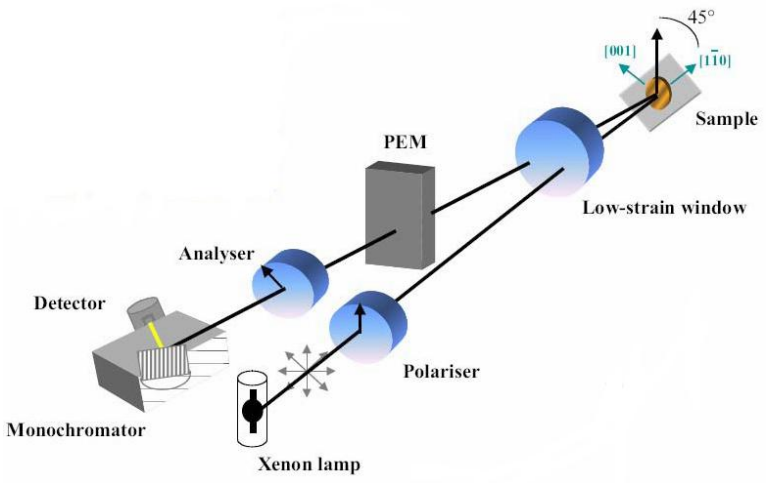

Figure 2.1: Schematic of the basic components of the RA Spectrometer. Reproduced from [6].

2.1.1 RA Spectrometer and its Components

RAS, originally known as Reflection Difference Spectroscopy (RDS), was developed in the 1980's by Aspnes *et al.* [4] and originally created as a real-time monitor of III-IV semiconductor growth at near atmospheric pressure [5]. RAS and SE instruments share several components and a similar experimental set up. However a significant difference between the two techniques is that SE monitors the reflection of light incident near to the Brewster angle [3] whereas RAS monitors light at near normal incidence ($\leq 5^{\circ}$). RAS has been successfully applied to study metal surfaces in UHV and air [6], the metal/liquid interface within an electrochemical environment [7] and the study of the adsorption of biological molecules onto electrode surfaces [8-12]. The individual components of an RA spectrometer can be seen in the schematic in figure 2.1. Each of the components are described in the order in which light passes through the system. Please note that mirrors are used to facilitate and enhance the position and focal length of light, the

mirrors, not shown in figure 2.1 are positioned before and after both the polariser and the analyser.

Xenon Lamp

The 75 Watt Super Quiet 9 short arc xenon discharge lamp (Hamamatsu) provides the necessary high intensity broad band light source for the spectrometer to function. The lamp is used in conjunction with a stabilised power supply (Hamamatsu C4621-02) which minimises fluctuations from the mains supply. Radiated light is generated by an arc discharge when high voltages are applied across the anode to the high performance cathode in a xenon gas environment. The light satisfies the requirements of the RA Spectrometer by providing a continuous steady output of light between the infrared (IR) and ultraviolet (UV) (1.5 – 5.5 eV) in the electromagnetic spectrum. For the first hour after power up the xenon gas pressure in the lamp can vary, preventing thermal equilibrium and therefore maximum radiant intensity to be reached. To ensure maximum and unchanged photon flux experiments only begin at least 1 hour after the lamp is switched on.

Mirrors

The mirrors have two main purposes in the RAS instrument. The first is to produce a parallel beam of focused light emitted from the xenon lamp. The second is to aid in ensuring as much light as possible reaches the detector, by introducing an astigmatism, which shapes the reflected light beam from the sample surface, into a narrow ellipse which is focused into the narrow entrance slit of the monochromator, thus reducing the amount of light lost. The mirrors used are front coated UV enhanced aluminium on glass, with a thin silica coating to prevent mechanical abrasion.

Polariser

The difference between the intensities of the reflections r_x and r_y in the *x* and *y* direction are typically very small. As a result the polariser and analyser must have a high extinction ratio $>10^5$, therefore prism type polarisers are used. Rochon and

Wollaston beam splitting type polariser and Glan prism polarisers, which separate the two polarised beam by total internal reflection, have been considered. Prism polarisers are commonly made of three different prism materials, calcite, quartz and magnesium fluoride. Calcite prisms cover the spectral range from IR to 300 nm while quartz extends this range to 200 nm and magnesium fluoride prisms can extend this to even shorter wavelengths into the UV. Glan prisms are advantageous in UHV conditions as there is only one beam emerging, meaning there is less restrictions on the location of components, with the two beams it is important to ensure they do not overlap, which can require larger distance between components. The RAS instrument that has been used in this thesis uses a Rochon type polariser, consisting of two attached quartz prisms that separate the ordinary and extraordinary polarised beams which are polarised perpendicular to each other, as it covers the full spectral range of interest in this thesis. A consequence of using Rochon type quartz polariser means that care must be taken to ensure the two emerging beam from the polariser do not overlap.

Low Strain Window

At the front of the electrochemical cell is a silica low strain window. Polarised light exiting the Rochon prism will pass through this window prior to interacting with the sample in the electrochemical cell. The window possesses a small inhomogeneous birefringence which will add a small contribution to the RAS signal. The spectrum of the window can be removed by subtracting it from all raw experimental data.

Photoelastic Modulator

Essentially the photoelastic Modulator (PEM) is a tuneable wave-plate, which, by manipulation of stress induced birefringence is capable of modulating the polarisation ellipse of light reflected from the sample, making it possible to collect both the real and imaginary parts of the waveform.

This is achieved by driving a quartz piezoelectric transducer coupled to a fused silica optical element at 50 kHz, the natural resonant frequency of the crystal, thus causing an oscillating birefringence. The reflected light can be considered as

having two orthonormal components linearly polarised parallel and perpendicular to the modulating axis. The induced oscillating birefringence introduces a phase difference, know as a retardation (Γ), between these two components. Light linearly polarised parallel to the modulation axis travels faster than the perpendicular component when the fused silica is compressed. Alternatively when the fused silica is stretched, the parallel component travels slower than the perpendicular component, which remains unchanged in each case.

This is a key component in the RAS instrument as elliptically polarised light from the sample surface will be phase modulated depending on the polarisation but linearly polarised light from the sample bulk will remain linearly polarised as it passes through the PEM as the intensity of the light is equal in all phases. The model used in this thesis is a Hinds Instrument Inc; PEM Quartz 90.

Analyser

The analyser, which is of the same design as the polariser, is used to covert the phase modulated signal from the PEM into an amplitude modulated signal which can be detected. The analyser is orientated at an angle of 45˚, with respect to the polariser, to produce a modulated signal switching between two linearly polarised states.

Monochromator

To obtain an RA Spectrum a monochromator with a computer controlled grating angle is required to split the light from the analyser into its constituent wavelengths. A Jobin Yvon monochromator (H10), consisting of a holographic grating with 1200 grooves mm^{-1} with a working spectral range of 1.5 to 6.2 eV is ideal for this purpose.

Detector

To measure the intensity of light a Hamamatsu multi alkali cathode photomultiplier tube (PMT) (Hamamatsu R955) is positioned immediately after the exit slit of the monochromator. The modulated waveform of light entering the PMT is converted into a small current, which is then amplified as the current is typically in the order of

nanoamps. The amplified signal is then converted into a voltage relative to the initial intensity of the incoming light. The signal consist of two components, an AC component, related to the anisotropy of the sample surface, which is superimposed onto a DC offset component, which relates to the reflectivity. The two components need to be separated, which requires the use of a lock in amplifier.

Other detectors that could be considered are Si photodiodes, however they do not function into the UV spectral range without the application of an appropriate coating to convert UV photons for detection within the visible range. This process causes a decrease in sensitivity in the visible range and ultimately the PMT was chosen as the preferred detector for this instrument

Lock-In Amplifier

A lock-in amplifier is used to analyse the resulting AC and DC signals produced from the PMT. An EG&G 5210 (dual phase) lock-in amplifier manufactured by PerkinElmer Instruments, which operates at a frequency range of 0 – 120 kHz, is used in the RAS instrument. To analyse the AC and DC signals the lock-in amplifier measures the Fourier coefficients of the first and second harmonics of the signal which carries the real and imaginary parts of the RA signal respectively. The successful detection of the RA signal is due to the lock-in amplifiers ability to detect a signal of very specific frequencies from an extremely noisy environment.

The lock-in works by identifying the frequency and phase relationship of a locked in reference voltage, which is supplied by the PEM. The difference in frequencies of the signal in interest with regard to its locked in signal can then be tracked.

2.2 The Propagation of Light through the System

To measure the RA signal accurately a comprehensive and well defined method of determining the polarisation state of light reflected from the sample surface is required. In this section the theoretical analysis of RAS is described in a quantitative manner using a well defined mathematical formulism. It is first important to define

the electric field vector, E, of light which can be represented as a superposition of two orthogonal states.

$$E(z,t) = E_x(z,t) + E_y(z,t) \tag{2.2}$$

where

$$E_x(z,t) = E_{0x}\cos(kz - \omega t + \phi_x) \tag{2.3}$$

and

$$E_y(z,t) = E_{0y}\cos(kz - \omega t + \phi_y) \tag{2.4}$$

The resulting wave, **E**, is therefore the vector sum of components,

$$E(z,t) = \hat{x}E_{0x}\cos(kz - \omega t) + \hat{y}E_{0y}\cos(kz - \omega t + \delta) \tag{2.5}$$

where the terms *k* is the wave number, *z i*s the position in space, ω is the angular frequency, *t* is the time, ϕ_x ϕ_y are the phases, and E_{0x} and E_{0y} represent the maximum amplitudes. In equation 2.5 $\delta = \phi_x - \phi_y$ is the relative phase between the two components and the resultant polarisation state of light is dependent on this value and the relative projection along each axis. The types of polarisation that can be achieved can now be discussed in terms of magnitudes, E_{0x} and E_{0y} and the relative phases between the two components δ. Linearly polarised light will occur when $\delta = m\pi$ for values of, m= 0, ±1, ±2, ±3…. as the wave will be confined to a single plane, this is also the case when either E_{0x} or E_{0y}=0, as the wave will be limited to displacements in the *x* or *y* axes respectively. Linearly polarised light with non-zero magnitudes is at an angle α to the *x* axis, defined below.

$$\alpha = \tan^{-1}\left(\frac{E_{0x}}{E_{0y}}\right)$$

Circularly polarised light is achieved when the phase lag, δ is an integer multiple of $\pm\pi/2$ and $E_{0x} = E_{0y}$. In circularly polarised light the magnitude remains

constant as the wave propagates through space but the direction of E fluctuates with time in a circular pathway with angular frequency ω.

Elliptical polarisation occurs when the resultant vector E fluctuates with time, as in circularly polarised light, but is also accompanied by variations in magnitude, for example if $E_{0x} \neq E_{0y}$ and δ is again an integer multiple of $\pm\pi/2$. Elliptical polarisation is also achieved when $E_{0x}=E_{0y}$ and δ is an arbitrary angle.

A convenient way of representing polarised light is to use the Jones vector notation, which was invented in 1941 by R. Clark Jones [13]. The method provides a mathematical description of the state of light in terms of the electric field vector Figures 2.2, 2.3 and 2.4 show the different polarisation states and their corresponding normalised Jones vector representation.

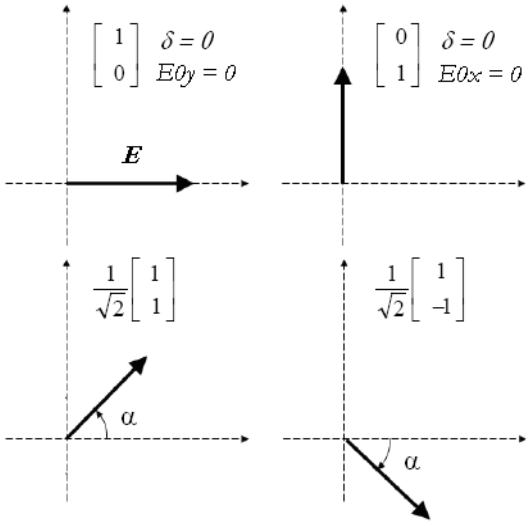

Figure 2.2: Common linear polarisation states

In the RAS system the light reflected from an appropriate sample will be either elliptically polarised or circularly polarised. Incident linearly polarised light reflected from the surface will be elliptically polarised due to surface anisotropy, whereas light reflected from the bulk of a cubic sample will be circularly polarised. This affect is significant as the PEM introduces retardation to the elliptically polarised light, so that it is possible to extract harmonics from the amplitude modulation, giving information which only derives from surface anisotropy.

Circularly polarised light from the bulk will pass through the PEM without modification as the intensity in the resultant vector is the same in all phases.

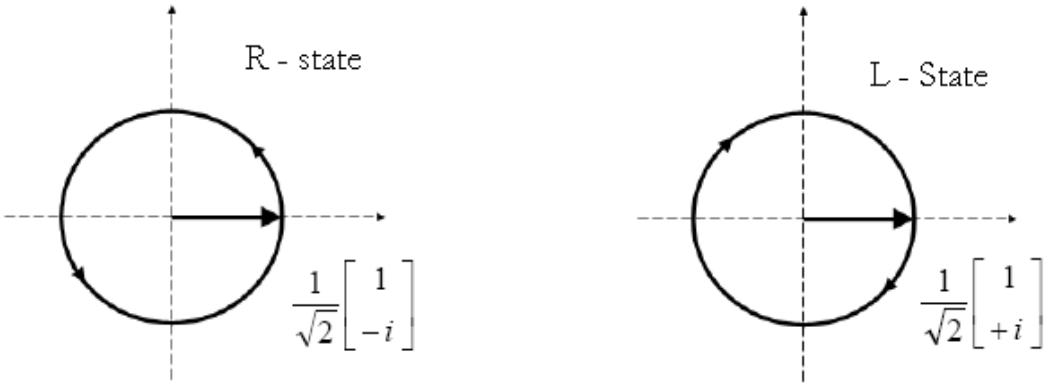

Figure 2.3: Circular polarised states

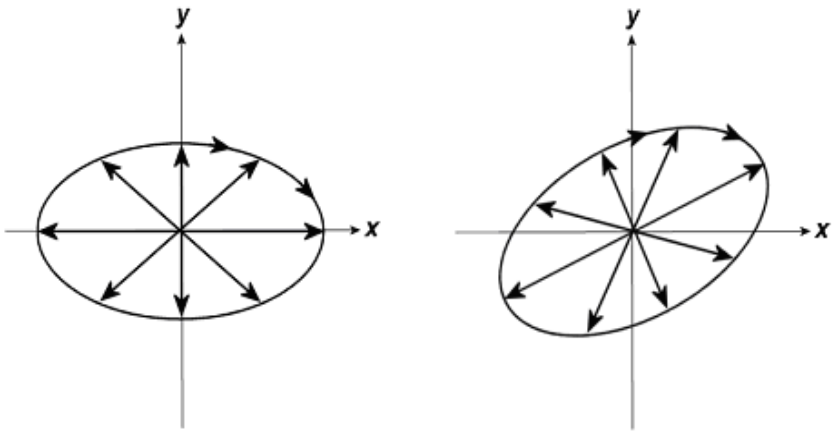

Figure 2.4: Ellipticaly polarised states

The RAS technique uses polarised light and consequently the analysis must follow that used for a polarising system. The Jones matrix formalism can not only describe the polarisation state of light but can also be used to calculate the effect of optical components on the input light of a given polarisation, the transmitted or reflected wave can then be expressed as (2 x 2) matrix, as such it is an ideal method for analysis of the RAS system and will now be used to describe the propagation of polarised light through the RAS set up.

2.2.1 The Jones Matrix Formalism

Light emitted from the xenon lamp, once polarised can be defined in a concise manner using the Jones matrix formalism, for example the resultant wave E from (2.5) written as a Jones vector is:

$$E(z,t) = \begin{bmatrix} E_{0x}e^{i\delta x} \\ E_{0y}e^{i\delta y} \end{bmatrix} \tag{2.6}$$

The polarisation state of light can be analysed as it passes through the system, from the initial state of the incident light E_i to the final sate E_f, arriving at the detector. The effect of each component in the RAS system modifies the Jones vector of the transmitted or reflected light. The Jones matrix, M in equation 2.7, fully describes the effect on light of all the optical components in the RAS instrument.

$$E_f = ME_i \tag{2.7}$$

The optical axes of each component need to be considered, both the polariser and analyser have a transmission axis, *t*, and an extinction axis, *e*, whilst the PEM, as it introduces retardation has a slow axis, *s* and a fast axis, *f*. For an Au(110) sample the axes (*x*,*y*) are in the $[1\bar{1}0]$ and [001] surface directions. These axes define the reference frame for each component, therefore rotational matrices, R, are used to convert the Jones vector representing the polarisation state of light to that of the optical component that it is interacting with.

$$R(\theta) = \begin{bmatrix} \cos(\theta) & -\sin(\theta) \\ \sin(\theta) & \cos(\theta) \end{bmatrix} \tag{2.8}$$

Azimuth angles P, A and M describe the orientations of the reference frames of the polariser, analyser and modulator respectively, which correlates to the transmission axes of the polariser and analyser and the fast axis of the modulator.

The first Jones matrix that can be assigned to the light wave is T_P^{te}. This is assigned after the light has passed through the polariser and is therefore in the *te* reference frame of the polariser.

$$T_P^{te} = \begin{bmatrix} 1 & 0 \\ 0 & 0 \end{bmatrix} \tag{2.9}$$

The rotation matrix R*(P)* is then used to get T_P^{te} into the *xy* reference frame of the sample and this is achieved by multiplying T_P^{te} by R*(P)*:

$$R(P)T_P^{te} = \begin{bmatrix} \cos P & \sin P \\ -\sin P & \cos P \end{bmatrix} \begin{bmatrix} 1 & 0 \\ 0 & 0 \end{bmatrix} = \begin{bmatrix} \cos P & 0 \\ -\sin P & 0 \end{bmatrix} \tag{2.10}$$

Before interacting with the sample surface the light will enter the electrochemical cell by passing through a strain free window. The orientation of the window axes is unknown and therefore it is assumed to coincide with the *xy* frame of the sample. The window posses some birefringence and this retards the light introducing a phase shift in *y* with respect to *x*, represented by the Jones matrix:

$$T_{WI}^{fs} = \begin{bmatrix} 1 & 0 \\ 0 & e^{i\delta_{WI}} \end{bmatrix} \tag{2.11}$$

where δ_{WI} is the retardation of the incident beam and δ is defined as:

$$\delta = \frac{4\pi d}{\lambda}\left(n_e - n_o\right) \tag{2.12}$$

where, d is the thickness of the window, λ is the wavelength of light and n_e and n_o are the refractive indices of the extraordinary and ordinary directions respectively. The light will then reflect from the sample surface. The Jones matrix for the sample is assumed to have different coefficients in x and y, r_x and r_y respectively.

$$T_S^{xy} = \begin{bmatrix} r_x & 0 \\ 0 & r_y \end{bmatrix} \tag{2.13}$$

Once the light is reflected from the sample surface it will once again pass through the window. Upon exiting the electrochemical cell the light will pass through a different part of the window which has an associated retardation, δ_{WO}, and is described by the Jones matrix:

$$T_{WO}^{fs} = \begin{bmatrix} 1 & 0 \\ 0 & e^{i\delta_{WI}} \end{bmatrix} \tag{2.14}$$

The next component in the RAS system is the PEM which is described by:

$$T_M^{fs} = \begin{bmatrix} 1 & 0 \\ 0 & e^{i\delta_M} \end{bmatrix} \tag{2.15}$$

Application of the rotation matrix R(M) is needed to change the reference frame from the xy frame of the sample to that of the PEM:

$$R(M) = \begin{bmatrix} \cos(M) & -\sin(M) \\ \sin(M) & \cos(M) \end{bmatrix} \tag{2.16}$$

Combining matrix 2.15 with 2.16 gives:

$$T_M^{fs}\mathrm{R(M)} = \begin{bmatrix} 1 & 0 \\ 0 & e^{i\delta_M} \end{bmatrix} \begin{bmatrix} \cos M & -\sin M \\ \sin M & \cos M \end{bmatrix} = \begin{bmatrix} \cos M & -\sin M \\ \left(e^{i\delta_M} \sin M\right) & \left(e^{i\delta_M} \cos M\right) \end{bmatrix} \tag{2.17}$$

The light will next interact with the analyser which converts the light from a phase-modulated signal to an amplitude-modulated signal. This requires the same Jones matrix used for the polariser:

$$T_A^{te} = \begin{bmatrix} 1 & 0 \\ 0 & 0 \end{bmatrix} \tag{2.18}$$

Once again the reference frame must be changed from that of the PEM to the analyser, requiring the rotation matrix R(A-M):

$$R(A-M) = \begin{bmatrix} \cos(A-M) & -\sin(A-M) \\ \sin(A-M) & \cos(A-M) \end{bmatrix} \tag{2.19}$$

Combining matrix 2.18 and 2.19 gives:

$$\begin{aligned} T_A^{te} R(A-M) &= \begin{bmatrix} 1 & 0 \\ 0 & 0 \end{bmatrix} \begin{bmatrix} \cos(A-M) & -\sin(A-M) \\ \sin(A-M) & \cos(A-M) \end{bmatrix} \\ &= \begin{bmatrix} \cos(A-M) & -\sin(A-M) \\ 0 & 0 \end{bmatrix} \end{aligned} \tag{2.20}$$

The Jones matrix, M, which describes the effect of all the optical components on the light wave can now be obtained by combining all the Jones matrices of each element. These must be combined in the order in which the light interacts. Due to matrices being non- commutative, M can now be written as:

$$M = T_A^{te} R(A-M) T_M^{fs} R(M) T_{WO}^{xy} T_S^{xy} T_{WI}^{xy} R(P) T_P^{te} \tag{2.21}$$

which after combining equations 2.10, 2.11, 2.13, 2.14, 2.16, 2.15, 2.19 and 2.18 evaluates to:

$$M = \begin{bmatrix} a_{11} & 0 \\ 0 & 0 \end{bmatrix} \tag{2.22}$$

where:

$$\begin{aligned} a_{11} = {} & (\cos(A-M)\cos M - \sin(A-M)(e^{i\delta_M}\sin M))(r_x \cos P) - \\ & (-\cos(A-M)\sin M - \sin(A-M)(A-M)(e^{i\delta_M}\cos M))(r_y e^{i\delta_{WO}} e^{i\delta_{WI}}\sin P) \end{aligned} \tag{2.23}$$

The values of the angles P, A and M are -45˚, 0˚ and 45˚ respectively therefore the following evaluations can be made:

$$\sin(\pm 45°) = \pm\frac{1}{\sqrt{2}}, \quad \cos(\pm 45°) = \frac{1}{\sqrt{2}}, \quad \sin(0°) = 0, \quad \cos(0°) = 1,$$

The above values can be inserted into equation 2.23 to give:

$$a_{11} = \frac{r_x}{2\sqrt{2}}(1 + e^{i\delta_M}) + \frac{r_y e^{i\delta_{WO}} e^{i\delta_{WI}}}{2\sqrt{2}}(e^{i\delta_M} - 1) \tag{2.24}$$

The matrix, M, contains one non-zero term and so the initial equation 2.7 becomes:

$$E_f = \begin{bmatrix} a_{11} & 0 \\ 0 & 0 \end{bmatrix}\begin{bmatrix} 1 \\ 0 \end{bmatrix} = \begin{bmatrix} a_{11} \\ 0 \end{bmatrix} \tag{2.25}$$

The window term can also be simplified:

$$e^{i\delta_{WO}} e^{i\delta_{WI}} = e^{i(\delta_{WO}+\delta_{WI})} = e^{i\delta_W} \tag{2.26}$$

The window induced retardation although finite, is small, meaning it is possible to expand the exponential in terms of a power series:

$$e^{i\delta_W} = 1 + i\delta_W + \frac{(i\delta_W)^2}{2!} + \frac{(i\delta_W)^3}{3!} + \ldots \approx 1 + i\delta_W \tag{2.27}$$

Using the above simplification, equation 2.24 becomes:

$$a_{11} = \frac{1}{2\sqrt{2}}[(r_x - r_y) + (r_x - r_y)e^{i\delta_M} - i\delta_W r_y(1 - e^{i\delta_M})] \tag{2.28}$$

The complex Fresnel coefficients, r_x and r_y in equation 2.13 can be written in terms of their real and imaginary components:

$$r_x = a + ib, \qquad r_y = c + id \tag{2.29}$$

The modulator retardation represented by $e^{i\delta_M}$ can be expressed using De Moivre's theorem:

$$e^{i\delta_M} = \cos(\delta_M) + i\sin(\delta_M) \tag{2.30}$$

With manipulation a_{11} becomes:

$$\left(2\sqrt{2}\right)a_{11} = \alpha + i\beta \tag{2.31}$$

where α and β are the real and imaginary parts of a_{11}. One can assume that the light wave beyond the analyser will not have I ts polarisation altered, and so the detector and monochromator can be thought of as polarisation independent. This implies that the detector only measures the time dependent intensity at each wavelength. The time dependent intensity measured, *I,* is proportional to the square of E_f from equation 2.25 which is dependent on the a_{11} term, thus:

$$I \propto \left|\left(2\sqrt{2}\right)a_{11}\right|^2 = \alpha^2 + \beta^2 \tag{2.32}$$

which, with, extensive algebraic manipulation, becomes:

$$\begin{aligned} I \propto |a_{11}|^2 = \frac{1}{4}\left[\left(a^2+b^2\right)+\left(c^2+d^2\right)+\left(c^2+d^2\right)\delta_W{}^2\right] \\ +\frac{1}{4}\left[\left(a^2+b^2\right)-\left(c^2-d^2\right)-\left(c^2+d^2\right)\delta_W{}^2\right]\cos\left(\delta_M\right) \\ +\frac{1}{2}\left[\left(ad-dc\right)-\left(ac+bd\right)\delta_W\right]\sin\left(\delta_M\right) \end{aligned} \tag{2.33}$$

This can be written in the form:

$$I = I_{dc} + I_{\omega}\sin\left(\delta_M\right) + I_{2\omega}\cos\left(\delta_M\right) \tag{2.34}$$

The retardation δ_M is varied sinusoidally by the PEM and can therefore be expressed as:

$$\delta_M = \alpha(\lambda)\sin(\omega t) \tag{2.35}$$

where ω is the resonant angular frequency of the modulator and $\alpha(\lambda)$ is the modulation amplitude, and is proportional to the applied excitation voltage and the wavelength of light. The frequency components of the signal can be determined by Fourier expansions of the $\cos(\delta_M)$ and $\sin(\delta_M)$ terms, which introduces Bessel functions of the first kind:

$$\cos\left(\alpha\sin\left(\omega t\right)\right) = J_0\left(\alpha\right) + 2\sum_{n=1}^{\infty} J_{2n}\left(\alpha\right)\cos\left(2n\omega t\right) \tag{2.36}$$

$$\sin\left(\alpha\sin\left(\omega t\right)\right) = 2\sum_{n=1}^{\infty} J_{2n-1}\left(\alpha\right)\sin\left(\left(2n-1\right)\omega t\right) \tag{2.37}$$

where $J_n(\alpha)$ is the Bessel function of order n and argument α. $J_0(\alpha) = 0$ is achieved, in this case, by adjusting the voltage applied to the PEM and equation 2.34 becomes:

$$I = I_{dc} + I_{\omega} 2J_1(\alpha)\sin(\omega t) + I_{2\omega} 2J_2(\alpha)\cos(2\omega t) + \ldots \qquad (2.38)$$

The first term in the above equation, 2.38, is time-independent, and is therefore considered as a DC component. Comparison of the terms in equations 2.33 and 2.38 enables the intensity coefficients to be determined. It is assumed that for small anisotropies $r_x \sim r_y$ for additive terms. If only the first order window strain terms are considered, the normalised frequency terms are found to be:

$$I_{dc} \sim \frac{\left\langle |r_x|^2 + |r_y|^2 \right\rangle}{2} = R \qquad (2.39)$$

$$\frac{I_{\omega}}{I_{dc}} \sim \mathrm{Im}\left(\frac{\Delta r}{r}\right) - \delta_W \qquad (2.40)$$

$$\frac{I_{2\omega}}{I_{dc}} \sim \mathrm{Re}\left(\frac{\Delta r}{r}\right) \qquad (2.41)$$

The time independent term, I_{dc}, is a measure of the reflectivity of the sample material. At frequency ω the imaginary component of $(\Delta r/r)$ is measured, which is found to be dependent on the first-order window strain terms, whereas the real component of $(\Delta r/r)$ is measured at 2ω and is only sensitive to window strain terms of the second order. Experimentally the frequency dependence of the real and imaginary parts of the signal allow the two parts to be separated. Measurements of the imaginary part of the signal have substantial window strain effects, which makes analysis of the signal significantly more complicated and as a result the majority of RAS measurements reported are of the real part of the RAS signal.

2.2.2 Errors

Misalignments of the optical components and the sample and sometimes insufficient linear polarisation of the light emitted from the Xe lamp are the source of the majority of errors in the RAS technique. The misalignment of polarisation dependent components will cause an offset in the measured Re($\Delta r/r$), which, although it does not introduce new features to the RA spectrum, creates problems when quoting absolute values of Re($\Delta r/r$). Changes between measured spectra can be more accurately investigated. A thorough discussion of the impact of misalignment on the RA spectra have been carried out in A. Maunder's thesis [14], where it was found that the relationship between the polariser and modulator is very sensitive to misalignment, but this has less of an effect on the analyser. Anisotropy induced by the window is another source of error in RA spectra and to remove the influence of this a window correction is subtracted from all RA spectra.

2.2.3 Rapid RAS

The rapid RAS is a recent development of the RAS technique. This development enables dynamic changes occurring over short time scales to be studied at multiple wavelengths. This can provide valuable information on dynamic changes in Au structure during surface reconstructions and other important changes that take place in biological systems adsorbed on suitable substrates.

The rapid RAS instrument has been developed to employ many of the components in the standard RAS instrument. It uses a 32 channel UV enhanced photodiode array (Hamamatsu S4114-35Q) to collect spectra in parallel and is developed from the 16 channel rapid RAS instrument described in detail earlier [15]. Each channel is individually amplified and digitised, the signals are processed using phase locked, signal averaging and fast Fourier transform (FFT) techniques which replaces the need of a lock-in amplifier and allows all 32 channels to be processed at once. The instrument is calibrated before use each time using filters of known wavelength to accurately establish the wavelength of each channel.

Dynamic effects in biological molecules can be crucial to their function and the rapid RAS allows the user to monitor dynamic effects and changes to RAS intensity over 32 channels at once. Data can be gathered and averaged to produce reasonably signal to noise RA spectra every 30-40 ms, which is a great advantage as changes in RAS intensity can occur at different time-scales at different wavelengths. The ability to monitor a large range of wavelength simultaneously allows this effect to be investigated.

2.3 Electrochemistry

Electrochemistry is an important branch of science and has applications across a wide range of industries including extraction of metals, solar cells, batteries, chemical synthesis and sensors which together make up a multi-million pound industry. Electrochemistry is concerned with chemical reactions which involve the transfer of electric charge, usually in the form of electrons across the interface of a chemical species and an electrode [16]. RAS has been used to study biological molecules adsorbed at electrode surfaces in electrochemical cells [8-12]. Reactions at the interfacial region are the core of electrochemistry and knowledge of this region is crucial. At a molecular scale the movement of negatively charged species between the electrode and a species in solution is driven by the potential gradient at the surface. This occurs at such small distances that the potential gradient can be in the order of 10^{10} Vm^{-1} [16]. To fully understand the interfacial region it is important to understand the movement of charged ions being attracted to the electrode surface, the structure of the adsorbed species and the effect the potential field has in this region.

A charged surface must have a balancing counter charge, which is in the solution. However this charge will not be uniformly distributed throughout the liquid phase but will be concentrated towards the electrode region. One of the earliest models to describe the interfacial region was created by Hermann Von Helmholtz in 1853 [17]. The model assumes that no electrons transfer and that the interface must be neutral overall, where the charge on the electrode is balanced by an equal and

opposite charge in the solution instigated by the redistribution of the electrolyte ions to the surface of the electrode, Helmholtz referred to this as the "electric double layer". The Helmholtz model likens the electrode/electrolyte interface to a parallel plate capacitor, with one of the plates representing the electrode surface and the second plate is thought of as the plane that passes through the centre of the solvated ions at the closet approach, this is known as the Outer Helmholtz Plane (OHP). This early model was subsequently improved, firstly by Gouy [18,19] and Chapman [20] by consideration that charge is free to move and subject to thermal motion, so that the largest concentration of counter ions is found close to the electrode, but excess charge will disperse away from the electrode into a diffuse layer with progressively decreasing concentration of ions until a homogeneous distribution of ions within the bulk of the electrolyte is reached [21]. Stern [22] modified this model further, stating that there must be a plane of closest approach, as in the Helmholtz model, as ions have a finite size. Stern combined ideas from the Helmholtz and Gouy-Chapman models to produce a new model.

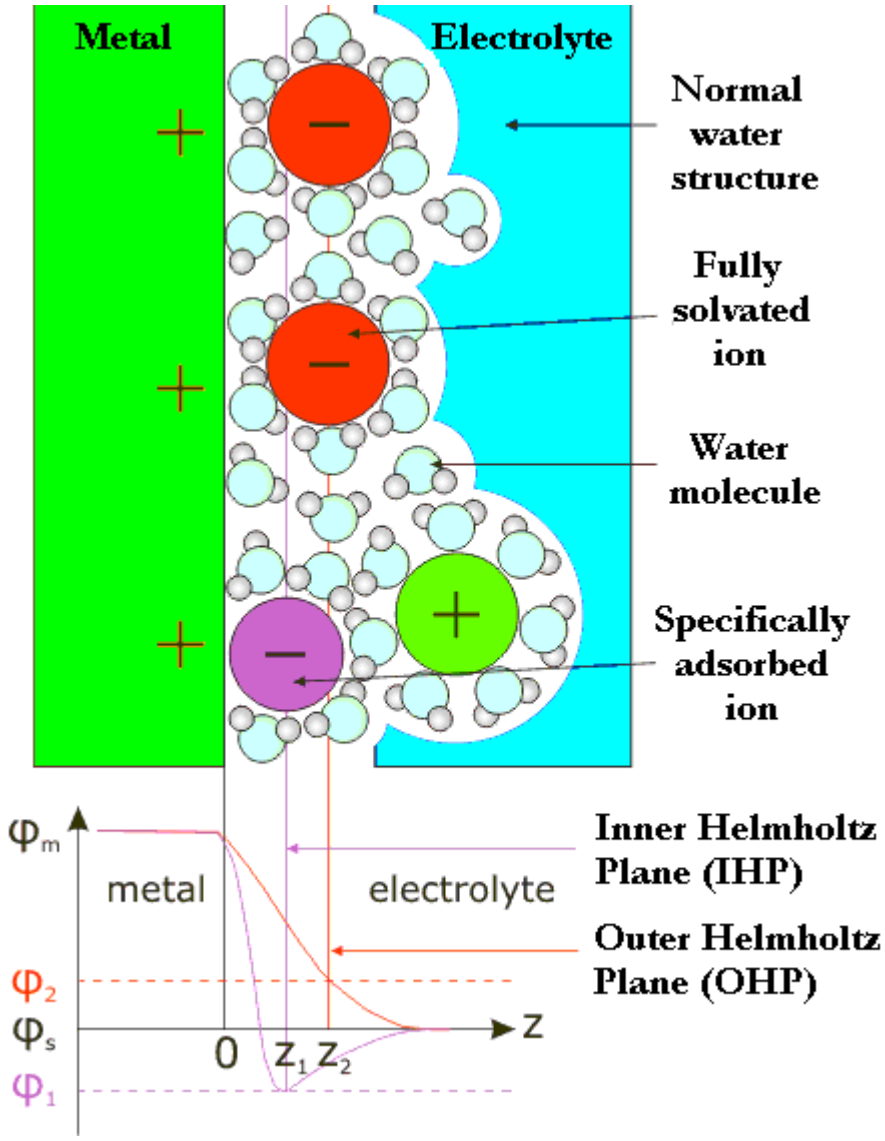

Figure 2.5: Schematic illustration of the interfacial region with a graph of the potential drop across the electrochemical interface (Reproduced from [23]).

The latest improvement to the model came in 1947 by Grahame [24], and is the current accepted model. Grahame introduced the concept of two types of adsorption present on the electrode surface, specifically adsorbed ions and non-specifically adsorbed ions. Grahame proposed that although the inner layer would be mostly occupied by solvent molecules, it is possible for some ions or molecules that have lost their weakly bound solvation shells to form a chemical bond to the surface of the electrode. This is only possible for certain types of molecules with certain types of electrodes and is therefore referred to as specifically adsorbed. This

introduces a new plane, the Inner Helmholtz Plane (IHP), which is the plane that runs through the centre of specifically adsorbed ions. This accepted model of the interfacial region is depicted in figure 2.5.

The specifically adsorbed molecules at IHP, shown in figure 2.5, typically show a steep potential drop across the interface (purple curve figure 2.5) with a over-shooting of the potential with respect to the bulk electrolyte value. It is assumed that non-specifically adsorbed molecules adsorbed at the OHP a linear potential drop across the interface (red line figure 2.5). The potential φ_m, φ_s, φ_1, and φ_2 correspond to potentials inside the metal, the electrolyte, the IHP at Z1 and the OHP at Z2 respectively.

Applying a potential to an electrode immersed in an electrolyte will cause the surface to become charged away from its neutral state. The value of the charge is not only dependent on the potential but also the electrode material and the electrolyte used. Applying a negative potential will cause electrons to flow into the electrode surface resulting in a negatively shifting surface charge and, if the potential applied is positive, the opposite is true: electrons will move from the surface and the charge will become less negative and eventually positive.

2.3.1 Measuring Electrode Potential

Electrochemical investigations in this thesis are supplemented with in situ RAS studies to monitor the adsorption of molecules at the electrode surface and changes occurring at the electrode surface as a result of changing the potential. It is therefore essential to have precise control and measurements of the potential across the electrode and the solution. Direct measurement of the electrode potential is not possible, for example in a one electrode cell the use of a standard digital voltmeter (DVM) to measure the potential drop will not work as it will not make electrical contact because free-electrons will not pass from the DVM probe to the solution. Indirect measurement of the potential is possible with the introduction of a second electrode, a reference electrode, in the reference half cell.

The role of the reference electrode is to provide a fixed potential which does not vary during the experiment [21]. A potentiostat will control the potential between the two electrodes. As a result of the reference electrode maintaining a fixed potential any change in the applied potential to the cell is across the working electrode and the solution and can therefore be measured. In fact this measurement is the difference of two metal/solution potential drops and can be represented as:

$$\begin{aligned}\Delta\Phi &= (\Phi_{(MetalA)} - \Phi_{(Solution)}) - (\Phi_{(MetalB)} - \Phi_{(Solution)}) \\ &= \Phi_{(MetalA)} - \Phi_{(MetalB)}\end{aligned} \tag{2.42}$$

In a two electrode system one electrode represents a test system and the other a reference system, the potential difference can be written as:

$$\Delta\Phi = (\Phi_{(Test)} - \Phi_{(Solution)}) - (\Phi_{(Reference)} - \Phi_{(Solution)}) \tag{2.43}$$

Due to the potential drop across the reference electrode/solution remaining constant this can be rewritten as:

$$\Delta\Phi = (\Phi_{(Test)} - \Phi_{(Solution)}) - \mathrm{k} \tag{2.44}$$

where k is a constant.

The value of $\Phi_{(Test)} - \Phi_{(Solution)}$ can still not be directly measured, however changes in this value can be determined against the constant k.

The work reported in this thesis involved the use of three electrodes, the purpose of the third ‘counter electrode’ is to supply the current required by the working electrode without in any way interfering with the measured response of the working electrode [21]. When a potential difference is applied across the working electrode/solution interface the current will be large, which can alter the ionic concentration in the solution, causing the difference between the reference and the measured potential to no longer be constant. The counter electrode prevents current

flowing from between the reference electrode and the working electrode by allowing the passage of current between itself and the working electrode.

A Standard Calomel Electrode (SCE) consisting of Hg/Hg_2SO_4 in saturated aqueous KCl is used as the reference electrode, the working electrode is a Au(110) crystal of 99.999 % purity and a piece of platinum gauze is used as the counter electrode given its inert nature and large surface area.

2.3.2 The Electrochemical Cell

The electrochemical cell used for RAS experiments described in this thesis is a purpose built three electrode spectro-electrochemical cell. An illustration of the cell can be seen in figure 2.6.

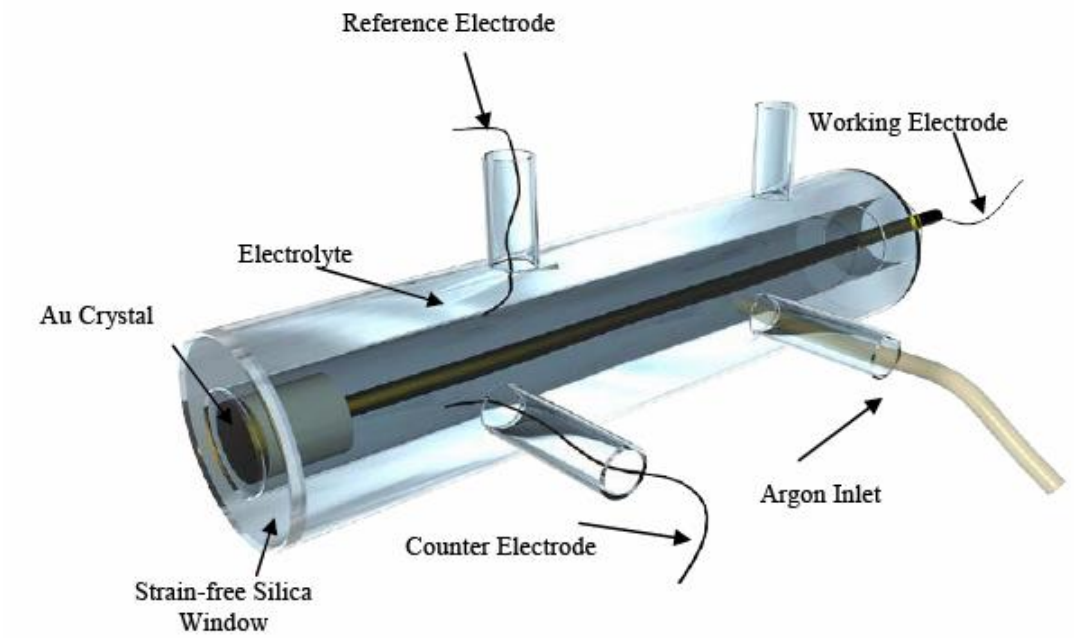

Figure 2.6: Schematic of the electrochemical cell used in potential controlled RAS experiments.

A closed Teflon tap is used to separate the SCE reference electrode from the electrochemical cell. This prevents any chloride ions leaking from the reference electrode and contaminating the working solution. The distance between the

working electrode and reference electrode is minimised to avoid any potential drop by using a luggin capillary, which consists of a thin glass pipe and is not shown in figure 2.6. The argon inlet allows argon gas to be bubbled through the cell preventing oxygen contamination of the electrolyte and degases the electrochemical cell. The potentiostat used in the research reported in this thesis was an Autolab PGSTAT 30.

2.4 Crystal Preparation

The Au(110) crystals used in RAS experiments throughout this thesis are in the form of discs of diameter 10 mm and thickness 2 mm with an exposed surface area of 0.5 cm^2. The Au(110) crystals are of 99.999% purity and are orientated to an accuracy of 0.1° by x-ray diffraction. The crystals were prepared for experiments by mechanically polishing on successively smaller grades of diamond paste, from 6 μm, 1 μm and finishing on 0.25 μm, between polishing at each grade of diamond paste the crystals were cleaned in an ultra sonic bath to remove the diamond paste. After being polished the crystals are flame annealed using a butane micro-torch, where the crystals are heated until glowing orange and then allowed to cool in air before being reheated in the flame of the torch, this process is repeated 15 times. The flame annealing process for preparing clean and well ordered surfaces was introduced by Clavilier *et al*. [25] and was later developed for the preparation of Au surfaces [26] After being flame annealed the crystals are allowed to cool in air before being protected by a drop of ultra pure water (Millipore Q Systems, 18 MΩcm), then transferred to the electrochemical cell.

2.5 Quartz Crystal Microbalance with Dissipation Monitoring (QCM-D)

The primary aim of this thesis is to develop and apply RAS to monitor, in real time, electron transfer induced conformational change in Cytochrome P450 Reductase (CPR) adsorbed onto an Au(110) surface. In order to understand conformational

events using RAS the protein must first be adsorbed onto the Au(110) substrate surface, therefore understanding the adsorption process is vital to the success of the research.

The interaction of biological molecules with solid surfaces is an area of huge interest. Understanding this interaction has application in biology, medicine, food processing and the area which has had rapid growth, the development of biomedical materials [27]. It is clear that monitoring of the adsorption of biological materials on solid surfaces is crucial, creating opportunities for the development of new adsorption monitoring techniques.

A Quartz Crystal Microbalance (QCM) is a nanogram sensitive device used to measure adsorbed mass per unit area. It utilises the resonant behaviour of the piezoelectric quartz crystal and the fact that the resonant frequency of the crystal changes when the mass of the crystal changes, therefore as mass is adsorbed onto the crystal accurate measurement of the frequency changes allows very small masses to be measured.

This was only possible after 1959, when Sauerbrey demonstrated the linear relationship of frequency changes of an oscillating material are related to the mass adsorbed on the material [28].

$$\Delta m=(C/n)\Delta f \tag{2.45}$$

where Δf is the frequency change, Δm is the mass adsorbed, n=1,3… is the overtone number and C is the mass sensitivity constant given by:

$$C=(t_q \rho_q)/f_0 \tag{2.46}$$

where t_q is the thickness of quartz, ρ_q is the density of quartz, f_0 is the resonant frequency of the crystal in Hz and C= 17.7 Hz ngcm^{-2} for a 5 MHz crystal.

The Sauerbrey relationship is accurate as long as three assumptions are held, i) the adsorbed mass is small relative to the mass of the quartz crystal, ii) the mass adsorbed is rigidly adsorbed and iii) the adsorbed mass is evenly distributed over the

active area of the crystal [29]. Initial studies using QCM's were carried out in gaseous or vacuum environments where metal oxidation [30], gas adsorption [31], dry etching and catalytic reactions [32] were the major areas of research.

The technique expanded into the liquid phase after Nomura and Okuhara [33] demonstrated that, if one face of the sensor is exposed to the liquid and the other to the gas phase it is possible to operate a QCM in the liquid phase. This expansion of the QCM capabilities created not only new experimental opportunities, but also introduced difficulties in the interpretation of the frequency changes. QCMs operating in the liquid phase introduced viscous and elastic contributions to the frequency change [29], which violates the assumption in the Sauerbrey relationship that the adsorbed mass is rigidly adsorbed, questioning the validity of the Sauerbrey relationship in the liquid phase.

The sensitivity of the QCM to the viscoelasticity of adsorbed layers can be the reason for experimentally observed deviations from the Sauerbrey linear relationship between frequency change and adsorbed mass [34]. The viscoelastic adsorbed layer brings the adjacent liquid layer into motion as a result of the crystal oscillating, which causes inaccuracies in the Sauerbrey relation. Voinova *et al.* [35] used continuum mechanics to show that the mechanical properties of viscoelastic materials are usually related to energy storage and dissipation processes resulting from the balance between applied stress and the ensuing relaxation process in the material. To use a QCM in the liquid phase, applying it to non-rigid overlayers, it is necessary to monitor the damping of the crystal oscillation or its dissipation factor along with the frequency change. The dissipation factor is defined as:

$$D=E_{Dissipated}/(2\pi E_{stored}) \tag{2.47}$$

where D is the dissipation, $E_{Dissipated}$ is the energy dissipated during one oscillating cycle and E_{Stored} is the energy stored in the oscillating system. Dissipation is the sum of various energy dissipating subsystems in the composite oscillator which can reveal the dissipative properties of the viscoelastic overlayers.

The Sauerbrey relation is not obeyed by non-rigid adsorbed layers. This causes a dissipation shift which has been shown to violate the Sauerbrey relation. Consequently just using this relation and measuring frequency alone would greatly underestimate the adsorbed mass of sufficiently non-rigid adsorbed layers [29]. It has been suggested that the failure of the Sauerbrey relationship derives from two sources. The first source is related to the propagation of the shear acoustic wave in the viscoelastic film. A thin and rigid film, adsorbed on the crystal acts as 'dead' mass, whereas viscoelastic or thicker films constitute a coupled oscillation for which the change in frequency is not proportional to the change in mass. The second source is related to the definition of mass. At solid liquid interfaces, mass is often defined as molar mass or 'dry' mass. In QCM measurements liquid may couple as additional mass through direct hydration or entrapment in cavities of the adsorbed film [36].

Voinova *et al.* [35] explained that the simplest way to account for dissipative losses in viscoelastic layers was to introduce a shear viscosity coefficient η and a shear elasticity modulus μ within one of the two basic models "Maxwell" or "Voight". The Voight model, unlike the Maxwell model, does not describe flow at a steady rate, instead the viscoelastic element is described by a complex shear modulus of which the real part (the storage modulus) is independent of frequency and the imaginary part (the loss modulus) increases linearly with frequency [35]. The two models are applicable when using different solutions. The Maxwell model is usually applied to polymer solutions with low shear rate that demonstrate purely liquid like behaviour, whereas the Voight model is applied for polymers that conserve their shape and do not flow [35].

The analysis of viscoelastic layers adsorbed on resonant crystal surfaces has lead to the development of commercial Quartz Crystal Microbalance with Dissipation monitoring (QCM-D). The first QCM-D devices were developed by Q-sense in 1996. These QCM-D devices have been used to monitor protein adsorption, and it has been shown that when a monolayer or a multilayer of biomolecules are adsorbed in the liquid phase the energy dissipated increases. The monitoring of the change in dissipation as well as frequency, at multiple harmonics of resonant frequencies in the millisecond timescale, can be modelled with theory to extract

meaningful data from the experimental data, such as mass, adsorbed layer thickness, viscosity or storage modulus [29]. This allows a much broader characterisation for viscoelastic systems that do not obey the linear Sauerbrey relation, than QCMs which monitor frequency changes alone. Biomedical material development is an area that has benefitted greatly from the development of QCM-D. An important factor in biomaterial development is the biocompatibility of the material. The ability of QCM-D to measure accurately the amount of protein adsorbed onto different surfaces provides insight into whether the material inhibits or promotes protein adsorption, which plays a crucial role in the development of biomedical material development and selection. Dissipation losses during protein adsorption have been shown to originate from several sources: interactions at the protein/substrate interface, interactions at the protein/liquid interface and/or processes within the protein layer (proteins plus trapped liquid) [37].

Figure 2.7: Q sense E4 QCM-D module. (Reproduced from www.q-sense.com).

In the research reported in this thesis, protein adsorption has been monitored uses a Q-Sense E4 Module QCM-D (figure 2.7). This is a 4 chamber module capable of monitoring the frequency and dissipation changes on four quartz crystals

at once. The frequency and dissipation changes are monitored using Q-Soft 401 software and analysis of layer thickness, viscosity and mass can be modelled and fitted to experimental data using Q-Tools 3.0 software. The frequency and dissipation changes can be monitored to an accuracy of 1 Hz and $1x10^{-6}$ units of dissipation respectively, for the protein solutions used in this research [38].

The quartz crystals are 'AT' cut which provides favourable stability properties and the crystal oscillates in a purely shear mode [39]. The crystals comprise a thin AT cut quartz disc sandwiched between two electrodes, which are used to establish an electric field across the crystal. The electrodes can be made of any metal material and in the case of this research gold is used, which is commonly used due to its inert nature. A polycrystalline Au coated sensor is shown in figure 2.8.

Figure 2.8: Q-Sense Au coated Sensor. (Reproduced from www.q-sense.com).

The E4 modules (figure 2.9) are temperature controlled and for the experimental research in this thesis the temperature was kept at 20˚C. All crystals were cleaned and UV-Ozone treated before use. Once placed inside the flow module ultra pure water was first pumped over the sensor until a steady trace for both frequency and dissipation was reached, which was then repeated with buffer solution to produce a baseline before a known concentration of protein was added to the solution, which was then pumped through the cell whilst the frequency and dissipation changes were monitored. It is important to rinse the cell thoroughly with buffer solution before the Δf and ΔD data are analysed, to ensure excess protein is rinsed off the crystal surface.

Figure 2.9: Q-Sense flow module with gold coated quartz sensor crystal in position. (Reproduced from www.q-sense.com).

2.6 Atomic Force Microscopy (AFM)

The capability of the Atomic Force Microscope (AFM) to produce very detailed three-dimensional images of the surface topography down to the nanometer or angstrom scale, has seen the AFM become an essential tool for imaging many surfaces with a wide range of applications.

AFM was first reported by G. Binnig *et al.* [40]. AFM measures the attractive and repulsive forces between a sharp probe tip mounted on a flexible cantilever and the sample surface. These forces cause the tip to deflect or approach the sample surface. Monitoring the tip deflections provides information on the sample surface structure. Originally the tip movements were monitored using a Scanning Tunnelling Microscope (STM) [40], however modern AFM's use optical detection systems. The detection systems utilise a laser which is reflected off the back of the cantilever onto a photodetector. The photodetector is usually separated into quadrants which allow changes in the position of the cantilever to be accurately detected [41]. The optical detection systems used can measure changes in the position of the laser beam as small as 1 nm [42]. The sample position is controlled by piezoelectric ceramics which allow very accurate positioning of the sample with respect to the tip. Alternatively the tip can be controlled by piezoelements and the

sample kept in a fixed position. Either way this allows the sample surface to be scanned in the *x*-*y* position very precisely [41].

The cantilever tip interacts with the sample surface and experiences repulsive and attractive forces. As the tip is brought to the surface it experiences long range weak attractive van der Waals forces between the tip and surface. As the tip is pushed into the surface stronger repulsive forces are detected as the tip is essentially trying to displace atoms on the surface [42].

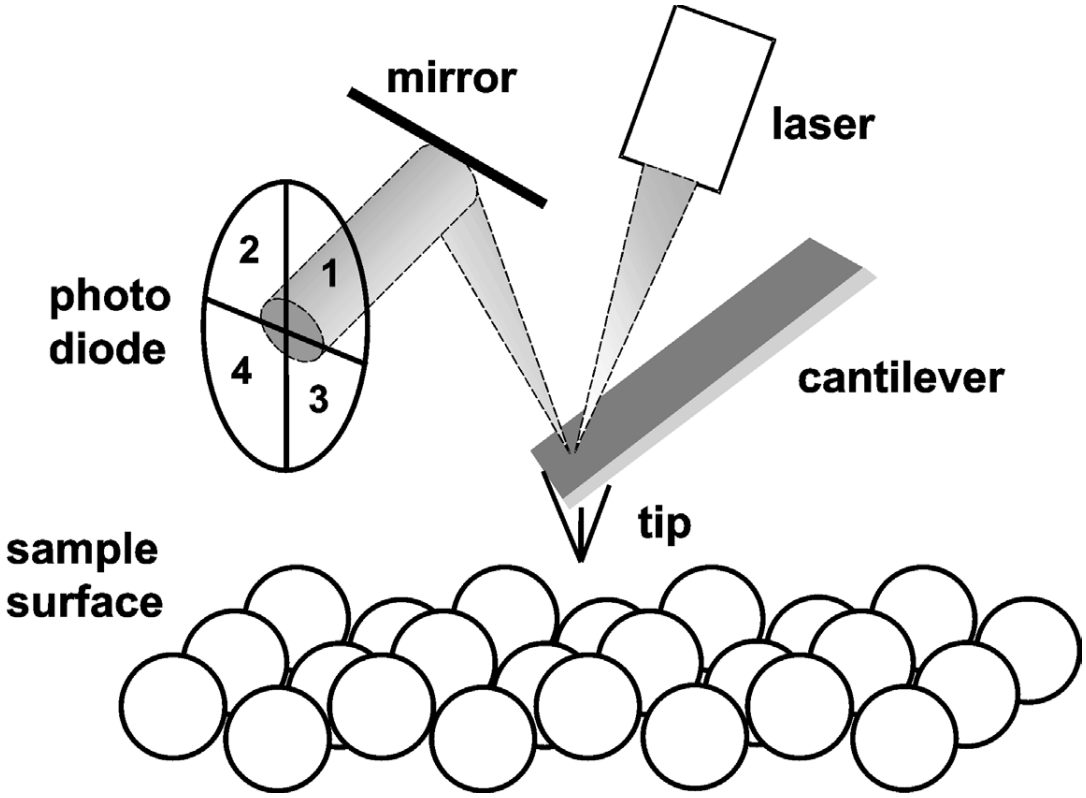

Figure 2.9: Schematic representation of an AFM. The cantilever-tip system is deflected by the surface topography of the sample. Cantilever deflections are detected with a laser-optical set-up. The four segment photodiode detects forces affecting the tip. In most AFM systems the sample rests on a piezotube scanner (not shown in this diagram) which allows the scanning to be rastered in the *x* and *y* surface direction as well as the *z* direction (reproduced from [42]).

The common modes of operation of AFM are contact mode, non-contact mode and tapping mode. In contact mode the tip is brought into contact with the

sample surface until a desired deflection of the cantilever is reached using piezoelements to control the *z*-position. The tip is then dragged over the sample surface, whilst keeping the deflection of the cantilever constant. This is achieved by moving the cantilever closer to or away from the surface. These changes in the *z*-position of the cantilever relate to the surface topography of the sample. Contact mode can cause problems when scanning soft samples as the dragging of the tip over the surface can damage the surface. Non-contact mode is were the tip is moved close to the sample surface, typically 5-15 nm above the surface. In this mode the attractive van der Waals forces are detected, these forces being much weaker than the forces in contact mode. Due to this the tip is oscillated close to or at the resonant frequency of the cantilever, which makes AC detection methods to detect forces between the cantilever and the sample surface possible. The forces will cause changes to the amplitude, phase or frequency of the oscillation. As a result of force gradients, an attractive force will lead to a decrease in resonant frequency whereas a repulsive force will lead to an increase in resonant frequency. Operating in non-contact mode is difficult in ambient conditions as the tip can experience a 'jump to contact' as it is brought close to the sample surface. This is caused by a small capillary bridge forming between the tip and the sample. A key advancement in the AFM technique is tapping mode. This allows high resolution images of the topography of samples that are easily damaged by contact mode because they are loosely held on the sample surface or soft with structures that can be subtly altered. In tapping mode the cantilever is oscillating at, or near to its resonant frequency: this is achieved using piezoelectric crystals. The oscillation of the cantilever has a high amplitude in air, typically 20 nm [41]. The tip is brought closer to the surface until it intermittently touches or 'taps' the surface. Tapping the surface reduces the cantilever oscillation due to energy loss and the reduction in the oscillation amplitude is used to measure surface features [44]. As the tip passes over the sample the amplitude of the oscillation will decrease as the tip passes over a bump, as there is less room to oscillate. Conversely the oscillation amplitude will increase as the tip passes over a depression, as at that moment the cantilever has more room to oscillate. Information of the oscillation amplitude is used to produce very accurate surface topography measurements without damaging surfaces or adsorbed surface

layers as this tip is not pulled or dragged across the surface, the tapping force being always applied vertically.

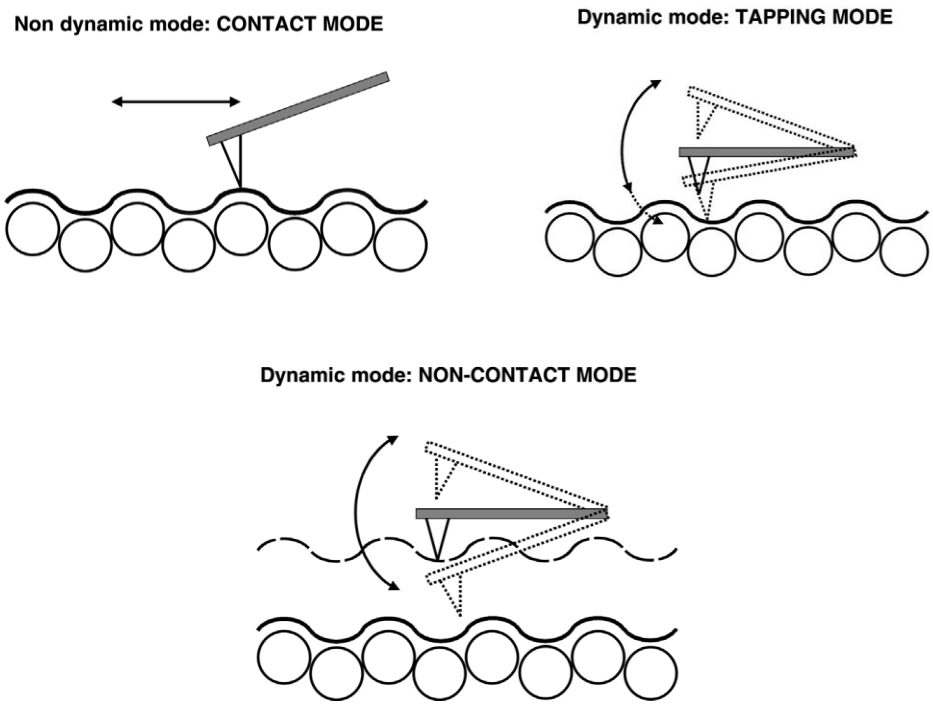

Figure 2.10: Common AFM imaging modes, showing contact mode, tapping mode and non-contact mode (reproduced from [43]).

The capability of AFM to operate in aqueous environments has seen the technique evolve from the original contact mode with metal or polymer samples to studies routinely carried out with the cantilever submersed in liquid, which allows biological molecules and living cells to be imaged in physiological conditions. AFM can measure local charge densities, mechanical properties and intermolecular forces with nanometer-scale spatial resolution, and is capable of manipulating biomolecules on a nanometer scale [41]. Therefore some of the most intriguing features of biological complexes, such as dynamic behaviour, their ability to interact with other molecules and their assembly patterns, are all possible to follow with AFM and as a result of this there has been a great increase in research using AFM to study biological systems, such as living cells [45], proteins and DNA [46], and there are several excellent review articles on the use of AFM to study biological molecules [41,47,48].

2.7 References

[1] T. E. Jenkins, *J. Phys. D: Appl. Phys.* **32**, R45 (1999)

[2] K. Vedam, *Thin Solid Films* **313**, 1 (1998)

[3] *Ellipsometery and Polarised Light*, R. M. Azzam and N. M. Bashara (Amsterdam: Elsevier, 1997)

[4] D. E. Aspnes, E. Colas, A. A. Stunda, R. Bhat, M. A. Koza and V. G. Keramidas, *Phys. Rev. Lett.* **61,** 2782 (1988)

[5] J. F. McGilp, *Prog. Surf. Sci*. **49**, 1 (1995)

[6] P. Weightman, D. S. Martin, R. J. Cole and T. Farrell, *Rep. Prog. Phys.* **68,** 1251 (2005)

[7] B. Sheridan, D. S. Martin, R. J. Power, S. D. Barrett, C. I. Smith, C. A. Lucas, R. J. Nichols and P. Weightman, *Phys. Rev. Lett.* **85** 4618 (2000)

[8] C. I. Smith, A. J. Maunder, C. A. Lucas, R. J. Nichols and P. Weightman, *J. Electrochem. Soc.* **150**, E233 (2003)

[9] C. I. Smith, G. J. Dolan, T. Farrell, A. J. Maunder, D. G. Fernig, C. Edwards and P. Weightman, *J. Phys.: Condens. Matter* **16**, S4385 (2004)

[10] R. LeParc, C. I. Smith, M. C. Cuquerella, R. L. Williams, D. G. Fernig, C. Edwards, D. S. Martin and P. Weightman, *Langmuir* **22**, 3413 (2006)

[11] C. I. Smith, A. Bowfield, G. J. Dolan, M. C. Cuquerella, C. P. Mansley, D. G. Fernig, C. Edwards, and P. Weightman, *J. Chem. Phys*. **130**, 044702 (2009)

[12] A. Bowfield, C. I. Smith, G. J. Dolan, M. C. Cuquerella, C. P. Mansley and P. Weightman, *e-J, Surf. Sci. Nanotech*. **7**, 225 (2009)

[13] R. C. Jones, *J. Opt. Soc. Am*. **31**, 488 (1941)

[14] A. Maunder, Ph. D. Thesis, The University of Liverpool (2001)

[15] P. Harrison, T. Farrell, A. Maunder, C. I. Smith and P. Weightman, *Meas. Sci. Technol.* **12**, 2185 (2001)

[16] *A First Course in Electrode Processes*, D. Pletcher (The Electrochemistry Consultancy, 1991)

[17] H. L. F. von Helmholtz, *Ann. Physik*, **89**, 211 (1853).

[18] G. Gouy, *Compt. Rend.* **149** 654 (1909)

[19] G. Gouy, *J. Phys*. **9**, 457 (1910)

[20] D. L. Chapman, *Phil. Mag*. **25**, 475 (1913)

[21] *Instrumental Methods in Electrochemistry*, The Southampton Electrochemistry Group, University of Southampton, Horwood Publishing (2001)

[22] O. Stern, *Z. Electrochem*. **30**, 508 (1924)

[23] D. M. Kolb, *Surf. Sci*. **500**, 722 (2002)

[24] D. G. Grahame, *Chem. Rev*. **41,** 441 (1947)

[25] J. Clavilier, R. Faure, G. Guinet and R. Durand, *J. Electroanal. Chem*. **107**, 205 (1980)

[26] N. Batina, A. S. Dakkouri and D. M. Kolb, *J. Electroanal. Chem*. **370**, 87 (1994)

[27] K. Nakanishi, T. Sakiyamu and K. Imamura, *J. Biosc. Bioeng*. **91**, 233 (2001)

[28] G. Sauerbrey, *Zeitschift Fut Physik* **155**, 206 (1959)

[29] M. C. Dixon, *J. Biomol. Techn.* **19,** 151 (2008)

[30] B. Kasemo, E. Tornquist, *Surf. Sci.* **77**, 209 (1978)

[31] T. A. P. Rocha, M. T. S. R. Gomes, A. C. Duarte and J. A. B. P. Oliveira, *Anal Commun* **35**, 415 (1998)

[32] B. Kasemo and E. Tornquist, *Phys. Rev. Lett* **44,** 1555 (1980)

[33] T. Nomura and M. Okuhara, *Anal. Chim. Acta* **142,** 281 (1982)

[34] M. V. Voinova, M. Jonson and B. Kasemo, *Biosens. Bioelectron*. **17,** 835 (2002)

[35] M. V. Voinova, M. Rodahl, M. Jonson and B. Kasemo, *Phys. Scripta* **59**, 391 (1999)

[36] F. Hook, T. Nylander, C. Fant, K. Sott, H. Elwig and B. Kasemo, *Anal. Chem*. **73**, 5796 (2001)

[37] M. Rodahl, F. Hook, C. Fredriksson, C. A. Keller, A. Krozer, P. Brzezinski, M. Voinova and B. Kasemo, *Faraday Discuss*. **107**, 229, (1997)

[38] F. Hook, Thesis. *Development of a novel QCM technique for protein adsorption studies.* Chalmers University of Technology, Goteborg University (2004)

[39] M. Rodahl, F. Hook, A. Krozer, P. Brzeeinski and B. Kasemo, *Rev. Sci. Instrum.* **66**, 3924 (1995)

[40] G. Binning, C. F. Quate and Ch. Gerber, *Phys. Rev. Lett.* **56**, 930 (1986)

[41] R. J. Colton, D. R. Baselt, Y. F. Dufrene, J. B. D. Green and G. U. Lee, *Curr. Opin. Chem. Biol.* **1**, 370 (1997)

[42] *Nanotechnology, basic science and emerging technologies,* M. Wilson, K. Kannangara, G. Smith, M. Simmons and B. Raguse, Chapman & Hall/CRC

[43] K. D. Jandt, *Surf. Sci.* **491,** 303 (2001)

[44] *Scanning Probe Microscopy and Spectroscopy, Methods and Applications,* R. Wiesendanger, Cambridge University Press (1994)

[45] J. A. DeRose and J. –P. Revel, *Thin Solid Films*, **331,** 194 (1998)

[46] H. G. Hansma and L. Pietrasanta, *Curr. Opin. Chem. Biol.* **2,** 579 (1998)

[47] D. Fotiadis, S. Scheuring, S. A. Müller, A. Engel and D. J. Müller, *Micron.* **33,** 385 (2002)

[48] M. Gaczynska and P. A. Osmulski, *Curr. Opin. Colloid. In.* **13** 351 (2008)

Chapter 3

The Au(110) Surface

The Au(110) surface has been the focus of a great deal of research in both ultra high vacuum (UHV) and electrochemical environments. The purpose of this chapter is to work through these previous studies and discuss how the physical and electronic structure of the Au(110) surface relate to features observed in the RA profile of Au(110) surface. This chapter will also introduce the three-phase model which enables simulations of RA spectra to be produced. The Au(110) surface is known to undergo surface reconstruction in varying electrolytes and electrode potentials: this work will be summarised and surface reconstructions will be assigned to spectral features in RA spectra.

3.1 The Need for a Substrate

Since it is difficult to monitor protein dynamics whilst the protein is in solution, as the molecules are able to move about randomly, we adopt the technique of fixing cytochrome P450 reductase (CPR) to a surface. This makes it easier to detect conformational changes.

The Au(110) surface that is used throughout this thesis is one of the low index faces of the gold face centred cubic (FCC) crystal structure. The surface structure of a Au(110) crystal, after the flame annealing and preparation process described in section 2.4 provides the intrinsic anisotropy that is necessary to produce a RA signal. The other two low-index faces of the Au, the unreconstructed (100) and (111), have inherently isotropic structures and so do not yield RA spectra.

The Au(110) surface offers a structured substrate which has been the focus of much reflection anisotropy spectroscopy (RAS) research and as a result the RA profile of Au(110) is well understood [1]. The flame annealing process makes it possible to prepare the Au(110) surface in conditions outside of the ultra high vacuum (UHV) environment. This has led to the use of Au(110) single crystal electrodes within an electrochemical environment being used to investigate biological molecules adsorbed at the Au(110)/electrolyte interface.

RAS investigations of biological molecules adsorbed at the Au(110)/electrolyte interface [2-13] have been shown to form ordered structures aligned along the principle axes of the substrate [3,5,7]. An advantage of adsorbing CPR onto the Au(110) surface in an electrochemical environment is that it allows the electrode potential to be changed to the known redox potentials of CPR which will induce electron transfer processes in the protein. This may make it possible for the RAS technique to monitor conformational changes in CPR during electron transfer processes. However a difficulty arises in understanding the RAS signatures of the surface reconstructions of the Au(110) surface. These reconstructions have been the focus of a great deal of experimental investigations. The surface reconstructions have been shown to be sensitive to crystal preparation, temperature, electrolyte solution, pH and electrode potential, and therefore a thorough

understanding of the Au(110) surface is required so that the effect of adsorbing protein can be monitored and analysed as accurately as possible.

3.2 Surface Phase Transitions

Phase transitions fall into two broad categories, first order transitions and second order transitions. Phase transitions occur in many physical systems: first order transitions are characterised by latent heats and occur mainly in a 'mixed phase' regime such as the solid/liquid/gas transition, where parts of the system have completed the transition and others have not. Second order transitions, which are not associated with latent heats, are also known as continuous transitions and include transitions to superconducting and superfluid states which occur in certain materials and in liquid He. Phase transitions occur due to the tendency of systems to minimise the free energy, F, whilst the system is in thermodynamic equilibrium at constant volume and temperature:

$$F = U - TS \tag{3.1}$$

Transitions occur at specific temperatures because different states can divide their energy between internal energy, U(T) and the entropy of the system, S(T) in different ways.

To characterise a phase transition, the degree of order in a system is measured: this is the order parameter. This parameter changes in a system as the transition temperature T_c is reached: the change in order is dependent on the type of phase transition involved. For first order phase transitions a discontinuous change is observed as one equilibrium phase changes to another. For second order transitions a continuous transition is seen. The order parameter typically varies as $(T-T_c)^{\beta}$ for second order transitions, where β is the critical exponent which belongs to a universality class and depends solely on the symmetry of the system, the dimensionality of the order parameter and the dimensionality of space.

3.3 The Physical Structure of the Au(110) Surface

It is necessary to gain a fundamental understanding of the phase transitions that occur at Au(110) surface in various environments before it is possible to interpret RA spectra of adsorbed material on the surface.

The nature of reconstructions of (110) surfaces has generated a great deal of interest within the scientific community and has been the focus of a significant amount of research. This section will provide an overview of the literature on the Au(110) surface reconstructions, in both UHV and electrochemical environments, where the phase transitions in the Au(110) can be induced through thermal treatment or by potential control. An excellent review of the literature on the Au(110) surface reconstructions has been recently carried out by N. J. Almond [14]. The next section of this thesis will highlight the main findings from that work together with a summary of more recent work.

3.3.1 Au(110) in the UHV Environment

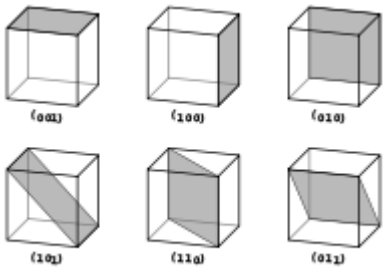

Figure 3.1: Schematic of low Miller index surfaces.

The schematic in figure 3.1 highlights some of the main low Miller index surfaces of Au. Of these surfaces the (110) is the most open of a FCC crystal and has the highest surface energy and the lowest atomic density. These characteristics mean the surface has a tendency to reconstruct. The unreconstructed Au(110) surface reveals the atoms exposed when a FCC crystal is sliced along the (110) plane. This unreconstructed surface is called a (1×1) surface structure and is shown in figure

3.2. The typical reconstruction of the Au(110) surface is the (1×2) surface structure. This is achieved by the removal of every other row of Au atoms along the $[1\bar{1}0]$ direction as shown schematically in figure 3.3.

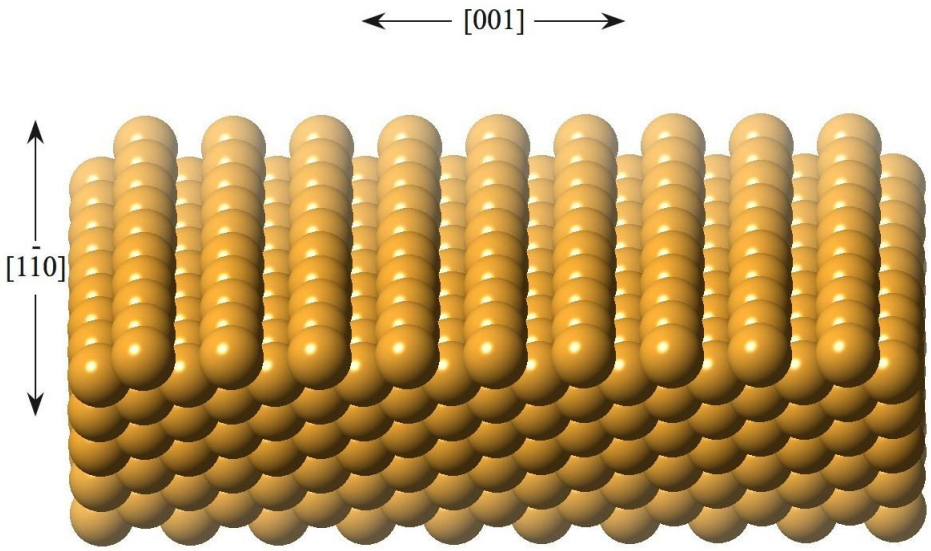

Figure 3.2: A schematic of the Au(110) unreconstructed (1×1) surface.

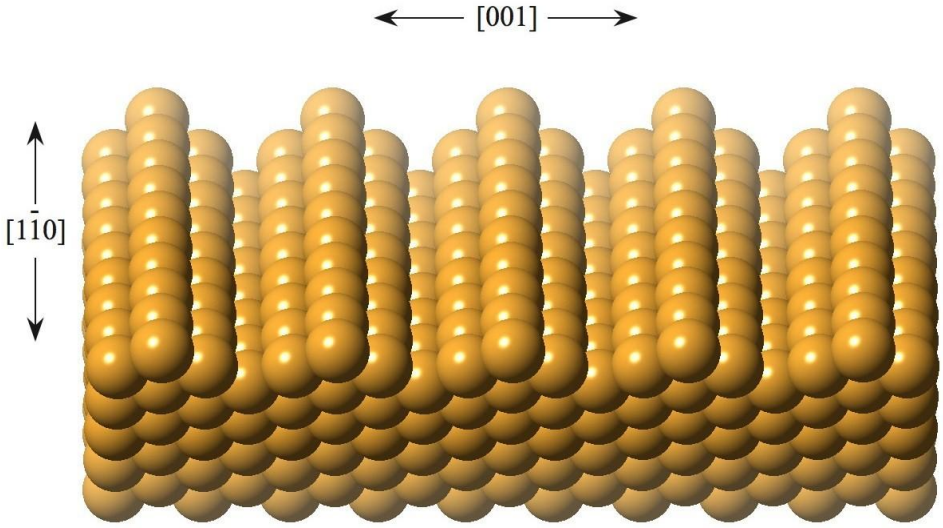

Figure 3.3: Schematic of the Au(110) (1×2) surface structure.

Early low energy electron diffraction (LEED) investigations by Fedak [15,16] first showed the (1×2) surface reconstruction on a clean Au(110) surface as shown in figure 3.3. These studies found that the transition from the unreconstructed (1×1) to (1×2) surface structure was reversible and temperature dependent in the UHV environment. The phase transition between these two surface structures involves extensive motion and reorganisation of the Au(110) surface atoms and understanding how these atoms achieve this rearrangement was at first unclear. Potential models describing the reorganisation of the surface atoms were proposed and tested by Chan *et al*. [17] to try to further understand the reconstruction process. R-Factor analysis of Ir(110)-(1×2) was used to test the potential models, which included the paired rows model, buckled surface model and the missing row model[17]. From their analysis Chan *et al.* [17] concluded that the most likely model for the structural reconstructions was the missing row model. Additional surface x-ray diffraction (SXRD) measurements carried out by Robinson [18] also suggested that the missing row model is the most likely model to describe the (1×2) surface structure. Further investigations followed [19,20], resulting in some disagreement over the validity of the missing row model due to the incompatibility of transition times with surface self diffusion times necessary for Au atoms to move the long distances necessary to allow the (1×1) to (1×2) reconstruction to occur. This became known as the "mass transport problem". Scanning Tunnelling Microscope (STM) studies of the Au(110) surface are extremely useful for investigating phase transitions as the technique is sensitive to structural changes such as step formation, microfaceting and anti-phase domain walls. Binnig *et al*. [21] carried out an STM investigation of the Au(110) surface confirming the (1×2) missing row surface structure. The missing row model describes the phase transition where every second row of atoms along the $[1\bar{1}0]$ direction is removed causing the exposure of (111) facets between the rows of atoms. Binnig *et al.* [21] suggested that the (111) faceted nature of the (110) surface is the driving force of the surface reconstruction as (111) microfacets create a more energetically stable surface. Scattering and recoil imaging spectrometry (SARIS) revealed that the displacement of surface atoms during the reconstruction is coupled to displacements in the underlying atomic layers [22].

To fully understand the structure of the Au(110) surface it is necessary to understand the mechanisms involved in the phase transitions between surface reconstructions. In particular an investigation into the phase transition was necessary to solve the mass transport problem. Campuzano *et al*. [23] suggested that the thermally induced (1×1) to (1×2) phase transition belongs to the two-dimensional Ising universality class [24], where the (1×1) phase can be considered as a disordered lattice gas phase, implying that the transition does not require significant mass transport as the top layer atoms are randomly placed on the surface rather than aligned in rows. STM experiments had already proven useful in obtaining structural information of the surface transitions [21], and the technique was subsequently used to reveal information on the dynamics of the surface during phase transitions [25-31]. STM experiments found step structure to be particularly important to phase transitions on this surface. Speller *et al*. [29] commented on observations of a mesoscopic "fish scale pattern" which is associated with large numbers of anti-phase domain boundaries of (111) step edges. The formation of large ordered terraces terminated by steps parallel to the closed packed rows are promoted by monatomic steps found predominately in the $[1\,\bar{1}\,0]$ direction on the Au(110) surface, as the movement of atoms in the [001] direction is inhibited at room temperature. The disordered gas model used to describe surface reconstructions suggested by Campuzano *et al*. [23] and a 2D Ising universality model describes the surface reconstruction as long as only wall defects are present on the surface. This however only provides an explanation for part of the process: if the surface contains only step defects then a roughening transition would occur. Since it has been demonstrated that the Au(110) surface contains both step and domain wall defects, the surface will undergo firstly a 2D Ising transition, at which point the surface deconstructs (T_D) and then at a higher temperature a roughening transition will occur (T_R), both transitions occurring within 100 K of each other.

Further STM analysis in UHV by Gritsch *et al*. [27] described the arrangement of (111) microfacets and (1×3) domain boundaries, and established that a perfect (1×2) structure cannot be terminated on both sides by (111) microfacets along the $[1\,\bar{1}\,0]$ direction. Adjacent (1×2) regions must be anti-phase to one another and separated by a (1×3) domain boundary. The stability of the (1×2)

structure has been investigated by Sturmat *et al*. [30], using STM to demonstrate the effect of raising the temperature close to the roughening temperature (T_D). STM measurements taken at progressively higher temperatures approaching T_D showed that the smooth step edges along the $[1\,\bar{1}0]$ change and the profile becomes jagged, characterised by an irregular sawtooth shape. The interior terrace regions were shown to still be a perfect (1×2) structure even at those elevated temperatures, highlighting the stability of the (1×2) structure. These findings oppose the lattice gas model suggested by Campuzano [23], as it shows that the main disorder process during the deconstruction transition is confined to step edges. The concentration of steps has been reported to vary significantly depending on the crystal preparation and crystal quality. This variation is echoed in the variation in T_D values of between 850 K and 1080 K reported for Au(110), highlighting the significant influence of surface steps in the transition. The (1×1) to (1×2) reconstruction requires the rearrangement of 50% of the surface atoms, this would be expected to involve the growth of terraces and large scale movement of steps, which would cause a variation in the step density at temperatures approaching T_D. Despite the variation in step density for different surfaces, STM investigations have shown that the step density of a crystal remains almost constant up to T_D. This suggests a possible solution for the mass transport. The assumption that the (1×1) consists of a disordered half monolayer of surface atoms means that the reconstruction will require only local movement of atoms over distances in the order of lattice spacing in order to generate the (1×2) structure.

The missing row (1×2) reconstruction seen on clean Au(110) surfaces is also seen on other 5*d* fcc metals, Ir and Pt. The interesting observation that the (110) surfaces of the isoelectronic 4*d* and 3*d* fcc metals do not reconstruct to the (1×2) structure but remain in a (1×1) structure has been investigated by Ho *et al*. [32]. Pseudopotential density function calculations showed that the (1×2) missing row reconstruction could be formed due to the need to lower the kinetic energy of *s-p* electrons. It was suggested that the stable (1×2) reconstruction occurs due to the larger orbitals in 5*d* fcc metals, which leave the electrons less "room" than in 4*d* and 3*d* fcc metals. This constraint causes an increase in the kinetic energy and the (1×2) structure promotes the lowering of the surface kinetic energy by delocalisation of the

s-p electrons though the formation of ordered (111) microfacets. The (1×2) missing row structure becomes more energetically favourable as it avoids the need to increase the number of broken bonds, whilst lowering the surface electronic density and retaining bulk cohesion [32]. The same mechanism can be used to explain how 4d and 3d fcc metals can reconstruct to the (1×2) structure however this is only possible following the adsorption of a submonolayer of alkali metals [33]. Charge transfer from the adsorbed alkali layers to the surface causes an increase in the surface electronic charge density of the *s-p* electrons. This causes the surface structure to reconstruct to the energetically favourable (1×2) missing row structure in order to reduce the kinetic energy of the *s-p* electrons.

3.3.2 Au(110) in the Electrochemical Environment

There is now a good understanding of the complicated surface of Au(110) crystals in UHV environments thanks to the extensive range of techniques used to examine the Au(110) surface in UHV. Information on the Au(110) surface in electrochemical environments is significantly more difficult to acquire, primarily due to the presence of the electrolyte. Electrochemical STM is able to yield local real-space structural information. This technique was used by Gao *et al.* [34] to study the Au(110) electrode in aqueous perchloric acid ($HClO_4$). This study showed that the Au(110) surface behaves similarly in the electrochemical environment to its behaviour in the UHV environment. A (1×2) surface structure was observed in STM for a potential corresponding to -0.3 V vs SCE, and the surface also contained small areas of (1×3) domains. The STM measurements also suggested that a relaxation occurs of the top and underlying layers of atoms in the (1×2) structure. At -0.3 V vs SCE the surface charge density will be negative, thus the (1×2) structure can be explained, as in UHV environments, as a need to reduce the surface kinetic energy, as the (1×2) structure offers a more energetically favourable structure. Goa *et al*. [34,28] found the transition to the unreconstructed (1×1) surface was achieved as the potential is made more positive. The transition occurred at 0.0 V vs SCE and within 2 seconds of changing the potential, and was shown to be largely reversible upon changing

back to a negative potential. The rapid and reversible nature of the (1×2) to (1×1) surface transition is attributed to the need for only short range motion of atoms and the low atomic density of the surface.

A further electrochemical STM investigation of the potential dependent (1×2) reconstruction on Au(110) was performed by Magnussen *et al*. [35]: the Au(110) surface was examined in perchloric acid, $HClO_4$ and sulfuric acid, H_2SO_4. The STM measurements showed a (1×2) surface structure with large terraces up to 700 Å wide separated by sequences of closely packed monatomic steps, which mirrored the results observed in UHV environments. STM images also revealed the existence of homogenously distributed anisotropic Au islands found on almost 50 % of all terraces. The anisotropic islands consist of only a few atomic rows along the $[1\bar{1}0]$ direction in (1×2) arrangement. The presence of these islands meant that large areas of perfect (1×2) domains were largely confined to the vicinity of step edges, where no Au islands are found. The domain boundaries between these Au islands consist of deep (1×3) troughs [35]. This observation of numerous anti-phase boundaries separating the (1×2) terraces implied that (1×3) domains play a crucial role in the phase transition, in agreement with work in UHV by Gritsch *et al*. [27]. The anti-phase structure results in a very stable configuration with (111) microfacets on both sides and a low kink density. The (1×2) surface reconstruction was observed at potentials below +0.05 V vs SCE, as the positive potential was increased to +0.25 V vs SCE the unreconstructed (1×1) surface is observed. The unreconstructed (1×1) surface was found to possess many isotropically shaped islands and holes each with a height or depth equivalent to an Au monolayer. STM measurements of the same surface area in a (1×2) reconstruction and a (1×1) structure revealed that the isotropic islands on the (1×1) were located in the same positions as the anisotropic Au island on a (1×2) surface, demonstrating the ability of the islands to be converted into each form. A roughening of the surface is observed at potentials of +0.8 V vs SCE and is explained by oxygen adsorption and the subsequent oxidation of the Au(110) surface.

Surface x-ray scattering (SXS) of Au(110) in electrolyte solution was used by Ocko *et al.* [36], to demonstrate the effect of potential on the surface structure. SXS results for Au(110) in $HClO_4$ a (1×2) structure were observed at slightly

negative potentials. This structure consisted of small regions of (1×3) domains, as seen in electrochemical STM [34,35]. Changing the electrolyte solution to various salt solutions allows the effect of more negative potentials to be investigated, as hydrogen gas evolution starts at a more negative potential. At the more negative potentials achieved in salt solutions the surface was shown to adopt a (1×3) structure. As the potential was made increasingly more positive the surface structure changed to the unreconstructed (1×1), avoiding the (1×2) reconstruction, which was not observed at any stage of the transition from (1×3) to (1×1). Experiments in UHV have demonstrated that it is possible to form the (1×3) surface reconstruction following the adsorption of alkali metals, due to charge transfer from the adsorbed alkali to the Au surface causing changes to the energy distribution and so promoting the (1×3) surface structure [37]. Studies of Au(110) in electrochemical environments have shown potential induced surface reconstructions. At potentials slightly negative of the point of zero charge (PZC) the surface adopts a (1×2) reconstruction, when the potential is made positive the unreconstructed (1×1) surface is observed. Several studies of the Au(110) surface have shown a potential induced (1×3) surface structure, at sufficiently negative potentials, as shown in figure 3.4 [38-40]. The transition from the (1×3) to the (1×1) directly without an intermediate (1×2) structure is not fully understood.

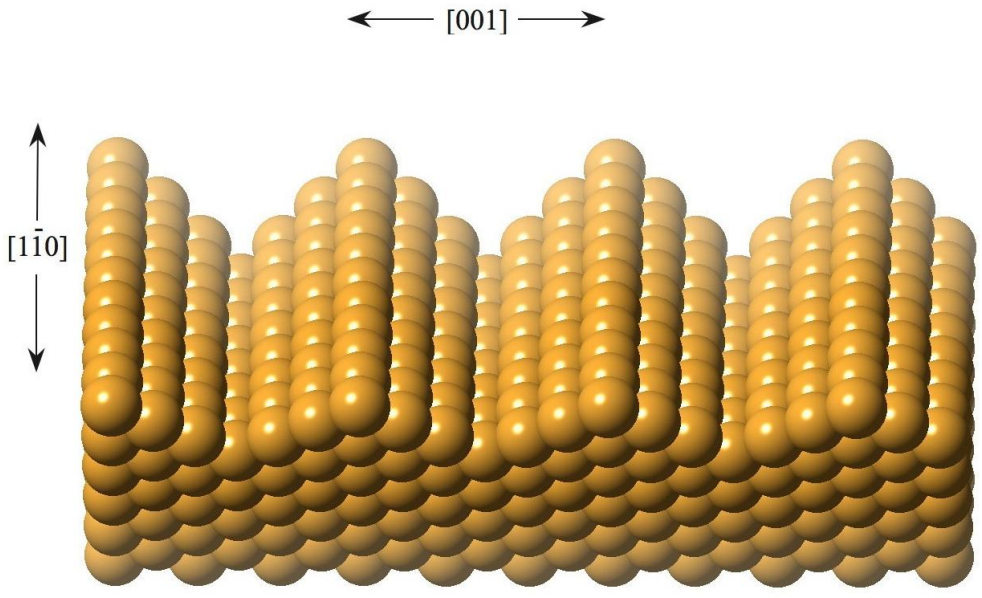

Figure 3.4: Schematic of the Au(110) (1×3) surface structure

In this thesis the Au(110) surface is studied exclusively in the electrochemical environment, as this environment is closer to the natural environment of biological molecules than UHV. The discussion of literature investigating the mechanisms of the Au(110) surface reconstructions highlights the intricate nature of these phase transitions. It is important that investigations in UHV and electrochemical environments are referenced as it has been demonstrated that work in the two environments is similar. The understanding of the Au(110) surface transitions, particularly potential induced reconstructions, is critical if one is to gain an understanding of RA spectra of adsorbed molecules under potential control.

3.4 The Electronic Structure of the Au(110) Surface

The features observed in RA spectral profiles of a material originate from single particle excitations between states in the band structure of the material. Therefore it is important to have an understanding of the electronic structure of Au in order to interpret RA spectral profiles of this surface. A detailed description of the Au(110) electronic structure is beyond the scope of this thesis, and so only a brief outline of this field will be described in this section.

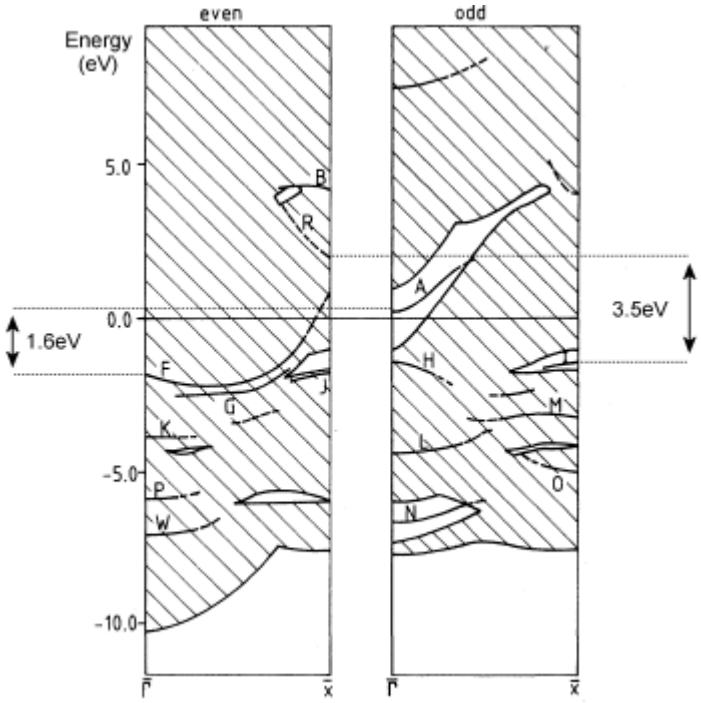

Figure 3.5: Calculated electronic structure of Au(110) (1×2) reconstructed surface. Reproduced from Xu *et al.* [43].

The electroreflectance spectra (ERS) of Au(110) revealed an anisotropic spectrum of Au(110) and highlight the sensitivity of the optical electron energy states to the surface distribution of atoms [41]. ERS data from Au(111), Au(110) and Au(100) crystals were compared to theoretical data from self-consistent pseudo-potential calculations from the bulk and surface electronic structure of Au. This suggested the presence of surface states at certain symmetry points in the Surface Brillouin Zone (SBZ) [42]. Important points in the SBZ relevant to optical transitions are the $\bar{\Gamma}$, $\bar{Y}$ and $\bar{X}$ points. The $\bar{\Gamma}$ point is found at the centre of the SBZ perpendicular from this and at the edge of the SBZ in the < 100 > direction is the $\bar{Y}$ point and similarly perpendicular from the $\bar{\Gamma}$ point but in the < 110 > direction is the $\bar{X}$ point. The investigation by Liu *et al.* [42] identified a transition between surface states at the $\bar{Y}$ point. However, this study does not account for the surface reconstruction and was based on a model of the unreconstructed (1×1) Au(110) surface. The difference between the surface electronic states of a (1×1) and

(1×2) is expected to be significant, since the reconstructed (1×2) involves the removal of half the atoms from the surface. Xu *et al*. [43] carried out self-consistent pseudo-potential calculations on a model (1×2) Au(110) surface, the calculated surface structure is shown in figure 3.6.

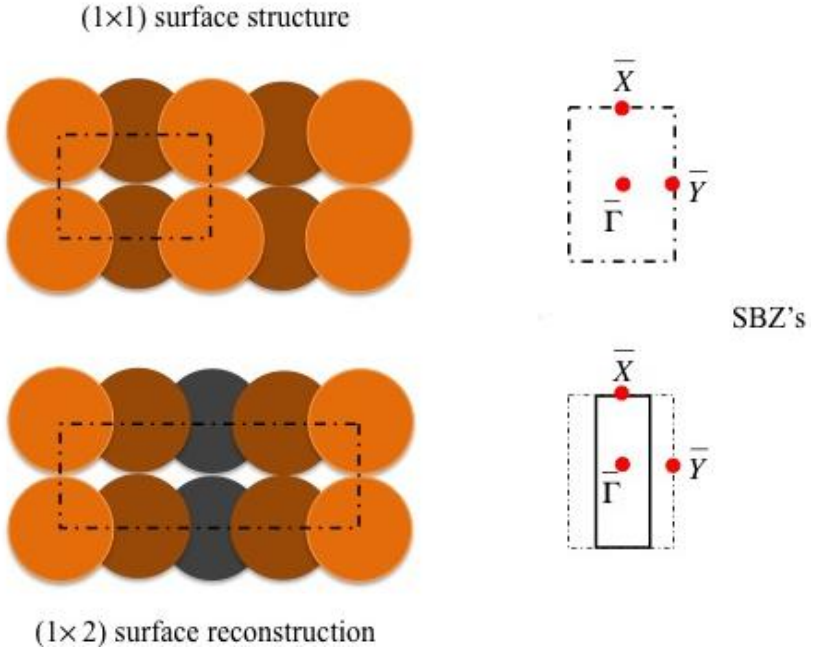

Figure 3.6: Calculated surface structure of Au(110) (1×1) and (1×2) surface structure. Reproduced from Xu *et al.* [43]

The data showed that the surface state assigned to the transition by Liu *et al.* [42] is not occupied on the reconstructed surface. These data were supported by photoemission measurements of the Au(110) (1×2) reconstructed surface [44], which agreed with the theoretical data presented by Xu *et al.* [43] and predict transitions between surface states at the $\bar{\Gamma}$ point.

3.5 RAS of the Au(110) Surface

In order to understand the origin of features in RA spectra it is useful to compare experimental data with theoretically simulated data. Theoretical simulation of experimental RAS data from first principles is not yet possible. However there have

been several attempts to link experiment with theoretical simulations of RA spectra of the Au(110) surface.

Mochán *et al.* [45] developed a theoretical model to describe the electromagnetic response of Ag(110) and Au(110) surfaces. They compared the theoretical data to RA spectra of Au(110) in ambient conditions. The model was based on surface-local-field effects (SLFE) and takes into account the contributions from *d* and *s-p* electrons as well as the lattice geometry of the surface. The theoretical results showed only a slight agreement with the experimental results. This however demonstrated that RAS is sensitive to surface effects of cubic crystals. A further model based on SLFE was later compared to RA spectra of Au(110) in UHV conditions [45]. In this work Hansen *et al*. [45] modelled data based on the reconstructed (1×2) and the (1×1) Au(110) surface. The modelled data was then compared to the experimental RA spectrum of the Au(110) (1×2) reconstructed surface. The (1×2) model was shown to be closer to the experimental data than the (1×1) model. However this again was not a convincing match. The theoretical data for the (1×2) and (1×1) show an increase in intensity of a predicted feature at ~2.5 eV during the transition from (1×1) to the (1×2) surface. This feature of the (1×1) to (1×2) phase transition has been observed in experimental RAS studies of the Au(110) surface [14, 47-49]. A combined RAS and STM study of Au(110) by Mazine *et al.* [50] did not observe this increase at 2.5 eV, actually observing a decrease in intensity from (1×1) to (1×2). The Authors [50] produced the first RA spectra of Au(110) under electrochemical conditions and induced the surface reconstruction through potential control, allowing them to produce RA spectra they associated with the (1×1), (1×3) and the (1×2) surface structure. The RA spectrum of the (1×2) was described as the spectrum of a intermediate poorly reconstructed surface which consists of (1×3) domains. A second paper by the same Authors published in 2002 [51] also reported a decrease in intensity at 2.5 eV during the transition from the (1×1) to (1×2) reconstructed Au(110) surface. Mazine *et al.* [51] again produced very similar RA spectra which they associated with the (1×1), (1×2) and (1×3) reconstructed Au(110) surfaces. They presented this data as the 'optical fingerprint' of the (1×3) and (1×2) structures, although the RA spectra look very similar to the RA spectra the Authors first reported in earlier work [50].

Through more recent RAS experiments on the Au(110) surface, it has been shown that once the (1×3) surface has been adopted it is difficult to observe a pure (1×2) reconstructed surface structure. A pure (1×2) surface has consistently been observed with RAS after going from a (1×1) surface. Mazine *at al*. [50,51] held the crystal at -0.6 V in a (1×3) reconstruction before their experiments and this could account for disagreements in the labelling of the RAS of a (1×2) reconstructed Au(110) surface. The work of Sheridan *et al.* [49] produced RA spectra of the Au(110) (1×1) and (1×2) surface reconstructions in the electrochemical environment, which were in disagreement with the work of Mazine *et al.* [50,51]. It was suggested by Weightman *et al*. [52] that the inconsistency in the identification of the RA spectra for the Au(110) surface reconstructions arise from the differing morphology in the Au(110) surfaces used in each experiment. Recent experiments have shown a more detailed signature of the Au(110) surface reconstructions [1]. These are significantly different to the ones first reported by Sheridan *et al.* [49]. This can be attributed to differences in crystal preparation, improvements to the RAS equipment used and a different crystal supplier.

The work of Sheridan *et al*. [49] utilised UHV techniques LEED and STM in order to correlate changes in surface structure to observed changes in RA spectra. A wide negative feature, found in the spectral region of 3.7 eV to 4.5 eV of the RA spectrum, was shown to be particularly sensitive to surface roughness. The intensity of this feature was greatest after prolonged annealing, which produced a clear (1×2) LEED pattern and STM images that showed many monatomic steps oriented along the $[1\bar{1}0]$ direction in the surface. The intensity of this feature decreased after a shortened annealing process. The LEED pattern of this surface showed a clear (1×2) reconstructed surface but the STM images showed a reduced number of monatomic steps [49]. The theoretical work of Xu [43] on the electronic structure of the Au(110) surface allowed Sheridan *et al*. [49] to associate features on the RA spectrum of Au(110) with transitions between surface states. The RA profile in the region 1.5 eV to 2.5 eV was attributed to contributions from a surface state and so is expected to be sensitive to the surface and electronic structure [41]. The 2.5 eV peak observed on the RA spectrum of Au(110) was associated with a transition at the Γ point between an occupied surface resonance of odd symmetry arising from *d* states

of *yz* character to an even symmetry surface state of predominantly *p* character at ~ 0.3 eV above the Fermi energy. The transition from a state of even symmetry and *sp* character to a surface state of odd symmetry and *d* character derived at ~ 1.6 eV above the Fermi energy, was attributed to the feature at 3.5 eV on the RA spectrum [49]. The fact that the states involved in this transition have significant contributions from the second layer of atoms means the higher energy feature found at 3.5 eV lacks surface sensitivity in comparison to the 2.5 eV feature.

The RA spectrum of a clean Au(110) (1×2) surface is shown in figure 3.7. The spectrum is characterised by a sequence of features, a positive feature between 1.5 eV and 2.3 eV, large negative region between 2.5 eV and 3.5 eV with two prominent negative peaks at these two energies and a positive feature between 4.0 eV and 5.0 eV. While the origin of some of these features have been discussed in terms of transitions between states in the electronic structure of the surface, the positive feature at 4.0 eV has been attributed to the presence of monatomic steps in the surface [49]. In a further study by Martin *et al.* [53] the effect of Ar bombardment on the surface morphology of Au(110) was studied by monitoring changes in the RA spectra and STM images as a function of increasing Ar bombardment. Martin *et al*. [53] showed large (1×2) reconstructed terraces terminated by long monatomic steps aligned along the $[1\,\bar{1}0]$ direction on the clean Au(110) surface. The surface morphology after successive Ar ion bombardment was observed using STM. The surface had changed from well ordered terraces of (1×2) reconstruction and continuous monatomic steps to a rippled morphology of elevated islands and valley regions [53]. Figure 3.7 below shows the STM image and the corresponding RA spectrum of the clean Au(110) surface in UHV, reproduced from [53].

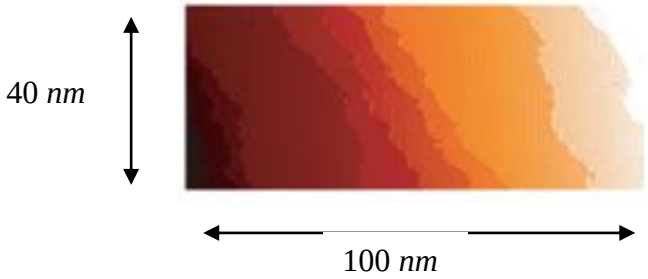

Figure 3.7: (a) Contrast STM image of annealed Au(110) surface in UHV showing monatomic steps and large terraces associated with the (1×2) reconstruction.

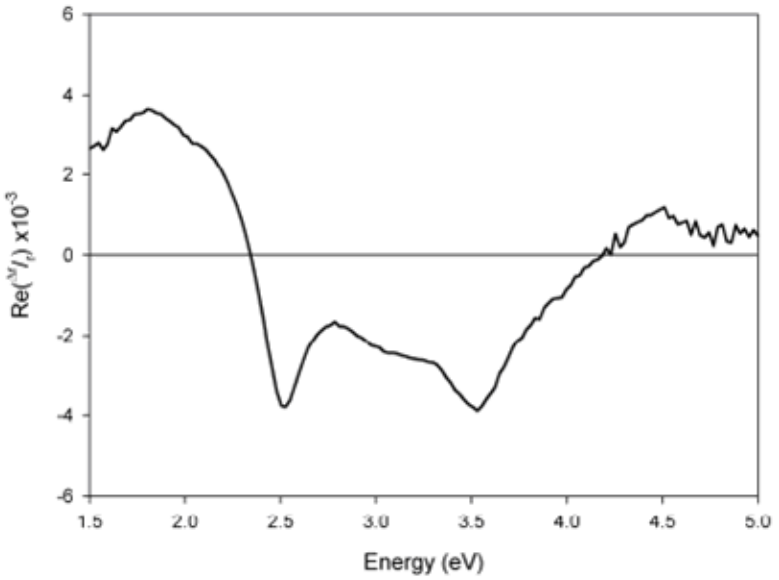

Figure 3.7: (b) RA spectrum associated with the crystal in a).

The removal of the step structure as a result of Ar ion bombardment has also been reported in RAS studies of Cu(110) [54]. A similar effect was observed in RA spectra of the Au(110) surface: a large change was observed in the region of 3.0 eV and 5.0 eV after Ar ion bombardment, which was attributed to the changes in surface roughness of the Au(110) surface as a result of Ar ion bombardment. The authors [53] found a slight intensity decrease in the 2.5 eV peak, however the feature retained its definition, even after 36 minutes of bombardment and so is considered insensitive to surface roughness and the slight decrease in intensity was attributed to the loss of (1×2) reconstruction in some regions of the surface, due to the Ar ion bombardment, which is in agreement with the other studies of the (1×2) to (1×1) transition [14,47-49].

The effect of temperature on the Au(110) surface has also been monitored using RAS firstly by Stahrenberg *et al.* [55] and more recently by Martin *et al.* [56]. RA spectra were taken between the temperature range 300 K to 800 K [55] and 300 K to 1000 K [56], the RA profile was characterised by features at 1.8 eV, 2.52 eV, 3.52 eV and 4.50 eV and these features were monitored as a function of temperature (figure 3.8). The initial RA spectrum produced for a clean Au(110) (1×2) reconstructed surface is in good agreement with earlier work [49-53]. The feature at 1.8 eV appears to be independent of temperature as it remains unchanged for temperatures up to 1000 K. The feature at 2.5 eV in the RA spectrum on the other hand does change, the intensity of the feature decreases and the peak broadens with increasing temperature, increasing the temperature above 580 K results in a slight positional peak shift of this feature to higher energy. When the temperature is increased beyond T_R ~ 800 K the feature at 2.5 eV is so broad and its intensity is so weak that it is difficult to distinguish from the background RA profile. The smooth decrease in RA intensity between 1.5 eV and 2.5 eV as the temperature is increased is consistent with the gradual increase in surface disorder during the phase transition from (1×2) to (1×1) structure [56]. The features at 3.5 eV and 4.5 eV change substantially as a result of increased temperature, both peaks shift to lower photon energies as the temperature was increased above 300 K. In addition to this positional shift both features also broaden and the similarity in behaviour of the two features suggested that they are closely related.

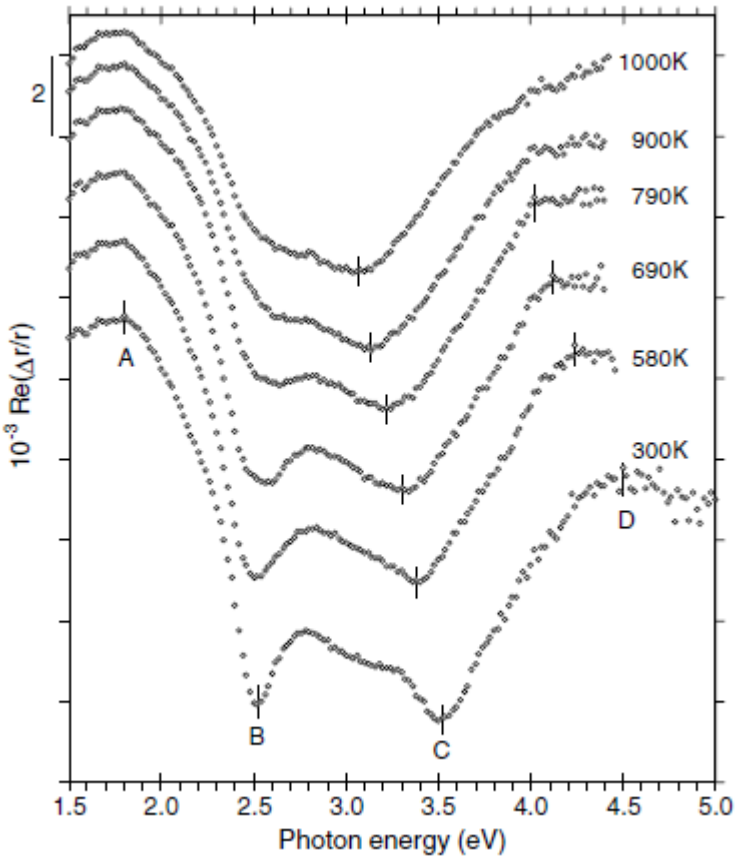

Figure 3.8: RA spectra of Au(110) as a function of temperature. Reproduced from [56].

Martin *et al*. [56] analysed the results of the temperature dependent RA spectra using a model derived by Russow *et al.* [57] and found good agreement with a thermovariation spectroscopy study of Au, Ag and Cu which showed that the main features contributing to the bulk dielectric, ε_b, for Au are from interband transition in the vicinity of the L point of the Brillouin zone (BZ) [56]. The consistency of the thermovariation spectroscopy study [58] with the variation in temperature and RA profile changes [56] allowed the 3.5 eV and 4.5 eV features on the RA spectra to be assigned with specific transitions, the $E_F \rightarrow L^u_1$ and the $L'_2 \rightarrow L^u_1$ respectively [56], thus establishing that the region between 2.5 eV and 4.5 eV on the RA spectrum of Au(110) is derived from contributions from surface modified bulk state transitions.

3.6 The Three Phase Model

Interpreting RA spectra from first principles is difficult. The Jones matrix formalism [59] described in chapter 2 of this thesis is used to describe the state of polarisation of light as it passes through the RAS instrument components, however to interpret RA spectra it is necessary to understand why changes in the polarisation state of light occur. The difficulty in developing *ab initio* theoretical treatments derived from first principles lead to the development of a linear approximation of the reflectivity expressions present in multiphase stratified systems such as the interfacial surface region of the Au(110) crystal in electrochemical and vacuum environments [60] with further development of the model following by Cole *et al*. [61]. The model represents the reflecting surface as three regions with each region referring to an isotropic semi-infinite bulk in between ambient layers of anisotropic thin film surface layers, as shown in figure 3.9.

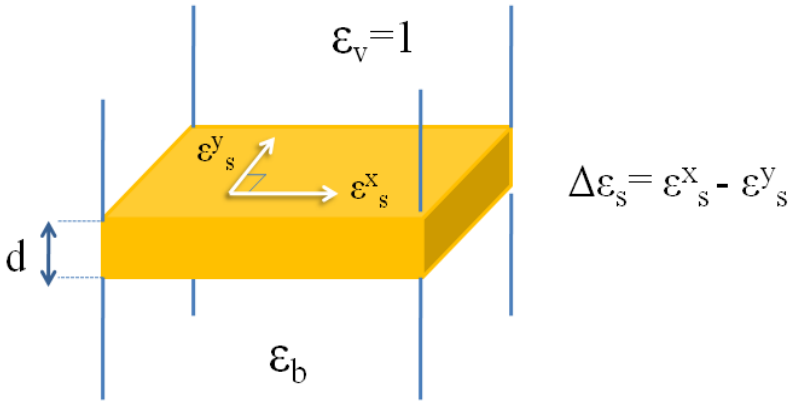

Figure 3.9: Schematic of the three phase model.

3.6.1 The Dielectric Function

The dielectric function of a material determines the interaction of light within the material. The three phase model is a simplified description of the interaction of light in three different media; the ambient/vacuum layer, the bulk of the sample and the surface of the sample. The dielectric function of the surface layer in the principle directions *x* and *y* of the surface are ε^y_s and ε^x_s. Due to the anisotropy of the surface these may not be equal and $\Delta\varepsilon_s$ is refered to as the surface dielectric anisotropy (SDA). The dielectric functions of the semi-infinite bulk and the ambient/vacuum layer are ε_b and ε_v respectively. A RAS signal arises when $\varepsilon^y_s \neq \varepsilon^x_s$ and the RAS equation can be expressed in terms of the dielectric functions by assuming that $\varepsilon_v = 1$ and using the thin film approximation ($d << \lambda$) which allows the probing of optical properties of the sample surface at optical wavelengths, leading to:

$$\frac{\Delta r}{r} = -\frac{2i\omega d}{c}\left[\frac{\varepsilon_s^x - \varepsilon_s^y}{1-\varepsilon_b}\right] \tag{3.2}$$

where ω is the angular frequency and $\hbar\omega$ is the photon energy. The RA spectra in this thesis are produced from the real part of the RAS signal, therefore equation 3.2 is expressed in terms of the real parts:

$$\mathrm{Re}\left(\frac{\Delta r}{r}\right) = \frac{2\omega d}{c}\,\mathrm{Im}\left[\frac{\Delta\varepsilon_s}{1-\varepsilon_b}\right] \tag{3.3}$$

where $\Delta\varepsilon_s = \varepsilon^x_s - \varepsilon^y_s$.

3.6.2 The Lorentzian Transition Model

Electric transitions in the surface are represented by Lorentzians. The bulk dielectric function, $\varepsilon_b(w)$ is represented in by the terms $A(\omega)$ and $B(\omega)$ defined as:

$$A(\omega) - iB(\omega) = \frac{1}{1 - \varepsilon_b(\omega)} \tag{3.4}$$

$A(\omega)$ and $B(\omega)$ are thus determined by the bulk dielectric function, which itself is calculated from the expression $\varepsilon = N^2$ where N is the refractive index and derived from, $N = n - ik$, where n is the refraction coefficient and k is the extinction coefficient. Spectroscopic ellipsometry can be used to obtain the values of n and k for Au as a function of photon energy, and the work of Blanchard *et al.* [62,63] provides the values for the optical constants in the photon energy range of 1.41 eV to 4.96 eV while data from Paliks review [64] is used for photon energies greater than 5.0 eV. The real parts of equation 3.2 can be written in terms of the functions $A(\omega)$ and $B(\omega)$:

$$\mathrm{Re}\left(\frac{\Delta r}{r}\right) = -\frac{2\omega d}{c}\left[A(\omega)\mathrm{Im}(\Delta\varepsilon_s) + B(\omega)\mathrm{Re}(\Delta\varepsilon_s)\right] \tag{3.5}$$

This equation allows RA spectra to be simulated in terms of the bulk optical properties of Au and a parameterised representation of surface electronic transitions. Simulation of the SDA is achieved by selecting appropriate values for energy, ω_t, relative strength, S and the full width at half maximum (FWHM) Γ for transitions within the surface layer in the x and y direction. Each simulated transition has the Lorentzian form given by:

$$\varepsilon_s^{x,y} = 1 + \sum_{n=1}^{m} \frac{S/\pi}{\omega_t - \omega + i\Gamma/2} \tag{3.6}$$

The shapes of the functions *A(ω)* and *B(ω)* are shown in figure 3.10. As a result of the change in data set, at 5.0 eV there is a small discontinuity is observed.

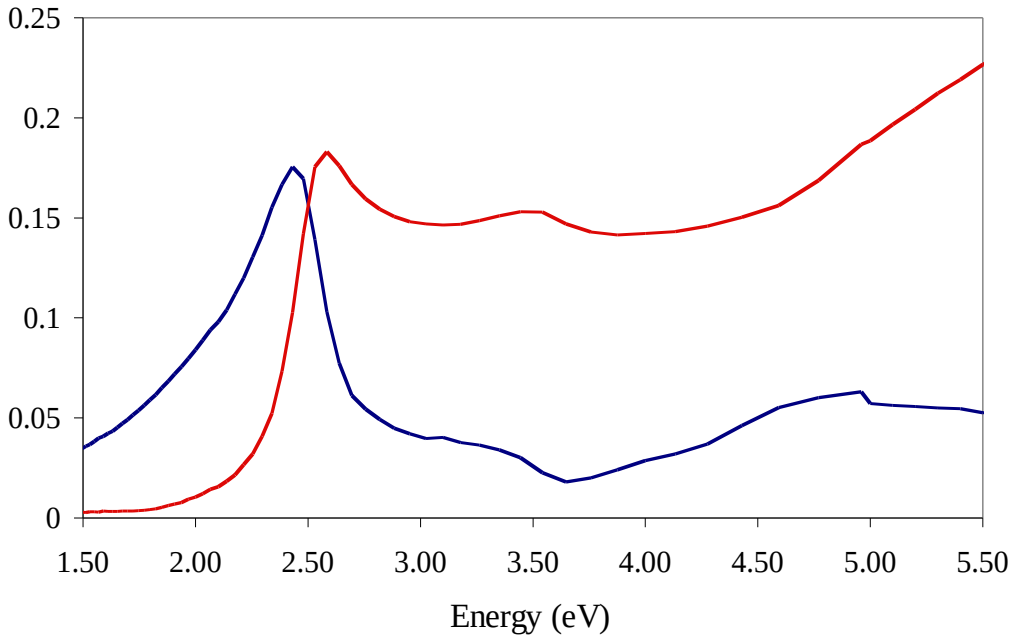

Figure 3.10: Line shape of the functions *A(ω)*(blue line) and *B(ω)* (red line).

Simulations of RA spectra have been used in previous work [47], however simulations of this nature have not been used in the work reported in this thesis.

3.7 Spectral Signatures of the Surface Reconstructions of Au(110)/electrolyte Interfaces

The earlier sections of this chapter have demonstrated the tendency of the Au(110) surface to reconstruct. It is therefore important to have a full understanding of the spectral signatures of the surface reconstructions in electrolyte solutions before it is possible to study and fully understand the effect of adsorbed molecules on the surface.

There has been some disagreement over identifying the RA spectral signatures of the Au(110) surface [49-53] which has been discussed previously. In this section the unique RAS profiles of the Au(110) (1×1) surface and the (1×2) and (1×3) reconstructed surfaces are presented, resolving the controversy surrounding the identification of the RA spectral signatures.

RA spectra were taken in three different electrolyte solutions, H_2SO_4/Na_2SO_4 (pH 1.2), $HClO_4/NaClO_4$ (pH 1.2) and $NaClO_4$ (pH 6.1), the solutions were selected to investigate the effect of pH and by using H_2SO_4/Na_2SO_4 and $HClO_4/NaClO_4$ both at pH 1.2 the effect of anions on the Au(110) reconstructions was also investigated. RA spectra were produced in three separate experiments in the different electrolyte solutions, taken at applied potentials of 0.0 V, 0.3 V and -0.6 V, in that order to prevent irreversible changes [62]. The RA spectra produced in each experiment were taken on the RAS instrument described in chapter 2 and the Au crystal was prepared as described in chapter 2 of this thesis. The extreme sensitivity of the polarizer makes it difficult to accurately produce a zero RAS signal in different experiments. Therefore the RAS signals in each experiment are offset from each other on the vertical axis. Changes in the shape of the RA profile as a result of varying the potential are only of interest so the zero positions in each of the three sets of experiments have been shifted to coincide in the spectra shown in figure 3.11. The shift corresponds to very small uncertainties of the order of minutes of arc in setting the polarizer. The zero shifts have been applied to all spectra taken in each experiment and are indicated by an insert in figure 3.11: these shifts do not effect the intensity or shape of the RAS profiles. The RA spectra features observed at 0.0 V

are almost identical in all three electrolyte solutions. Two clear negative peaks are observed in the spectra at 2.6 eV and a more intense peak at 3.6 eV. The two peaks are separated by an almost linear negative slope. At -0.6 V again the RA spectra are almost all identical with only a slightly lower intensity of the 3.6 eV peak seen in the sulphate solution. The different electrolytes seem to have the biggest effect at 0.3 V, where the RA spectra in the three different solutions show significant differences below 3.6 eV: above 3.6 eV all three RA spectra are identical. The RA spectra observed in perchlorate solution at 0.3 V are very similar above 2.4 eV, below this energy the spectra have the same shape but adopt different intensities, whereas in sulfate solution the spectrum is shifted to more positive values between 2.0 eV and 3.4 eV.

Differences between the RA spectra in the three electrolytes at the potentials 0.0 V and -0.6 V occur predominately below 4.5 eV. As the potential is changed from -0.6 V to 0.0 V a sharpening of the negative peak at 3.6 eV is observed along with the emergence of a negative peak at 2.6 eV. There is also a decrease in intensity of the broad positive peak below 2.5 eV. The higher energy regions, above 3.6 eV have a very similar line shape in all three electrolyte solutions at 0.0 V and -0.6 V with the only difference observed as the potential was changed was in absolute intensity however a clear difference in the RAS shape at 5.5 eV was observed at 0.3 V. An earlier RAS study of the Au(110) surface by Sheridan *et al.* [49] associated this higher energy region of the RA spectrum with the presence of $[1\,\bar{1}\,0]$ orientated surface steps. It is therefore reasonable to associate changes in this energy region with variations in the number of surface steps produced by the annealing procedure.

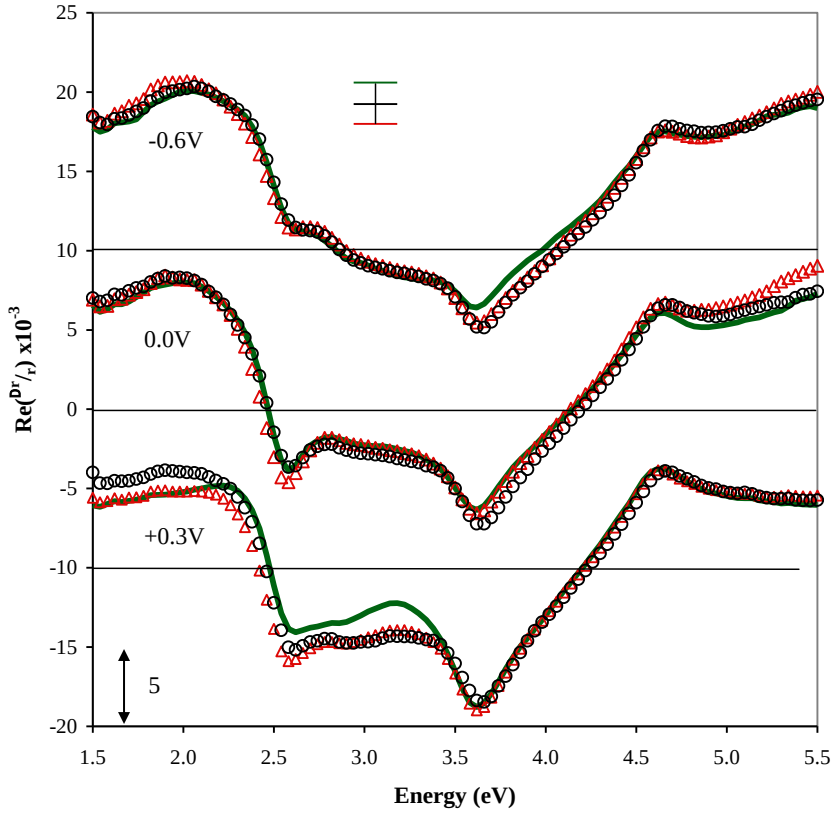

Figure 3.11: RA spectra of Au(110) at -0.6 V, 0.0 V and 0.3 V in 0.1 M $HClO_4/NaClO_4$ (Δ), in 0.1 M $NaClO_4$ (○) and in 0.1 M H_2SO_4/Na_2SO_4 (green line). The spectra have been offset on the *y*-axis in each electrolyte, this offset is demonstrated by the arrow in the top of the figure.

As the potential is taken to 0.3 V the intensity of the broad positive feature below 2.5 eV decreases continuing the trend seen between -0.6 V and 0.0 V. The intensity of the peak at 2.6 eV decreases slightly and also broadens, while the intensity of the 3.6 eV peak is shown to increase. A steady positive increase in intensity is observed in the region of 4.5 eV with increasing photon energy at 0.0 V and -0.6 V potentials, which changes to a slow decrease in intensity at 0.3 V.

At -0.6 V the RA spectra observed in all three electrolytes are assigned to the (1×3) reconstruction (figure 3.12). They are very similar to the RA spectra obtained by Mazine *et al.* [50,51] assigned to the (1×3) reconstruction. Data from in situ X-ray scattering by Tidswell *et al.* [39] showed the conditions in which a (1×3)

reconstruction is adopted. Very similar RA spectra [65] to the ones observed at -0.6V in this study were observed in the conditions outlined by Tidswell e*t al.* [39].

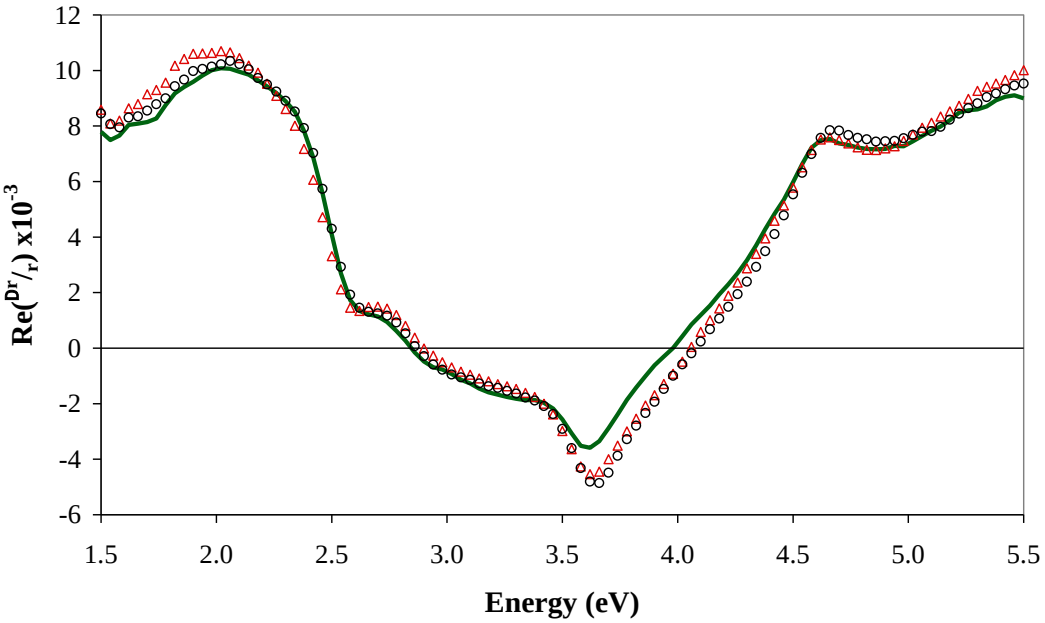

Figure 3.12: RA spectra of Au(110) at -0.6 V in 0.1 M $HClO_4/NaClO_4$ (Δ), in 0.1 M $NaClO_4$ (○) and in 0.1 M H_2SO_4/Na_2SO_4 (green line).

An assignment of the (1×2) and (1×1) RA spectral signatures in sulfate electrolytes have previously been made by Mazine *et al.* [50, 51] at 0.0 V and 0.6 V vs Ag/AgCl reference electrodes respectively, the RA spectra produced in this work are significantly different to those. The RAS of the Au(110) (1×2) reconstructed surface has been observed in UHV many times. In the UHV environment it is possible to confirm the surface reconstruction with LEED which has been shown previously [55,67]. The RAS profiles of the (1×2) reconstruction in UHV are similar to the ones observed for all three electrolytes at 0.0 V in this work. Furthermore Magnessun *et al.* [35] observed with in situ STM measurements of the Au(110) surface in sulfuric acid and perchlorate electrolyte solution a (1×2) reconstruction between the potentials -0.3 V and 0.2 V. Therefore the RA Spectra observed in this work at 0.0 V in all three electrolytes can be assigned to the (1×2) reconstructed Au(110) surface (figure 3.13).

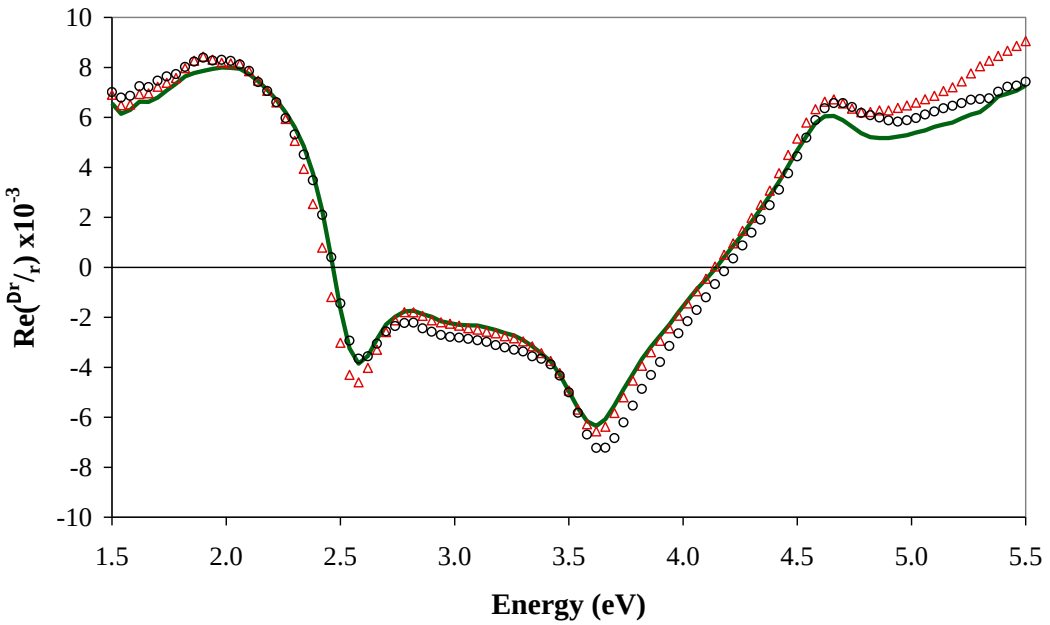

Figure 3.13: RA spectra of Au(110) at 0.0 V in 0.1 M $HClO_4/NaClO_4$ (Δ), in 0.1 M $NaClO_4$ (○) and in 0.1 M H_2SO_4/Na_2SO_4 (green line).

In situ STM experiments established that in sulfate electrolyte the Au(110) surface adopts a (1×2) reconstruction below 0.05 V and the (1×1) unreconstructed surface is observed at potentials above 0.25 V. The three RA spectra produced in this work at 0.3 V in the three different electrolyte solutions are different for each of the electrolyte solutions. The two RA spectra produced in perchlorate solution show a similar shape but a different intensity of the peak below 2.4 eV, whereas the RA spectrum produced in the sulfate solution is different below 3.4 eV, these more obvious differences being attributed to the different properties of the perchlorate and sulfate ions. The sulfate ion is a more strongly adsorbing anion than the perchlorate anion and the adsorption of sulphate has been shown to lift the (1×2) reconstruction to the unreconstructed (1×1) [35, 68-70]. Therefore it is more likely that the sulfate electrolyte will lead to the lifting of the (1×2) reconstruction to the (1×1) structure than the perchlorate electrolyte at the same potential. The RA spectral signature of the (1×1) unreconstructed surface is attributed to the 0.3 V RA spectrum in H_2SO_4/Na_2SO_4 shown in figure 3.14.

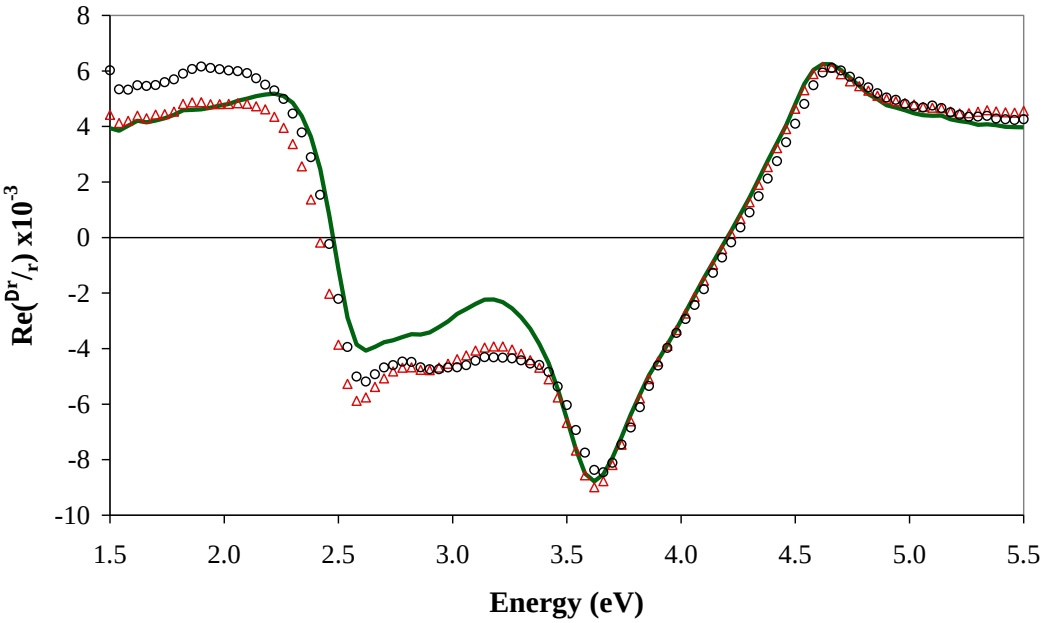

Figure 3.14: RA spectra of Au(110) at 0.3 V in 0.1 M $HClO_4/NaClO_4$ (Δ), in 0.1 M $NaClO_4$ (○) and in 0.1 M H_2SO_4/Na_2SO_4 (green line).

The RAS profile of the Au(110) (1×1) structure is characterised by a line shape in which the peak at 3.6 eV is significantly more intense than the 2.6 eV peak. In sulfate solution changes in the RA spectrum are observed as low as 0.1 V as the potential is changed to more positive potentials, with the 3.6 eV peak reaching a maximum intensity when the potential is 0.3 V (figure 3.14). In the perchlorate solution, pH 1.2, different RA spectra are observed for this potential change, a slight increase in the 3.6 eV peak intensity at 0.2 V may indicate a (1×1) surface structure for some regions. However the RA spectrum assigned to the unreconstructed (1×1) surface is not observed at increasing positive potentials up to 0.6 V. The reason the RA spectra produced at 0.3 V in the three different electrolyte are not identical is attributed to the (1×2) reconstructed surface not being fully lifted in the perchlorate electrolyte solutions. This is consistent with the absence of strongly adsorbing anions in the perchlorate solution, which are present in the sulfate solution. The adsorption of anions has been shown to lift the (1×2) reconstruction to the (1×1) surface structure. The possible mechanism for the lifting of the (1×2) reconstruction has been discussed by Kolb *et al.* [70], who suggested the reconstruction could be

due to the adsorption anions or a consequence of the specific charge on the Au surface as a result of changing the potential. Distinguishing between these two mechanisms is extremely difficult. Magnessun *et al.* [35] commented that the presence of anionic adsorbates means that the two processes go hand in hand, as any change in surface charge is accompanied by the loss or gain of anionic adsorbates making the two processes difficult to distinguish. It is clear from the differences in RA spectra at 0.3 V that the presence of strongly adsorbing anions, as in the sulfate solution, is the dominant mechanism for the lifting of the (1×2) reconstruction. In the presence of weakly adsorbing anions as in the perchlorate solution it is the potential induced surface charge that is the main driving force of the phase transition. The effect of the different anions is clearly seen at 0.3 V. However the effect of pH is more subtle, though it is important to note that in $NaClO_4$ and $HClO_4/NaClO_4$ electrolyte solutions of pH 6.1 and pH 1.2 respectively there are also differences in the RAS at 0.3 V, specifically in the intensity of the broad peak below 2.4 eV. This difference is attributed to the change in pH, as the RA spectra are produced at the same applied potential and in solutions of the same anion. The differences are probably a result of the number of (1×2) regions which have not changed to the (1×1) surface structure on the Au(110) surface. The similarity of the RAS profiles at -0.6 V and 0.0 V compared to the differences at 0.3 V would suggest that there are more areas of (1×1) in pH 6.1 solution than in the pH 1.2 solution of the same anion. This conclusion has been supported by evidence that the pH of the solution can effect the potential range in which the (1×2) reconstruction is observed [36,70].

This identification of the RA spectral signatures of the (1×1), (1×2) and (1×3) reconstructed Au(110) surfaces is significantly different to those presented as optical signatures of the (1×1) and (1×2) reconstruction by Mazine *et al.* [50, 51]. The RAS profile for the (1×2) reconstructed surface presented here are similar to the RA spectrum observed in UHV of a Au(110) (1×2) surface structure confirmed in UHV by LEED. Mazine *et al.* [50] concluded from their STM measurements that the Au(110) surface showed a poorly reconstructed (1×2) surface structure. One reason for that study to yield a poor intermediate reconstructed surface could be the possible sequence in which the RA spectra were produced. If the electrode potential

was varied from -0.6 V to -0.2 V to 0.6 V, as it was for their STM measurements, then the (1×2) reconstruction may not have been produced fully due to an incompletely reversible phase transition from (1×3) to (1×2) reconstructions. It has been observed that the RAS profile for the (1×2) reconstruction is not fully reproduced after the electrode potential has been changed to an electrode potential that is only -0.1 V. Therefore it is reasonable for one to expect that the RA spectrum attributed to the Au(110) (1×2) reconstructed surface by Mazine *at al.* [50, 51] is a mixed surface structure of (1×2) and (1×3) regions.

The RAS profile attributed to the Au(110) (1×1) surface structure in this work is also different to the RA spectrum identified for the same surface structure by Mazine *et al.* [50,51]. In this work the RAS profile is characterised by a line shape in which the intensity of the 3.6 eV peak is significantly greater than the intensity of the 2.6 eV peak, whereas the RAS profile in the work of Mazine *et al.* [50,51] the 3.6 eV peak is not as intense and the 2.6 eV peak has a comparable intensity. The RA spectrum associated with the (1×1) surface structure in this work was observed at an applied potential of 0.3 V. However the RA profile observed by Mazine *et al.* [50,51] was found at an applied potential of 0.645 V. Increasing the applied potential in the sulfate electrolyte from 0.3 V to 0.6 V and to 0.7 V for the perchlorate solution the three RAS profiles change and become very similar in both shape and intensity with a decrease in intensity of the 3.6 eV peak and a slight increase in intensity of the 2.6 eV peak observed (figure 3.15). The RA spectra at 0.6 V and 0.7 V are very similar in shape to the RAS profile associated with the (1×1) surface structure by Mazine *et al.* [50,51]. This convergence of the RA spectra at higher potentials suggests there is a common process occurring at the interface, which is associated with the formation of an ordered layer of adsorbed anions, which is both independent of pH and the nature of the anion. The higher applied potential needed to create this RAS profile in perchlorate solution is consistent with the ions in that solution being weakly adsorbing, and so an increased potential is required for their adsorption in comparison to the strongly adsorbing sulfate ions. These RA profiles correspond to a surface structure influenced by an ordered layer of anions which results in an anion-induced (1×1) structure which is significantly different to the RAS profile of the (1×1) structure.

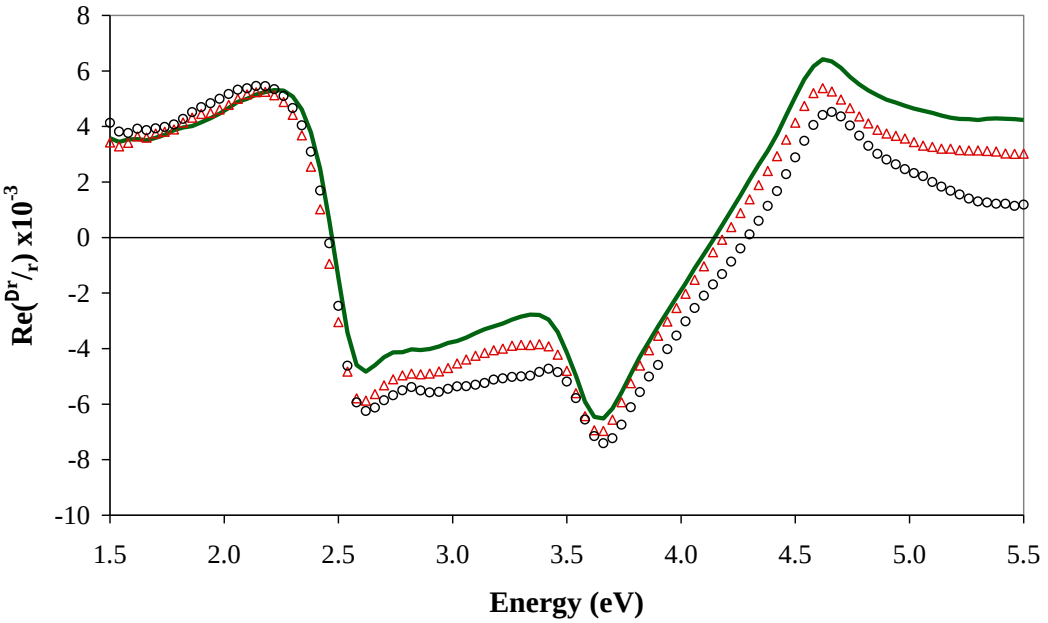

Figure 3.15: RA spectra of Au(110) at 0.6 V in 0.1 M $HClO_4/NaClO_4$ (Δ), in 0.1 M $NaClO_4$ (○) and in 0.1 M H_2SO_4/Na_2SO_4 (green line).

3.7.1 RA Spectral Signatures in 0.1 M NaH_2PO_4/K_2HPO_4

RA spectra in 0.1 M NaH_2PO_4/K_2HPO_4 have been obtained at pH 7.1 and pH 7.2 and are shown in figure 3.16. This slight change in pH causes a change in the RA profile at 0.0 V. The line shape of the RA spectra in each pH value is similar but the intensity of the 3.6 eV peak reduces when going from pH 7.1 to pH 7.2 whilst the peak at 2.6 eV increases slightly with the same change in pH. As this change in the RA profile is very similar to the change that is observed between the (1×1) surface structure and an anion-induced (1×1) surface structure, it is possible to conclude that as the pH is changed from pH 7.1 to pH 7.2 in the same anion solution and at the same potential, the change in pH causes the surface to adsorb anions and thus the observation of the RAS profile of an anion-induced (1×1) surface structure.

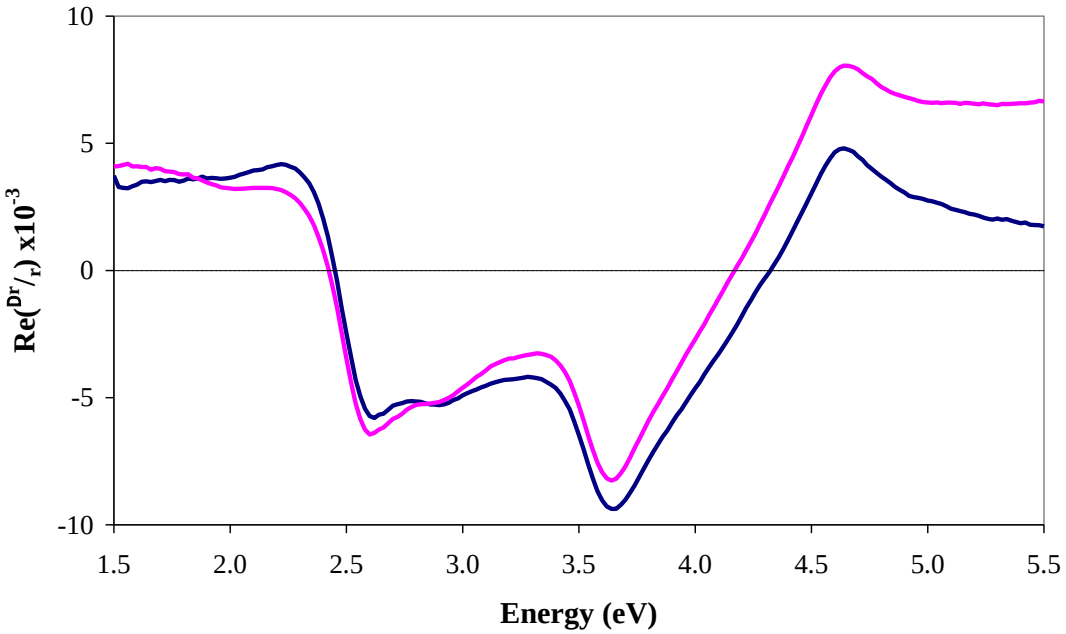

Figure 3.16: RA spectrum of Au(110) in 0.1 M NaH_2PO_4/K_2HPO_4 at pH 7.1 (blue line) and at pH 7.2 (pink line)

Further investigation of the effect of pH on the Au(110) surface is needed, and the pH value should be changed whilst using the same electrolyte solution, but this is beyond the scope of this thesis. However it is important to note the change observed in this electrolyte solution as the same solution is used for the adsorption of protein onto the Au(110) surface.

3.8 Monitoring the Adsorption of Molecules at the Au(110)/Electrolyte Interface using RAS.

This chapter has shown how the Au(110) surface has been studied in UHV and electrolyte conditions. The RAS technique has proved to be sensitive to the Au(110) surface reconstructions that can be induced by changes in temperature [56], potential, crystal preparation and pH. RAS can provide information on the kinetics of these reconstructions and has been used to identify the RA profiles of the Au(110) reconstructed surfaces. The detailed understanding of the Au(110) surface is an

essential prerequisite for its use as a substrate for the adsorption of molecules. This section will discuss the application of RAS to monitor the adsorption of molecules on the Au(110) surface.

RAS was first used to monitor the adsorption of pyridine on the Au(110) surface in the electrochemical environment [71]. RAS is a microscopic probe of macroscopic anisotropy and the resultant RA spectrum after the adsorption of pyridine [71] demonstrated that the molecule forms an ordered structure on the Au(110) surface. A disordered surface would yield a zero RAS signal. Changes in the RA spectrum after the adsorption of molecules on the surface can be associated with transitions in the molecule and information on these transitions is available from the absorption spectra of the molecule. The Authors [71] concluded that pyridine adsorbs through the N atom of pyridine onto the Au surface. A later investigation demonstrated that the RAS technique can distinguish between the adsorption of pyridine and two bipyridine species, 2,2´-bipyridine and 4,4-bipyridine [73]. Differences in the shape of RA spectra for each species of pyridine was attributed to the different orientation of each adsorbed species on the Au(110) surface, highlighting the sensitivity of the RAS technique.

The relationship between the optical axis of the Au(110) surface and the optical axes of transitions arising from adsorbed molecules can be used to establish the orientation of adsorbed molecules on the Au(110) surface. It has been shown by Weightman *et al.* [67] that the intensity of the RA spectrum of Au(110) varies as a function of $\cos 2\theta$, where θ is the azimuthal angle between the plane of polarisation of the incident light and the crystal axis of the surface. This intensity dependence as a function of azimuthal rotation can be utilised to provide information on the orientation of adsorbed molecules on the Au(110) surface. If the plane of the adsorbed molecule is parallel to the Au(110) surface then the RAS intensity takes on a more complicated dependence on θ, as the RA signal is now a product of more than one optical axis, this dependence has been described in detail by Macdonald and Cole *et al*. [74]. As a consequence of this relationship, if the molecule is vertically orientated along one of the crystal axes of the Au(110) surface then the contribution from the molecular transitions will vanish at $\theta = 45^{\circ}$ across the entire spectral range. Therefore the azimuthal rotation of the Au(110) surface with

adsorbed molecules is a powerful technique that provides information on the orientation of adsorbed molecules.

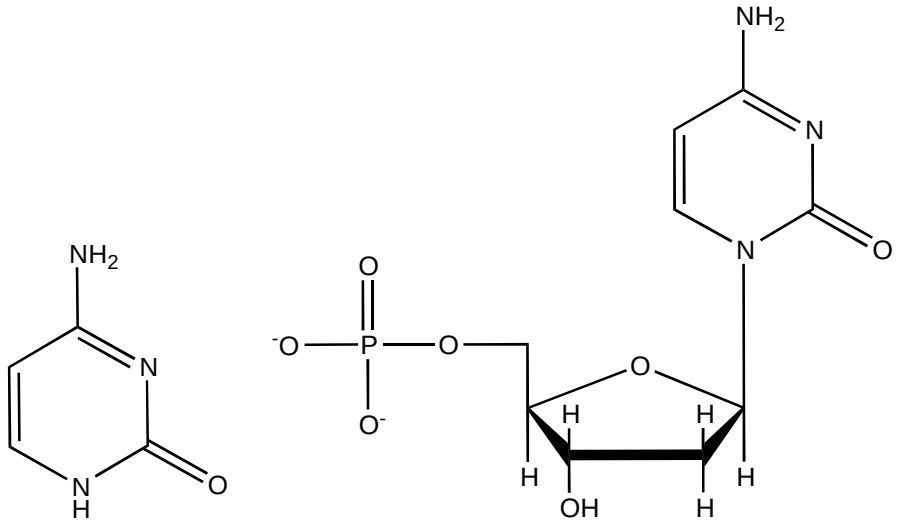

Figure 3.17: Structure of cytosine and cytidine 5´-monophosphate.

The adsorption of the Deoxyribonucleic acid (DNA) base cytosine and cytidine 5´-monophosphate on Au(110) [3] produced two similar RA profiles, which implied that the molecules adsorb in a similar orientation. STM results showed that each molecule adsorbed at saturation coverage of the Au surface. The RA spectra of both cystosine and cytidine 5´-monophosphate vanishes at an angle $\theta = 45^{\circ}$ which indicated that the molecules are orientated vertically on the Au(110) surface and aligned along one of the principle axes of the Au(110) surface. This information coupled with the similarity of the RAS of the two molecules made it extremely likely that both molecules adsorb on the Au(110) surface through the same mechanism, and the structure of the two molecules (figure 3.17) suggests that they adsorb via the lone pairs in the N and O atoms. Several studies of the adsorption of the nucleic acid adenine and adenosine 5´ monophosphate [7-9] (figure 3.18) showed that adenine adsorbs orientated vertically on the Au surface along the $[1\,\bar{1}\,0]$ direction by bonding through the NH_2 group and possibly N(7) [7-9].

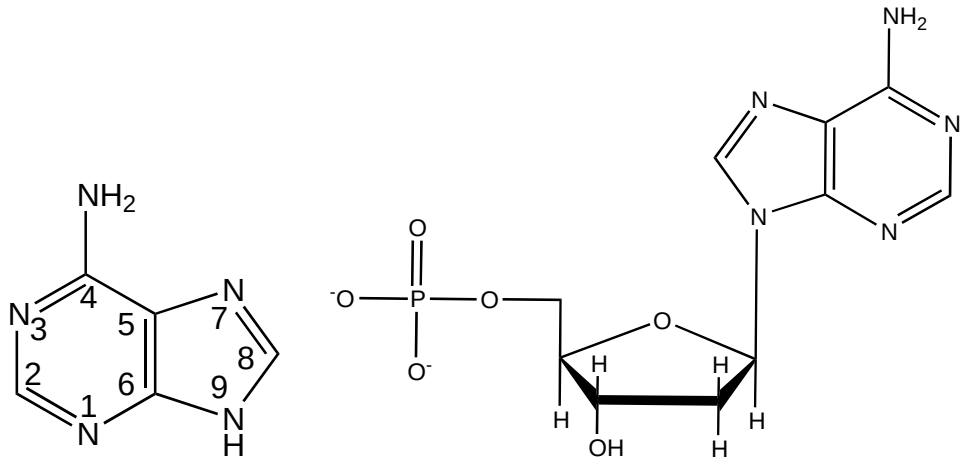

Figure 3.18: Structure of adenine and adenosine 5´ monophosphate.

The RA spectra of adenine were also shown to change as a function of concentration [8] and pH [9]. At lower concentrations it was also shown that sub-saturation coverage is achieved and even at this coverage the molecules adsorb in the same orientation [8].

RA spectra after the adsorption of the DNA bases of cytosine, adenine, cytidine 5´-monophosphate [3] and adenosine 5´-monophosphate [7], has revealed information on the orientation of these molecules adsorbed at the Au(110)/liquid interface. Sub saturation coverage of both adenine and cytosine was shown to have no effect on the orientation of the molecule on the Au surface [8,10]. RA spectral changes as a function of applied potential for adenine [7-9] and cytosine [10] have shown that adenine changes its orientation as a function of potential, whereas cytosine does not change orientation on the Au(110) surface but was found to freeze the Au(110) surface in the (1×1) surface structure. This observed difference in behaviour is attributed to the difference in the strength of the bonding of each molecule to the Au surface. The Authors [10] suggest that the cytosine molecule bonds through three sites, the NH_2, the N(3) and O(8) to three Au atoms along the $[1\bar{1}0]$ row, while the adenine molecule is known to bond via the N(7) site and possibly also the NH_2 group at 0.0 V [7].

An important step towards studying larger biological molecules and proteins has been the study of amino acids adsorbed onto the Au(110) surface. It is important to understand the adsorption of amino acids as a precursor to monitoring the

adsorption of protein. The adsorption of three amino acids; cysteine, cystine and methionine have been monitored using RAS [2]. Cysteine contains a highly reactive sulfur containing functional group, which can form a disulfide bond with another cysteine to form cystine, whilst methionine contains a thiolether as shown in figure 3.20. These thiol groups are found on the surface of proteins and interact strongly with surfaces to form strong bonds which can provide an anchor point for proteins to a surface.

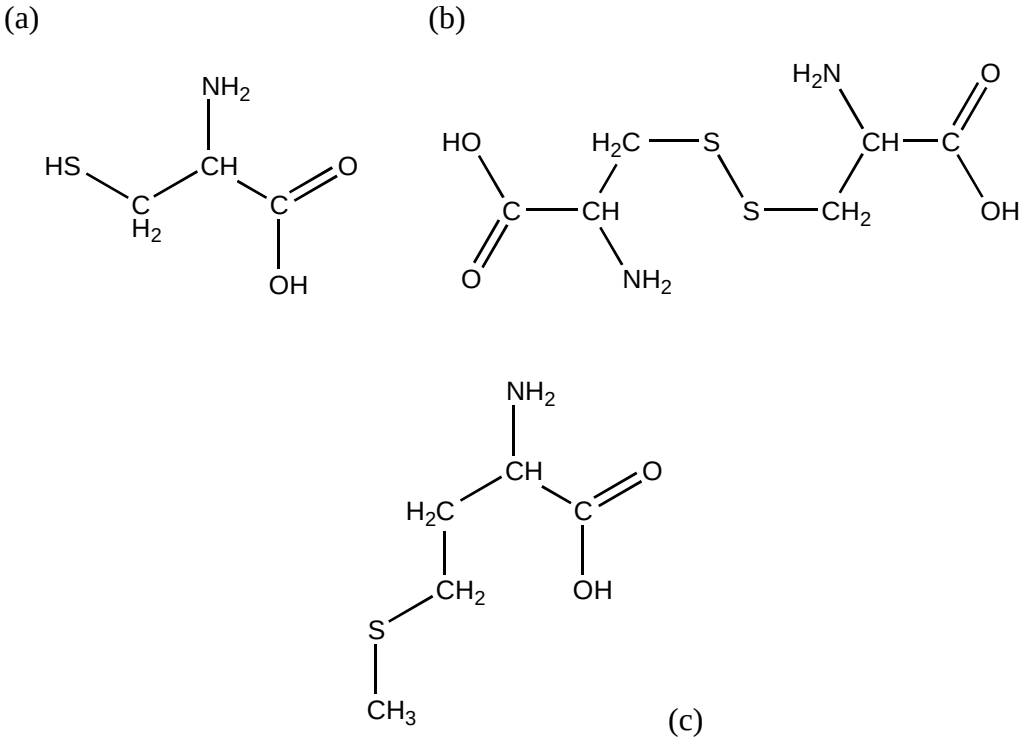

Figure 3.20: Structure of (a) cysteine, (b) cystine and (c) methionine.

The RAS investigation [2] suggested that the amino acids adsorb via the formation of a thiolate Au-S bond which is associated with an increase in intensity of a negative 2.5 eV peak. The authors [2] demonstrated how changes in the RA spectra are induced by variations in pH and voltage, the change in RA profile is associated with changes to the adsorption mechanism and orientation. A similar mechanism and response to voltage was observed for the adsorption of cysteine-tryptophan on the Au(110) surface [11].

The adsorption of molecules is important for understanding the effect binding to a surface has on the structure of a molecule. The adsorption of single-stranded DNA and double-stranded DNA (ss-DNA and ds-DNA respectively) on Au(110) surface was also monitored with RAS [4]. The study showed that both ss-DNA and ds-DNA formed similar ordered structures on the Au(110) surface. At 0.0 V the RA profiles are very similar for both forms of DNA, however there was significant increase in the RAS response for ss-DNA. This difference was linked to the different adsorption mechanisms: ss-DNA adsorbs through the bases, optical transitions of the bases can couple to the dielectric response of Au and cause an increase in the RAS intensity. The adsorption of ds-DNA is through the phosphate backbone, and this backbone shields the bases from interacting with the Au surface and therefore a lower intensity RA spectrum is produced. The study also demonstrated that the adsorption mechanism is sensitive to voltage and ss-DNA adsorbs through the phosphate backbone at +0.6V, as does ds-DNA, and at negative potentials both forms of protein desorb from the Au surface. A further study into the orientation of ds-DNA and ss-DNA [5] found that the optical axes of the molecules are aligned with that of the Au(110) surface.

The sensitivity of RAS to the orientation and dipole transitions of adsorbed molecules makes it an ideal instrument to study protein conformational change, the understanding of interactions of the amino acid cysteine with the Au(110) surface has shown that the molecule forms a strong Au-S bond at negative potentials [2].

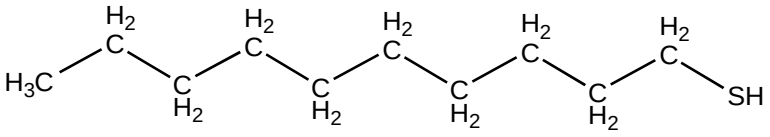

Figure 3.21: Structure of decanethiol

Previous research has demonstrated that a negative peak at 2.54 eV is a signature of the formation of the Au-S bond which has also been observed with the adsorption of decanethiol on the Au(110) surface [75]. The research reported in this thesis utilises this information and the strength of the Au-S bond by introducing

surface exposed cysteine molecules into the structure of the protein thus allowing a strong anchor point between the protein and the Au surface to be established. An earlier preliminary experiment utilising this technique showed that protein adsorbed onto the Au(110) surface by forming the thiolate-Au bond [6]. The adsorption of protein via the Au-thiolate bond has shown to anchor the protein to the Au surface in a specific predetermined orientation that allows the rest of the protein to function normally. This study showed that changes in the RA spectra of adsorbed protein as a function of potential could be associated to changes in the protein conformation. The work in this thesis goes a long way into identifying the coverage, orientation and interaction of the protein with the Au(110) surface and provides more information on possible conformational changes that are associated with changes in the RA spectra.

3.9 Summary

The Au(110) surface has been discussed in detail in this chapter both in terms of its physical and electronic structure. Research both in electrochemical and UHV environments have been discussed and summarised highlighting key experiments and studies. The (1×1), (1×2) and (1×3) surface reconstructions have been introduced and the transition between these surface reconstructions has been the focus of much research which has also been discussed in this chapter. Importantly the conditions in which the surface reconstructions are induced has also been explained, along with the introduction of the RA spectral signatures of each reconstruction which have been discussed in detail, highlighting the importance of the electrolyte solution, pH and potential. RA spectra have been shown to adopt an anion-induced (1×1) surface structure making the anion of the electrolyte an important factor to take into account.

Previous RAS experiments which have utilised the Au(110) surface as a suitable substrate for the adsorption of biological molecules demonstrate the reproducibility of the RA spectrum of the Au(110) surface and the sensitivity of the RAS technique to surface orientation of the adsorbed molecule. A thorough

understanding of previous RAS studies where biological molecules have been adsorbed onto the Au(110) surface is key to the development of the experimental procedures and techniques used throughout the research reported in this thesis.

3.10 References

[1] C. I. Smith, A. Bowfield, N. J. Almond, C. P. Mansley, J. H. Convery and P. Weightman, *J. Phys.: Condens. Matter* **22**, 392001 (2010)

[2] R. LeParc, C. I. Smith, M. C. Cuquerella, R. L. Williams, D. G. Fernig, C. Edwards, D. S. Martin and P. Weighman, *Langmuir* **22**, 3413 (2006)

[3] P. Weightman, G. J. Dolan, C. I. Smith, M. C. Cuquerella, N. J. Almond, T. Farrell, D. G. Fernig, C. Edwards and D. S. Martin, *Phys. Rev. Lett.* **96**, 086102 (2006)

[4] M. C. Cuquerella, C. I. Smith, D. G. Fernig, C. Edwards and P. Weightman. *Langmuir* **23**, 2078 (2007)

[5] C. P. Mansley, C. I. Smith, M. C. Cuquerella, T. Farrell, D. G. Fernig, C. Edwards and P. Weightman, *Phys. Status Solidi C* **5**, 2582 (2008)

[6] H. L. Messiha, C. I. Smith, N. S. Scrutton and P. Weightman, *Euro. Phys. Lett*. **83**, 18004 (2004)

[7] C. I. Smith, A. Bowfield, G. J. Dolan, M. C. Cuquerella, C. P. Mansley, D. G. Fernig, C. Edwards and P. Weightman, *J. Chem. Phys* **130**, 044702 (2009)

[8] A. Bowfield, C. I. Smith, G. J. Dolan, M. C. Cuquerella, C. P. Mansley and P. Weightman, *e-J. Surf. Sci. Nanotech*. **7**, 225 (2009)

[9] A. Bowfield, C. I. Smith, C. P. Mansley and P. Weightman, *Phys. Status Solidi* B **247**, 1937 (2010)

[10] C. P. Mansley, C. I. Smith, A. Bowfield, D. G. Fernig, C. Edwards and P. Weightman, *J. Chem. Phys*. **132**, 214708 (2010)

[11] B. Morozzo della Rocca, C. I. Smith, C. Teasuro, A. Desideri and P. Weightman, *Surf. Sci.* **604**, 2170 (2010)

[12] A. L. Schofield, C. I. Smith, V. R. Kearns, D. S. Martin, T. Farrell, P. Weightman and R. L. Williams, *J. Phys. D: Appl. Phys*. **44**, 335302 (2011)

[13] J. H. Convery, C. I. Smith, B. Khara, N. S. Scrutton, P. Harrison, T. Farrell, D. S. Martin and P. Weightman, *Phys. Rev. E* **86**, 011903 (2012)

[14] N. J. Almond, *Ph. D. Thesis*, The University of Liverpool (2008)

[15] D. G. Fedak and N. A. Gjostein *Acta Metallugrica* **15**, 827 (1967)

[16] D. G. Fedak and N. A. Gjostein, *Surf. Sci.* **8**, 77 (1067)

[17] C. –M. Chan, K. L. Luke, M. A. Van Hove, W. H. Weinberg and E. D. Williams, *J. Vac. Sci. Technol.* **16**, 642 (1979)

[18] I. K. Robinson, *Phys. Rev. Lett.* **50**, 1145 (1983)

[19] J. R. Noonan and H. L. Davis, *J. Vac. Sci. Technol.* **18**, 587 (1979)

[20] B. Reihl and B. I. Dunlap, *Appl. Phys. Lett.* **37**, 941 (1980)

[21] G. Binnig, H. Rohrer, Ch. Gerber and E. Weibel, *Surf. Sci.* **131**, L379 (1983)

[22] C. Hofner and J.W. Rabalais, *Surf. Sci.* **400**, 189 (1998)

[23] J. C. Campuzano, M. S. Foster, G. Jenings and R. F. Willis, *Phys. Rev. Lett.* **54**, 2684 (1985).

[24] L. Onsager, *Phys. Rev.* **65**, 117 (1944)

[25] Y. Yuk, P. J. Silverman and H. Q. Nguyen, *J. Vac. Sci. Technol. A.* **6**, 524 (1988)

[26] J. K. Gimzewski, R. Berndt and R. R. Schlittler, *Surf. Sci* **247**, 327 (1990)

[27] T. Gritsch, D. Coulman, R. J. Behm and G. Ertl, *Surf. Sci.* **257**, 297 (1991)

[28] R. Koch, M. Borbonus, O. Haase and K. H. Rieder, *Appl. Phys.* **A55**, 417 (1992)

[29] S. Speller, S. Molitor, C. Röthig, J. Bömermann and W. Heiland, *Surf. Sci.* **312**, L748 (1994)

[30] M. Sturmat, R. Kock and K. H. Rieder, *Phys. Rev. Lett.* **77**, 5071 (1996)

[31] R. Koch, M. Sturmat and J. J. Schluz, *Surf. Sci.* **454-456**, 543 (2000)

[32] K. –M. Ho and K. P. Bohnen, *Phys. Rev. Lett.* **59**, 1833 (1987)

[33] J. W. M. Frenken, R. L. Krans, J. F. van der Veen, E. Holub-Krappe and K. Horn, *Phys. Rev. Lett.* **59**, 2307 (1987).

[34] X. Gao, A. Hamelin and M. J. Weaver, *Phys. Rev. B* **44**, 10983 (1991).

[35] O. M. Magnussen, J. Wiechers and R. J. Behm, *Surf. Sci.* **289**, 139 (1993)

[36] B. M. Ocko, G. Helgesen, B. Schrdt and J. Wang, *Phys. Rev. Lett.* **69**, 3350 (1992)

[37] P. Häberle, P. Fenter and T. Gustafsson, *Phys. Rev. B.* **39**, 5810 (1989).

[38] X. Gao and M. J. Weaver, *Surf. Sci.* **313**, L775 (1994)

[39] I. M. Tidswell, N. M. Marković, and P. N. Ross, *Surf. Sci.* **317**, 241 (1994)

[40] X. Gao, G. J. Edens, A. Hamelin and M. J. Weaver, *Surf. Sci.* **318**, (1994)

[41] R. Kofman, P. Cheyssac and J. Richard, *Surf. Sci.* **77**, 537 (1978)

[42] S. H. Liu, C Hinnen, C. Nguyen Van Huong, N. R. De Tacconi and K. M. Ho, *J. Electroanal. Chem.* **176**, 352 (1984)

[43] C. H. Xu, K. M. Ho and K. P. Bohnen, *Phys. Rev. B.* **39**, 5599 (1989)

[44] M. Sastry, K. C. Prince, D. Cvetko, A. Morgante and F. Tommansi, *Surf. Sci.* **271**, 179 (1992)

[45] W. L. Mochán, R. G. Barrera, Y. Borrensztein and A. Tadjeddine, *Physica. A.* **207**, 334 (1994)

[46] J. –K. Hansen, J. Bremer, L. Seime and O. Hunderi, *Physica A* **298**, 46 (2001).

[47] A. Bowfield, *Ph. D. Thesis.* The University of Liverpool (2009)

[48] G. J. Dolan, *Ph. D. Thesis,* The University of Liverpool (2007)

[49] B. Sheridan, D. S. Martin, J. R. Power, S. D. Barrett, C. I. Smith, C. A. Lucas, R. J. Nichols and P. Weightman, *Phys. Rev. Lett.* **85**, 4618 (2000)

[50] V. Mazine, Y. Borensztein, L, Gagnon and P. Allongue, *Phys Status Solidi* **175**, 311 (1999)

[51] V. Mazine and Y. Borensztein, *Phys. Rev. Lett.* **88**, 147403 (2002)

[52] P. Weightman, C. I. Smith, D. S. Martin, C. A. Lucas, R. J. Nichols and S. D. Barrett, *Phys. Rev. Lett.* **92**, 199707 (2004)

[53] D. S. Martin, N. P. Blanchard and P. Weightman, *Surf. Sci.* **532**, 1 (2003)

[54] J. Bremer, J. –K. Hansen and O, Hunderi, *Surf. Sci.* **436**, L735 (1999)

[55] K. Stahrenberg, Th. Herrmann, N. Esser, W. Richter, S. V. Hoffmann and Ph. Hofmann, *Phys. Rev. B* **65**, 035407 (2001)

[56] D. S. Martin, R. J. Cole, N. P. Blanchard, G. E. Isted, D. S. Rosenburgh and P. Weightman, *J. Phys.: Condens. Matter* **16**, S4375 (2004)

[57] U. Rossow, L. Mantese and D. E. Aspnes, *J. Vac. Sci. Technol. B* **14**, 3070 (1996)

[58] P. Winsemius, F. F. van Kampen, H. P. Lengkeek and C. G. van Went, *J. Phys. F: Metal Phys.* **6**, 1583 (1976)

[59] R. C. Jones, *J. Opt. Soc. Am.* **31**, 488 (1941)

[60] J. D. E. McIntyre and D. E. Aspnes, *Surf. Sci.* **24**, 417 (1971)

[61] R. J. Cole, B. G. Frederich and P. Weightman, *J. Vac. Sci. Technol. A.* **16**, 3088 (1998)

[62] N. P. Blanchard, C. Smith, D. S. Martin, D. J. Hayton, T. E. Jenkins and P. Weightman, *Phys. Status Solidi C* **0**, 2931 (2003)

[63] N. P. Blanchard PhD Thesis, University of Liverpool (2009)

[64] *Handbook of Optical Constant of Solids* E. D. Palik (Academic, New York 1985)

[65] C. I. Smith, private communication

[66] C. I. Smith, unpublished work

[67] P. Weightman, D. S. Martin, R. J. Cole, and T. Farrell, *Rep. Prog. Phys.* **68**, 1251 (2005).

[68] A. Hamelin, *J. Electroanal. Chem.* **329**, 247 (1992)

[69] F. Silva and A. Martins, *Electrochimica. Acta.* **44**, 919 (1998)

[70] D. M. Kolb, *Prog. Surf. Sci.* **51**, 109 (1996)

[71] C. I. Smith, A. J. Maunder, C. A. Lucas, R. J. Nichols and P. Weightman, *J. Electrochem. Soc.* **150**, E233 (2003)

[72] F. Henglein, D. M. Kolb, L. Stolberg and J. Lipkowski, *Surf. Sci.* **291**, 325 (1993)

[73] C. I. Smith, G. J. Dolan, T. Farrell, A. J. Maunder, D. G. Fernig, C. Edwards and P. Weightman, *J. Phys.: Condens. Matter.* **16**, S4385 (2004)

[74] B. F. Macdonald and R. J. Cole, *Appl. Phys. Lett.* **80**, 3527 (2002)

[75]` A. Bowfield, C. I. Smith, M. C. Cuquerella, T. Farrell, D. G. Fernig, C. Edwards and P. Weightman, *Phys. Status Solidi C* **5**, 2600 (2008)

Chapter 4

Preliminary Studies of Protein Adsorbed at the Au(110)/Electrolyte Interface

Two forms of mutant P499C cytochrome P450 reductase (CPR) have been adsorbed onto the Au(110) surface, the full length protein and a truncated form of the protein containing just the flavin adenine dinucleotide (FAD) domain. The mutant protein adsorbed through the surface exposed cysteine which form strong Au-S bonds. A series of electron transfer processes driven by variations in the potential applied to the Au(110) electrode have been monitored using RAS. The data presented in this chapter was produced following similar experimental procedures used in previous RAS experiments, were a full coverage of adenine and cytosine was adsorbed on the Au(110) surface. Further experimental data presented in later chapters of this thesis demonstrates that these techniques may not have resulted in the desired adsorption of a monolayer of the two mutant forms of P499C CPR. However the data discussed in this chapter is an important step in understanding the adsorption of P449C CPR onto the Au(110) surface, and describes the behaviour of the protein during the adsorption process and reports changes in the RA spectra of the adsorbed proteins as a result of changes in the applied electrode potential.

4.1 Introduction

The reflection anisotropy spectroscopy (RAS) technique has been proven to be extremely sensitive to changes induced in the RAS of Au(110) after the adsorption molecules [1-10]. This sensitivity has been used to study changes in the RAS of cytochrome P450 reductase (CPR) adsorbed on the Au(110) surface as the molecules are adsorbed and as the potential applied to the electrode is varied. CPR, a 78 *kDa* protein shown in figure 4.1, has a modular structure consisting of distinct redox domains: flavin adenine dinucleotide/nicotinamide adenine dinuctleotide phosphate (FAD/NADP) and flavin mononucleotide (FMN). Each domain is bonded to a flavin cofactor which, as part of the natural catalytic cycle is successively oxidised and reduced [11]. The tightly bound cofactors FAD and FMN, which catalyse electron transfer reactions, play an important role in delivering electrons to cytochrome P450 enzymes which catalyse the detoxification of a wide range of xenobiotics and drugs [12]. The electron transfer process is expected to be linked to domain motion [13-15]. The FMN domain is joined to the rest of the protein by a flexible peptide hinge. The crystal structure of CPR reveals a conformation ideal for interflavin electron transfer. However this conformation is less suitable for the subsequent transfer of electrons to large acceptor proteins. It is therefore suggested that domain motion plays a key role in the function of CPR during electron transfer processes. Evidence for these dynamic models have been explored using small angle X-ray scattering (SAXS), pulsed electron-electron double resonance (ELDOR) spectroscopy and high pressure and temperature jump studies of the kinetics of interflavin electron transfer [13-15].

a)

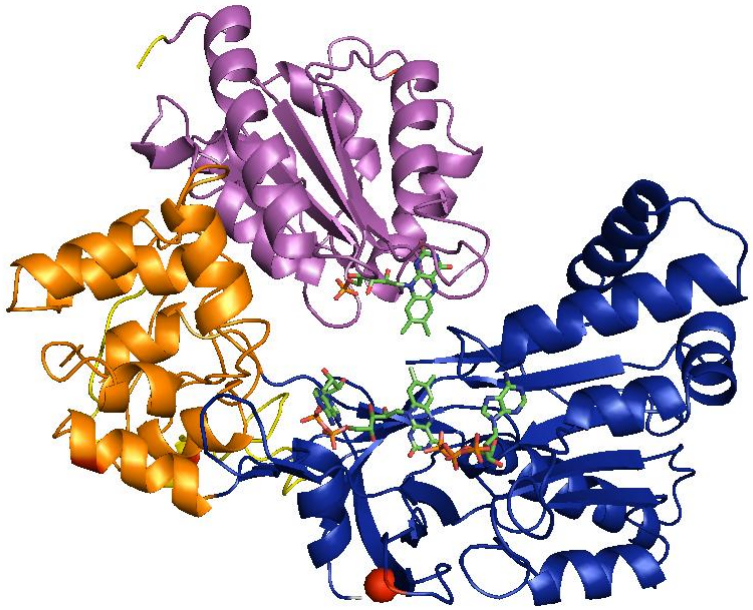

b)

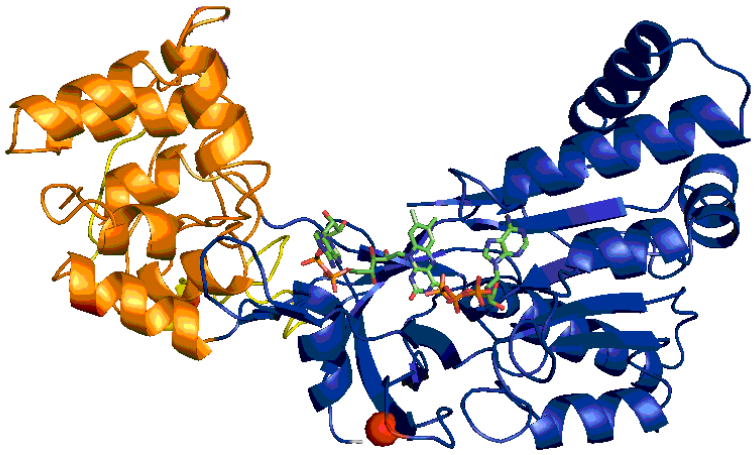

Figure 4.1: Molecular graphics ribbon diagram representation for the structure of a) cytochrome P450 reductase and b) the isolated FAD variant The Pro-499 residue that was targeted by site directed mutagenesis to produce the P499C variant is shown by the red sphere. The FMN-binding domain is shown in purple, the connecting domain in orange, and the FAD/NADP domain in blue. The FAD and FMN cofactors are shown as green sticks.

The aim of these experiments is to use RAS to monitor these dynamic changes that are thought to be key to electron transfer processes in CPR. The molecule is adsorbed onto the Au(110) surface through a cysteine residue. X-ray crystallography provides structural information of the protein which has been used

to select a position to introduce surface cysteine residues. The variant form (Pro-499 to Cys-499; P499C) of CPR was obtained by site-directed mutagenesis using ‘forward’ and ‘reverse’ oligonucleotide primers. The mutated gene was completely sequenced to verify no illegitimate changes had taken place during the mutagenesis procedure. Cysteine was chosen as it has been shown to form a strong bond through the thiol group to the Au surface [4,5,9]. This bond acts as an anchor point on the protein and its position is carefully selected to ensure the protein adsorbed onto the Au(110) surface in an orientation that allows optimum potential to observe conformational events as the protein functions. Two forms of the protein have been investigated: the full length form containing both the FMN and FAD domain (full length CPR) and a truncated version containing only the FAD domain (FAD). The isolated FAD only version acts as a control as it is not expected to undergo any significant conformational events during the electron transfer process.

The reduction potentials of CPR are revealed through redox potentiometry conducted on both wild type and mutant P499C full length CPR by titration and have been described previously [11]. Redox potentials for the flavin couples were calculated by global analysis of data obtained from reductive titrations of protein samples against dithionite under anaerobic conditions. This process was conducted at Manchester Interdisciplinary Biochemistry centre (MIB) as part of this research. The techniques used are not discussed as this is beyond the scope of this thesis. The redox potentials were shown to not be substantially different to those of the wild-type CPR as shown in tables 4.1 and 4.2.

Redox Potentials	Oxidised	$1e^-$ reduced	$2e^-$ reduced	$3e^-$ reduced	$4e^-$ reduced
Wild Type	0.036V	-0.394V	-0.504V	-0.574V	-0.744V
P499C	0.056V	-0.376V	-0.465	-0.557V	-0.652V
Possible Redox States	FMN FAD	FMN FADH•	FMNH• FADH•	FMNH• $FADH_2$	$FMNH_2$ $FADH_2$
Possible Redox States		FMNH• FAD	FMN $FADH_2$	$FMNH_2$ FADH•	
Possible Redox States			$FMNH_2$ FAD		

Table 4.1: The redox potentials for wild-type and the P499C variant of CPR are shown, as well as the possible sites for the electron, denoted by the •, in the P499C full length CPR.

Redox Potentials	Oxidised	$1e^-$ reduced	$2e^-$ reduced
P499C (truncated)	0.056V	-0.492V	-0.657V
Possible Redox States	FAD	FADH•	$FADH_2$

Table 4.2: The redox potential for P499C variant of CPR as well as the possible sites for the electron, denoted by the •, for the truncated FAD only version.

The isoalloxazine ring within the flavin cofactors is successfully oxidised and reduced by accepting or donating electrons, and hydride ions are donated to the FAD from electron donor species NADPH. The FAD then in turn donates electrons to the FMN cofactor [16]. Figure 4.2 is a representation of the oxidation and reduction states of the isoalloxazine ring, showing the possible positions of the hydride ion, and the structure of both FMN and FAD are shown in figure 4.3.

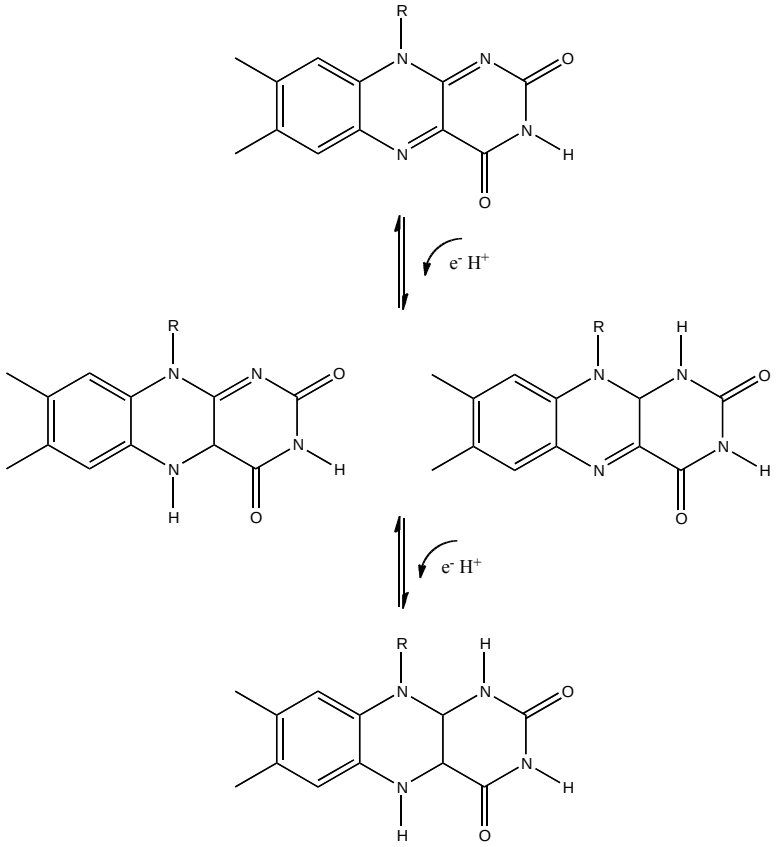

Figure 4.2: Diagram showing the oxidation and reduction of the isoalloxazine ring.

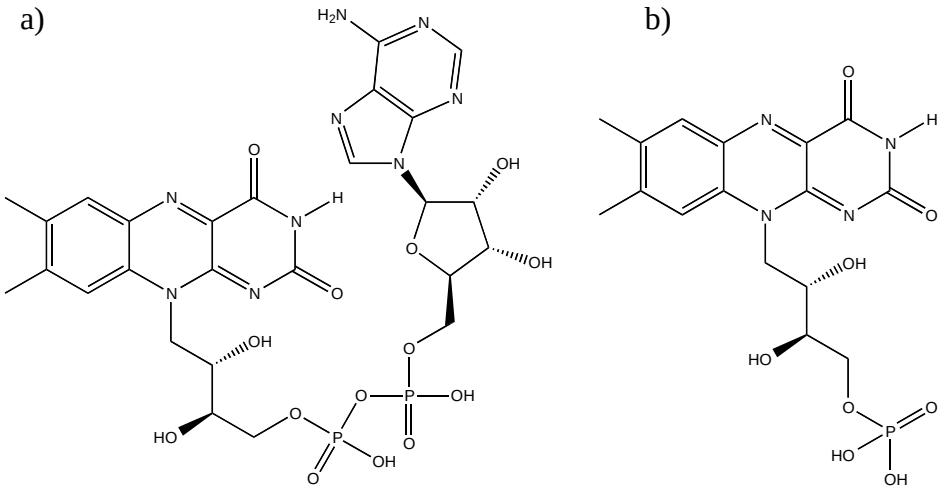

Figure 4.3: Structure of a) FAD and b) FMN showing the isoalloxazine ring

4.2 RAS of the Au(110) Surface in 0.1 M NaH_2PO_4/K_2HPO_4

The Au(110) surface was prepared following the technique and procedure outlined in section 2.4 of this thesis. The Au crystal was then immersed in 0.1 M NaH_2PO_4/K_2HPO4 pH 7.1 buffer solution, which was made anaerobic by bubbling with argon gas prior to the insertion of the Au(110) crystal into the electrochemical cell. RA spectra of the Au(110) surface were produced at the redox potential for the corresponding variant of CPR prior to the adsorption of CPR. The RAS technique is sensitive to surface states, steps and reconstructions [17,18,19,20] and the flame annealing process has been shown to affect the number of monatomic steps observed in STM images, which was shown to induce changes in the RAS [18]. Therefore careful control of the flame annealing process is necessary to maximise the reproducibility of RA spectra of the Au(110) surface. This is achieved by ensuring that the duration and sequence of the flame annealing process is consistently maintained. This strict and consistent Au preparation procedure results in accurately reproducible RA spectra of the Au(110) surface, indicating that a reproducible and well formed Au substrate surface structure can be produced prior to the adsorption of CPR.

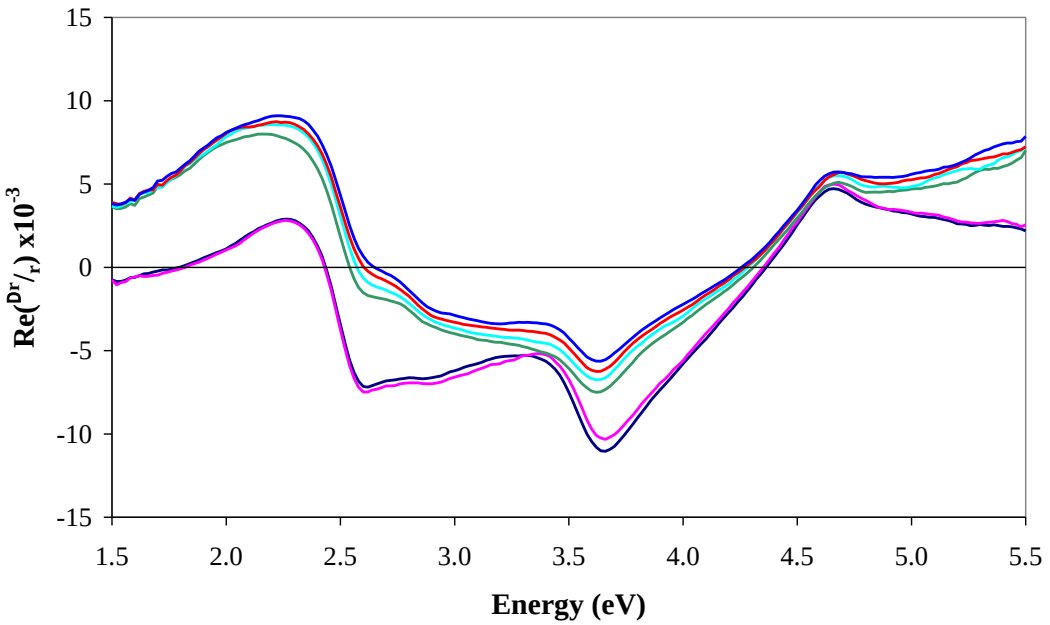

Figure 4.4: RA spectra of the Au(110) in 0.1 M NaH_2PO_4/K_2HPO_4 pH 7.1 at 0.0 V (dark blue line), 0.056 V (pink line), -0.376 V (green line), -0.465 V (turquoise line), -0.557 V (red line) and -0.652V (blue line) vs SCE

The RA spectra produced at an applied electrode potential of 0.0 V and redox potential 0.056 V correspond to an anion induced (1×1) surface structure, whilst at the negative redox potentials of -0.376 V, -0.465 V -0.557 V and -0.652 V the RA spectral signature of the (1×3) [21] is observed and shown in figure 4.4. This is an important observation and demonstrates that over the range of the redox potentials of the mutant CPR molecules the Au(110) surface undergoes a major surface reconstruction.

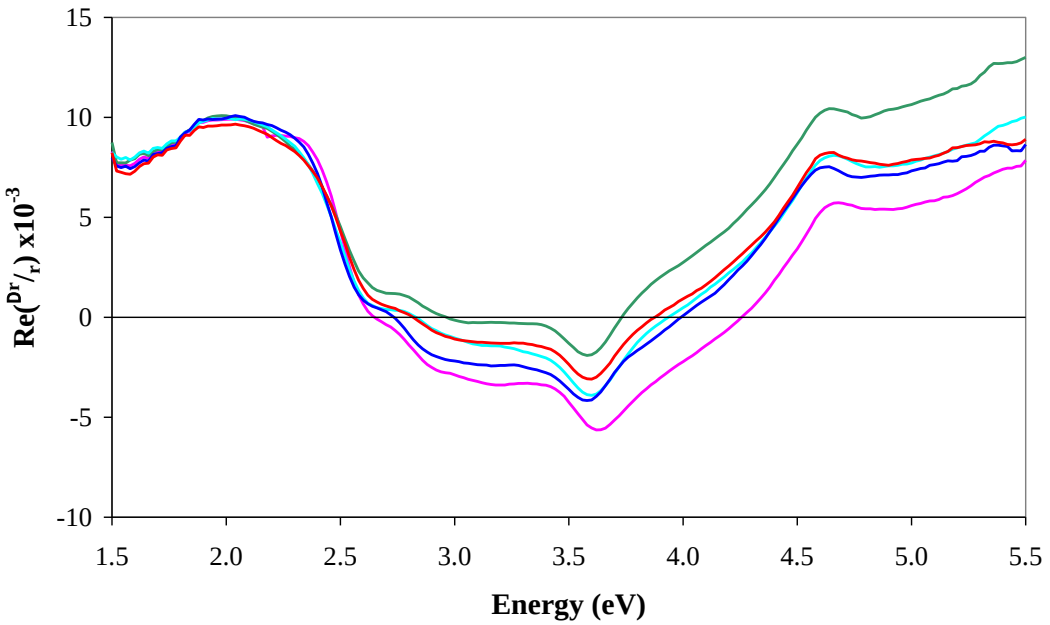

Figure 4.5: RA spectra of Au(110) in 0.1M NaH_2PO_4/K_2HPO_4 pH 7.1 at -0.652 V taken on five separate experiments over the course of 12 months.

RA spectra of Au(110) produced at the applied potential of -0.652V on five separate occasions over a 12 month period are shown in figure 4.5, highlighting the reproducibility of the RA spectra. The overall RA spectral shapes obtained in different experiments are very similar and correspond to a (1×3) surface structure. The slight differences observed in the RAS profiles in figure 4.5 above 3.0 eV could be attributed to slight variations in the flame annealing procedure which has been shown to induce changes in the RAS [17-20]. Sheridan *et al.* [18] showed in an earlier RAS study that the RAS of the Au(110) surface is sensitive to the number of monatomic steps along the $[1\bar{1}0]$ direction, therefore variations in the number of surface steps which are produced during the flame annealing procedure could also account for the slight variation in RAS profile observed in figure 4.5.

4.2.1 The Adsorption of P499C Full Length CPR onto the Au(110) Surface

A dithiotheitol (DTT; 2 mM) protecting group supplemented during the purification of the mutant CPR is used to maintain the reduced form of the engineered cysteine residues when transferring the specimens between Manchester and Liverpool and also whilst in storage. This was removed by eluting on a column immediately prior to use in experiments. Previous RAS experiments have shown that the thiol of the cysteine forms a strong bond to the Au(110) surface at negative potentials [4,5,9]. The formation of this bond has been observed to result in the increase in intensity of the 2.54 eV negative peak in the RAS. To allow the mutant CPR molecules to adsorb via the formation of the Au-S bond between the mutant cysteine molecule and the Au surface, the protein was adsorbed onto the Au(110) surface at -0.652 V, which coincides with the potential at which the protein is in a fully reduced form.

The Au(110) surface adopts a (1×3) structure at -0.652 V, which was confirmed by the observation of the RA spectral signature of this Au(110) surface structure. Protein was then added to the electrochemical cell whilst the applied potential was held at -0.652 V. After the addition of protein solution the RAS intensity of the 2.54 eV peak was recorded as a function of time. The negative increase in intensity of this peak is associated with the formation of the Au-S bond and therefore signals the adsorption of CPR molecules onto the Au(110) surface. In previous RAS studies of the adsorption of cytosine, cytidine 5´-monophosphate and adenine [1,2,6], it was found that a full coverage was achieved upon saturation of the Au(110) surface. Therefore in the preliminary work discussed in this chapter, CPR was added to the electrochemical cell until the intensity at the 2.54 eV peak reached a maximum, at which point it was assumed that monolayer coverage of CPR had been achieved. The adsorption was monitored in this way as it is important to get as close to a full coverage of adsorbed protein on the Au(110) surface as possible in order achieve the maximum RAS signal from the adsorbed CPR molecules. However further experimental data presented in later chapters of this thesis demonstrates that the adsorption of CPR onto the Au(110) surface is sensitive to protein concentration and

the data in these preliminary experiments may not have resulted in a the desired monolayer adsorption of CPR. The data presented in this chapter is an important step in understanding the adsorption of P449C CPR onto the Au(110) surface, and as well as demonstrating that CPR appears to adsorb via the formation of the Au-S bond it also reports changes in the RA spectra of the adsorbed proteins as a result of electron transfer processes.

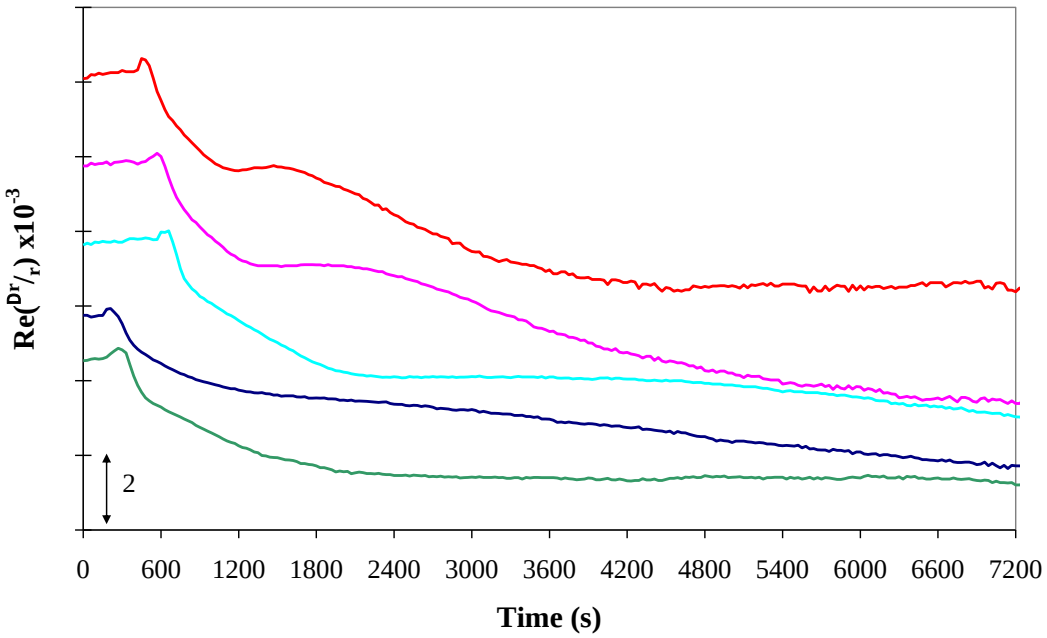

Figure 4.6: The RAS intensity at 2.54 eV monitored as a function of time measured after the addition of P499C full length CPR to the electrochemical cell at -0.652 V. Each curve corresponds to a separate experiment completed over a 12 month period.

Figure 4.6 shows the increase in intensity of the negative peak at 2.54 eV, as a result of the adsorption of P499C full length CPR onto the Au(110) surface. The data is taken from 5 separate experiments produced over a 12 month period. The curves have been shifted on the y-axis to separate them for clarity. The difference in the time before the intensity starts to decrease in each curve is arbitrary and caused by variations between the point at which RAS intensity was recorded and the point at which the protein solution was injected into the electrochemical cell. The

observed increase in intensity of the 2.54 eV peak is indicative of the formation of the Au-S bond and suggests that the protein has adsorbed via interaction between the engineered cysteine residue and the Au surface.

A similar initial negative increase in intensity between 600 and 1200 seconds was observed in all the curves in figure 4.6. However after 1200 seconds a much more varied behaviour in RAS intensity between the experiments was observed. The pink curve (figure 4.6) appears to plateau after 1200 seconds, before another slower more steady increase in intensity is observed after 2400 seconds. This secondary process flattens out after 6600 seconds which was interpreted to signal that adsorption had finished. The red curve (figure 4.6) follows a similar shape to the pink curve with a secondary adsorption process also observed after an initial plateau in the RAS intensity. However the plateau between the two adsorption processes is shorter, only lasting ~300 seconds and the intensity then reaches a maximum after 4400 seconds. The overall intensity changes by ~ 6 units in both the pink and red curves (figure 4.6). The turquoise curve in figure 4.6 has a much slower and steadier initial increase in intensity than both the red and pink curves, the intensity plateaus after 2000 seconds after which a very subtle increase in intensity of only 0.5 units was observed before the RAS intensity maximised at 6500 seconds. The blue curve again shows a slow initial increase in intensity, which starts to steady off after 1200 seconds before continuing to increase at a very slow rate until 7000 seconds. This increase in intensity of the blue curve (figure 4.6) is a much smaller and steadier increase in intensity, with an overall intensity increase of only 4 units. The green curve is similar in overall shape to the turquoise curve, however again the overall increase in intensity observed was only ~ 3 units.

The data in figure 4.6 demonstrate that the adsorption process is complex, and appears to contain several stages. Monitoring the intensity change of the 2.54 eV peak provides information on the formation of Au-S bonds between the engineered cysteine of CPR and the Au(110) surface. The differences between the curves in figure 4.6 highlight possible differences in the adsorption process, with a clear secondary process observed in the red and pink curves, and only a small overall increase in intensity observed in the blue and green curves. The strength of the 2.54 eV peak can be associated with the number of Au-S bonds formed [9], and

so the larger increase in intensity, seen in the pink and red curves could indicate a greater coverage of protein on the Au(110) surface. If this is the case, it demonstrates the difficulty in adsorbing a consistent coverage of CPR onto the Au(110) surface.

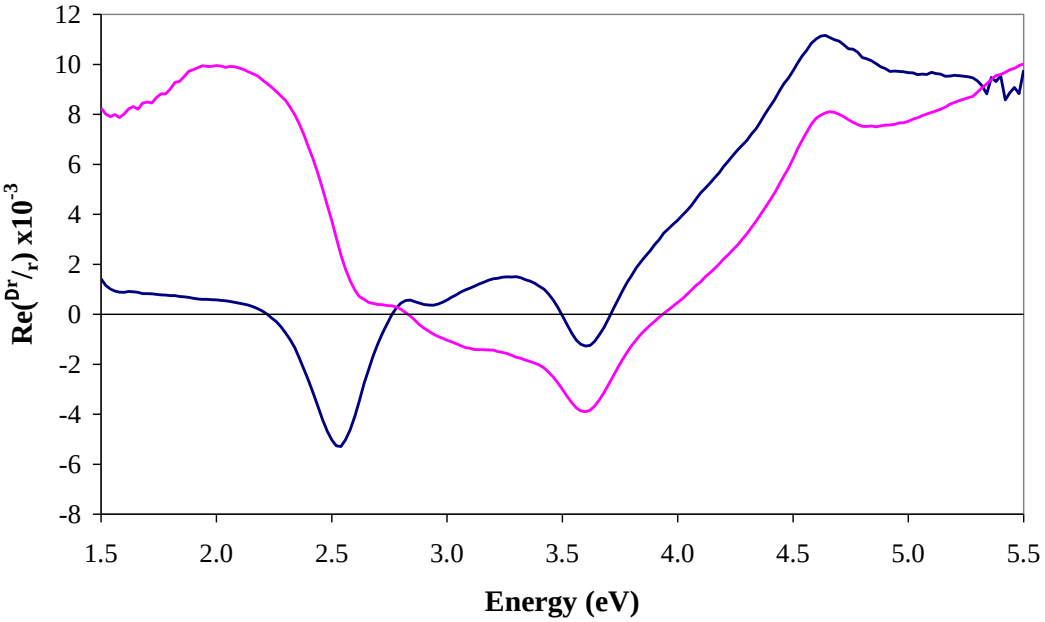

Figure 4.7: RA spectra of Au(110) at -0.652 V (pink line) and Au(110) + P499C full length CPR at -0.652 V (blue curve).

The adsorption of CPR onto the Au(110) surface gave rise to changes in the RA spectrum of Au(110). The resultant RA spectra after the addition of CPR indicated that CPR adsorbed in an ordered structure on the Au(110) surface. RA spectra taken immediately after the adsorption of CPR at -0.652 V are shown in figure 4.8. The coloured lines in this figure 4.8 are colour coded to correspond to the adsorption curves of the same colour in figure 4.6. RA spectra of Au(110) and Au(110) + CPR at -0.652 V are shown in figure 4.7. An obvious change in the RA spectrum of Au(110) after the adsorption of CPR was observed. The positive feature seen in the RA spectrum of Au(110) at ~ 2.0 eV is no longer observed after the adsorption of CPR. Instead an almost horizontal line close to the zero was observed. The emergence of a large negative peak at 2.54 eV was also observed, which is

assumed to be the signature of the formation of Au-thiol bond. After the 2.54 eV peak a steady positive increase in the RAS profile intensity connects the 2.54 eV peak to the 3.6 eV peak, which has decreased in intensity but become more prominent as a result of the adsorption of CPR. At higher energies, between 3.6 eV and 4.5 eV, the RA spectra of both the clean Au(110) surface and Au(110) + CPR, (figure 4.7) follow a similar RA spectral shape. The high energy feature at 4.6 eV increased in intensity after the addition of CPR, and the RAS profile then followed a slight negative slope until 5.5 eV. This is in contrast to a slightly positive slope observed between 4.6 eV and 5.5 eV in the RAS of the clean Au(110) surface.

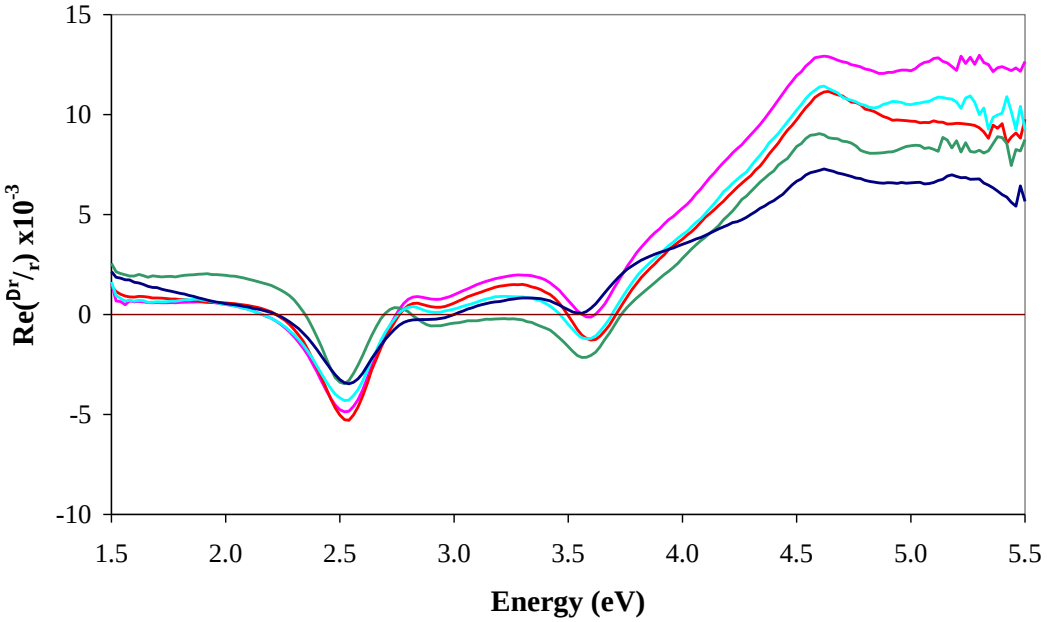

Figure 4.8: RA spectra of Au(110) + P499C full length CPR at -0.652 V vs SCE in 0.1 M NaH_2PO_4/K_2HPO_4 pH 7.1 produced in 5 separate experiments over a 12 month period. The colours of the curves correspond to the same adsorption profile as shown in figure 4.6.

The data shown in figure 4.6 showed differences in the RA intensity profiles at 2.54 eV during the adsorption of CPR onto the Au(110) surface. It was suggested that these differences could relate to variations in the adsorbed protein coverage and orientation on the Au(110) surface. Figure 4.8 shows the RA spectra produced

immediately after the adsorption of CPR in the same experiments at -0.652 V. The RA spectra in figure 4.8 follow a similar spectral shape but clear variations in the intensity of features were observed. These differences echo the differences seen in the adsorption spectra (figure 4.6), and support the theory that the changes observed between each experiment are the result of a different coverage of CPR molecules on the Au(110) surface. This demonstrates the difficulty in producing a consistent reproducible coverage of adsorbed CPR molecules on the Au(110) surface, despite following the same procedures and techniques for each experiment.

The differences in the intensity of the 2.54 eV peak observed between experiments in figure 4.8 is associated with the number of Au-thiol bonds between the Au(110) surface and the engineered cysteine molecule on CPR. The intensity of the 2.54 eV peak was linked to the coverage of adsorbed decanethiol in previous RAS studies [9]. The study found that an increased intensity of the 2.54 eV peak was observed in conjunction with a corresponding decrease in RAS intensity of the 3.6 eV peak. Therefore the observed reduction in intensity of the 3.6 eV peak after the adsorption of CPR, as shown in figure 4.7 may also be a feature of adsorbed CPR.

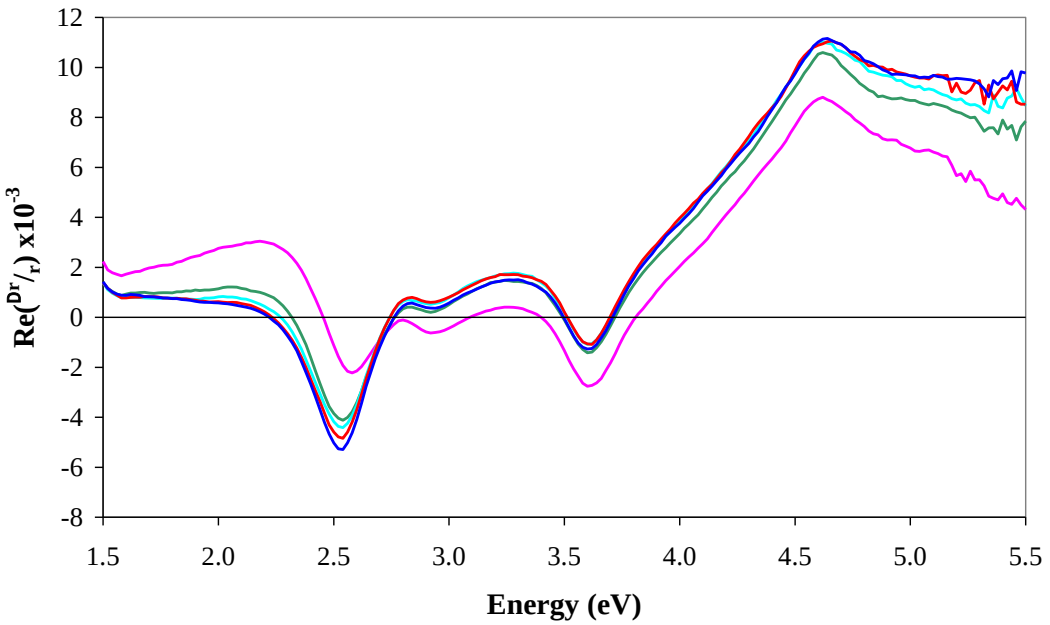

Figure 4.9: RA spectra of Au(110) + CPR in 0.1 M NaH_2PO_4/K_2HPO_4 pH 7.1 at 0.056 V (pink line), -0.376 V (green line), -0.465 V (turquoise line), -0.557 V (red line) and -0.652V (blue line) vs SCE.

The RA spectral shape of Au(110) + CPR produced at the applied potentials -0.652 V, -0.557 V, -0.465 V and -0.376 V are all very similar (figure 4.9), with only a very slight decrease in overall intensity observed as the potential was changed towards increasingly positive potentials. The RA spectrum of Au(110) + CPR obtained at 0.056 V however, shows a more obvious change in RAS profile, with the decrease in intensity of the 2.54 eV peak and an increase in the 3.6 eV peak observed at 0.056 V. The Au(110) surface is known to reconstruct from the (1×3) to anion induced (1×1) surface structure as the potential is changed from the negative potentials to 0.056 V [21]. This same change in applied potential induced the largest change in the RA spectral shape of Au(110) + CPR. It is therefore possible that the observed change in the RA spectral shape of Au(110) + CPR at 0.056 V is associated with a change in the Au(110) substrate surface structure. However the RA spectral signature of the Au(110) (1×1) surface is very different to RA spectral shape of Au(110) + CPR observed at 0.056 V. The potential induced surface reconstruction of Au(110) from (1×3) to the anion induced (1×1) gives rise to a

negative increase in RAS intensity across the full spectral range. Whereas the same change in applied potential after the adsorption of CPR gives rise to a positive shift in RAS intensity below 2.6 eV and a negative increase above this point, it also sees the reduction of the 2.54 eV peak intensity, as shown in figure 4.10.

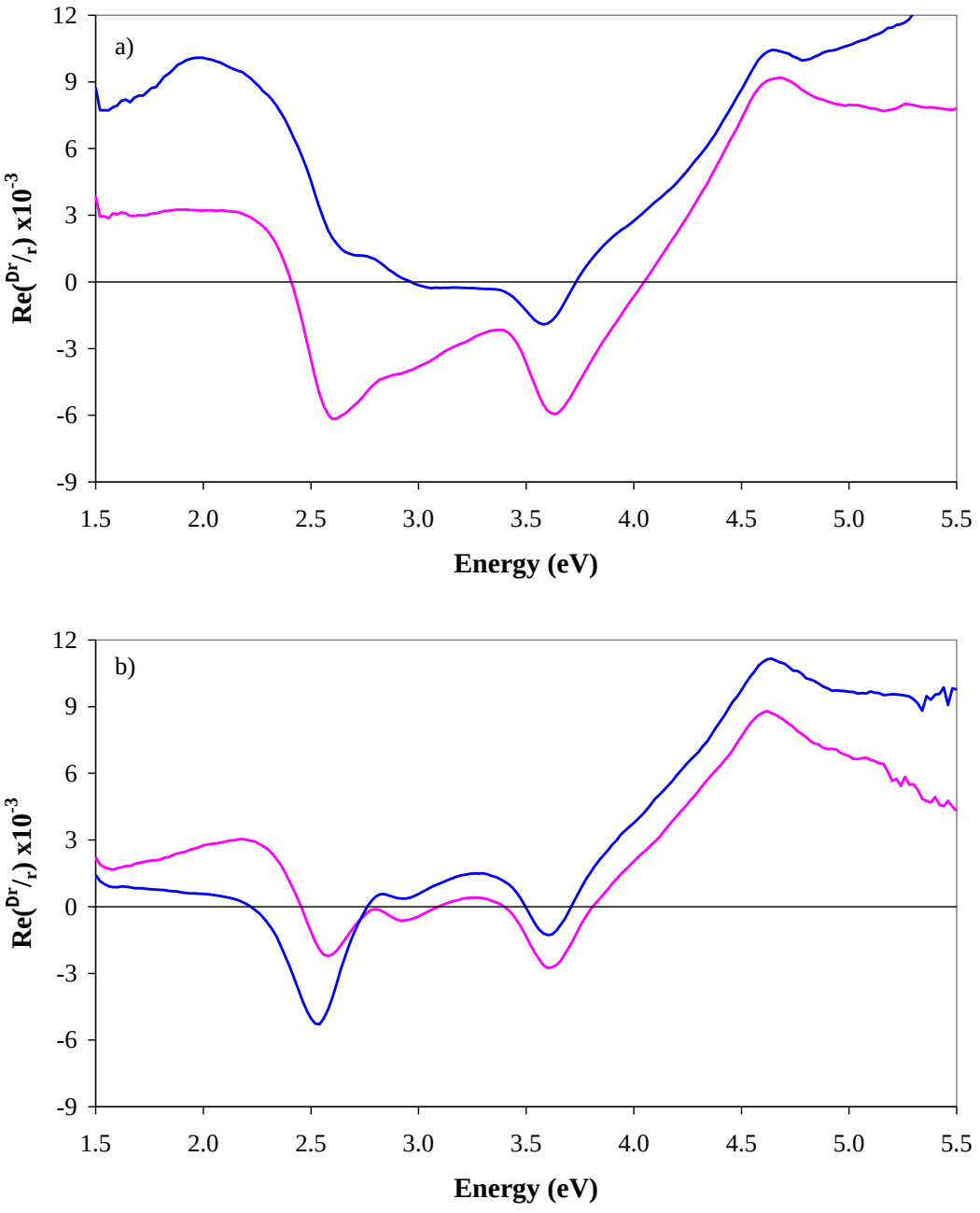

Figure 4.10: RA spectra of a) clean Au(110) at -0.652 V(blue line) and 0.056 V (pink line) and b) after the adsorption of full length CPR at -0.652 V (blue line) and 0.056 V (pink line) all recorded in 0.1 M NaH_2PO_4/K_2HPO_4 pH 7.1.

The RA spectra recorded after the adsorption of CPR (figure 4.9) can be considered as the product of RAS contributions from the Au(110) substrate and the adsorbed protein. The differences in RA spectral shape as a function of potential could therefore be attributed to changes in the orientation and conformation of the adsorbed CPR molecules and slight changes in the Au(110) surface structure. A deeper investigation into the effect of changing the potential is discussed in a later section of this chapter.

The changes induced in the RA spectra of Au(110) after the adsorption of CPR can be more clearly observed following the subtraction of the RA spectra of the clean Au(110) surface. The resultant RA spectra are considered to be the RAS contribution from the adsorbed CPR: this methodology has been used in previous RAS experiments following the adsorption of molecules onto the Au(110) surface [1-10]. RA spectra of CPR as a function of applied potential have been produced and are shown in figure 4.11. The RA spectra of CPR at negative potentials follow a very similar spectral profile, however a significant change in both spectral shape and intensity was observed at 0.056 V (figure 4.11). The main changes observed in the RA spectra of CPR at negative potentials saw a gradual positive shift in intensity with the softening of the 2.5 eV shoulder and slight shift of the small positive feature at 3.2 eV to 3.4 eV as the potential was changed in order from -0.652 V to -0.376 V. These slight variations in spectral shape observed between the negative redox potentials could be attributed to a change in conformation or orientation of the adsorbed CPR molecules. Significant changes in the RA spectral shape and intensity were observed across the full spectral range of CPR at 0.056 V as shown in figure 4.11. This large change in spectral shape observed at the applied potential of 0.056 V could be due to the Au(110) surface undergoing a reconstruction and causing a large change in the orientation of the adsorbed CPR molecules. However the adsorbed protein would be in a fully oxidised state at this potential and is expected to undergo a large change in conformation, with the adsorbed CPR molecules expected to adopt a more compact and rigid structure at this potential [14,15]. It is therefore possible that the large changes observed in the RA spectra of CPR at an applied potential of 0.056 V could be the result of a natural change in

conformation of the adsorbed CPR molecules, rather than a change in orientation induced by a surface reconstruction of the Au(110) substrate.

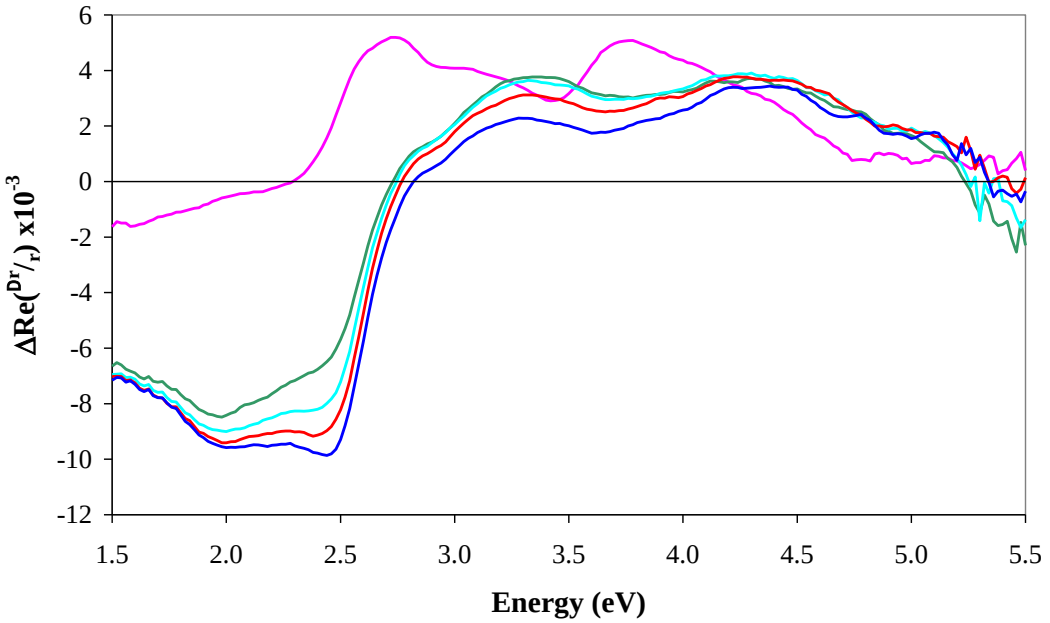

Figure 4.11: RA spectra of the P499C full length CPR in 0.1 M NaH_2PO_4/K_2HPO_4 pH 7.1 produced by subtraction of the RA spectra of Au(110) from Au(110) + P499C full length CPR at corresponding potentials , 0.056 V (pink line), -0.376 V (green line), -0.465 V (turquoise line), -0.557 V (red line) and -0.652V (blue line) vs SCE.

It has been shown in previous RAS studies that molecules adsorbed at the Au(110)/electrolyte interface can prevent the Au(110) surface from reconstructing [22]. Mansley *et al*. [22] showed that the adsorption of cytosine on the Au(110) surface in a (1×1) surface structure prevented the reconstruction to the (1×2) and (1×3) surface structures as the applied potential was changed. It is possible that the adsorption of CPR on the Au(110) surface causes a similar effect, freezing the Au(110) surface in the (1×3) reconstruction which is the surface structure at which the protein was adsorbed. This view is supported by the fact that there was no evidence of the RA spectral signature of the (1×1) surface structure at 0.056 V after the adsorption of CPR. To test this hypothesis figure 4.12 shows the effect of

subtracting the RA spectrum of Au(110) at -0.652 V from the spectra of Au + CPR at all the redox potentials, replicating the effect of a frozen (1×3) substrate surface. Following this subtraction the spectra of CPR at all potentials follow a very similar spectral profile, although changes in intensity are observed as a function of applied potential, with significant changes in the intensity observed at 0.056 V. The similarity of the spectra suggests that there is some evidence that the adsorption of the protein freezes the Au(110) surface at negative potentials. If the Au(110) substrate is frozen then the changes in RAS intensity as a function of applied potential observed in figure 4.12 could be attributed to a change in conformation or orientation of the adsorbed molecules. This is discussed further in later chapters.

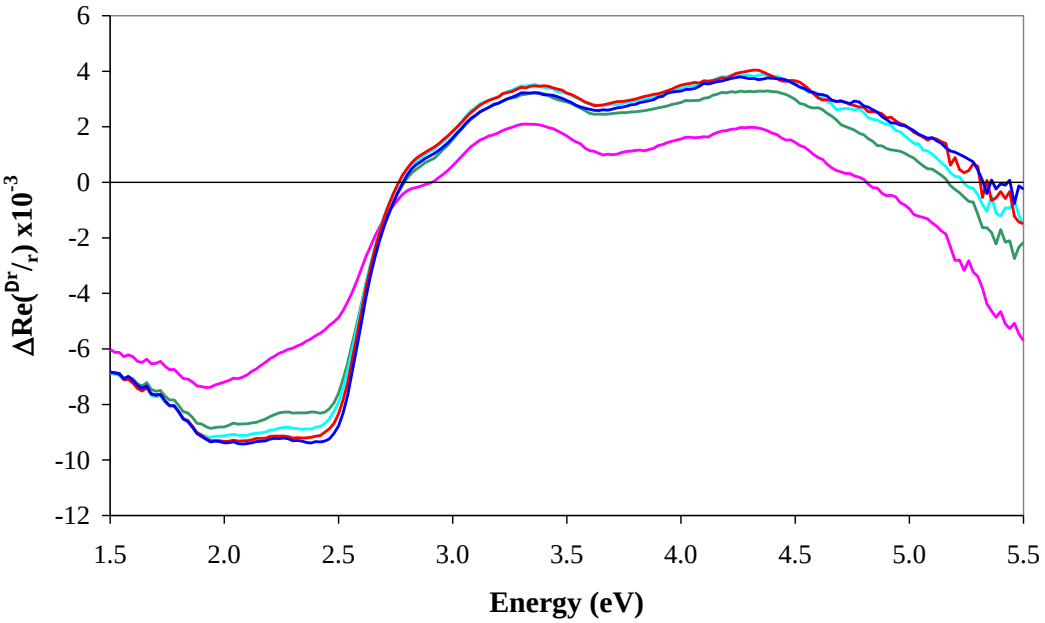

Figure 4.12: RA spectra of the P499C full length CPR in 0.1 M Na_2HPO_4/K_2HPO_4 pH 7.1 produced by subtraction of the RA spectra of Au(110) at -0.652 V from RA spectra of Au(110) + P499C full length CPR at all potentials, 0.056 V (pink line), -0.376 V (green line), -0.465 V (turquoise line), -0.557 V (red line) and -0.652V (blue line) vs SCE.

4.2.2 The Adsorption of Isolated P499C FAD Variant onto the Au(110) Surface

The isolated mutant FAD domain of the CPR protein which does not contain the FMN domain, was also adsorbed onto the Au(110) surface. This was achieved by following the same procedures used for the adsorption of the full length version of mutant CPR. Again the RAS intensity at 2.54 eV was monitored as a function of time during the adsorption of isolated FAD, as a signature of the formation of the Au-S bond. The RAS intensity at 2.54 eV during the adsorption of isolated FAD onto the Au(110) substrate in three separate experiments is shown in figure 4.13 and have been shifted on the *y*-axis for clarity.

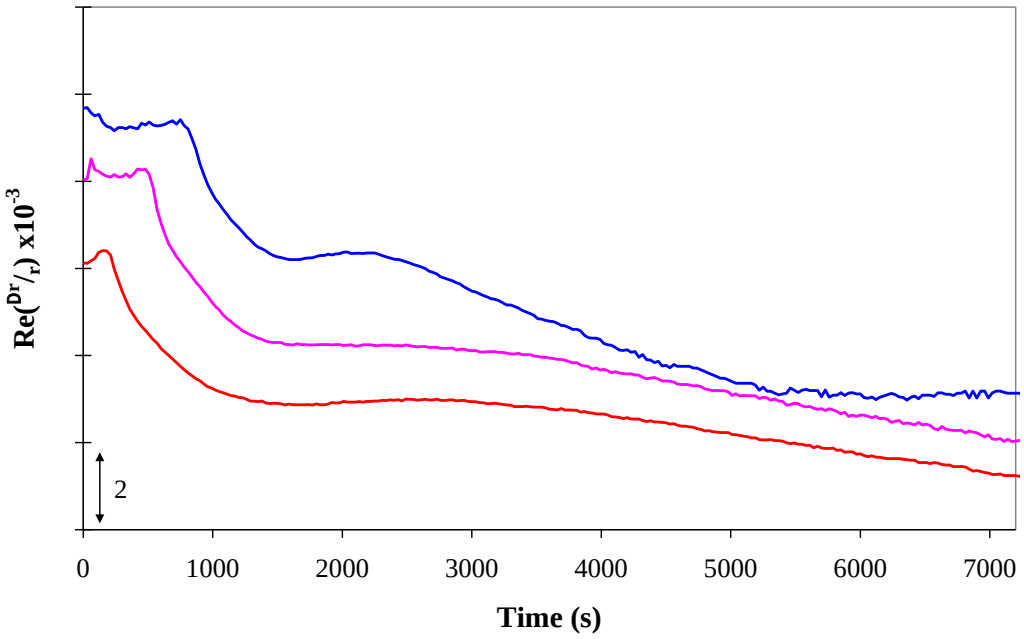

Figure 4.13: RAS intensity at 2.54 eV as a function of time measured during the adsorption of P499C FAD.

The FAD only variant of CPR was injected into the electrochemical cell at the applied potential of -0.657 V, inducing the fully reduced state of the protein and a (1×3) Au(110) surface structure. The intensity of the 2.54 eV peak was monitored

for 2 hours, similar to the adsorption of full length CPR. During this 2 hour period the RAS intensity reached a maximum and plateaued indicating that no more Au-S bonds were being formed and that a full coverage of protein on the Au surface had been achieved. The adsorption curves in figure 4.13 appear to follow a two stage adsorption process, where a fast initial negative increase in intensity is followed by a slower steadier increase in intensity. The two stages appear to be separated by a region in which the intensity remains constant. As with the adsorption dynamics of full length CPR, shown in figure 4.6, there are some differences in adsorption dynamics of FAD between experiments. The secondary increase in intensity is clearly greater in the blue curve (figure 4.13). The two stage adsorption process could be associated with the initial adsorption of the protein via the formation of Au-S bonds followed by a slower organisation process caused by interactions between the protein molecules.

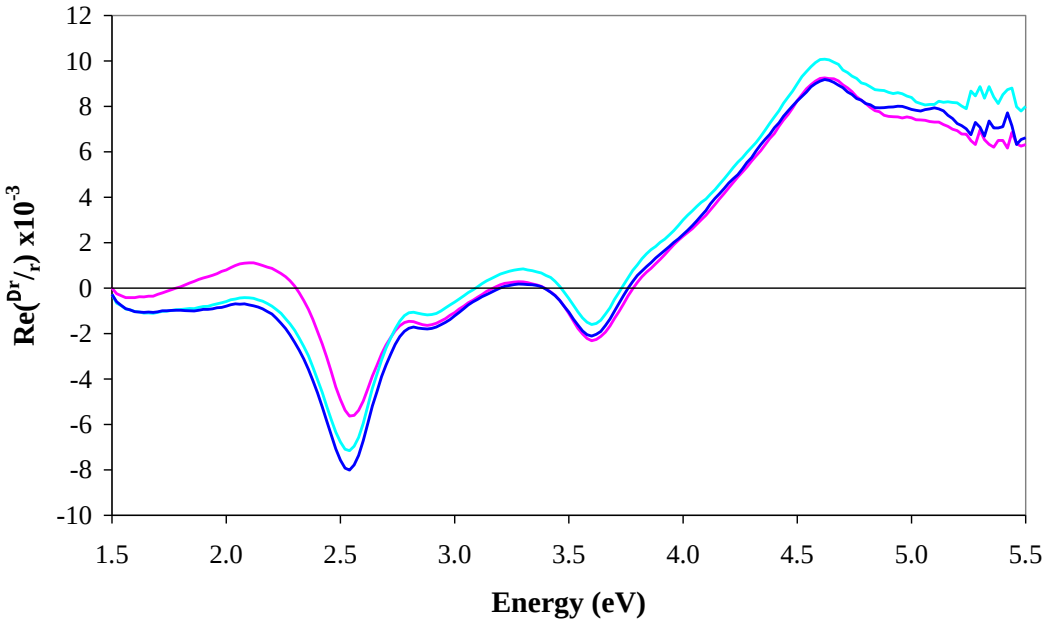

Figure 4.14: RA spectra of Au(110) + FAD at 0.056 V (pink line), -0.492 V (turquoise line) and -0.657 V (blue line).

RA spectra of the Au(110) + FAD produced at -0.657 V, -0.492 V and 0.056 V redox potentials follow a similar line shape. As the potential is changed

from -0.657 V to -0.492 V and finally to 0.056 V a decrease in intensity between 1.5 eV and 3.0 eV is observed whilst an increase in negative intensity between 3.0 eV and 5.5 eV is also observed, as shown in figure 4.14. The decrease in intensity is clearly observed at the lower energies and specifically at the 2.54 eV peak, whilst the increase in intensity in the higher energy regions is much more subtle.

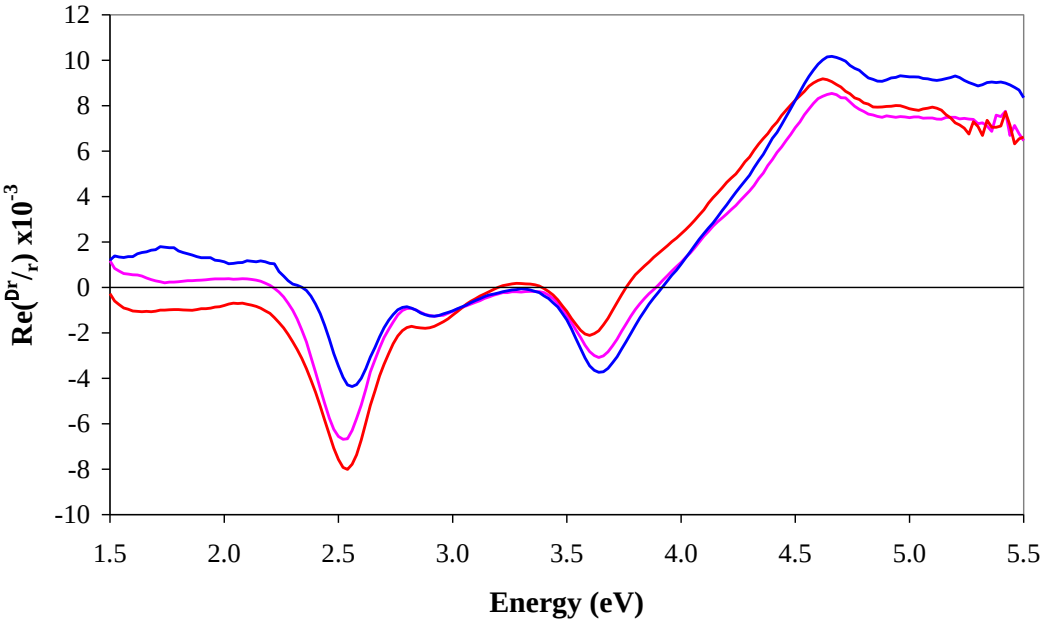

Figure 4.15: RA spectra of Au(110) + FAD at -0.657 V, data produced during 3 separate experiments completed over a 12 month period. The colours of the curves correspond to the same adsorption profile shown in figure 4.13.

The RA spectra shown in figure 4.15 were produced immediately after the adsorption of FAD onto the Au(110) surface and were recorded during the same experiments that gave rise to the adsorption spectra discussed earlier in figure 4.13. The RA spectral profiles shown in figure 4.15 were all recorded at -0.657 V and, although they follow a similar spectral shape, there are clear differences in the intensity of the features at 2.54 eV, 3.6 eV and 4.6 eV between each of the spectra. The differences in the intensity of these features could be due to slight variations in sample orientation or in the Au(110) surface structure between experiments, caused

during the flame annealing process. However the difficulty of producing consistent identical RA spectral profiles after the adsorption of FAD demonstrates the difficulty in achieving saturation coverage of adsorbed molecules on the Au(110) surface, which could account for the variation in intensities of features observed in the RAS shown in figure 4.15. The similarities between the RA spectra obtained after the adsorption of full length CPR and isolated FAD suggests that both variants of CPR adsorb in similar orientation on the Au(110) surface.

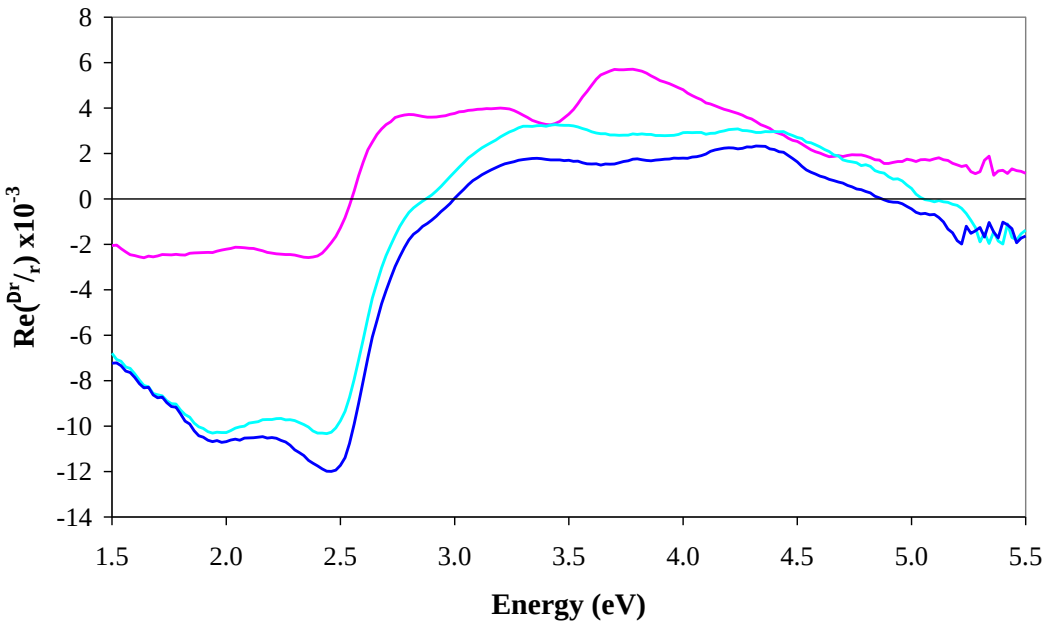

Figure 4.16: RA spectra of the FAD only variant CPR in 0.1 M NaH_2PO_4/K_2HPO_4 pH 7.1 produced by subtraction of the RA spectra of Au(110) from the RA spectra of Au(110) + P499C FAD CPR at corresponding potentials, 0.056 V (pink line), -0.492 V (turquoise line) and -0.657V (blue line) vs SCE.

Subtracting the RA spectra of Au(110) from the RA spectra of Au(110) + FAD reveals the RA spectra attributed to the isolated FAD variant of CPR: these spectra are shown in figure 4.16. The shapes of the two RA spectra produced at negative potentials are very similar to each other, with only a slight change in intensity observed. However after the potential was changed to the positive 0.056 V redox potential, a large change in spectral intensity and shape was

observed, as shown in figure 4.16. As with the full length CPR system the 0.056 V potential relates to the fully oxidised state of the protein as such the large change in spectral shape observed at this potential could be associated with a change in conformation of the adsorbed protein molecules. However the isolated FAD variant of CPR is expected to be less dynamic and is not expected to undergo large conformational events like those expected in the full length CPR system. As discussed after the adsorption of full length CPR in the previous section the 0.056 V applied potential is also known to induce a surface reconstruction of the clean Au(110) surface, and it is unclear if the adsorption of protein prevents the Au(110) substrate from reconstructing. Without this knowledge it is possible that the observed change in spectral shape at each potential (figure 4.16) could be attributed to the Au(110) surface reconstruction. On the other hand if the adsorption of FAD does prevent the Au(110) surface from reconstructing, then the difference between the spectra in figure 4.16 could be artificially exaggerated by the subtraction of the RAS of Au(110) in an anion induced (1×1) structure from the RAS of Au(110) + FAD at 0.056 V on a (1×3) substrate, making the majority of this subtraction the difference between an anion induced (1×1) and (1×3) surface structure with a small contribution from the adsorbed molecule.

The effect of a frozen substrate has been investigated by subtracting the RA spectrum of the clean Au(110) surface produced at -0.657 V from all the RA spectra of Au(110) + FAD produced at the applied potentials of -0.492 V, -0.657 V and 0.056 V (figure 4.17). The RA spectra of FAD produced after this subtraction all follow a very similar shape (figure 4.17). The largest change in intensity is observed between approximately 1.8 eV and 2.5 eV between the spectrum produced at 0.056 V and the spectra produced at the negative potentials -0.492 V and -0.657 V.

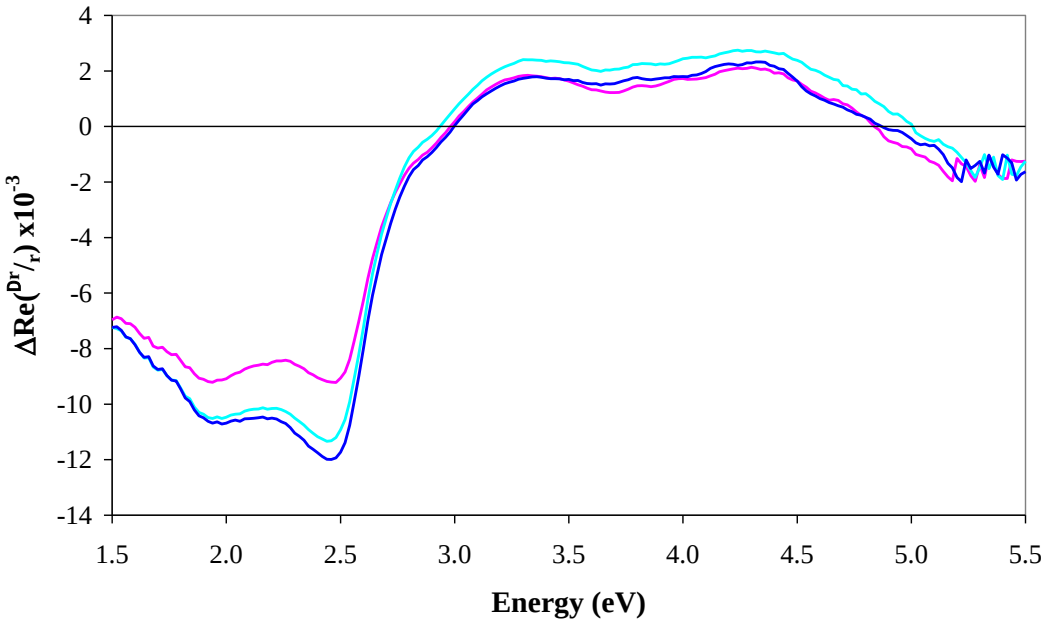

Figure 4.17: RA spectra of the FAD only variant CPR in 0.1 M $Na_2H_2PO_4/K_2HPO_4$ pH 7.1 produced following the subtraction RA spectra of Au(110) at -0.657 V from the RA spectra of Au(110) + P499C FAD CPR at all redox potentials, 0.056 V (pink line), -0.492 V (turquoise line) and -0.657V (blue line) vs SCE.

The similarity of RA spectra in figure 4.17 suggest that the adsorption of isolated FAD prevents the reconstruction of the Au(110) surface. This effect was also observed with the adsorption of the full length variant of CPR (figure 4.12) and is discussed in depth in a later chapter of this thesis.

4.2.3 Summary of the Adsorption of Variant CPR onto the Au(110) Surface

The work presented in the previous two sections of this chapter has demonstrated that both variant forms of CPR adsorbed in an ordered structure on the Au(110) surface and induce changes in the RA spectrum of the clean Au(110). Monitoring the intensity of the 2.54 eV peak as a function of time during the adsorption process suggests that the protein adsorbs onto the Au(110) surface via the formation of Au-S

bond formed between the thiol group of the mutant engineered cysteine in the protein, and the Au(110) surface[4,5,9]. The rate at which intensity of the 2.54 eV peak changed during the adsorption of full length CPR and isolated FAD appeared to vary between experiments (figures 4.6 and 4.13). These differences could be attributed to variations in the adsorption process, which may result in a difference in the coverage [9], orientation and alignment of the adsorbed molecules on the Au(110) surface between experiments. This is supported by differences in the RA spectra recorded immediately after the adsorption of CPR and isolated FAD observed between experiments, as shown in figures 4.8 and 4.15. The adsorption of a consistent ordered monolayer of protein on the Au(110) surface is an important prerequisite to monitoring conformational change in CPR, and has been investigated further using QCM-D. This is discussed in detail in a later chapter of this thesis.

4.3 Preliminary Investigation of the Effect of Switching the Applied Potential on the RAS of Adsorbed Protein

The difficulty in calculating the RAS of adsorbed molecules on surfaces from first principles prevents a fundamental interpretation of spectral features observed in RA spectra. Consequently the work discussed in this thesis concentrates on interpreting changes in the RAS which were induced by varying the applied electrode potential. Previous work by Messiha *et al.* [10] has already demonstrated the potential of the RAS technique as a real time monitor of conformational events in proteins. A similar approach to the one adopted by Messiha *et al.* [10] has been utilised in this work to interpret changes in RA spectra as a function of the applied electrode potential. Electrochemical techniques allow accurate control of the applied electrode potential which makes it possible to cycle the applied potential between the known redox potentials of the two CPR variants. The sensitivity of the RAS technique to dipole transitions means that changes in the orientation of adsorbed molecules is expected to induce changes in the RA spectrum. The intensity of dipole transitions observed in RA spectra is determined by the geometrical relationship between the direction of the dipole transition and the electric field vector (E) of the incoming

polarised light. Therefore changes in RA spectral features can be associated with a change in orientation of the adsorbed molecules provided there are no other influences on the spectral profile.

A range of interflavin electron transfer rates of CPR in solution have been measured using t-jump spectroscopy [11,15]. The relatively slow rates of 55 s^{-1} and 20 s^{-1} that were observed in that work suggest that the rate of interflavin electron transfer is limited by the rate of conformational change. UV-visible spectra of CPR from 300 to 700 nm (4.1 to 1.7 eV) produced from reduced and oxidised CPR in solution produced in anearobic stopped-flow diode array data by Brenner *et al.* [23] are shown in figure 4.16. Changes in the absorption spectra were induced by mixing stoichiometric amounts of NADPH to oxidised CPR [23]. The reduction of oxidised CPR molecules induced a large change in the UV-visible spectrum, between ~ 370 nm and 460 nm as shown in figure 4.18. The large change observed at 460 nm (2.7 eV) coincides with maximum absorption of the isoalloxazine rings [24-28]. As each flavin domain contains an isoalloxazine ring, and conformational events are expected to involve the relative motion of the two domains, monitoring changes in RAS intensity at 2.7 eV as a function of applied potential is expected to provide information on conformational events involving relative domain motion in CPR during electron transfer processes.

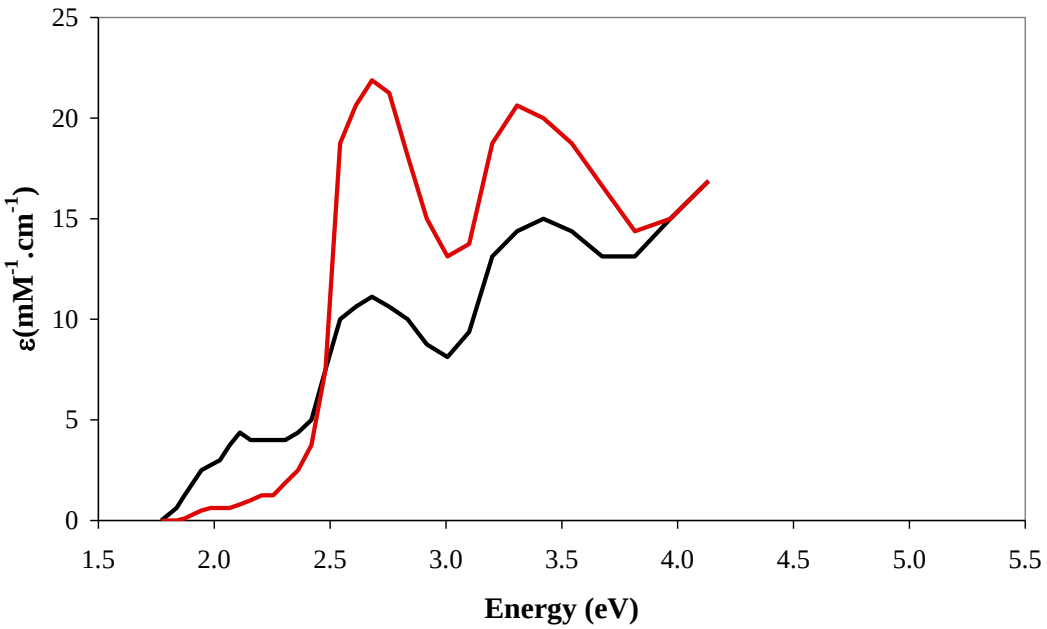

Figure 4.18: Absorbance spectra produced during stopped-flow experiments, where stoichiometric amounts of NADPH were mixed with oxidised CPR in solution. Absorbance spectra corresponding to oxidised (red line) and fully reduced (black line) CPR as shown in table 4.1. Data reproduced from [23].

After the adsorption of P499C full length CPR onto the Au(110) surface in a preliminary experiment, the applied electrode potential was cycled between the redox potentials of CPR. The electrode potential was changed every 60 seconds starting at the fully reduced potential of -0.652 V and then changed in order to -0.557 V, -0.465 V, -0.376 V and 0.056 V. The potential was then changed back down in reverse order to -0.652 V. The RAS intensity monitored at 2.7 eV as a function of these changes in the applied potential is shown in figure 4.19.

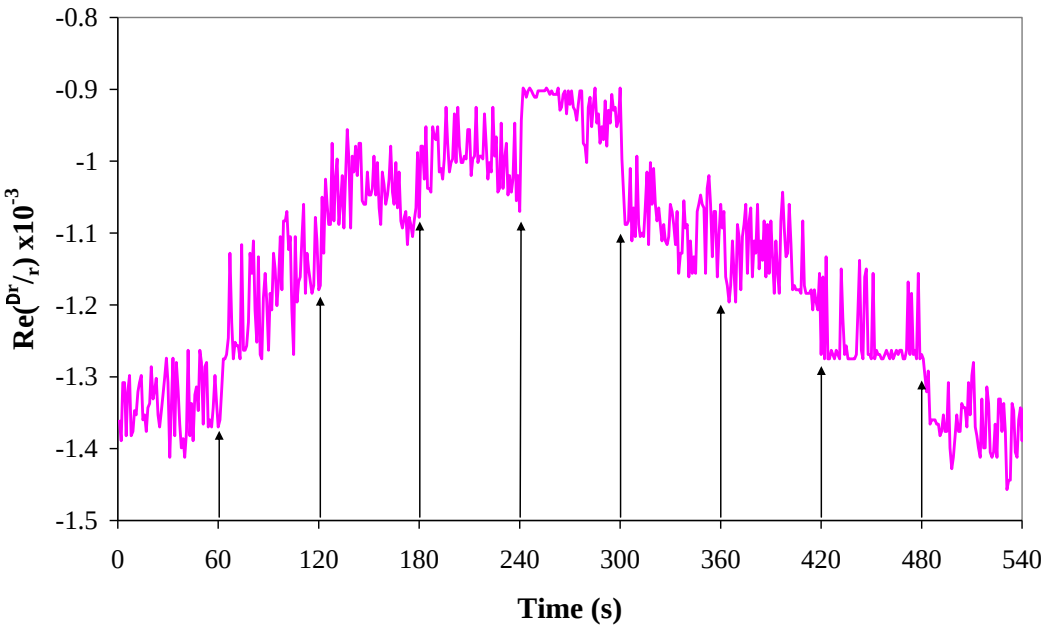

Figure 4.19: Changes in peak intensity of the RAS of Au(110) + full length CPR as a function of time recorded at 2.7 eV, as the potential is cycled through -0.652 V, -0.557 V, -0.465 V, -0.376 V and 0.056 V at 60 second intervals, marked by arrows.

The data in figure 4.19 is extremely noisy and determination of the absolute RAS intensity at each potential is difficult. However the RAS intensity appears to increase in steps which correspond to changes in the applied potential, the reverse change in RAS intensity is observed as the potential is cycled back through the redox potentials. This behaviour reveals that the RAS intensity changes in stages as the potential is changed, which is consistent with the idea that the adsorbed CPR molecules adopt several conformations on a fast time scale rather than a smooth continuous change in conformation between the fully reduced and oxidised states. Comparisons of the final and initial RAS intensity observed at an applied potential of -0.652 V (0-60 seconds and 480-540 seconds figure 4.19) appear to be very similar before and after stepping through all the redox potentials. This indicates that the reaction is reversible and that no permanent changes occurred during the oxidation and reduction of the adsorbed CPR molecules. However the RAS intensities at other potentials do not appear to show the same reversibility. For example the intensities at -0.376 V before and after the potential was changed to

0.056 V between 180-240 seconds and 300-360 seconds in figure 4.19 are clearly different. The RAS intensity increased by ~ 0.07 units as the potential was changed from -0.376 V to 0.056 V, whereas the reverse potential step saw the RAS intensity decrease by ~ 0.16 units. Clearly the direction of the potential step influences the observed change in RAS intensity. This could imply that, depending on the direction of the potential change, the CPR molecules adopt different conformations provided all other influences on the intensities are negligible.

The data in figure 4.19 demonstrates that there is a considerable amount of noise in the RAS response at 2.7 eV as a function of applied potential. To improve the signal to noise, the RAS intensity was monitored as the applied potential was stepped between two redox potentials every 60 seconds repeatedly. This allowed the RAS intensity obtained from several repeated potential steps to be averaged which significantly improved the signal to noise ratio. All possible combinations of potential steps were investigated initially before the potential step from -0.465 V to 0.056 V was chosen to be monitored as a function of repeated potential steps. This is a good choice for observing conformational events as this potential step induces a reversible two electron transfer process from the 2 electron reduced state at -0.465 V to the fully oxidised species of CPR at 0.056 V and is expected to be accompanied by a change in conformation. This potential step is also of interest as the -0.465 V potential induces the 2 electron reduced species of CPR which can exist in three possible redox states, as shown in table 4.1. An example of the observed changes in RAS as a function of the stepping between the applied potentials -0.465 V and 0.056 V is shown in figure 4.20. Several scans similar to the one shown in figure 4.20 were produced in each experiment to provide a sufficiently large data set from which the average change in RAS intensity can be obtained.

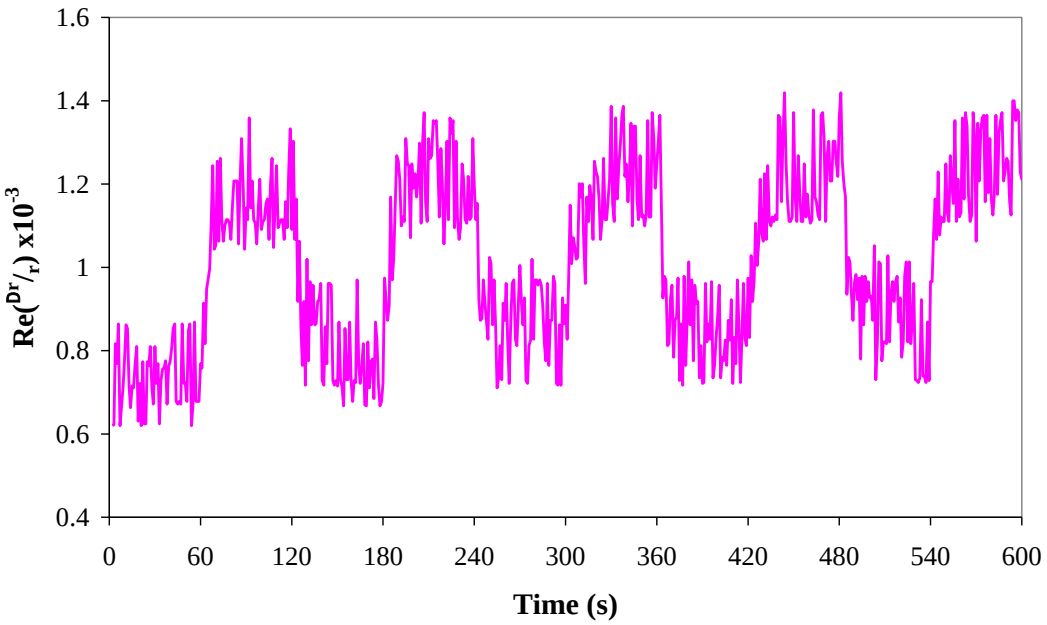

Figure 4.20: Change in RAS intensity of Au(110) + full length CPR at 2.7 eV, as a function of changing the applied potential between -0.465 V and 0.056 V every 60 seconds.

The RAS intensity as a function of this repeated potential step has been studied at two energies, 2.7 eV which corresponds to the isoalloxazine rings [24-28] and 2.54 eV which is associated with the Au-S bond [4,5,9]. The intensity was monitored at these energies during the potential steps for the clean Au(110) surface and following the adsorption of both full length CPR and isolated FAD. The data shown in figure 4.21 shows the average RAS intensity and a 5 point smoothing of this average at 2.7 eV and 2.54 eV as the potential was changed from -0.652 V to 0.056 V at 60 seconds for the clean Au(110) surface and after the adsorption of full length CPR and isolated FAD onto the Au(110) surface.

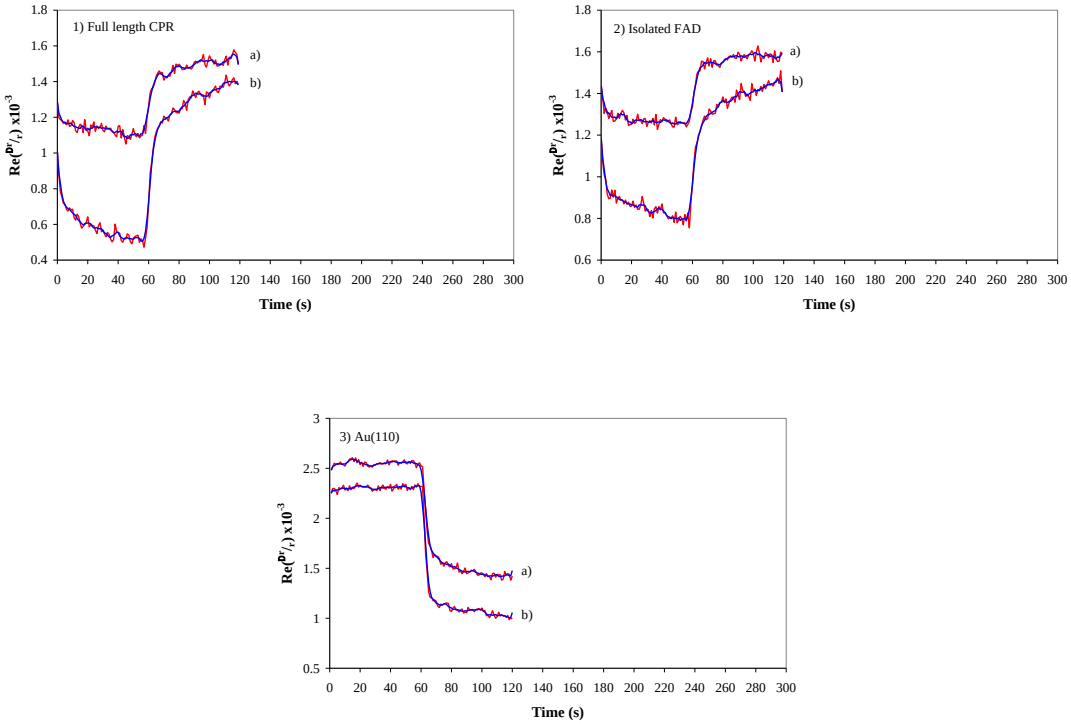

Figure 4.21: Average RAS intensity over 50 steps(red line) and the 5 point smoothed averaged (blue line) at a) 2.7 eV and b) 2.54 eV for 1) Au(110) + full length CPR, 2) Au(110) + isolated FAD and 3) the clean Au(110) surface as a function of stepping the potential from -0.465 V to 0.056 V at 60 seconds. The data in each chart have been shifted on the *y*-axis for clarity.

As the applied potential was changed to 0.056 V a rapid change in the RAS intensity was induced which reached a maximum after approximately 10 seconds. The RAS intensity increased in the positive direction after the adsorption of CPR and isolated FAD whereas a negative change in intensity was observed in the clean Au(110) data, as shown in figure 4.21. After the adsorption of full length CPR and isolated FAD the RAS intensity increased by a greater amount following the potential step at 2.54 eV than at 2.7 eV, as shown in all three graphs in figure 4.21. It is also clear from the data in figure 4.21 that changing the applied potential to 0.056 V induces a greater overall change in intensity in the RAS of clean Au(110), with a change of ~ 1.0 units observed in comparison with a ~0.5 to ~0.75 units change in intensity observed in the CPR and FAD data at each energy.

The adsorption of full length CPR and isolated FAD clearly alters the RAS response of Au(110) as a function of applied potential. It was hoped that these changes observed in the RAS intensity after the adsorption of protein would reveal information on conformational events associated with the electron transfer process. Since full length CPR is expected to be more dynamic than the isolated FAD molecule it is important to compare the RAS intensity after the adsorption of the two variants of CPR at 2.7 eV and 2.54 eV, as shown in figure 4.22.

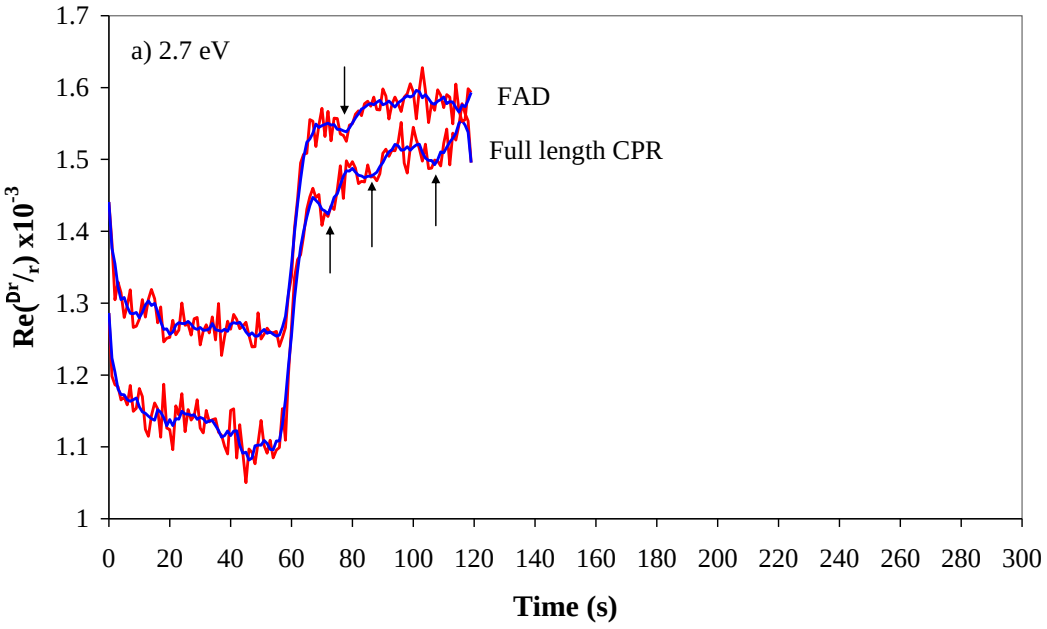

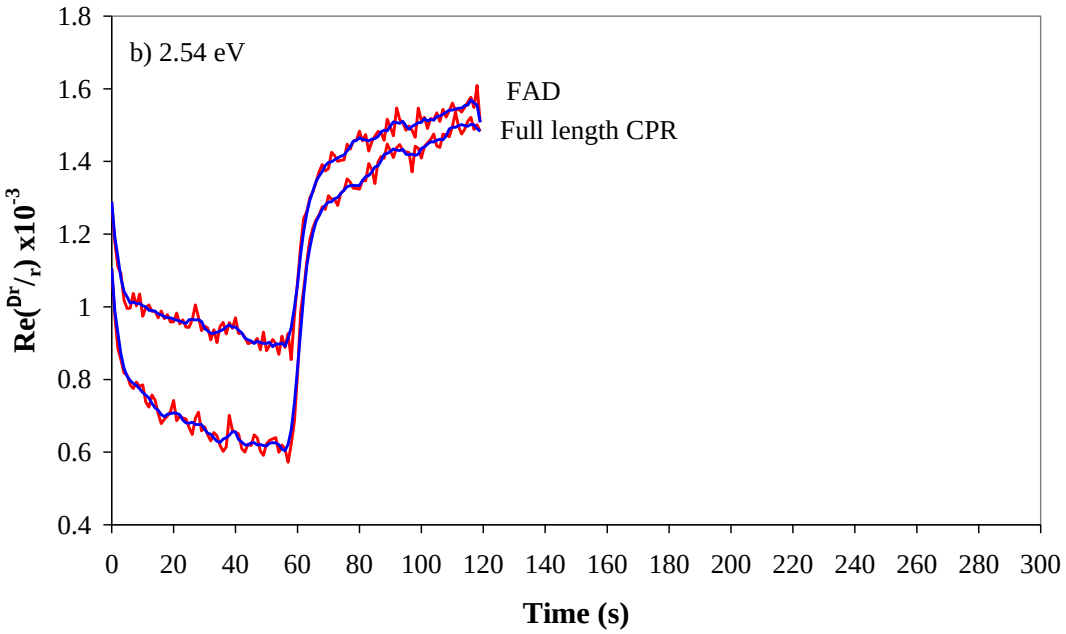

Figure 4.22: The average RAS intensity (red line) and 5 point smoothed average (blue line) as a function of stepping the applied potential from -0.465 V to 0.056 V for full length CPR and -0.492 V to 0.056 V for isolated FAD, monitored at a) 2.7 eV and b) 2.54 eV.

Following the adsorption of both variants of CPR a similar initial increase in intensity was observed as the potential was changed at both energies (figure 4.22). However differences in the RAS intensity after this initial increase have been observed. Three small negative features were observed in the full length CPR data at 2.7 eV, shown by the arrows in figure 4.22 a). These features were observed 5, 30 and 50 seconds after changing the potential to 0.056 V (figure 4.22 a). In the RAS intensity of FAD a similar intensity single negative feature was observed ~20 seconds after the potential was changed to 0.056 V at 2.7 eV as shown in figure 4.22 a). The RAS intensity at 2.54 eV, shown in figure 4.22 b) appears to follow a much smother change as a function of applied potential in comparison to the data produced 2.7 eV and does not appear to reveal any similar features with only a very slight possible feature observed in the full length CPR data at 2.54 eV. The observed difference in the RAS response following the potential step between 2.7 eV and 2.54 eV suggests that the features observed at 2.7 eV are local to that energy region and may be associated with changes in the orientation of the isoalloxazine rings. As

the FMN and FAD domains each contain an isoalloxazine ring then the changes observed in the RAS at 2.7 eV following the potential change may be associated with relative motions and changes in the orientation of the FMN and FAD. The observation of only a single feature in the FAD data and three features in the full length CPR data supports this association since the isolated FAD domain is expected to be less dynamic than the full length CPR molecule and the main conformational change is expected to involve the motion of the FMN domain about the rest of the protein.

Despite the possible association of these features with conformational events in the protein, it has not been possible to investigate this further due to the difficulty in reproducing the data. This difficulty in reproducing the data may be attributed to a variation in the coverage and orientation of the adsorbed protein molecules as suggested by the observed differences between experiments in the adsorption dynamics and subsequent RA spectra produced after the adsorption of CPR and FAD. In order to improve the reproducibility it was concluded that accurate control of the adsorption process is necessary to ensure that a well ordered monolayer of adsorbed molecules is achieved each time.

4.4 The Effect of Repeated Potential Steps on the RAS of Au(110) + Protein

As discussed in the previous section the signal to noise ratio was improved by monitoring the RAS intensity as a function of repeated potential steps and finding the average RAS intensity. Improvements to the computer software controlling the RAS instrument and the potentiostat were introduced during the process of collecting these data. The new software allowed the RAS and potentiostat, which were initially controlled separately, to be controlled simultaneously by one programme. Not only did this eliminate difficulties in synchronising the RAS instrument with the potentiostat but it also provided the user with accurate knowledge of the moment the potential was changed and also allowed the user to automatically repeat a user defined scan routine many times. This improvement to

the software allowed more data to be gathered other longer periods. This meant that the applied potential was frequently stepped overnight in an attempt to produce accurate data. However the effect of repeatedly stepping the potential between -0.652 V and 0.056 V and oxidising and reducing the adsorbed protein induced long term changes in the RAS of Au(110) + CPR. These changes induced as a result of repeated oxidation are shown in figure 4.23.

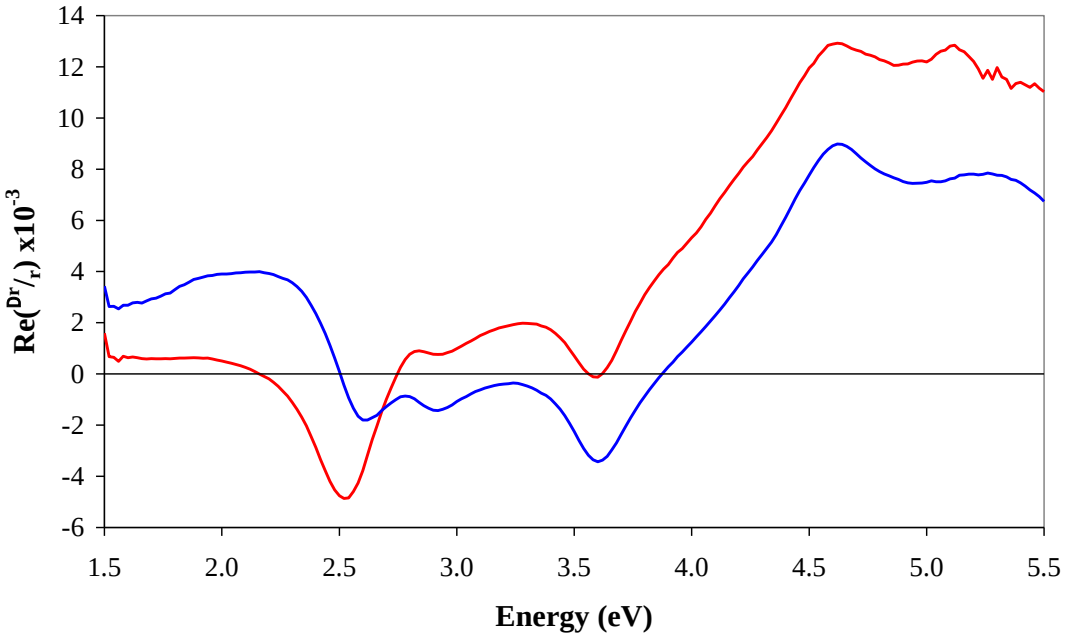

Figure 4.23: RA spectra of Au(110) + full length CPR at -0.652 V produced before stepping (red line) and after repeated overnight stepping between the applied potentials -0.652 V and 0.056 V (blue line).

The effect of repeatedly stepping the applied potential caused a decrease in intensity of the 2.54 eV peak and an increase in the 3.6 eV peak. As the intensity of a feature in the RA spectrum is a product of the intrinsic strength of the feature, the number of dipoles that give rise to the feature and the degree of anisotropy, the observed decrease in intensity of the 2.54 eV peak could arise from a reduction in the number of Au-S bonds [9]. The decrease in the number of Au-S bonds could be associated with desorption of CPR molecules from the Au(110) surface. The RA spectrum recorded at -0.652 V after overnight stepping of the potential shows a

remarkable similarity to the RA spectrum recorded at 0.056 V as shown in figure 4.24. The spectra in figure 4.24 follow a very similar shape, however the total intensities of the 2 spectra are different, and the 3.6 eV peak is more intense in the spectrum recorded at -0.652 V after stepping to the oxidised potential overnight. The similarities in RA spectral shape suggests that adsorbed CPR molecules could remain in the oxidised state after repeated potential steps between redox potentials, -0.465 V and 0.056 V.

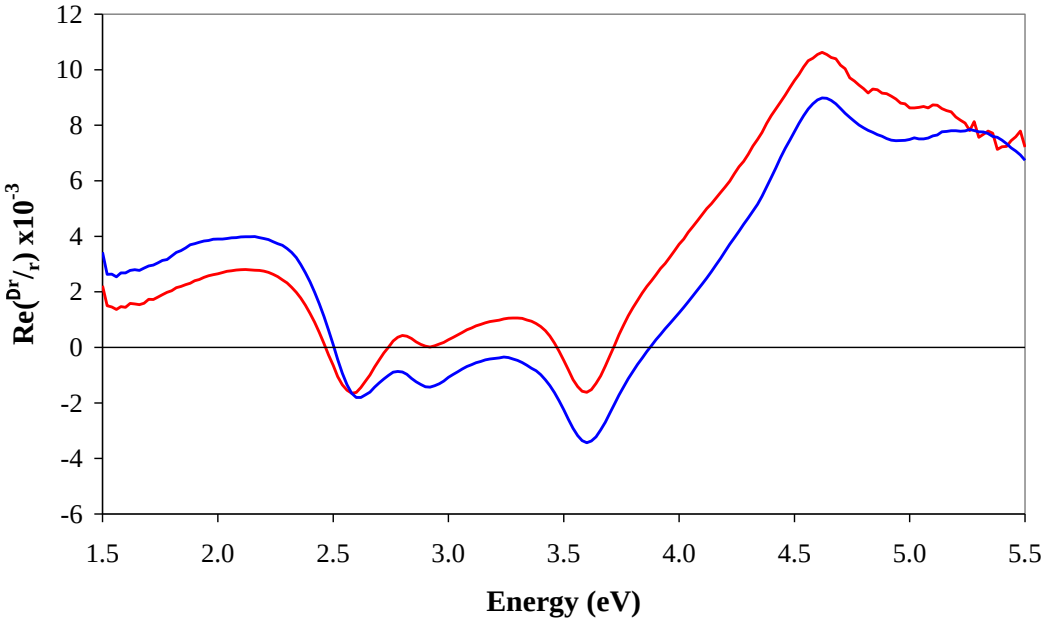

Figure 4.24: RA spectra of Au(110) + full length CPR at 0.056 V (red line) and at -0.652 V after repeated overnight stepping between the applied potentials -0.652 V and 0.056 V (blue line).

It is difficult to determine the origin of these RA spectral changes induced by the repeated potential steps. However the idea that the RAS spectral changes are a result of the desorption of the CPR molecules is not supported be previous experimental work by Leparc *et al.* [4] who showed that cysteine only started to desorb from the Au(110) surface at the applied potential of 0.6 V, which is significantly greater than the potential range explored during overnight stepping. It is possible that the observed RA spectral changes are associated with the protein

molecule denaturing as a function of repeated potential steps. If the protein structure is damaged it is possible that parts of the molecule could detach from the main structure of the protein. As a result of this is it might be expected that the RAS signal from the adsorbed protein may reduce, due to a decrease in coverage and anisotropy. This may also expose areas of the Au(110) substrate thus strengthening the RAS contribution from the Au(110) surface and inducing changes in the total RAS. If the protein molecule becomes denatured this may also prevent the protein from functioning, which may prevent the protein from changing conformation, which could explain how the CPR appears to remain in an oxidised state after repeated potential steps.

4.5 Summary of the Preliminary Data

This chapter has shown that both variant forms of CPR, full length and isolated FAD adsorbed onto the Au(110) surface and induce changes in the RA spectral shape. The resultant RA spectra produced for FAD and full length CPR are very similar in spectral shape and intensity, which considering the similarity of the two variants of CPR is not surprising. The RAS intensity at 2.54 eV was monitored as a function of time during the adsorption process. The intensity of this peak increased which is attributed to the formation of Au-S bonds and the adsorption of the CPR molecules on the Au(110) surface. The RAS intensity adsorption dynamics demonstrated that the adsorption of CPR may follow a two stage process. This also highlighted variations in the adsorption processes between experiments which was accompanied by differences in the resultant RA spectral shape after the adsorption of CPR.

A technique was developed for monitoring the RAS intensity as a function of repeated oxidation and reduction of the adsorbed CPR molecules. This involved producing large data sets to produce an average RAS intensity change in order to improve the signal to noise. Updated computer software was introduced which enabled simultaneous control of both the RAS instrument and potentiostat allowing automated repeat scans to be set up, which meant data could be generated over larger time scales and even overnight. The potential step experiments showed that

changing the applied potential between the redox potentials of both adsorbed CPR and isolated FAD molecules induced changes in the RA spectra. These changes are different to the induced spectral changes observed in the RAS of clean Au(110) after the same potential step. Monitoring these spectral changes at key energies has revealed features observed in full length CPR and FAD data which may be associated with conformational events linked to electron transfer processes. There are clear differences between the features observed in the data produced after the adsorption of CPR and isolated FAD. Three small features were observed in the CPR data following stepping the applied potential between -0.465 V and 0.056 V whilst one feature was observed from the isolated FAD system following stepping the applied potential between -0.492 V and 0.056 V. If these features are associated with conformational events in the protein, this difference would indicate a difference in protein dynamics of the isolated FAD and full length CPR protein. However reproducing the data has proved extremely difficult. This is probably associated with the observed variation in the adsorption dynamics which may result in different RAS responses depending on the coverage and orientation of the adsorbed molecules.

The effect of repeated oxidation and reduction of the adsorbed molecules has been shown to induce permanent changes in the RA spectral shape. These changes could be associated with the desorption of the protein molecules off the Au(110) surface or the protein becoming denatured. Again further analysis of this effect was difficult owing to the difficulty in reproducing the data.

4.6 References

[1] C. I. Smith, A. Bowfield, G. J. Dolan, M. C. Cuquerella, C. P. Mansley, D. G. Fernig, C. Edwards and P. Weightman, *J. Chem. Phys.* **130**, 044702 (2009)

[2] A. Bowfield, C. I. Smith, G. J. Dolan, M. C. Cuquerella, C. P. Mansley and P. Weightman, *e-J. Surf. Sci. Nanotech.* **7**, 225 (2009)

[3] A. Bowfield, C. I. Smith, C. P. Mansley and P. Weightman, *Phys. Status Solid. B.* **247**, 1937 (2010)

[4] R. LeParc, C. I. Smith, M. C. Cuquerella, R. L. Williams, D. G. Fernig, C. Edwards, D. S. Martin and P. Weightman, *Langmuir* **22**, 3413 (2006)

[5] B. Morozzo della Rocca, C. I. Smith, C. Teasuro, A. Desideri and P. Weightman, *Surf. Sci.* **604**, 2170 (2010)

[6] P. Weightman, G. J. Dolan, C. I. Smith, M. C. Cuquerella, N. J. Almond, T. Farrell, D. G. Fernig, C. Edwards and D. S. Martin, *Phys. Rev. Lett.* **96**, 086102 (2006)

[7] M. C. Cuquerella, C. I. Smith, D. G. Fernig, C. Edwards and P. Weightman, *Langmuir* **23**, 2078 (2007)

[8] C. P. Mansley, C. I. Smith, M. C. Cuquerella, T. Farrell, D. G. Fernig, C. Edwards and P. Weightman, *Phys. Status Solidi C* **5**, 2582 (2008)

[9] A. Bowfield, C. I. Smith, M. C. Cuquerella, T. Farrell, D. G. Fernig, C. Edwards and P. Weightman, *Phys. Status Solidi C* **5**, 2600 (2008)

[10] H. L. Messiha, C. I. Smith, N. S. Scrutton and P. Weightman, *Euro. Phys. Lett.* **83**, 18004 (2008)

[11] A. Gutierrez, L. Y. Lian, C. R. Wolf, N. S. Scrutton and G. C. Roberts, *Biochemistry* **40**, 1964 (2001)

[12] M. B. Murataliev, R. Feyereisen and F. A. Walker, *Biochim. Biophys. Acta* **1698**, 1 (2004)

[13] J. Ellis, A. Gutierrez, I. L. Barsukov, W. C. Huang, J. G. Grossmann and G. C. Roberts, *J. Biol. Chem.* **284**, 36628 (2010)

[14] S. Hay, S. Brenner, B. Khara, A. M. Quinn, S. E. Rigby and N. S. Scrutton, J. *Am. Chem. Soc*. **132**, 9738 (2010)

[15] A. Gutierrez, M. Paine, C. R. Wolf, N. S. Scrutton and G. C. Roberts, *Biochemistry* **41**, 4626 (2002)

[16] C. Xia, D. Hamdane, A. L. Shen, V. Choi, C. B. Kasper, N. M. Pearl, H. Zhang, S-C. Im, L. Waskell and J-J. P. Kim, *J. Biol. Chem*. **286**, 16246 (2011)

[17] V. Mazine, Y. Borensztein, L. Gagnon and P. Allongue, *Phys Status Solidi* A **175**, 311 (1999)

[18] B. Sheridan, D. S. Martin, J. R. Power, S. D. Barrett, C. I. Smith, C. A. Lucas, R. J. Nichols and P. Weightman, *Phys. Rev. Lett.* **85**, 4618 (2000)

[19] V. Mazine and Y. Borensztein, *Phys. Rev. Lett.* **88**, 147403 (2002)

[20] P. Weightman, C. I. Smith, D. S. Martin, C. A. Lucas, R. J. Nichols and S. D. Barrett. *Phys. Rev. Lett.* **92**, 199707 (2004)

[21] C. I. Smith, A. Bowfield, N. J. Almond, C. P. Mansley, J. H. Convery, P. Weightman, *J. Phys.: Condens. Matter* **22**, 392001 (2010)

[22] C. P. Mansley, C. I. Smith, A. Bowfield, D. G. Fernig, C. Edwards and P. Weightman, *J. Chem. Phys.* **132**, 214708 (2010)

[23] S. Brenner, S. Hay, A. W. Munro and N. S. Scrutton, *FEBS Journal* **275**, 4540 (2008)

[24] M Sun, T. A. Moore and P. –S. Song, *J. Am. Chem. Soc*. **94**, 1730 (1972)

[25] W. A. Eaton, J. Hofrichter, M. W. Makinen, R. D. Andersen and M. L. Ludwig, *Biochemistry* **14**, 2146 (1975)

[26] L. B. -A. Johansson, A. Davidson, G. Lindblom and K. R. Naqvi, *Biochemistry* **18**, 4249 (1979)

[27] T. Climent, R. González-Luque, M. Merchán and L. Serrano-Andrés, *J. Phys. Chem. A* **110**, 13584 (2006)

[28] M. Salim, U. Siddiqui, G. Kodali and R. J. Stanley, *J. Phys. Chem. B* **112**, 119 (2008)

Chapter 5

Controlling the Formation of a Monolayer of Cytochrome P450 Reductase onto the Au(110) Surface

This chapter describes the use of the quartz crystal microbalance with dissipation (QCM-D) technique to study the adsorption process of cytochrome P450 reductase onto the Au(110) surface. The chapter establishes the conditions necessary to control the adsorption of a monolayer of protein molecules onto the Au(110) surface. These conditions are then examined using atomic force microscopy (AFM) and reflection anisotropy spectroscopy (RAS) to establish the RA spectrum of a monolayer of cytochrome P450 reductase (CPR) adsorbed onto the Au(110) surface.

5.1 The Adsorption of Variant CPR onto Au Substrate Monitored Using QCM-D

The previous chapter has demonstrated the difficulty in accurately reproducing RA spectra after the addition of cytochrome P450 reductase (CPR) onto the Au(110) surface. These inconsistencies in the RA spectra produced in chapter 4 have been associated with variations in the adsorption process. This chapter explores the use of other techniques to further understand and control the adsorption process.

Quartz crystal microbalance with dissipation (QCM-D) is an extremely sensitive technique used to measure the mass of adsorbed molecules on a quartz crystal. Accurate measurements of the frequency (*f*) and dissipation (*D*) following the adsorption of material onto a crystal surface allow the thickness of the adsorbed layer of material to be calculated [1]. This information along with knowledge of the dimensions of the individual molecules can provide information on the orientation of adsorbed molecules on the substrate surface.

The CPR molecules are expected to attach via the mutant cysteine at position 499, shown by the red sphere in figure 5.1. The dimensions of the two variant forms of CPR have been deduced from the crystal structure of rat CPR [2] and are 5.9 nm, 5.2 nm and 5.1 nm with 5.9 nm referring to the vertical dimension in figure 5.1. Considering that adsorbed CPR molecules are dynamic and may adopt a variety of orientations on the surface a layer thickness of 6 to 7 nm has been considered to represent a monolayer of adsorbed protein.

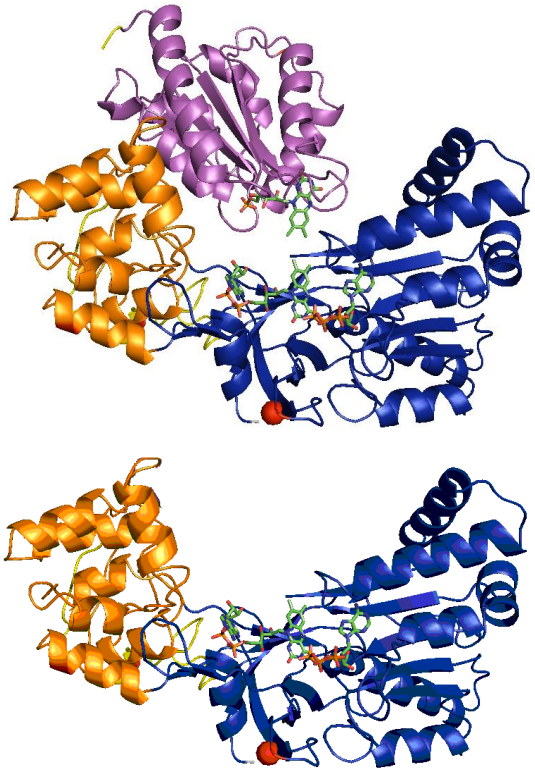

Figure 5.1: Molecular graphics ribbon diagram representation for the structure of cytochrome P450 reductase, (top diagram) and the isolated FAD/NADPH-domain (lower diagram). The Pro-499 residue that was targeted by site directed mutagenesis to produce the P499C variant is shown by the red sphere. The FMN-binding domain is shown in purple, the conecting domain in orange, and the FAD/NADP-domain in blue. The FAD and FMN cofactors are shown as green sticks.

5.2 Experimental

The QCM-D technique has been described in detail previously in chapter 2.5. Polycrystalline Au coated crystals were placed in the temperature controlled E4 module which was maintained at 20 °C during all QCM-D experiments reported in this thesis. Ultra pure water was then pumped over the sensors until a steady trace for both frequency and dissipation was obtained, this was then repeated with buffer solution to produce a baseline before a known concentration of protein solution was pumped over the sensors. Once a steady trace for both *f* and *D* was obtained for the

protein solution the sensors were then rinsed with fresh buffer solution to rinse off any excess protein.

5.2.1 Preliminary Experiment

The initial QCM-D experiments used the same conditions as those in the preliminary RAS studies reported in chapter 4. The adsorption of CPR onto polycrystalline Au coated quartz crystals was monitored under potential control and via self assembly. In both cases it took ~ 16 hours to achieve a steady trace for both (*f*) and (*D*) after the addition of CPR. The frequency and dissipation values were used to estimate the adsorbed layer thicknesses [3-5] which were 40 nm for potential control and 45 nm for self assembly adsorption. This layer thickness relates to a height of almost ten times higher than that of the individual CPR molecules and therefore it was considered that a multilayer of CPR molecules had been adsorbed onto the substrate surface rather than the desired monolayer. Each of these preliminary experiments indicates that the protein adsorbs in a similar manner whether under potential control or via self assembly, and multiple layers of CPR adsorbed in each case.

This indicated that the adsorption of a monolayer of CPR is complex and does not follow a similar adsorption process to that observed in previous RAS experiments [6-11]. The observed similarity between the adsorption of CPR via self assembly and under potential control implies that applied potential does not strongly influence the adsorption of CPR onto the polycrystalline Au surface. Further experiments were monitored using self assembly as this allowed the E4 module with four sensors to be used. This increased the number of experiments and range of variable that could be investigated during each experiment.

The adsorbed layer of CPR molecules achieved in the preliminary QCM-D experiments was significantly thicker than a monolayer of CPR molecules, which suggests that the concentration of protein used was too high to produce a monolayer of adsorbed protein. An initial investigation into the effect of concentration found significant differences in the estimated layer thickness when using similar concentrations of protein. Subsequently it was shown that the pH of the buffer

fluctuated between experiments considerably. It was therefore assumed that both protein concentration and pH of the buffer solution affect the adsorption of CPR onto the polycrystalline Au surface and careful control of both these was necessary.

5.2.2 Controlled Experiments

The preliminary data which saw the adsorption of a protein layer many times thicker than the individual dimensions of a single CPR molecule, demonstrated how protein molecules can aggregate which can result in the formation of multilayers adsorbed on surfaces. It is also assumed to be unlikely that every protein molecule would adsorb via the Au-S bond in an adsorbed layer of that thickness. This suggests that protein-protein interaction can allow further layers to adsorb on top of each other. It is therefore important to minimise protein-protein interactions during the adsorption process.

Controlled QCM-D experiments focused on finding the conditions for monolayer adsorption of full length CPR: the same conditions would later be tested on the adsorption of the isolated FAD variant of CPR. The experimental procedure was subsequently altered to follow a more systematic approach. The concentration of CPR was monitored closely as was the pH of the buffer. The protein concentration was calculated after each experiment using UV-Visible spectroscopy (Genesys 10 Bio, Thermo Scientific).

As with the preliminary QCM-D experiments a steady trace for both (f) and (D) was obtained. This baseline trace was recorded for 2 minutes before the protein samples were pumped over the sensors at a rate of 100 µl/min which was then reduced after 5 minutes to 10 µl/min. The protein samples were pumped over the sensors at the lower pump rate for a further 25 minutes the cell was then rinsed thoroughly with pure buffer solution for an hour after the adsorption of CPR. It was hoped that this rinsing would remove any excess protein molecules that have not formed a strong Au-S bond with the substrate surface.

5.3 QCM-D Results for Adsorption of Full Length CPR

The change in resonant frequency is related to changes in the mass of the sensor due to the adsorption of protein [12]. The changes in dissipation are a measure of all the mechanisms that dissipate energy during one period of oscillation [4]. The origin of dissipative changes following the adsorption of protein have been studied in detail by F. Hook *et al.* [4] who concluded that there are several causes of dissipative loss due to the viscosity of the adsorbed layer. Monitoring the *D*-shifts allows an accurate calculation of the layer thickness, taking into account the viscosity and mass of the adsorbed layer.

The adsorption of P499C full length CPR in pH 7.0 buffer solution is indicated by the observed changes in (*f*) and (*D*) as shown in figure 5.2. The bottom pink curve is the result of frequency changes and the top blue curve is the result of changes in the dissipation. Both the frequency and dissipation changed quickly over the first 5 minutes after the addition of protein and then followed a steady trace for the remainder of the scan with only slight fluctuations in the dissipation observed.

The data in figure 5.2 show the frequency and dissipation changes induced after a 0.18 μM concentration of protein was pumped over the sensor, this concentration of protein is similar to the concentration used in the preliminary experiments discussed in chapter 4. These frequency and dissipation values resulted in a calculated adsorbed layer thickness of 7.4 nm, which was considered a monolayer of CPR. The frequency and dissipation profiles in figure 5.2 indicates that the protein adsorbs quickly into a monolayer and does not take 16 hours as observed in the preliminary QCM-D data. This also indicates that once the monolayer has formed there is no secondary adsorption process of further layers.

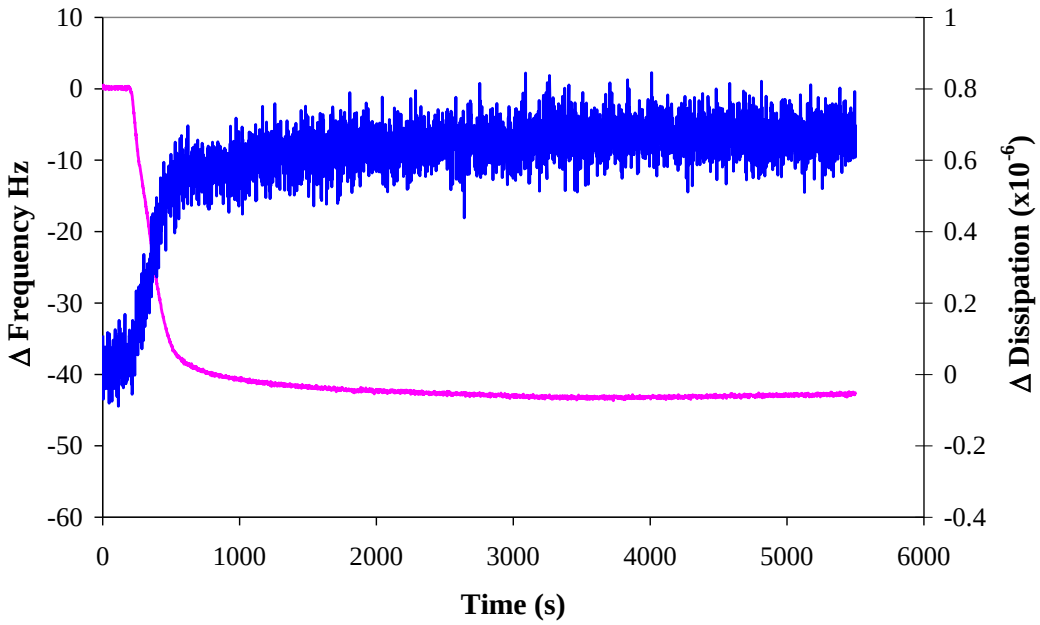

Figure 5.2: Change in frequency (pink curve) and dissipation (blue curve) as a function of time during the adsorption of P499C full length CPR in 0.1 M buffer solution pH 7.0.

The data in figure 5.3 was produced after increasing the protein concentration above 0.18 μM. Increasing the protein concentration resulted in a calculated layer thickness of ~12 nm which is approximately double the height of the individual CPR molecule and therefore showed that a bilayer of CPR had adsorbed onto the polycrystalline substrate. In this case the adsorption process follows a similar shape as observed in figure 5.2, where the *f* and *D* changed rapidly over the first 1000 seconds and then levelled out to an almost steady trace for the remainder of the scan. This indicated that a bilayer and monolayer form over a similar timescale and bilayer adsorption does not appear to consist of two separate processes. The overall change in frequency and dissipation is greater after the adsorption of a bilayer of CPR as shown in figure 5.3.

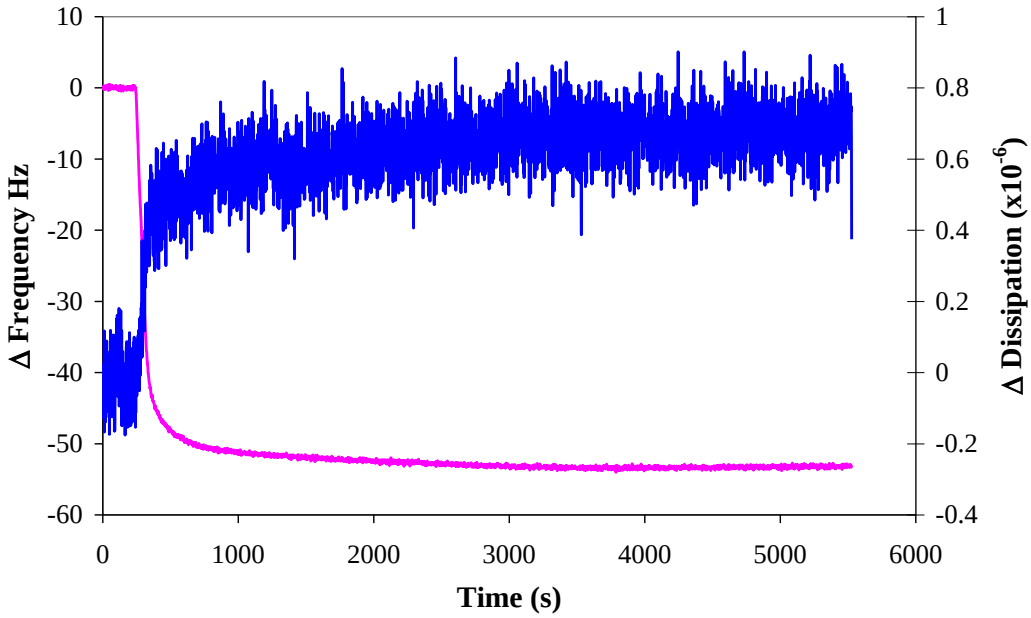

Figure 5.3: Change in frequency (pink curve) and dissipation (blue curve) as a function of time during the adsorption of P499C full length CPR in 0.1 M buffer solution pH 7.0.

The effect of varying the concentration of protein was initially investigated using pH 7.0 buffer. The data in figure 5.4 shows the adsorbed layer thickness as a function of protein concentration. This demonstrates that a monolayer is formed at a very low concentration of CPR, and that a slight increase in protein concentration causes a bilayer to adsorb. This behaviour suggests that adsorption of a monolayer is extremely dependent on the protein concentration. The concentration of protein needed to produce a monolayer of CPR is very low, and would potentially prove difficult to achieve in the electrochemical cell during RAS experiments. The concentration is so low that it is close to the limit of being detectable in the UV-Vis spectrometer, which makes it very difficult to measure concentrations of protein lower than the one that produced a monolayer. This difficulty is compounded by the slight difference between the concentration needed to produce a monolayer and bilayer of adsorbed CPR. It was therefore deemed very difficult to control the formation of a monolayer at pH 7.0 and it was decided to investigate the effect of varying the pH of the solution.

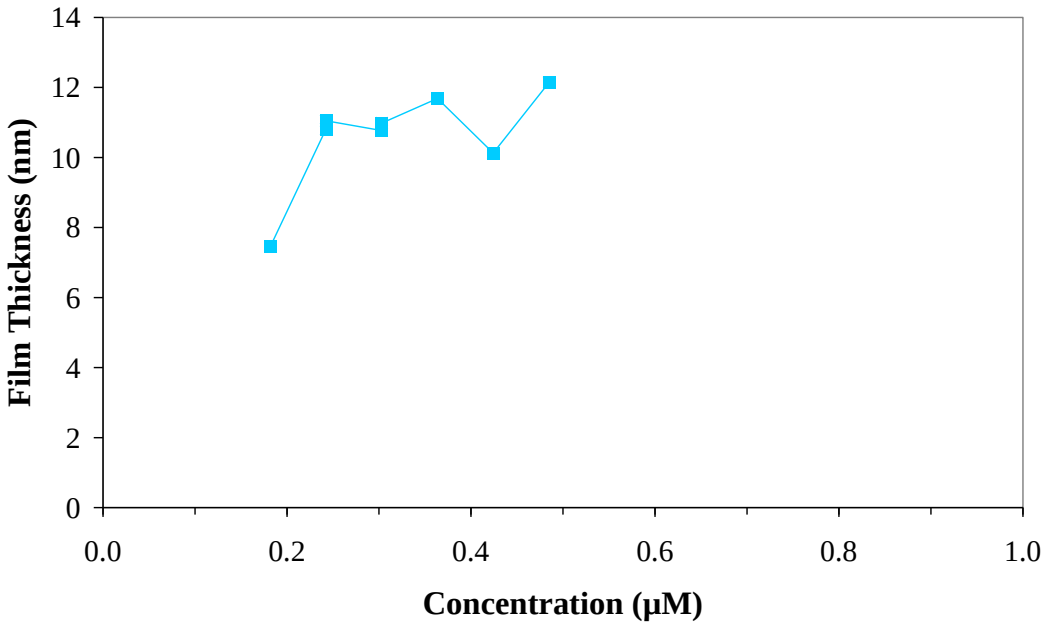

Figure 5.4: Film thickness as a function of P499C full length CPR concentration in 0.1 M NaH_2PO_4/K_2HPO_4 at pH 7.0.

5.3.1 The Effect of pH and Concentration on the Formation of a Bilayer and Monolayer of P499C Full Length CPR

The pH range that has been investigated was from pH 6.2 to pH 7.8, which allowed a thorough investigation of the effects of pH whilst still remaining within the range of the phosphate buffer system and so preventing the need to change buffer systems. The same experimental procedures were used as with the experiments in pH 7.0 buffer solution, with the same pump rates and same procedure of rinsing with pure buffer after the adsorption of CPR molecules.

The variation of pH of each buffer solution investigated has shown a similar effect of concentration on the adsorbed layer thickness and the adsorption appears to follow the same process where a rapid shift in both *D* and *f* was observed over the first 1000 seconds, after which a steady trace for both frequency and dissipation was observed, indicating that CPR adsorbs rapidly at either a monolayer or bilayer coverage. The concentration at which a monolayer is formed, however, has been

shown to fluctuate as a function of the pH value of the buffer solution. The following figure shows the calculated film thickness as a function of concentration produced in phosphate buffer solution with varying pH values.

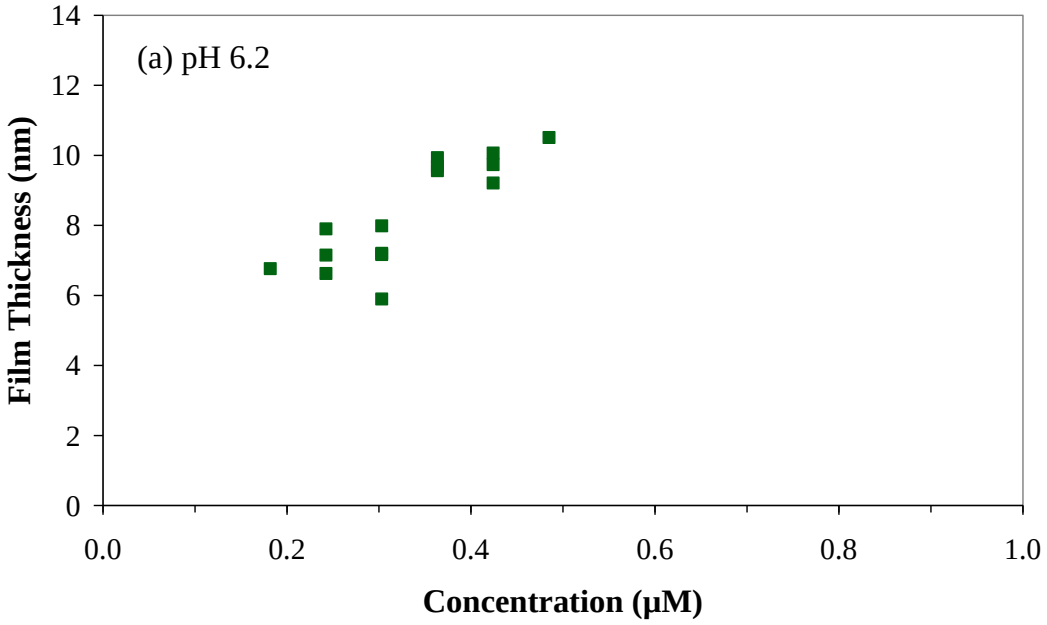

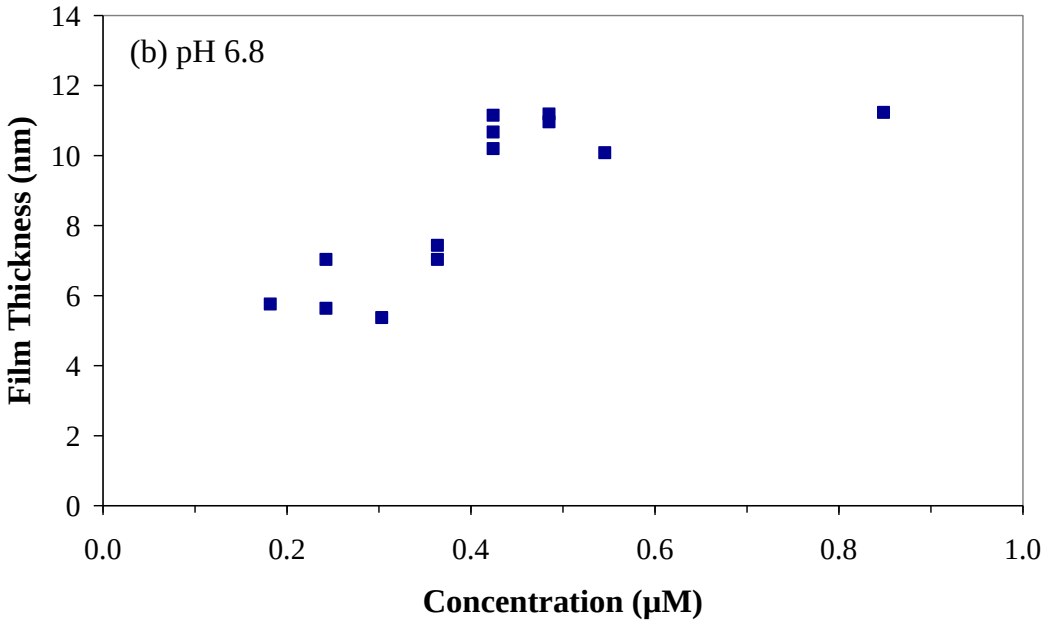

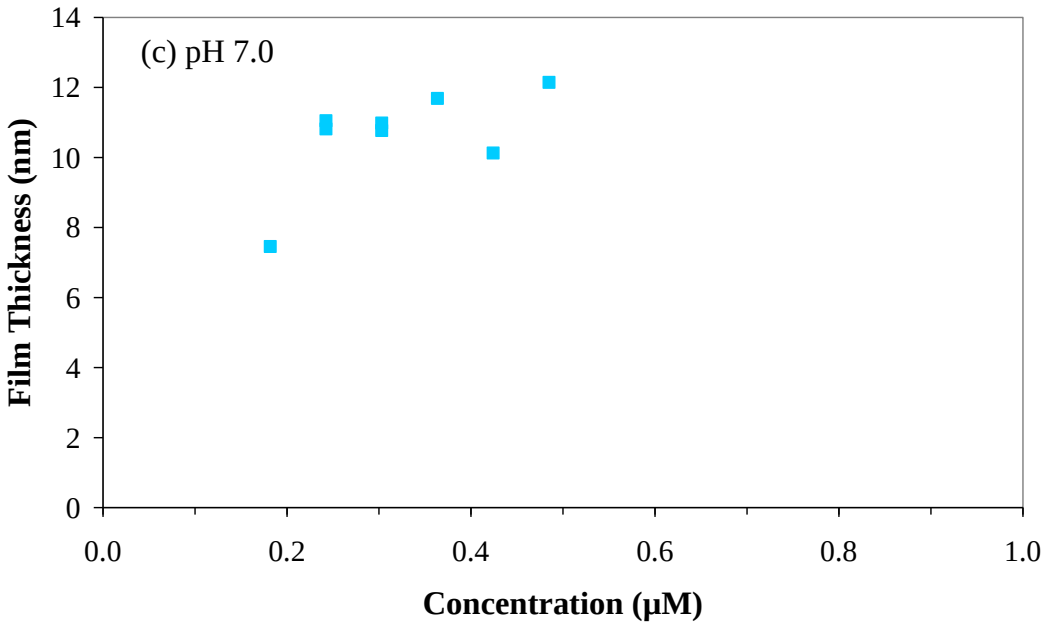
(c) pH 7.0
Film Thickness (nm)
Concentration (μM)
0
2
4
6
8
10
12
14
0.0
0.2
0.4
0.6
0.8
1.0

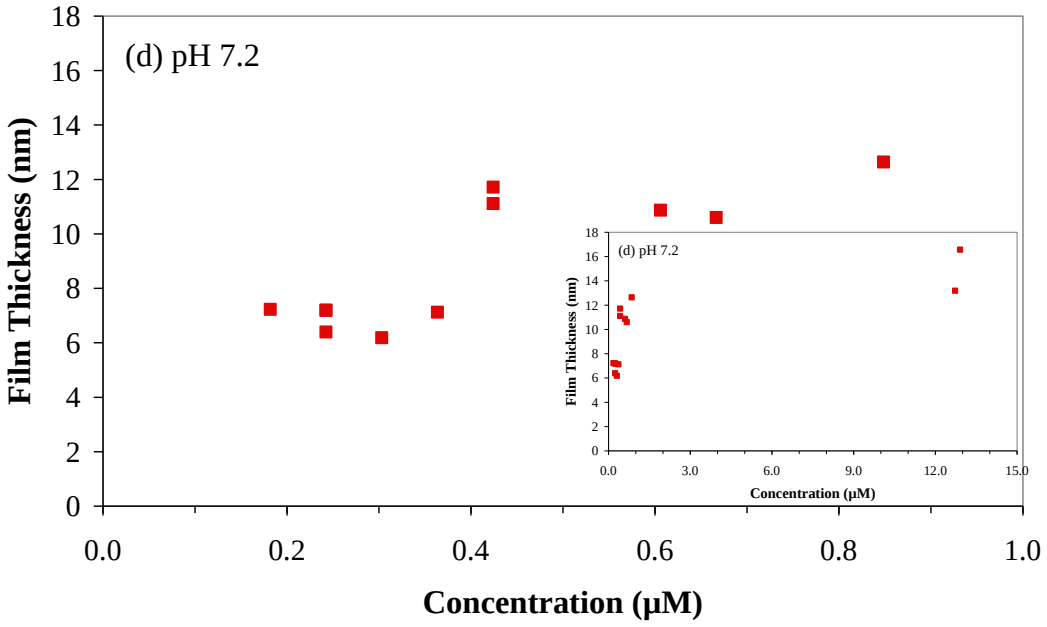
(d) pH 7.2
Film Thickness (nm)
Concentration (μM)
0
2
4
6
8
10
12
14
16
18
0.0
0.2
0.4
0.6
0.8
1.0
(d) pH 7.2
Film Thickness (nm)
Concentration (μM)
0.0
3.0
6.0
9.0
12.0
15.0

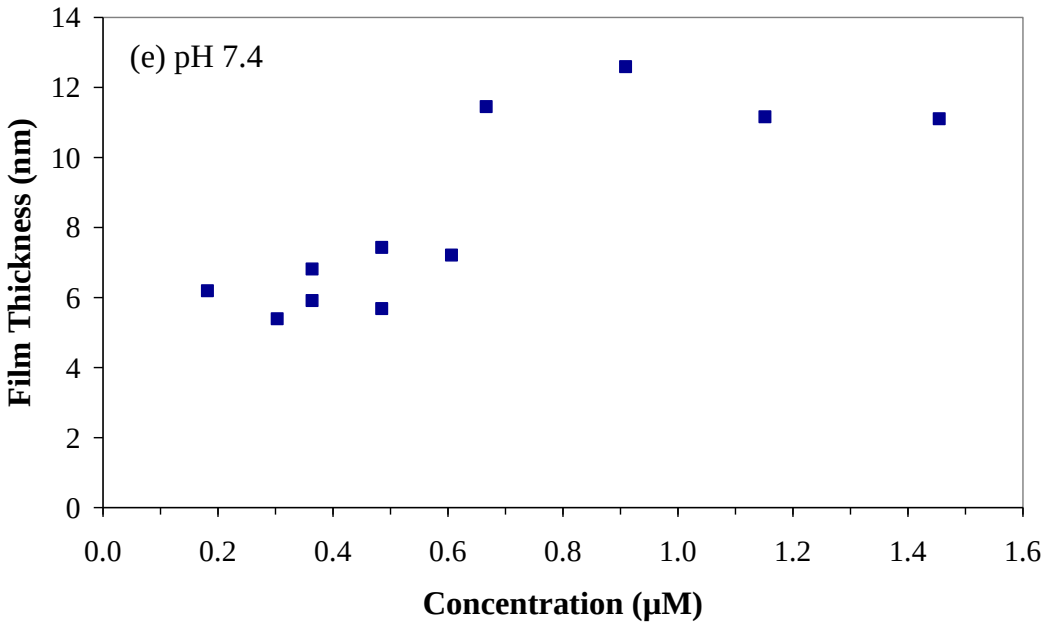

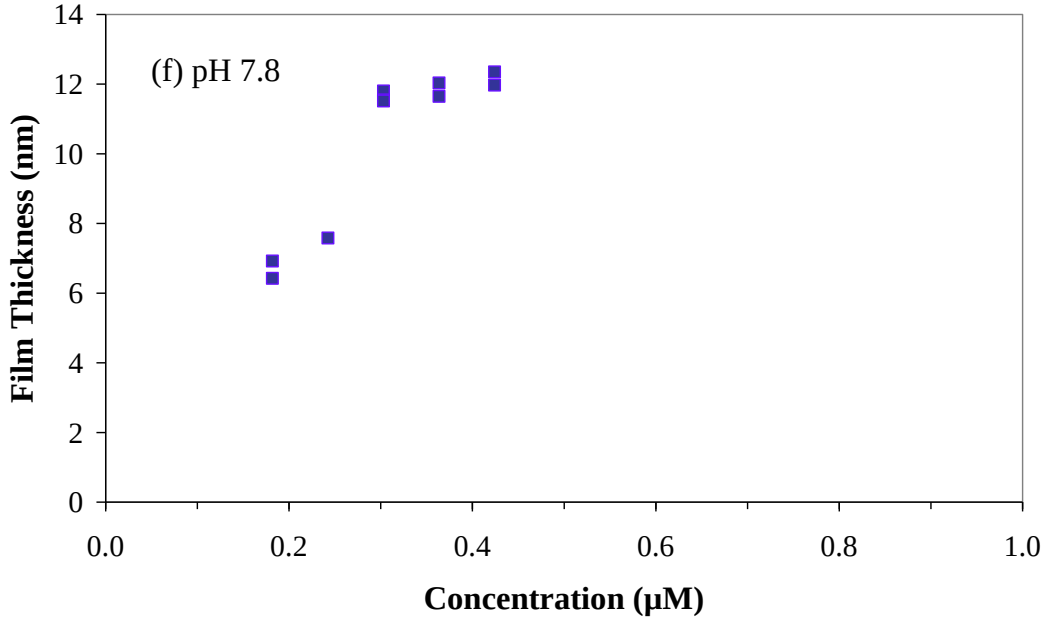

Figure 5.5: Film thickness as a function of P499C full length CPR concentration in 0.1 M NaH_2PO_4/K_2HPO_4 at a) pH 6.2 b) pH 6.8 c) pH 7.0 d) pH 7.2 e) pH 7.4 and f) pH 7.8.

The concentration of protein needed to produce a bilayer is increased as the pH is changed from pH 7.0 to pH 7.2, this increase in range of concentrations that

form a monolayer of CPR is beneficial as it provides a larger window in which to control the formation of a monolayer coverage. The formation of a monolayer or bilayer appears to be extremely sensitive to the pH of the buffer solution. By changing the pH by only 0.2 units from pH 7.0 to pH 7.2 the concentration at which a bilayer is observed increased from 0.24 μM to 0.42 μM as shown in table 5.1

pH	Concentration for Monolayer Adsorption
6.2	< 0.36 +/- 0.03 μM
6.8	< 0.42 +/- 0.03 μM
7.0	< 0.24 +/- 0.03 μM
7.2	< 0.42 +/- 0.03 μM
7.4	< 0.67 +/- 0.03 μM
7.8	< 0.30 +/- 0.03 μM

Table 5.1: Summary of QCM-D results showing the maximum concentration of P499C full length CPR to achieve a monolayer as a function of solution pH.

The thickness of the adsorbed protein layer does not show a linear dependence on solution concentration, however the QCM-D data demonstrates that there are critical concentrations at which a monolayer and bilayer of CPR adsorb, as shown in figure 5.5, these concentrations vary as a function of pH, which is summarised in table 5.1.

In pH 7.0 buffer solution a bilayer is adsorbed at the lowest concentration, this may indicate that at this pH the protein is more reactive and the interactions necessary for a bilayer to form occur more readily than at any other pH value investigated.

The investigation into the effect of pH and concentration has provided information on the conditions necessary to produce a monolayer of adsorbed full length CPR on polycrystalline Au. As the pH plays an important part in influencing the formation of a monolayer it is therefore crucial to choose a pH that allows a

monolayer to form over a large of protein concentrations, whilst maintaining a pH close to that of the biological system. For these reasons all further experiments were carried out in pH 7.2 buffer solution. Further QCM-D analysis of the effect of concentration on the adsorption of the isolated FAD variant of CPR was necessary. This was carried out by investigating the effect of concentration at pH 7.2 as the similarities of FAD and full length CPR structures are expected to produce similar QCM-D data.

5.4 QCM-D Results for the Adsorption of the Isolated P499C FAD Variant of CPR

The same experimental procedures as discussed in section 5.2 were used to monitor the adsorption of the truncated P499C FAD variant of CPR on to the polycrystalline Au surface. A similar adsorption process was observed for the adsorption of FAD, where a fast initial shift in both *f* and *D* was followed by a steady trace for both after the first 1000 seconds of the scan. The shifts in *f* and *D* as a result of the adsorption of a monolayer of FAD onto the polycrystalline Au surface are shown in figure 5.6, and the data show that the change in frequency is similar to that observed after the adsorption of a monolayer of full length CPR. However the dissipation shift is smaller for a monolayer of FAD. This indicates that the FAD molecule forms a more rigid structure on the Au surface [1,3-5]. This is consistent with theory as the isolated FAD molecules are expected to be a more rigid and less dynamic molecule than the full length variant of CPR.

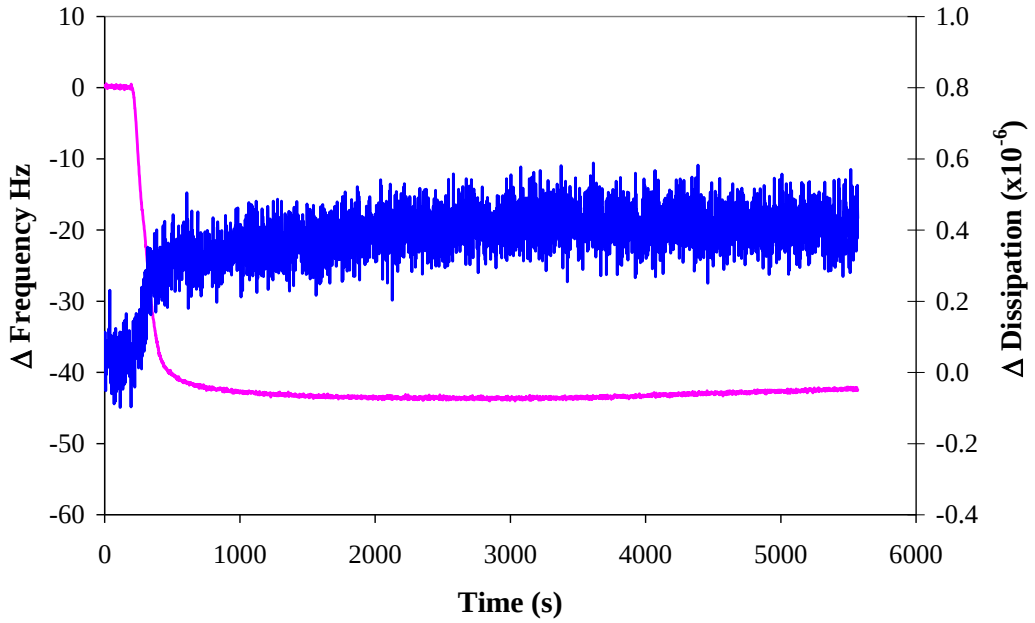

Figure 5.6: Change in frequency (pink curve) and dissipation (blue curve) as a function of time during the adsorption of P499C FAD CPR in 0.1 M buffer solution pH 7.2.

As with full length CPR the adsorption of a monolayer or bilayer of molecules is dependent on the concentration of the protein sample. A sample concentration above 0.6 μM has been shown to result in the adsorption of a bilayer of FAD. At lower concentrations a monolayer is adsorbed as shown in figure 5.7. The data demonstrated that a higher concentration of FAD molecules than full length CPR molecules was needed to form a bilayer of adsorbed molecules.

The removal of the FMN domain does not result in a major difference in height of the CPR molecule. This is due to the fact that the FMN domain sits within a cavity thus increases the dimensions in the vertical axis only very slightly. Therefore the same values of layer thickness associated with a monolayer and bilayer adsorption were used to analyse data produced by both variants of CPR.

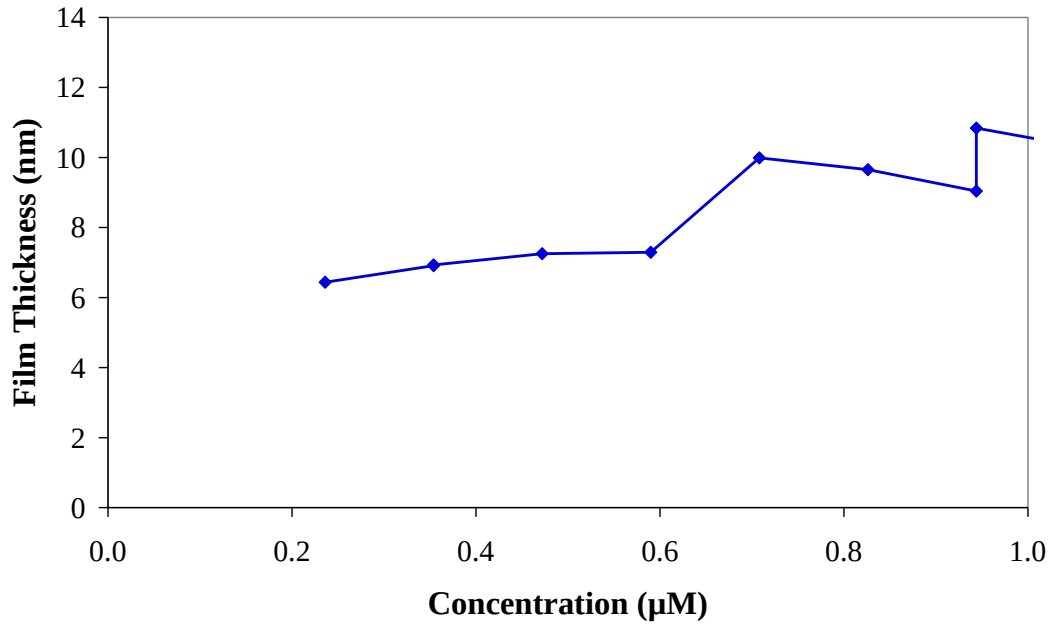

Figure 5.7: Film thickness as a function of P499C FAD CPR concentration in 0.1 M NaH_2PO_4/K_2HPO_4 at pH 7.2.

pH	Concentration for Monolayer Adsorption of P499C FAD CPR
7.2	< 0.60 +/- 0.3 µM

Table 5.2: Summary of QCM-D results showing the maximum concentration of P499C FAD CPR to achieve a monolayer in 0.1M NaH_2PO_4/K_2HPO_4 pH 7.2.

5.5 QCM-D Monitoring the Adsorption of Wild Type CPR

Wild type CPR is the naturally occurring form of the CPR molecule and so it does not contain the mutant cysteine molecule that was engineered in the two variants of P499C CPR. The effect of the mutant cysteine molecules on the adsorption of CPR was investigated by monitoring the adsorption of wild type CPR. The cysteine molecule is expected to act as an anchor point forcing each protein molecule to adsorb in a certain orientation.

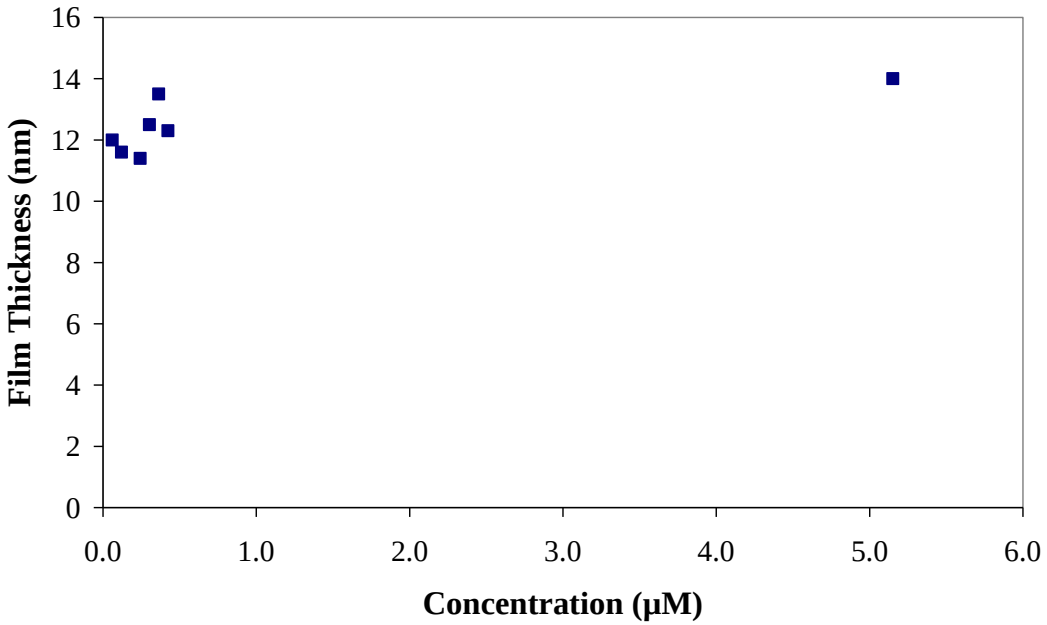

Figure 5.9: Film thickness as a function of Wild Type CPR concentration in 0.1 M NaH_2PO_4/K_2HPO_4 pH 7.2.

Figure 5.9 shows the adsorbed film thickness as a function of concentration for wild type CPR and shows that a bilayer of CPR was adsorbed at all concentrations examined. Even at a sample concentration as low as 0.06 µM a bilayer is adsorbed.

The wild type CPR molecule contains both the FMN and FAD domains and has the same dimensions as the P499C full length CPR variant, but crucially does not contain the mutant cysteine anchor point, therefore observed differences in the adsorption behaviour between the mutant and wild type CPR may be associated with the mutated cysteine residue. This suggests that the mutant cysteine molecule enables the protein to adsorb at a monolayer coverage, which is essential for accurate RAS investigations. The formation of a bilayer at all sample concentrations may be the result of interactions between the CPR molecules. These interactions could occur in solution before the protein adsorbs onto the surface, as the *f* and *D* shifts suggest that the adsorption of a bilayer of wild type CPR does not involve a multiple stage adsorption process. The formation of a bilayer of adsorbed mutant CPR molecules maybe due to the same protein interactions. However these

interactions may only occur in the mutant forms of CPR after a certain critical concentration in solution is reached. This could be due to competing factors such as the comparative strength of the Au-S bond and the protein-protein interactions. However this is beyond the scope of this research and the aim of the QCM-D experiments were to establish the conditions of monolayer adsorption of the variant forms of CPR.

5.6 AFM Measurements of a Monolayer and Bilayer of Variant CPR Molecules

Having established the conditions at which a monolayer and bilayer of CPR adsorbs in the previous QCM-D experiments, these were then used to produce samples of a monolayer and bilayer coverage of P499C full length CPR onto the polycrystalline Au sensors. QCM-D analysis confirmed the layer thickness of the samples before they were transported from the QCM-D sensor modules to the AFM instrument. The samples were protected from air by being submerged in pure phosphate buffer solution. AFM images were produced of each sensor by Dr D. S. Martin and are shown in figure 5.7.

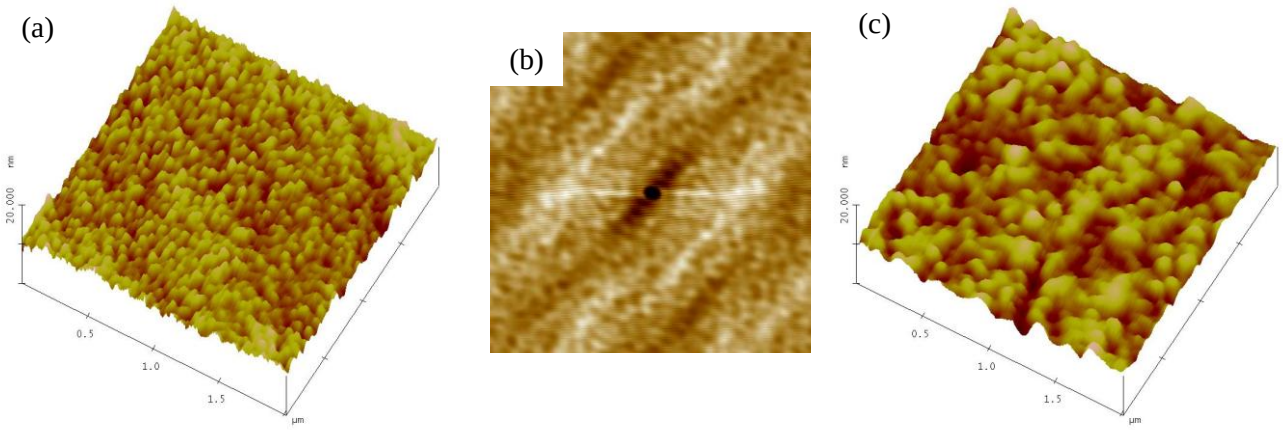

Figure 5.7: AFM images of 2 µm x 2 µm area of a polycrystalline Au sensor obtained from the QCM-D after deposition of (a) monolayer, (b) the autocorrelation image obtained from the monolayer and (c) bilayer film thickness.

The AFM images were produced by carefully positioning the sample sensors whilst protecting the adsorbed protein layer under a drop of ultra pure water. The morphology of both films was of the type produced by molecular aggregates. Small holes occurred occasionally in the monolayer sample revealing the exposed Au substrate surface. The AFM tip was used to 'scratch' away small areas of the protein layer in order to expose larger areas of the Au substrate so that the height of the protein layer could be measured accurately form the substrate surface. The height was measured at various positions on the monolayer sample surface and the height of the aggregates varied between 4 and 6 nm. Whilst the AFM imaging was optimized to minimize the applied force on the substrate, the probe tip may compress the protein and result in a reduced height being measured. Values for the height of 4 nm to 6 nm are consistent with the dimensions of the molecules as deduced from crystallography [2] and with the monolayer film thickness measured with the QCM-D instrument. The AFM images were subject to autocorrelation analysis using Image SXM [13]. The Autocorrelation function (ACF) describes the spatial correlation between objects in an image, which in this case is dependent on the distribution of light and dark regions corresponding to the topography of the AFM image. The ACF can be described as the correlation of an image with itself as a function of displacement of the image with respect to itself [14], which can be mathematically represented as the convolution of the two-dimensional gray value function G(x,y) with itself:

$$G(x,y) \otimes G(x,y) = \int_{-\infty}^{\infty} \int_{-\infty}^{\infty} G(x',y') \cdot G(x+x', y+y') dx' dy' \qquad (5.1)$$

where *x* and *y* are the coordinates, and x' and y' are the displacements. Fourier Transforms are used to calculate the ACF in Image SXM, a method that is mathematically equivalent to equation 5.1, yet computationally more efficient [14].
The ACF can reveal the level and range of correlation of statistical patterns as a function of orientation, reflecting the shape, symmetry, anisotropy and orientation of

particles in AFM images, therefore providing a powerful method of image analysis [14].

Autocorrelation analysis of the monolayer sample showed weak striation directed along the diagonal of the square image shown in figure 5.7 b). A similar autocorrelation result was observed for the clean Au substrate, which displays a granular morphology of 1 to 2 nm height variation over areas of 2 μm. The autocorrelation result indicates that there is some similarity in both (i) the granular pattern of the clean substrate and (ii) the monolayer aggregates, along one particular direction over a length scale of a few microns. This suggests that the substrate contributes to the localised ordering effect in the monolayer. No such pattern was observed for the bilayer, indicating that the effect is lost at this coverage. The striation observed in the autocorrelation image of the monolayer is observed from areas of side length 1 to 2 μm (figure 5.7 b)), this effect, however is lost over larger areas. The area size of these striations provides and indication of the spatial correlation of the molecules on the polycrystalline Au surface.

Analysis of the bilayer sample showed that it was not possible to determine the location of the underlying Au substrate, however, aggregates having a maximum height of ~ 8 nm were measured. The height of the aggregates could not be accurately measured from the Au substrate surface, however the AFM results show larger aggregate heights in the bilayer compared to those in the monolayer sample (figure 5.7). The increase in height of the aggregates is in general agreement with the QCM-D which distinguished between monolayer and bilayer thickness.

5.7 QCM-D Measurements of the Adsorption of Variant CPR Molecules under Potential Control

After the conditions for monolayer adsorption of the two variant forms of CPR had been established the effect of potential on the adsorption process has been investigated.

Two electrochemical QCM-D modules have been used to investigate the adsorption of CPR. However difficulties in producing accurate data under potential

control were associated with the design of the modules. One of the modules used has much larger volume than the modules used in the concentration and pH investigations. Pumping protein solution through this larger module frequently resulted in a frothing of the protein sample, which is associated with aggregation of the protein. This made it extremely difficult to pump the solution through the cell and produce an accurate trace for both *f* and *D*. The other electrochemical module used was a new design cell produced by Q-Sense which incorporated electrochemical control within a window cell. Again this cell was problematic in that it proved extremely difficult to pump through solution without trapping small air bubbles in the module. These trapped bubbles can cause shifts in both *f* and *D* and also introduce severe inaccuracies in controlling the applied potential, thus the potential can not be controlled properly and the experiment had to be abandoned.

Despite these difficulties early electrochemical QCM-D experiment indicated the potential did not affect the adsorption conditions for a monolayer coverage.

5.8 Summary

The adsorption of protein from a sample of similar concentration as used in the preliminary RAS experiments discussed in chapter 4 was monitored using the QCM-D instrument. The QCM-D results discussed in this chapter suggest that the concentration of protein used in the preliminary RAS experiments results in the adsorption of multiple layers of protein, therefore indicating that the RAS data discussed in chapter 4 may have been produced after the adsorption of multiple layers of CPR molecules onto the Au(110) surface.

It has been shown that the formation of both monolayer and bilayer coverage is dependent not only on concentration but also on pH as shown in table 5.1. These results also show that there is no simple relationship between the pH and concentration at which a monolayer is formed but that, apart from the results at pH 7.0 and 7.8, the maximum concentration at which adsorption is limited to a monolayer increases with increasing pH.

The conditions for producing a monolayer of the mutant full length CPR and isolated FAD CPR have been established. All future experiments were carried out using a pH 7.2 phosphate buffer solution and a protein concentration less than 0.4 μM for full length CPR and 0.6 μM for the isolated FAD variant of CPR was used.

5.9 References

[1] M. C. Dixon, *Journal of Biomolecular Techniques* **19**, 151 (2008)

[2] M. Wang, D. L. Roberts, R. Paschke, T. M. Shea, B. S. S. Masters and *J-J. P. Kim, Proc. Natl. Acad. Sci.* **94**, 8411 (1997)

[3] M. Rodahl, F. Hook, C. Fredriksson, C. A. Keller, A. Krozer, P. Brzezinski, M. Voinova and B. Kasemo, *Faraday Discuss*. **107**, 229, (1997)

[4] F. Hook, Thesis. *Development of a novel QCM technique for protein adsorption studies.* Chalmers University of Technology, Goteborg University (2004)

[5] F. Hook, T. Nylander, C. Fant, K. Sott, H. Elwig and B. Kasemo, *Anal. Chem*. **73**, 5796 (2001)

[6] P. Weightman, G. J. Dolan, C. I. Smith, M. C. Cuquerella, N. J. Almond, T. Farrell, D. G. Fernig, C. Edwards and D. S. Martin, *Phys. Rev. Lett.* **96**, 086102 (2006)

[7] A. Bowfield, C. I. Smith, M. C. Cuquerella, T. Farrell, D. G. Fernig, C. Edwards and P. Weightman, *Phys. Status Solidi* C **5**, 2600 (2008)

[8] C. I. Smith, A. Bowfield, G. J. Dolan, M. C. Cuquerella, C. P. Mansley, D. G. Fernig, C. Edwards and P. Weightman, *J. Chem. Phys.* **130**, 044702 (2009)

[9] A. Bowfield, C. I. Smith, G. J. Dolan, M. C. Cuquerella, C. P. Mansley and P. Weightman, *e-J. Surf. Sci. Nanotech*. **7**, 225 (2009)

[10] A. Bowfield, C. I. Smith, C. P. Mansley and P. Weightman, *Phys Status Solidi* B **247**, 1937 (2010)

[11] C. P Mansley, C. I. Smith, A. Bowfield, D. G. Fernig, C. Edwards and P. Weightman, *J. Chem. Phys*. **132**, 214708 (2010)

[12] G. Sauerbrey, *Zeitschift Fut Physik*, **155** 206 (1959)

[13] Image analysis carried out using Image SXM, S. D. Barrett [http://www.ImageSXM.org.uk] (2011)

[14] *Image Analysis in Earth Science,* Renée Heilbronner and Steve Barrett, Springer Berlin Heidelberg (2013)

Chapter 6

RA Spectra of Monolayer and Bilayer Adsorption of P499C Truncated FAD and Full Length CPR Molecules

This chapter provides the RA spectral signatures of both monolayer and bilayer coverage of P499C truncated FAD and full length CPR molecules adsorbed on the Au(110) surface. Conditions under which a monolayer and bilayer adsorb were provided from QCM-D experiments discussed in the previous chapter.

6.1 Introduction

Having established the conditions under which monolayers and bilayers of the mutant P499C variants of CPR adsorb on polycrystalline Au in QCM-D experiments, it was necessary to reproduce these conditions in the electrochemical cell to enable RAS studies of monolayer adsorption of variant CPR molecules. The RAS experiments presented in this chapter closely followed the procedures used in preliminary RAS experiments in chapter 4, relating to the preparation of both the protein samples and the Au(110) surface. However slight changes to the experimental procedure were made to accommodate the conditions for monolayer adsorption. These were, to firstly ensure that buffer solutions of appropriate pH were prepared and secondly the concentration of protein in each sample was carefully controlled. The pH of the buffer solution was checked prior to each experiment and the concentration of protein in solution was monitored using the UV-Vis spectrometer. During QCM-D experiments the sensors were rinsed with fresh buffer solution after the adsorption of protein, which was done to try to prevent protein aggregation and to rinse off any additional weakly bonded protein molecules. To replicate this procedure in RAS experiments the electrochemical cell was rinsed with fresh buffer solution, immediately after the adsorption of protein onto the Au(110) surface.

6.2 RA Signature of Monolayer and Bilayer Coverage of P499C Full Length CPR on the Au(110) Surface

QCM-D results discussed in chapter 5 indicated that potential control does not affect the adsorption conditions under which a monolayer of mutant CPR is adsorbed. However it is necessary for the RAS experiments to be under potential control in order to induce electron transfer processes in the adsorbed CPR molecules. The ability to control the electrode potential also ensures the Au(110) surface is in a known surface reconstruction prior to the adsorption of protein. Full length CPR was adsorbed onto the Au(110) electrode surface at an applied potential of -0.652 V.

This potential is known to result in the Au(110) surface adopting a (1×3) surface reconstruction [1] and the fully reduced state of CPR. Two different protein concentrations were added to the electrochemical cell. These concentrations related to those used in QCM-D experiments that resulted in the formation of bilayer and monolayer coverage of mutant CPR. Changes in the RA spectrum of Au(110) at -0.652 V after the addition of bilayer and monolayer concentrations full length CPR to the electrochemical cell are shown in figure 6.1. These changes are associated with the adsorption of protein onto the Au(110) surface. There are clear differences between the resultant RA spectra in figure 6.1 b) which are attributed to the adsorption of a monolayer and bilayer of P499C full length CPR onto the Au(110) surface at -0.652 V. The RA spectra in figure 6.1 b) are presented as the spectral signature of a monolayer (red line) and bilayer (blue line) of CPR on the Au(110) electrode at -0.652 V.

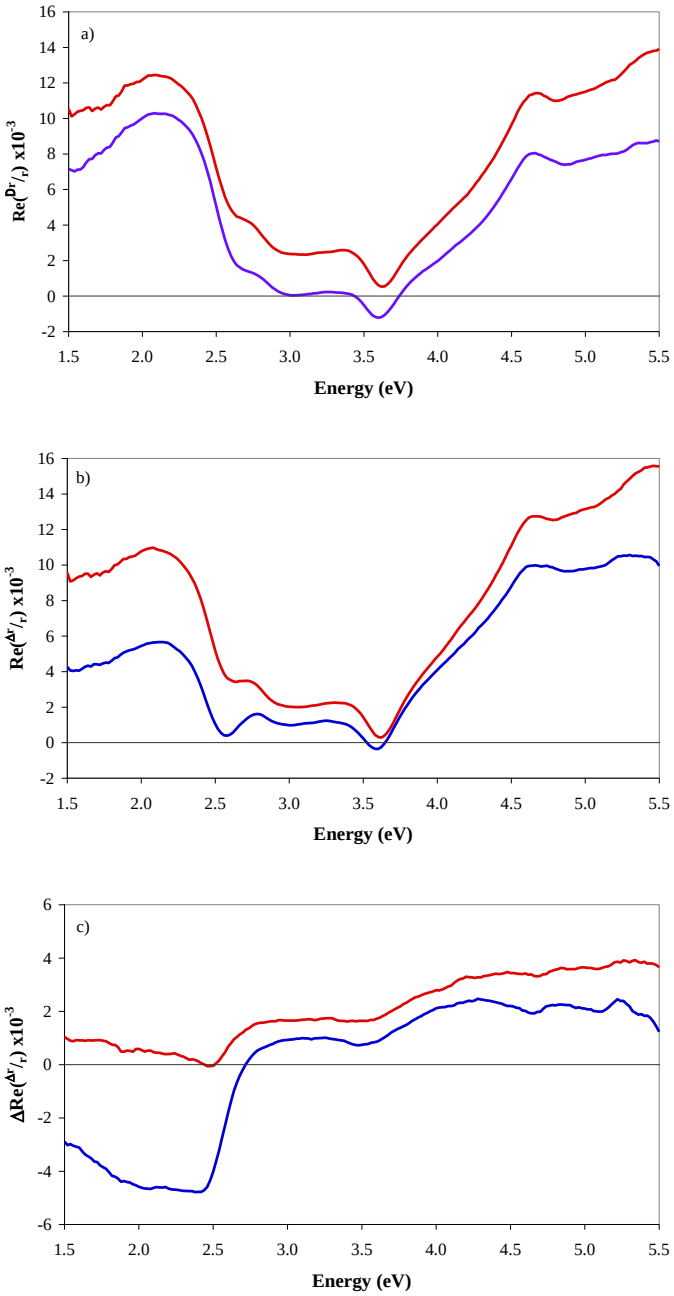

Figure 6.1: RA spectra of a) clean Au(110) at -0.652 V, b) Au(110) + P499C full length CPR at -0.652 V and c) P499C full length CPR at -0.652 V obtained by subtracting the corresponding Au(110) spectrum from the Au(110) + protein spectrum all recorded in 0.1 M NaH_2PO_4/K_2HPO_4 (pH 7.2) monolayer experiment (red line) and bilayer experiment (blue line). The RA spectra corresponding to the (red line) have been shifted on the *y* axis for clarity and the RA spectra corresponding to the blue line corresponds to the *y* axis scale.

It has previously been discussed that the mutant P499C protein molecules are expected to adsorb onto the Au(110) surface via the formation of a Au-S linkage between the substrate and the mutant cysteine molecule. The formation of this linkage should lead to the observation of the characteristic Au-S peak in the RA spectrum at 2.54 eV as observed in previous RAS experiments after the adsorption of S-containing amino acids [2], decanethiol [3] and a cysteine-tryptophan dimer [4]. The RA spectra produced after the adsorption of P499C full length CPR onto the Au(110) surface show an enhanced intensity in the low energy region and the emergence of the negative peak at 2.54 eV (figure 6.1 b)). The presence of the 2.54 eV peak was observed in the RA spectrum of both a monolayer and bilayer as shown in figure 6.1 b). This increase in intensity at 2.54 eV suggests that the protein molecules adsorbed via the formation of the Au-S bond, although it is possible that this is not the only residue involved in the adsorption process and many others may also be involved. The bilayer spectrum has a much stronger contribution in the low energy region and an increased intensity of the 2.54 eV peak. The negative peak at 2.54 eV, although associated with the formation of the Au-S bond, this region of the RA spectrum is also expected to overlap with the contribution from the adsorbed molecules, since the absorption spectrum of the CPR species in solution shows a rather broad feature in the range of 2.5 eV to 3.0 eV (figure 6.2). This feature in the absorption spectrum of the molecule is expected to be associated with the isoalloxazine rings [5-9] which have a maximum absorption spectrum at 2.7 eV.

RA spectra produced after the adsorption of P499C full length CPR onto the Au(110)/electrode surface are expected to be the sum of RAS contributions from the adsorbed molecules and from the clean Au(110) surface. In previous RAS studies of the adsorption of molecules onto the Au(110) surface [2-4,10-13], it was possible to find the RA spectrum of the adsorbed molecules by subtracting the RAS of the Au(110) substrate. The RA spectra of the adsorbed CPR molecules has been produced following a similar procedure, whereby the RA spectrum of the clean Au(110) (figure 6.1 a)) was subtracted from the RA spectra of Au(110) + P499C full length CPR (figure 6.1 b)). The resultant spectra following this subtraction are attributed to the RAS of the adsorbed molecules for both a monolayer and bilayer coverage and are shown in figure 6.1 c). The RA spectra in figure 6.1 c) follow a

similar spectral shape, with an increased negative intensity observed below 2.5 eV. However the bilayer spectrum has a much stronger contribution in the low energy region.

Comparison of the RA spectrum of clean Au(110) at -0.652 V (figure 6.1 a)), and the RA spectrum of Au(110) + P499C full length CPR (figure 6.1 b)), suggests that the RAS of the adsorbed molecules is strongly influenced by that of the RAS of the Au(110) substrate. This is consistent with the autocorrelation analysis [15] of the AFM images of an adsorbed monolayer of CPR on polycrystalline Au, which suggested that the substrate contributes to the localised ordering effect of the adsorbed molecules. However this effect was not observed after the adsorption of a bilayer on polycrystalline Au. The autocorrelation analysis [15] was performed after the adsorption of CPR onto polycrystalline Au, while the Au(110) surface provides a much more ordered substrate. Therefore it is likely that the Au(110) substrate would influence the order of both a monolayer and bilayer of adsorbed molecules.

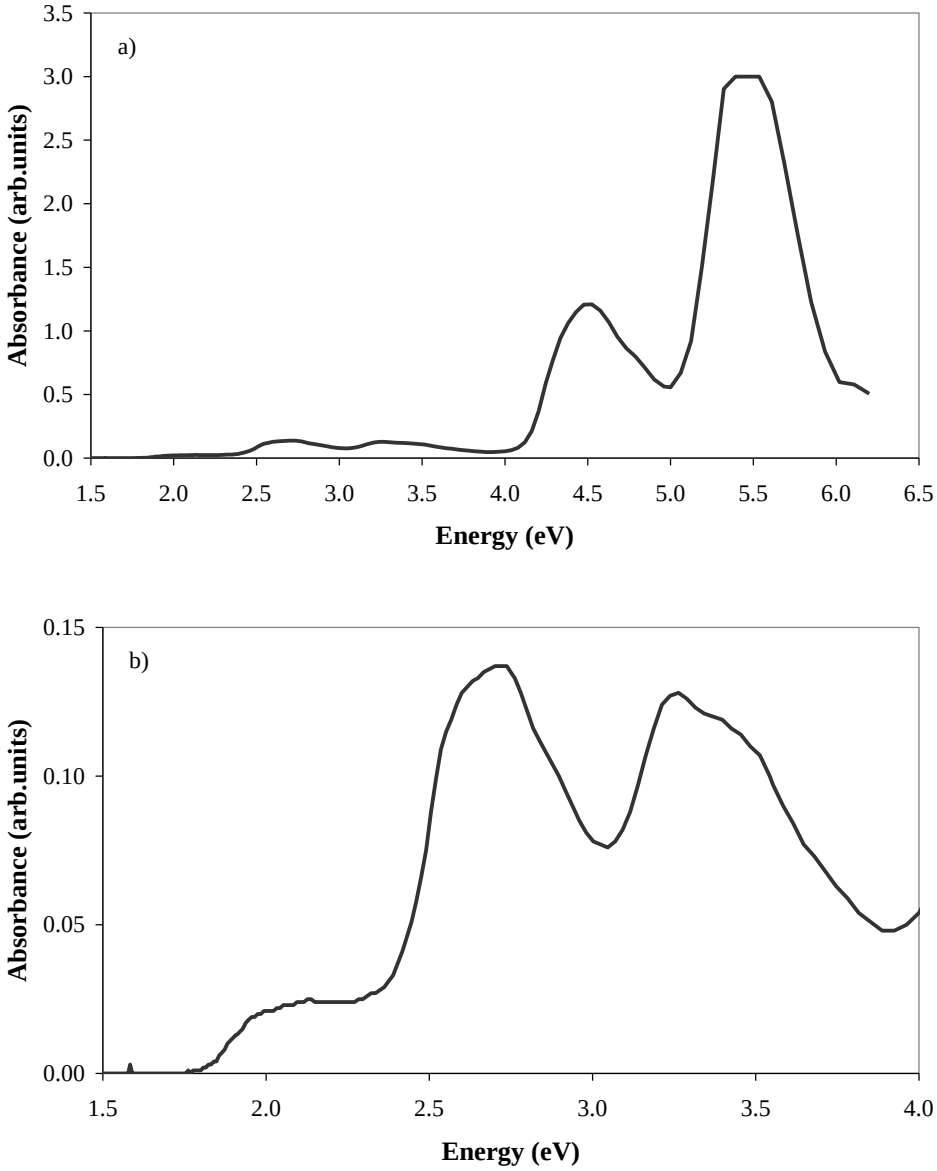

Figure 6.2: UV-VIS absorbance spectrum for 8.3 μM P499C full length CPR in 0.1 M NaH_2PO_4/K_2HPO_4 at pH 7.2 as a function of photon energy a) from 1.5 eV to 6.5 eV and b) shows the absorbance over the photon energy range of 1.5 eV to 4.0 eV over an expanded absorbance scale. These spectra are in agreement with those of Ref [7].

Further information on the process of protein adsorption onto the Au(110) surface has been obtained by monitoring the RAS intensity at selected energies as a function of time during the adsorption process. The RAS intensity was monitored as

a function of time in two separate experiments at 2.54 eV and 2.7 eV during the adsorption of protein onto the Au(110) surface and is shown in figure 6.3. Despite the potential overlapping of the signals from the formation of the Au-S bond and the isoalloxazine rings, there are clear differences between the adsorption kinetics observed at these two energies (figure 6.3). At both energies a strong decrease in RAS intensity is observed between 500 and 1000 seconds, however after this the behaviour at each energy differed. At 2.7 eV (blue line figure 6.3) the RAS intensity saturated after 1000 seconds whereas at 2.54 eV (red line figure 6.3) the RAS intensity continued to decrease, but at a much slower rate. The kinetic behaviour observed at 2.54 eV has been observed in a previous RAS investigation of the adsorption of pyridine onto the Au(110) surface [14]. This behaviour was interpreted as an initial saturation of the surface followed by a much slower ordering process of the adsorbed species that increases the overall anisotropy [14].

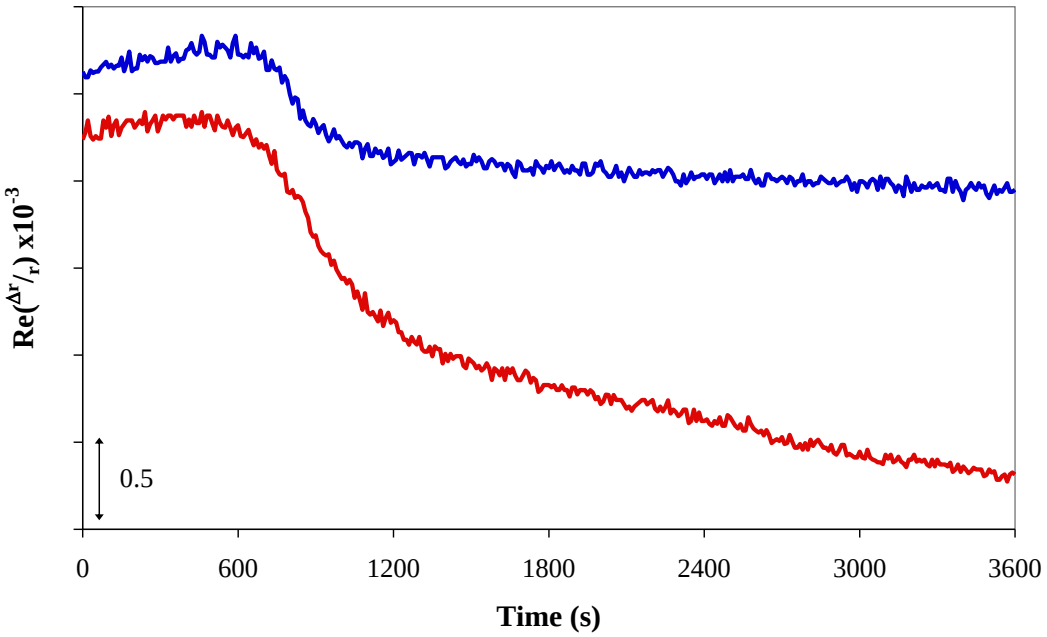

Figure 6.3: Changes in RAS intensity as a function of time during the adsorption of a monolayer of full length CPR monitored at 2.7 eV (red line) and 2.54 eV (blue line). The RAS intensity profiles have been shifted on the *x* axis for clarity.

In order to characterise the adsorption process further the Rapid RAS instrument was used to monitor RAS intensity across a larger spectral range from 2.0 eV to 4.0 eV in 32 channels simultaneously during the adsorption of a monolayer of P499C full length CPR. Selected adsorption curves at a range of energies monitored using the Rapid RAS instrument are shown in figure 6.4.

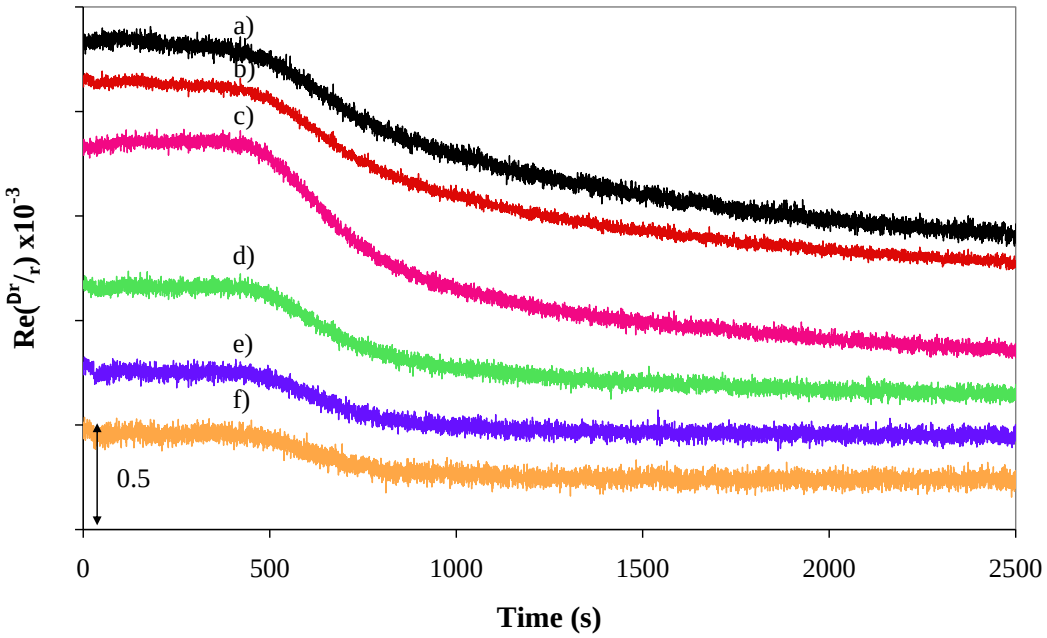

Figure 6.4: Changes in RAS intensity as a function of time during the adsorption of a monolayer of P499C full length CPR onto the Au(110) surface at -0.652 V monitored at a) 2.02 eV, b) 2.25 eV, c) 2.53 eV, d) 2.66 eV, e) 2.73 eV and f) 3.06 eV.

The data from the Rapid RAS instrument, shown in figure 6.4, shows that the adsorption curves at lower energies are significantly different to the adsorption curves at higher energies. The RAS intensity at 2.02 eV, 2.25 eV and 2.53 eV shows a strong decrease between 500 to 1000 seconds followed by a much slower but steady decrease in intensity as a function of time. This behaviour is similar to that observed at 2.54 eV using the standard RAS instrument. The higher energy adsorption curves also follow a similar intensity decrease over the first 1000 seconds but the signal then saturates, similar to that observed at 2.7 eV using the standard

RAS kit. The intensity of a feature in the RA spectrum is a product of the intrinsic strength of the feature, the number of dipoles that give rise to the feature and the degree of anisotropy. The secondary decrease in intensity observed at energies below 2.54 eV is expected to be the product of a slower ordering process which increases the negative strength of the RAS signal and could be due to an increase in anisotropy. This secondary ordering process has only been observed at energies below 2.54 eV and does not change the strength of the RAS signal at higher energies. This behaviour could be explained if the ordering process does not change the net orientation of the dipoles that give rise to the higher energy RAS response of the adsorbed molecules.

The information on the adsorption process provided by monitoring changes in the RAS intensity at these energies, suggested that the adsorption of CPR involves secondary ordering process, which appears to take place after the initial adsorption of the molecule. In order to gain information on the orientation of the adsorbed protein molecules RA spectra were collected as a function of azimuthal angle. This utilises the relationship between the optical axes of the Au(110) surface and the optical axes of transitions arising from adsorbed molecules on the Au(110) surface which has been discussed in detail by Macdonald and Cole [16]. This relationship is a powerful tool for determining the orientation of adsorbed molecules, as has been demonstrated in previous work [10-13] and discussed earlier in this thesis (chapter 3.8). The intensity of the RAS of Au(110) varies as a function of $\cos 2\theta$, where θ is the azimuthal angle between the plane of polarization of the incident light and the crystal axis of the surface [17]. RA spectra were obtained as a function of azimuthal angle after the adsorption of a monolayer of full length CPR on to the Au(110) surface (figure 6.5). The RA spectra in figure 6.5 are essentially flat when measured along the principle axis of the Au(110) surface. This observation establishes that the optical dipole transitions that give rise to the spectra of a monolayer of full length CPR must be roughly orientated in a plane normal to the surface and directed along either the $[1\bar{1}0]$ or [001] axes of the Au(110) surface This behaviour has been observed previously for smaller molecules adsorbed on the Au(110) surface [10-13].

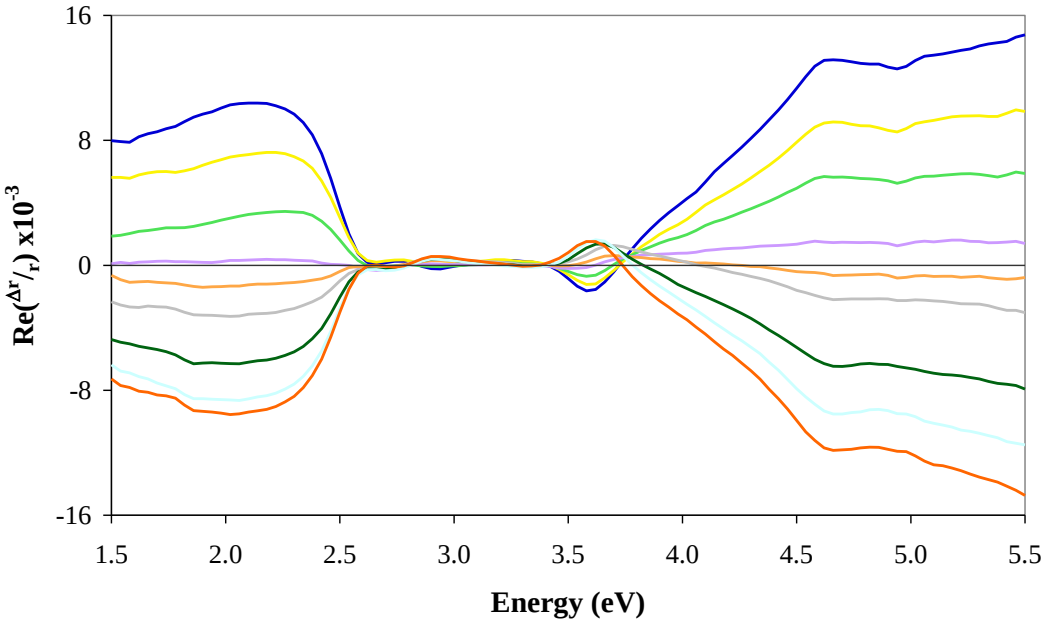

Figure 6.5: RA spectra of Au(110) + monolayer of P499C full length CPR at -0.652 V as a function of azimuthal angle defined with respect to the Au[001] axis. Recorded at 45° (blue line), 65° (yellow line), 75° (green line), 85° (purple line), 90° (orange line), 95° (grey line), 105° (dark green line), 115° (sky blue line) and 135° (red line).

The UV-VIS absorption spectrum of CPR molecules in solution (figure 6.2) shows strong broad features between 2.5 eV and 3.0 eV which are expected to be a contribution from the isoalloxazine rings. However the effect of the adsorption of a monolayer of full length CPR induces only a small change in this region of the RAS of Au(110), which is shown by comparison of the RA spectra in figure 6.1 a) and b). It is also notable that the region between 1.5 eV and 2.5 eV is the weakest region of the absorption spectrum of the free molecules (figure 6.2) but produces one of the strongest changes in the RAS of Au(110) surface as shown in figure 6.1 c), while the strongest regions of the absorption spectrum of the free molecules induce very little change in the RAS of the Au(110) surface. These changes induced in the RAS of Au(110) after the adsorption of full length CPR are much smaller than the changes observed after the adsorption of smaller molecules [2-4,10-13]. The adsorption of cysteine molecules onto the Au(110) surface at -0.652 V causes a large negative

shift in intensity between 1.5 eV and 3.0 eV including the emergence of an intense negative peak at 2.54 eV (figure 6.6). The reason for the increased contribution to the RAS after the adsorption of smaller molecules is probably due to a much higher concentration of ordered dipoles on the surface. The reduction in the contribution to the RAS intensity from adsorbed P499C CPR is probably due to the dimensions of the P499C CPR molecule as the number of pairs of isoalloxazine rings on a given area of the Au(110) surface will be significantly reduced in comparison to the number of cysteine molecules in the same area after the adsorption of cysteine only.

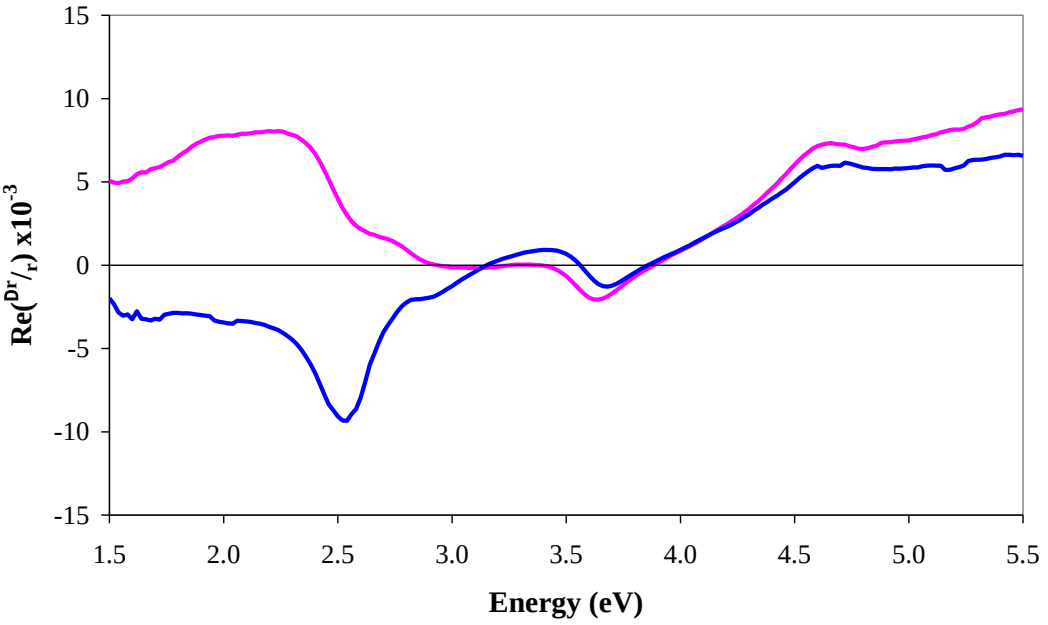

Figure 6.6: RAS of Au(110) (pink line) and RAS of Au(110) + cysteine (blue line) in 0.1 M NaH_2PO_4/K_2HPO_4 at -0.652 V.

The intensity of the 2.54 eV peak observed after the adsorption of a monolayer of CPR is also much smaller than those that have been observed in previous RAS studies of the adsorption of sulfur containing amino acids [2]. The intensity of the 2.54 eV peak has been monitored using RAS as a function of coverage of decanethiol [3]. It was shown to take approximately 60 minutes for a full saturated coverage of dacanethiol to adsorb onto the Au(110) surface. The Authors observed that the 2.54 eV peak increased in intensity as the coverage of

adsorbed decanethiol increased, as shown in figure 6.7. Therefore the authors associated a reduced intensity 2.45 eV peak with a low coverage of decanethiol [3]. The intensity of 2.54 eV peak observed after the adsorption of full length CPR is comparable to the intensity observed after the adsorption of a low coverage of decanethiol. This could indicate that a lower number of Au-S bonds are formed after the adsorption of a monolayer CPR. However the comparative size of the protein molecule to decanethiol means that significantly fewer protein molecules are needed to form a full monolayer coverage on the Au(110). Therefore it is expected that far fewer Au-S bonds would form after the adsorption of CPR in comparison to the adsorption of decanethiol on the Au(110) surface. This suggests that despite the observation of only a small negative increase in the 2.54 eV peak, P499C full length CPR adsorbs by the formation of the Au-S bond.

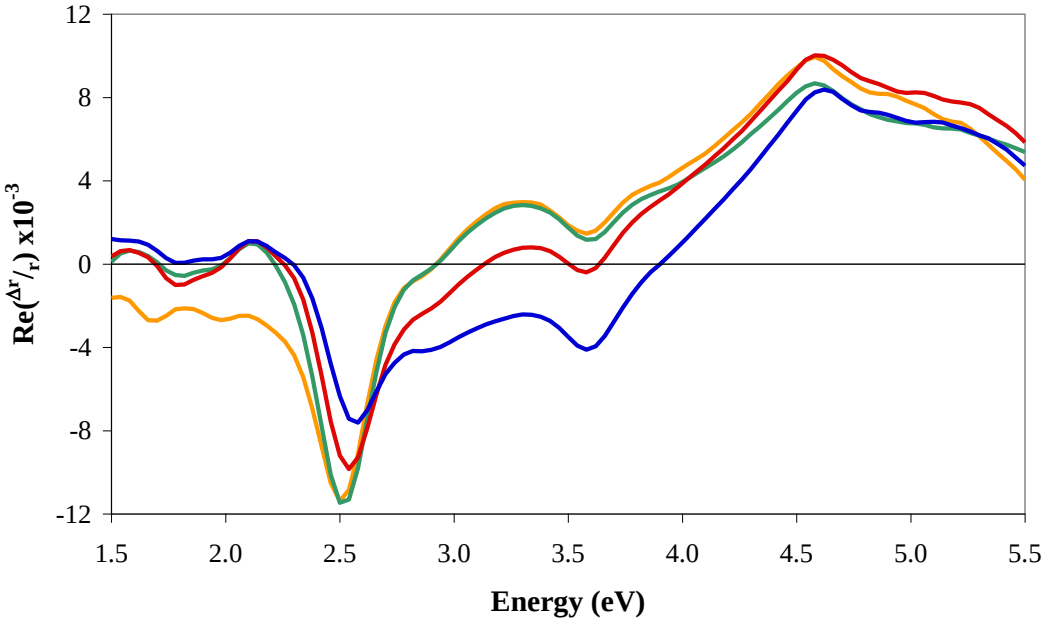

Figure 6.7: RA spectra of Au(110)/ethanol + decanethiol after 15 mins (blue line), 30 mins (red line), 45 mins (green line) and 60 mins (orange line). Reproduced from [5].

The disordered orientation of the dipoles that give rise to the optical spectrum of the molecules on the Au(110) surface can also account for the small

contribution to the RAS of Au(110) induced by the monolayer adsorption of P499C full length CPR. In the spectral region probed in these experiments there will be two main contributions to the molecular spectrum, the isoalloxazine rings and the aromatic amino acids phenylalanine, tyrosine and tryptophan. Detailed analysis of the spectrum of the isoalloxazine ring has been carried out previously [5-9] and was found to have three main contributions, a peak at 2.7 eV which is ~ 1.0 eV wide, a band between 3.3 eV and 3.8 eV and a stronger band peaking at ~ 4.6 eV. These features have been observed in the spectrum of the free molecules in figure 6.2. The dipole transitions that give rise to these features are roughly orientated along the long axis of the ring (figure 6.8), being offset by 32°, 7° and 29° respectively in one analysis [7] and 0 °, 11 ° and 3 °, respectively in an alternative analysis [9]. Cytochrome P450 reductase contains two isoalloxazine rings, the position of these rings is shown in figure 6.9 in the 'closed', fully oxidised state. In this position the long axis of the two rings are roughly parallel to each other. If the long axes of these rings are orientated roughly vertically to the Au(110) surface, as suggested by the molecular ribbon diagram in figure 6.9, then this could account for the weak contribution made to the RAS of the Au(110) surface by the features in the molecular absorption spectrum of the rings lying between the 2.5 eV and 5.0 eV. Further evidence that suggests that the plane of the rings are orientated roughly vertical to the Au surface was provided by the observation that the RAS of the adsorbed molecules is essentially flat when measures at an azimuthal angle of ~90°, which corresponds to one of the principle axes of the Au(110) substrate. If the long axes of the isoalloxazine rings are orientated vertically on the Au(110) surface then the azimuthal variation results indicate that the short axes of the rings would need to be orientated roughly along one of the principle directions of the Au(110) surface either the $[1\,\bar{1}\,0]$ or [001]. The behaviour of the RAS signal monitored above 2.6 eV during the adsorption of a monolayer of P499C full length CPR could be explained by the initial adsorption process resulting in a configuration in which the long axes of the isoalloxazine rings were vertical to the surface and that the subsequent ordering process, revealed by the adsorption kinetics observed at lower energies, involves only lateral movements of the molecules on the surface, therefore not affecting the orientation of the isoalloxazine rings.

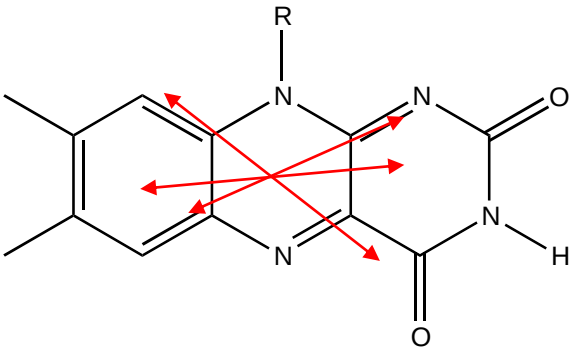

Figure 6.8: Diagram showing the structure of the isoalloxazine ring. The red arrows show the possible direction of the transition moments determined by L. B. -Å. Johnson *et al.* [7].

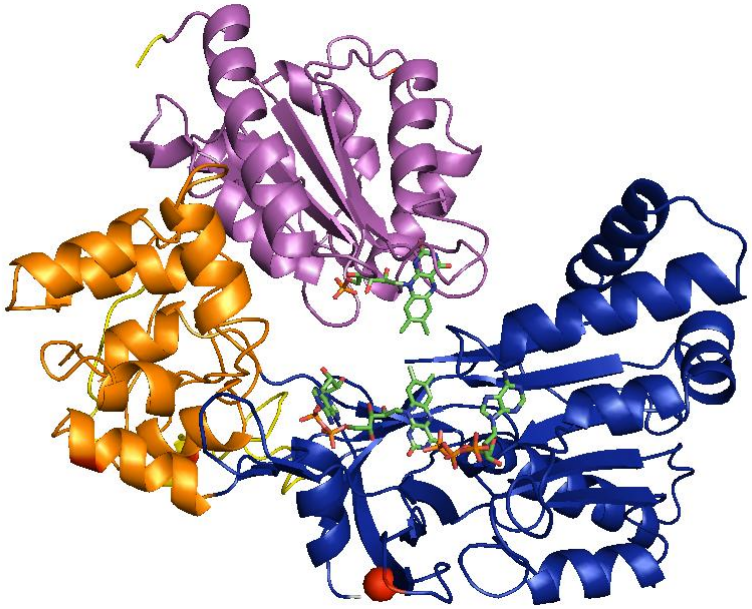

Figure 6.9: Molecular graphics ribbon diagram representation for the structure of cytochrome P450 reductase. The Pro-499 residue that was targeted by site directed mutagenesis to produce the P499C variant is shown by the red sphere. The FMN-binding domain is shown in purple, the conecting domain in orange, and the FAD/NADP-domain in blue. The FAD and FMN cofactors are shown as green sticks.

CPR contains 28 phenylanine, 31 tyrosine and 9 tryptophan amino acids which are widely distributed through the molecular structure of the protein [18]. It is therefore important to consider the contributions that these amino acids make to the RAS of the adsorbed molecule. The amino acids are expected to make a strong contribution to the two intense peaks at higher energies observed in the absorption spectrum of the free molecule (figure 6.2). The higher energy peak is associated with contributions from the peptide bonds of all the amino acids. Despite the intensity of these peak in the absorption spectrum (figure 6.2) the features are remarkably weak in the RAS of the adsorbed molecules (figure 6.1 b) and c)). It is unreasonable to suppose that the weakness of these contributions to the RAS arise from all the dipoles being orientated roughly vertical on the Au(110) surface as with the dipoles of the isoalloxazine rings. Therefore a much more likely explanation for the weakness of these contributions is that there is no significant order in the orientation of these dipoles in the molecular structure so that even if the molecules adopt an ordered arrangment on the Au(110) surface there is no significant net anisotropy in the orientation, resulting in a very weak RAS signal.

The induced changes in the RAS of Au(110) after the adsorption of P499C full length CPR has been compared to changes induced by the adsorption of smaller molecules [2-4,10-13] earlier, where it was also noted that the strongest contribution to the RAS of the adsorbed molecules was observed below 2.5 eV (figure 6.1 c)). However, this spectral region is very weak in the absorption spectrum of the molecules (figure 6.2). The origin of this weak contribution to the absorption spectrum of the molecules is unclear. However the stronger contributions observed in the RAS of the adsorbed molecules in this spectral region could arise from dipole transitions in individual molecules which become orientated in roughly the same direction during the slow ordering process that appears to follow the initial adsorption. This would result in an increase of the net anisotropy of the optical response of the adsorbed molecules and explain why the intensity of this region of the molecular spectrum is enhanced in the RAS. This would also explain the adsorption kinetics observed at lower energies (figure 6.4).

6.3 RA Spectral Signature of a Monolayer and Bilayer of P499C FAD

Having demonstrated the ability of RAS to determine the difference between a monolayer and bilayer of mutant P499C full length CPR adsorbed at the Au(110)/electrode. The remainder of the work presented in this thesis will be aimed at monitoring conformational events in a monolayer of full length CPR adsorbed on the Au(110)/electrode surface. However for completion the RA spectra obtained after the adsorption of both a monolayer and bilayer of the isolated FAD variant of mutant CPR is presented in the following section of this chapter.

The adsorption of the mutant isolated FAD molecules onto the Au(110) surface was achieved by following the conditions for both a monolayer and bilayer adsorption outlined in the QCM-D experiments in chapter 5. As with the full length CPR the concentrations of isolated FAD samples were accurately controlled to enable both a monolayer and bilayer adsorption onto the Au(110) surface. The pH of the buffer solution was also carefully controlled to ensure the buffer used in each experiment had a pH value of 7.2 and the electrochemical cell was thoroughly rinsed after the adsorption of FAD. The applied electrode potential was held at -0.657 V which relates to the fully reduced state of the isolated FAD variant of CPR, and also induces the (1×3) surface structure in the Au(110) substrate [1]. RA spectra of the Au(110) surface before and after the addition of both monolayer and bilayer concentrations P499C FAD are shown in figure 6.10.

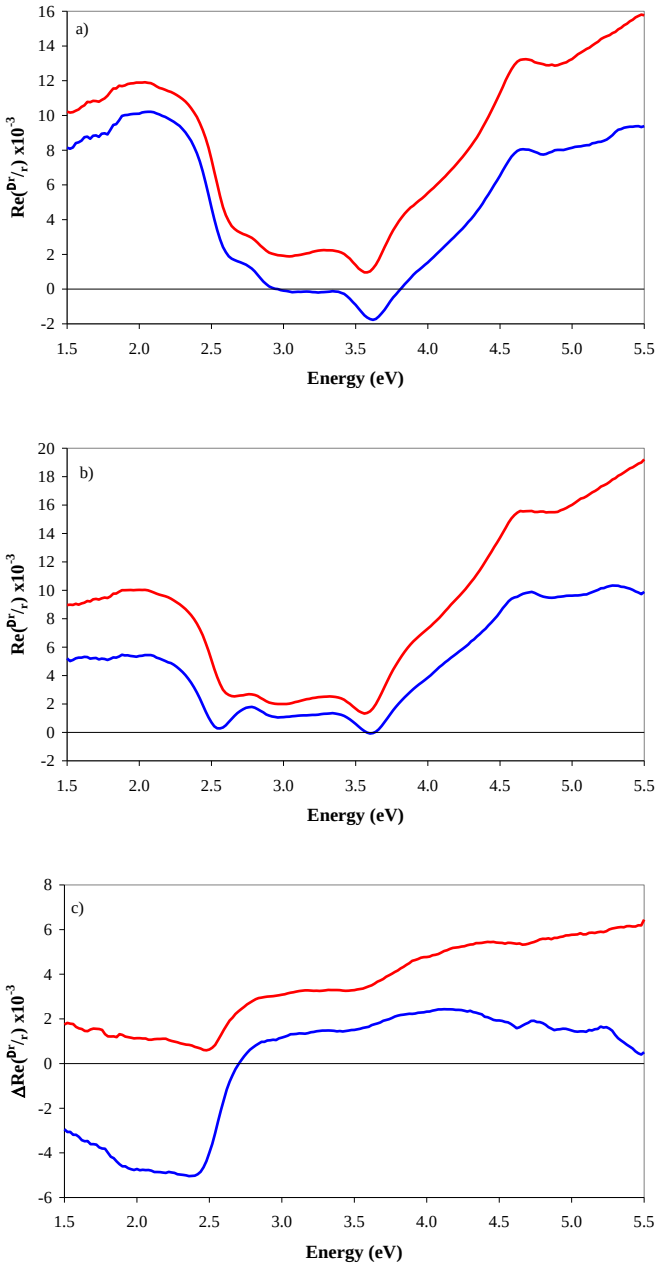

Figure 6.10: RA spectra of a) clean Au(110) at -0.657 V, b) Au(110) + P499C FAD at -0.657 V and c) P499C FAD at -0.657 V obtained by subtracting the corresponding Au(110) spectrum from the Au(110) + protein spectrum. All spectra were recorded in 0.1 M NaH_2PO_4/K_2HPO_4 (pH 7.2) monolayer experiment (red line) and bilayer experiment (blue line). The RA spectra produced after a monolayer adsorption (red line) have been shifted on the *y* axis for clarity, whilst the RA spectra corresponding to the bilayer (blue line) correspond to the *y* axis scale

The RA spectra of the clean Au(110) surface, in figure 6.10 a) are very similar with only a slight difference in the overall intensity of the spectra, which could be associated with slight variations in the Au(110) surface induced during the flame annealing process [19-22]. The addition of the two concentrations of isolated FAD induced changes in the RAS of Au(110), which are associated with the adsorption of a monolayer and bilayer of FAD and are shown in figure 6.10 b). The emergence of the 2.54 eV peak, observed in both spectra in figure 6.10 b) suggests that the isolated FAD molecules have adsorbed via formation of the Au-S bond. The increased concentration of the mutant isolated FAD induced greater changes in the RA spectrum, which is attributed to the formation of a bilayer of adsorbed molecules. The RA spectra in figure 6.10 b) are very similar to the RA spectra produced after the adsorption of a monolayer and bilayer of the full length variant of CPR which are shown in figure 6.1 b).

The spectrum associated with the adsorbed FAD molecules is shown in figure 6.10 c). The main contribution from the adsorbed FAD molecules is in the low energy region as shown in figure 6.10 c), which is observed in both the RAS of the monolayer and bilayer coverage. The strength of the 2.54 eV peak is stronger in the bilayer than the monolayer as is the contribution in the spectral range below 2.6 eV. Both spectrum of a bilayer and monolayer of isolated FAD follow a very similar spectral shape until ~ 4.25 eV were the bilayer spectrum follows a steady negative change in intensity and the monolayer spectrum follows a steady positive change in intensity, as shown in figure 6.10 c). This behaviour was not observed following the adsorption of a monolayer and bilayer of the full length variant of CPR. This difference could be due to slight variation in orientation of the adsorbed molecules in bilayer and monolayer coverage. If so then this difference in behaviour between the isolated FAD and full length variants of CPR could indicate that the difference in orientation between a monolayer and bilayer involves a larger change to the orientation of the FAD domain than the FMN domain, which may account for the difference in spectral shape observed at ~ 4.25 eV after the adsorption of isolated FAD. It is however difficult to determine information on the difference in orientation of the FAD molecules when adsorbed in monolayer or bilayer coverage, and this is not the focus of this research, but it is important to demonstrate the

sensitivity of RAS and the ability of RAS to monitor the difference between a monolayer and bilayer coverage. The identification of the RAS signature of a monolayer adsorption of isolated FAD is a vital prerequisite for monitoring conformational events during electron transfer processes.

Having established that RAS is capable of determining the difference between what is expected to be a monolayer and bilayer coverage of adsorbed CPR molecules, the remainder of the work discussed in this thesis will be aimed at monitoring conformational events occurring on monolayer coverage of full length CPR. This is because it is the full length CPR form of the molecule which is expected to involve the largest conformational events linked to electron transfer process to occur.

6.4 Comparison of RAS of a Monolayer P499C FAD and Full Length CPR

The work presented in this chapter has shown the RA spectra produced after the adsorption of a monolayer and bilayer of both the isolated and full length variant of mutant CPR as shown in figures 6.1 and 6.10. The RA spectra attributed to the monolayer adsorption of isolated FAD and full length CPR have been compared in and are shown in figure 6.11. The RA spectra follow a very similar shape, however there are subtle differences between the monolayer FAD and monolayer full length CPR data as shown in figure 6.11.

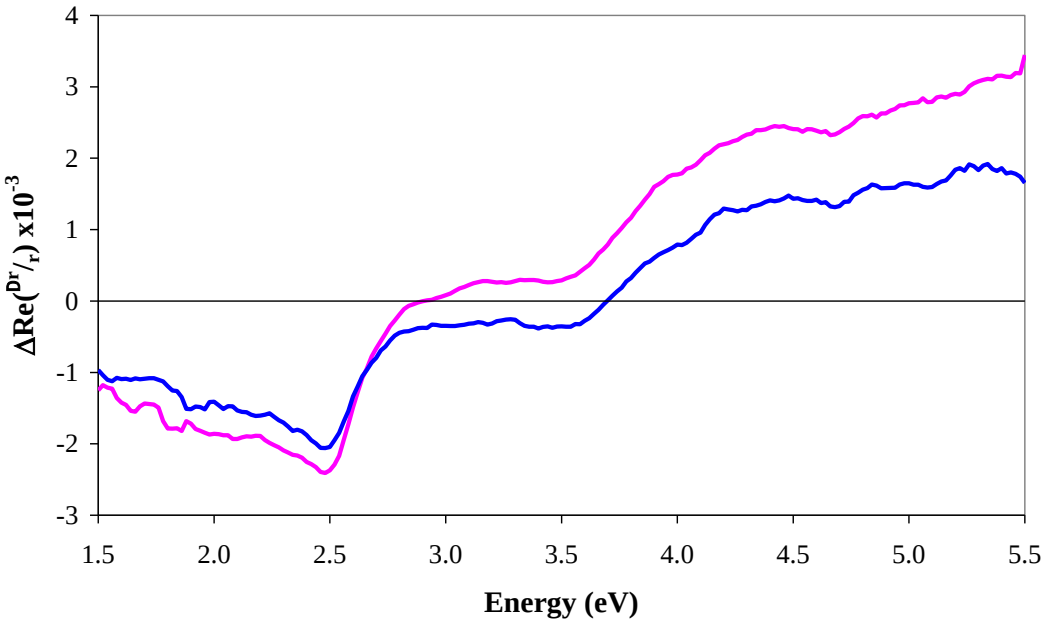

Figure 6.11: RA spectra of monolayer of P499C FAD at -0.657 V (pink line) and P499C full length CPR (blue line) obtained by subtracting the corresponding Au(110) spectrum from the Au(110) + protein spectrum all recorded in 0.1 M NaH_2PO_4/K_2HPO_4 (pH 7.2).

The similarity of the RA spectral shapes in figure 6.11, indicates that both FAD and full length CPR molecules adsorb in a very similar orientation, it also suggests that the RAS contribution from the FMN domain is relatively weak. Although the two spectra follow a very similar spectral shape it is interesting to note that the intensity of the FAD spectrum is greater across the full range spectral range. This difference could be attributed to the difference in surface morphology of the Au(110) substrate between experiments caused by slight variations in the flame annealing procedure [19-22] However it is also possible that the FAD molecules adsorb with a greater overall anisotropy than the full length CPR molecules causing an increase in the RAS signal. This is possible as the FMN domain is expected to be relatively mobile, whereas the FAD molecule is expected to be more rigid. The flexibility of the FMN domain may result in a decrease in the net anisotropy.

6.5 Summary

The RA spectral signatures of both a monolayer and bilayer coverage of variant CPR adsorbed on the Au(110) surface has been reported in this chapter. The conditions were determined after a detailed QCM-D analysis of the adsorption of P499C full length and isolated FAD, which was presented in chapter 5. These RA spectral signatures allow rapid determination of CPR coverage, which aids in ensuring that an ordered monolayer of CPR has been adsorbed. This is an important prerequisite before an accurate investigation of potential induced conformational events in CPR can be studied. The data reported in this chapter is therefore part of a crucial step in the use of the RAS technique to investigate conformational change during electron transfer in CPR.

Replicating the conditions for bilayer and monolayer adsorption determined in QCM-D analysis allowed the RA spectral signatures of both a monolayer and bilayer adsorption of CPR on the Au(110) surface to be established, which have been presented in this chapter. The characteristic Au-S peak at 2.54 eV was observed in the RA spectra of both monolayer and bilayer coverage of CPR, indicating that both form via the interaction between the mutant cysteine molecules and the Au substrate. Clear differences between the RA spectrum of a monolayer and bilayer demonstrated the capability and sensitivity of RAS. A more intense peak at 2.54 eV and a stronger contribution at lower energies were observed in the RA spectrum produced after the adsorption of a bilayer compared to the spectrum of a monolayer of CPR. Further analysis of the adsorption process was carried out using the Rapid RAS instrument, which monitored the RAS intensity at a range of energies as a function of time during the adsorption process. The Rapid RAS data demonstrated that there is a clear difference in the adsorption kinetics at 2.54 eV and 2.7 eV. The adsorption kinetics at 2.5 eV implies that the adsorption process is dynamic, where an initial saturation of the surface is followed by a slower ordering process of the adsorbed CPR molecules, which increases the intensity. This secondary slower ordering was only observed at energies below 2.54 eV which suggested that the secondary ordering process does not change the net orientation of

the dipoles that give rise to the higher energy RAS response of adsorbed CPR molecules.

The effect of azimuthal angular variation on the RA spectral intensity has provided information on the possible orientation of the adsorbed CPR molecules on the Au(110) surface which implies that the optical dipole transitions that give rise to the spectrum must be roughly orientated in a plane normal to the surface and along either the $[1\bar{1}0]$ or [001] axes of the Au(110) surface. The comparison of the strength of features observed in the optical absorption spectrum of the molecule in solution with the RAS of the adsorbed molecules suggests that the reduced contribution to the RAS at higher energies is associated with the orientation of the molecules on the surface, specifically the weak contribution from the isoalloxazine rings could be associated with a nearly vertical orientation of the long axis of the isoalloxazine rings with respect to the Au(110) surface. Whereas the weak contribution from aromatic amino acids in the RAS has been associated with a lack of specific order in the orientation of these dipole moments due to the spread of these molecules throughout the CPR structure.

The identification of the RA spectral signature of a monolayer of full length CPR adsorbed on the Au(110) surface presented in this chapter allowed the preparation of consistent coverage of CPR protein in subsequent RAS experiments.

6. 6 References

[1] C. I. Smith, A. Bowfield, N. J. Almond, C. P. Mansley, J. H. Convery and P. Weightman, *J. Phys. Condens. Matter* **22**, 392001 (2010)

[2] R. Leparc, C. I. Smith, M. C. Cuquerella, R. L. Williams, D. G. Fernig, C. Edwards, D. S. Martin and P. Weightman, *Langmuir* **22**, 3413 (2006)

[3] A. Bowfield, C. I. Smith, M. C. Cuquerella, T. Farrell, D. G. Fernig, C. Edwards and P. Weightman, *Phys. Status Solidi C* **5**, 2600 (2008)

[4] B. M. della Rocca, C. I. Smith, C. Tesauro, A. Desideri and P. Weightman, *Surf. Sci.* **604**, 2170 (2010).

[5] M Sun, T. A. Moore and P. –S. song, *J. Am. Chem. Soc.* **94**, 1730 (1972)

[6] W. A. Eaton, J, Hofrichter, M. W. Makinen, R. D. Andersen and M. L. Ludwig, *Biochemistry* **14**, 2146 (1975)

[7] L. B. -Å. Johansson, Å. Davidson, G. Lindblom and K. R. Naqvi, *Biochemistry* **18**, 4249 (1979)

[8] T. Climent, R. González-Luque, M. Merchán and L. Serrano-Andrés, *J. Phys. Chem. A* **110**, 13584 (2006)

[9] M. Salim, U. Siddiqui, G. Kodali and R. J. Stanley, *J. Phys. Chem. B* **112**, 119 (2008)

[10] P. Weightman, G. J. Dolan, C. I. Smith, M. C. Cuquerella, N. J. Almond, T. Farrell, D. G. Fernig, C. Edwards and D. S. Martin, *Phys. Rev. Lett.* **96**, 086102 (2006)

[11] C. I. Smith, A. Bowfield, G. J. Dolan, M. C. Cuquerella, C. P. Mansley, D. G. Fernig, C. Edwards and P. Weightman, *J. Chem. Phys.* **130**, 044702 (2009)

[12] C. P. Mansley, C. I. Smith, A. Bowfield, D. G. Fernig, C. Edwards and P. Weightman. *J. Chem. Phys.* **132**, 214708 (2010)

[13] A. Bowfield, C. I. Smith, G. J. Dolan, M. C. Cuquerella, C. P. Mansley and P. Weightman. *e-J. Surf. Sci. Nanotech.* **7**, 225 (2009)

[14] C. I. Smith, A. J. Maunder, C. A. Lucas, R. J. Nichols and P. Weightman. *J. Electrochem. Soc.* **150**, E233 (2003)

[15] Image analysis carried out using Image SXM, S. D. Barrett, [http://www.ImageSXM.org.uk] (2011).

[16] B. F. Macdonald and R. J. Cole, *Appl. Phys. Lett.* **80**, 3527 (2002)

[17] P. Weightman, D. S. Martin, R. J. Cole, and T. Farrell. *Rep. Prog. Phys.* **68**, 1251 (2005)

[18] M. Wang, D. L. Roberts, R. Paschke, T. M. Shea, B. S. Siler-Masters and J. J. P. Kim, Proc. Natl. Acad. Sci. USA **94**, 8411 (1997)

[19] B. Sheridan, D. S. Martin, J. R. Power, S. D. Barrett, C. I. Smith, C. A. Lucas, R. J. Nichols and P. Weightman, *Phys. Rev. Lett*. **85**, 4618 (2000).

[20] V. Mazine, Y. Borensztein, L. Cagon and P. Allongue, *Phys. Status Solidi A* **175**, 311 (1999)

[21] V. Mazine and Y. Borensztein, *Phys. Rev. Lett*. **88**, 147403 (2002)

[22] P. Weightman, C. I. Smith, D. S. Martin, C. A. Lucas, R. J. Nichols and S. D. Barrett, *Phys. Rev. Lett* **92**, 199707 (2004)

Chapter 7

Monitoring the Effect of Changing the Applied Potential on the RAS of a Monolayer of P499C Full Length CPR on the Au(110) Surface

Having established the RA spectral signature of monolayer coverage of P499C full length CPR this repeats the results of the studies of changes in the RAS intensity profile of a monolayer of P499C full length CPR during electron transfer processes induced by potential control of the Au(110) electrode.

7.1 Introduction

The ability of RAS to monitor changes in spectral intensity as a function of electrode potential was demonstrated in chapter 4 of this thesis. However this earlier study was carried out on what was later shown to be a multilayer adsorption of CPR molecules onto the Au(110)/electrode surface. Having established the conditions for monolayer adsorption of CPR and demonstrated the ability of the RAS technique to distinguish between bilayer and monolayer coverage of CPR, it was then possible to study the effect of electron transfer processes on the RAS of the adsorbed molecules.

In chapter 4 a technique of monitoring the RAS intensity at key energies during repeated potential changes was established. This involved recording the effects of repeated potential steps and averaging the data to reduce the noise. This technique has been used to obtain the data discussed in this chapter. The automated computer software package which allows repeated scans to start automatically and continue until a pre-determined time was also employed. The preliminary data reported in chapter 4 suggested that stepping to the 0.056 V redox potential induced irreversible changes in the RA spectral shape. These changes are thought to be associated with a changes in orientation or coverage of CPR on the Au(110) surface. Therefore to avoid changes to coverage or orientation and allow the RAS intensity to be monitored over multiple repeat potential steps, the 0.056 V electrode potential was avoided for the majority of experiments reported in this chapter, in order to minimise any inaccuracies in the data that might arise from a change in CPR coverage.

The electrode potential was repeatedly stepped between -0.652 V, the $4e^-$ reduced potential where the CPR molecule is expected to adopt an open conformation and -0.465 V, the $2e^-$ reduced potential where the CPR molecule is expected to adopt a more compact conformation [1-4]. Table 4.1 shows the redox potential for P499C full length CPR and also illustrates the likely sites for the electrons in each redox state. From this it is clear that at -0.652 V, the fully reduced state, there is only one possible redox state, whereas at the redox potential -0.465 V there are as many as three different redox states that can be adopted. Each redox

state may involve the CPR molecule adopting a different conformation [4]. It is not clear which redox state is preferred at -0.465 V, therefore by stepping to the electrode potential between the $4e^-$ and $2e^-$ reduced states is likely to involve conformational change in the CPR structure, whilst hopefully avoiding any irreversible changes to coverage of CPR orientation as observed in chapter 4 after potential steps to 0.056 V.

7.2 The Effect of Electron Transfer in a Monolayer of Adsorbed P499C Full Length CPR

The Au(110) crystal was prepared following the procedures outlined in Chapter 2 of this thesis. Careful control of the flame annealing process was followed to ensure that reproducible RA spectra of the clean Au(110) surface were produced. The consistent preparation of the Au(110) surface is an important prerequisite to the adsorption of CPR as it was shown in AFM autocorrelation data [5] that the substrate appears to contribute to the local order of the adsorbed molecules.

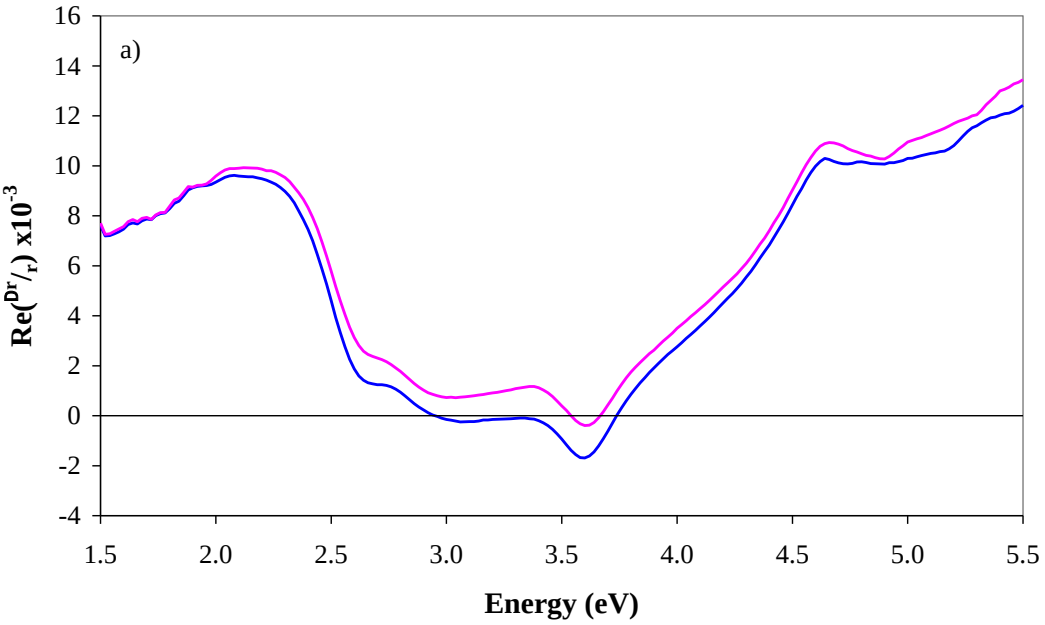

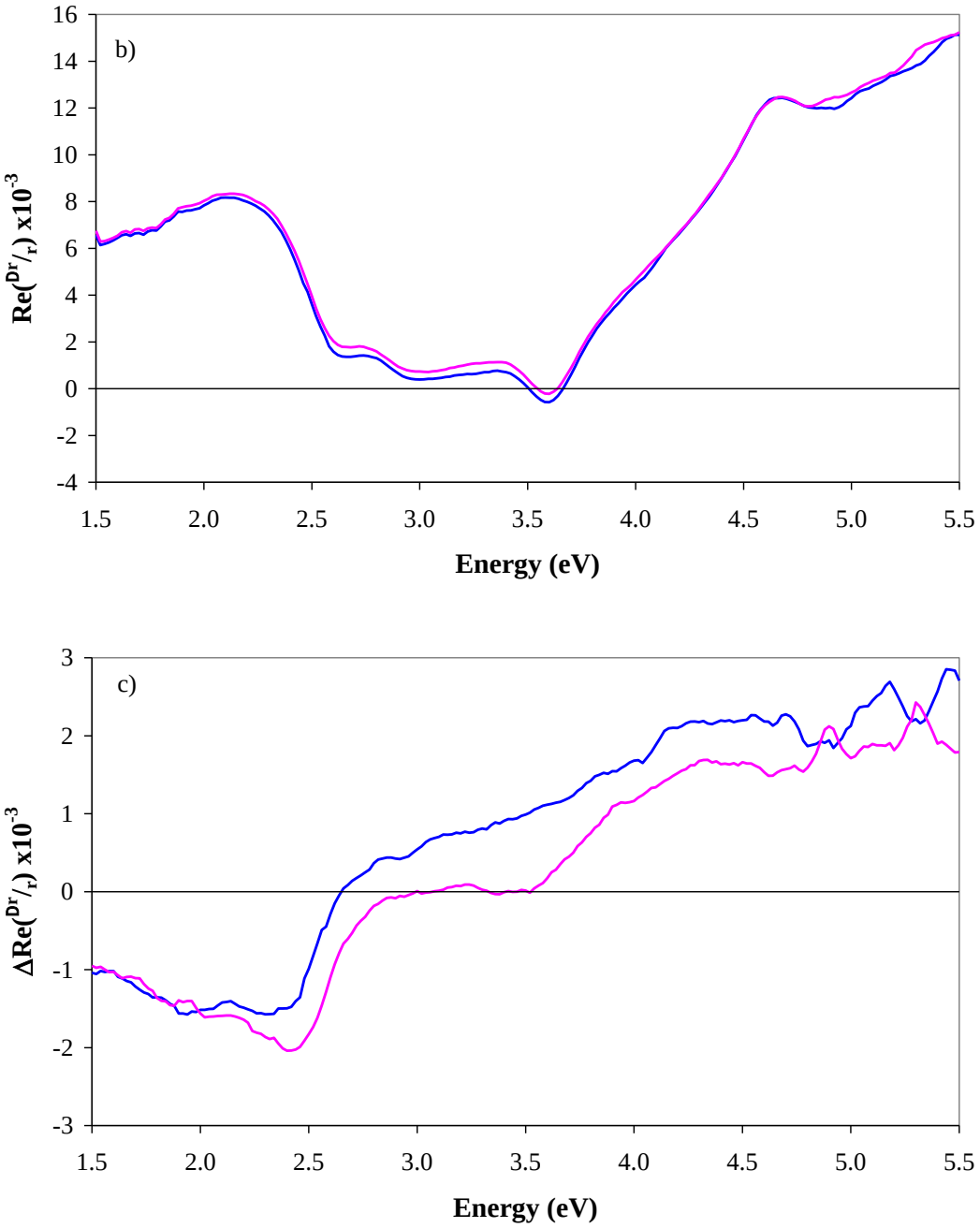

Figure 7.1: RA spectra produced at the applied electrode potentials of -0.652 V (pink line) and -0.465 V (blue line) of a) the clean Au(110), b) Au(110) + P499C full length CPR after monolayer adsorption and c) P499C full length CPR obtained after the subtraction of the RAS of clean Au(110) from the RAS of Au(110) + CPR at the corresponding potentials. All RA spectra were produced in 0.1M NaH_2PO_4/K_2HPO_4 pH 7.2.

The adsorption of a monolayer of P499C full length CPR induced changes in the RA spectrum of the clean Au(110). These changes are shown in figure 7.1. The RA spectra in figure 7.1 were produced at -0.652 V and -0.465 V for clean Au(110) (figure 7.1 a)) and again after the adsorption of a monolayer of full length CPR (figure 7.1 b)) during the same experiment. The RA spectral shape remained very similar at each of the applied electrode potentials of -0.652 V and -0.465 V, however the change in potential caused a negative increase in the RAS intensity across the full spectral range in the RA spectra of both the clean Au(110) (figure 7.1 a)) and of Au(110) + CPR (figure 7.1 b)). The greatest increase in RAS intensity as the potential was changed was observed between 2.5 eV and 4.0 eV. However the change in RAS intensity as the potential was changed from -0.652 V to -0.465 V was significantly reduced after the adsorption of full length CPR (figure 7.1 b)). The intensity changed by ~ 0.3 units after the adsorption of CPR, in comparison with a change in intensity of ~ 1.3 units observed in the RA spectra of clean Au(110). The RAS contribution from the adsorbed CPR molecules shown in figure 7.1 c), was produced following the subtraction of the RAS of clean Au(110) from the RAS of Au(110) + CPR at the corresponding potentials [6-9]. The intensity of the resultant RA spectra in figure 7.1 c) shifts in the positive direction as the potential was changed from -0.652 V to -0.465 V, this change in intensity being accompanied by the reduction in intensity of the peak at ~ 2.54 eV and the loss of the shallow negative peak at ~ 3.5 eV. These observed changes in the RA spectra of CPR could be associated with a change in the orientation of the CPR molecules on the Au(110) surface which could be the result of conformational change induced by the change in applied potential.

The RAS of Au(110) + full length CPR is expected to be the sum of the individual RAS contributions of the Au(110) and the adsorbed ordered CPR layer. The change in potential from -0.652 V to -0.465 V results in a more negative RAS profile over almost the whole spectral range for Au(110). After the adsorption of CPR this change in potential produced a similar but significantly reduced shift in profile. The relatively small intensity of the RAS of CPR (figure 7.1 c)) shows that the individual RAS contribution from the adsorbed CPR is small. The RAS profiles of Au(110) + CPR (figure 7.1 b)) are closer together than those of the clean Au(110)

surface (figure 7.1 a)) as a function of the applied potential. This could arise if the change in potential from -0.652 V to 0.056 V induces Au(110) and CPR changes in opposite directions.

This is supported by the results discussed in chapter 4 for the multilayer adsorption of CPR which showed that the RAS intensity of Au(110) + CPR shifted in the opposite direction to that of the clean Au(110) as a result of increasing the applied potential from the negative to the more positive redox potentials. The RAS signal from adsorbed multilayer of CPR will be stronger than that of a monolayer and dominates the contribution from the Au surface.

The Au(110) surface does not to undergo a large surface reconstruction as the applied potential is changed from -0.652 V to -0.465 V [10] so the negative increase in RAS intensity of Au(110) is not associated with a large surface reconstruction but is more likely to be associated with slight variations and movements of Au atoms on the surface. Regardless of the source of these changes in the RAS intensity of clean Au(110) the adsorption of a monolayer of full length CPR does not appear to prevent it from occurring.

7.2.1 Monitoring the RAS Intensity of Au(110) + P499C Full Length CPR During Repeated Potential Steps Between -0.652 V and -0.465 V

The changes in the RAS intensity of Au(110) + CPR induced by changing the applied electrode potential have been monitored in real time at the two energies 2.7 eV and 2.54 eV in two separate experiments. Monitoring the RAS intensity at these energies is expected to offer a good chance of observing any conformational events linked to the electron transfer process. The 2.7 eV energy range is associated with the λ_{max} of the isoalloxazine rings[11-15], whereas 2.54 eV is associated with the Au-S bond [16-18]. Changes in CPR conformation are expected to involve the relative movement of the FMN and FAD/NADPH domains [1-4,19]. Monitoring changes in the RAS intensity at 2.7 eV might be expected to reveal any relative motion of the FAD and FMN domains since each domain contains an isoalloxazine,

RAS intensity was monitored during repeated potential steps using the same procedures described in chapter 4, following the adsorption of an ordered monolayer of P499C full length CPR onto the Au(110)/liquid interface. The applied electrode potential was stepped between two potentials ten times per scan in order to induce reversible electron transfer processes. Each scan was repeated several times and the RAS intensity was averaged over an increasing number of potential steps in order to improve the signal to noise. Further smoothing of the data was also performed by calculating a five point average. The applied potential was stepped between -0.652 V (0 – 60 seconds) and -0.465 V (60 – 120 seconds). This change in applied potential is expected to induce a two electron transfer process in the adsorbed CPR molecules, from a fully reduced state to the two electron reduced state, at -0.652 V and -0.465 V respectively (Table 4.1). The two electron reduced state at -0.465 V can correspond to several possible redox states, the di-semiquinone: FAD•/FMN• state or the hydroquinone states: FAD/$FMNH_2$ and $FADH_2$/FMN, as shown in table 4.1 [20].

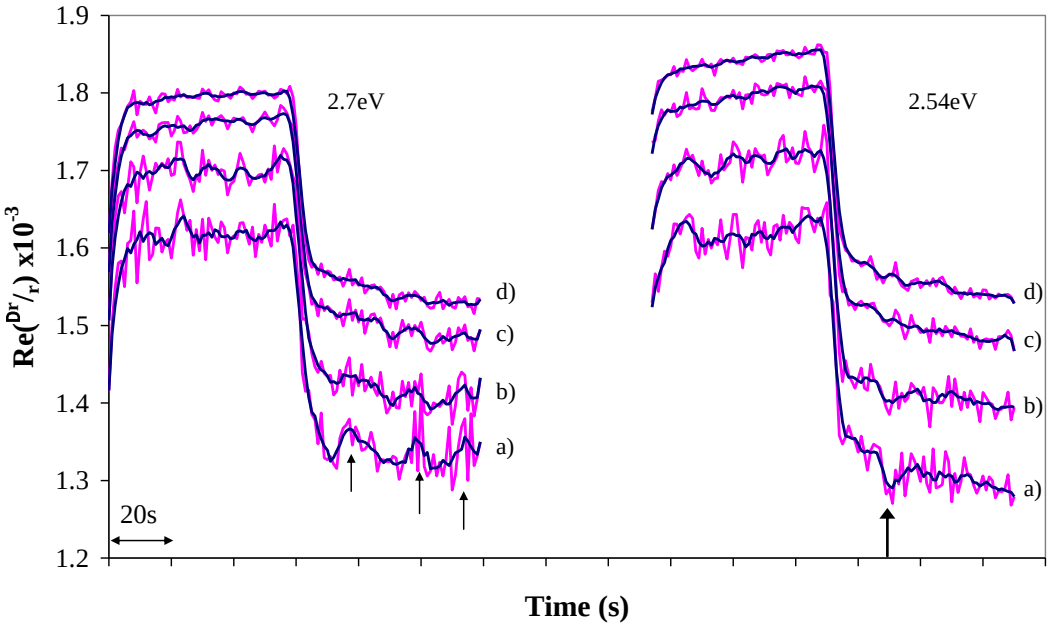

Figure 7.2: RAS intensity as a function of stepping the applied potential between -0.652 V and -0.465 V after the adsorption of a monolayer of P499C full length CPR at 2.7 eV (left side of chart) and 2.54 eV (right side of chart). In each case the average RAS intensity (pink line) was obtained after a) 5 b) 10 c) 25 and d) 50 potential steps and is shown with the corresponding 5 point smoothing average (blue line). The RA spectra at each energy have been shifted on the *y*-axis allowing them to be stacked for clarity. The 2.54 eV RAS intensity data has also been shifted on the *x*-axis to allow side by side comparison between the two energies, the arrow on the *x*-axis corresponds to 20 seconds.

The data on the left of figure 7.2 show the average RAS intensity at 2.7 eV as a function of the repeated potential step produced after averaging the RAS intensity obtained after 5, 10, 25, and 50 potential steps. As the potential was changed from -0.652 V to -0.465 V at 60 seconds, an initial negative change in the RAS intensity of ~ 0.3 units was observed at 2.7 eV which occurred over approximately 10 seconds (figure 7.2). After the initial negative increase in intensity, 3 small positive features ~ 0.04 units in intensity were observed in the RAS intensity at 2.7 eV which were observed approximately 20, 40 and 55 seconds after the potential was changed to 0.056 V as shown by the arrows in figure 7.2 left

side of chart). Averaging the RAS intensity over an increasing number of potential steps resulted in the significant reduction in noise but also in the intensity of the 3 features, as shown in figure 7.2 a)-d) left hand side of chart.

The RAS intensity monitored at 2.54 eV during the same potential step in a separate experiment is shown in the right hand side of the graph in figure 7.2, which also shows the average RAS intensity obtained after 5, 10, 25 and 50 potential steps and the 5 point smoothing average. The RAS intensity at 2.54 V again shifts in the negative direction by ~ 0.3 units as the potential was changed to -0.465 V after 60 seconds at -0.652 V. Following this large initial shift in intensity a small feature approximately 0.04 units high was also observed in the RAS intensity at 2.54 eV. This small negative feature was observed approximately 20 seconds after the potential was changed to -0.465 V. The intensity of this feature also reduced significantly as the RAS intensity was averaged over an increasing number of potential steps (figure 7.2 a) -d) right hand side of chart).

The features observed in the RAS intensity at 2.7 eV are similar in intensity and occur on a similar time scale to those observed at the same energy in chapter 4. The 3 features occur on a much slower timescale than the initial ~ 0.3 unit change in RAS intensity, which could be associated with a change in orientation of the adsorbed CPR molecules on the Au(110) surface. The change in potential from -0.652 V to -0.465 V is expected to induce a change in conformation of CPR [1-4]. The 3 oscillations observed at 2.7 eV could be a signal of a subtle change in conformation, possibly involving the relative change in orientation of the FAD and FMN domains. The observation of a small negative feature of similar intensity in the RAS at 2.54 eV (figure 7.2 right side of graph) could also be associated with changes in conformation of two domains as the broad 2.7 eV peak associated with the isoalloxazine rings which was observed in the absorption spectrum of P499C full length CPR shown in figure 7.4, may overlap with the signal from the Au-S bond at 2.54 eV [13]. The overlapping of the RA signals from the isoalloxazine rings and the Au-S bond has been discussed previously in chapter 6. It is important to note that the features observed at both 2.54 eV and 2.7 eV as a result of stepping the applied potential reduced significantly as the intensity was averaged over an increasing number of potential steps. This suggests that the features could result from noise.

However it is also possible that as the number of potential steps is increased the adsorbed CPR molecules may lose some of their functional ability or even start to desorb from the Au(110) surface, which might also cause the signal to reduce as a function of the number of potential steps. Evidence for this was shown in chapter 4, where significant changes were observed in RA spectra after repeated potential steps. This suggested that the adsorbed CPR molecules had possibly become denatured or partially desorbed from the Au(110) surface. Therefore it is likely that the adsorbed protein becomes damaged after repeated cycling of the applied potential.

7.2.2 Monitoring the RAS Intensity of Clean Au(110) During Repeated Potential Steps Between -0.652 V and -0.465 V

In order to probe the origin of the oscillations observed in the RAS intensity after the adsorption of a monolayer of CPR, the RAS intensity of clean Au(110) at 2.7 eV has been monitored during the same repeated potential step. The RAS intensity was averaged over increasing numbers of potential steps and again this was carried out following the procedures described in chapter 4.

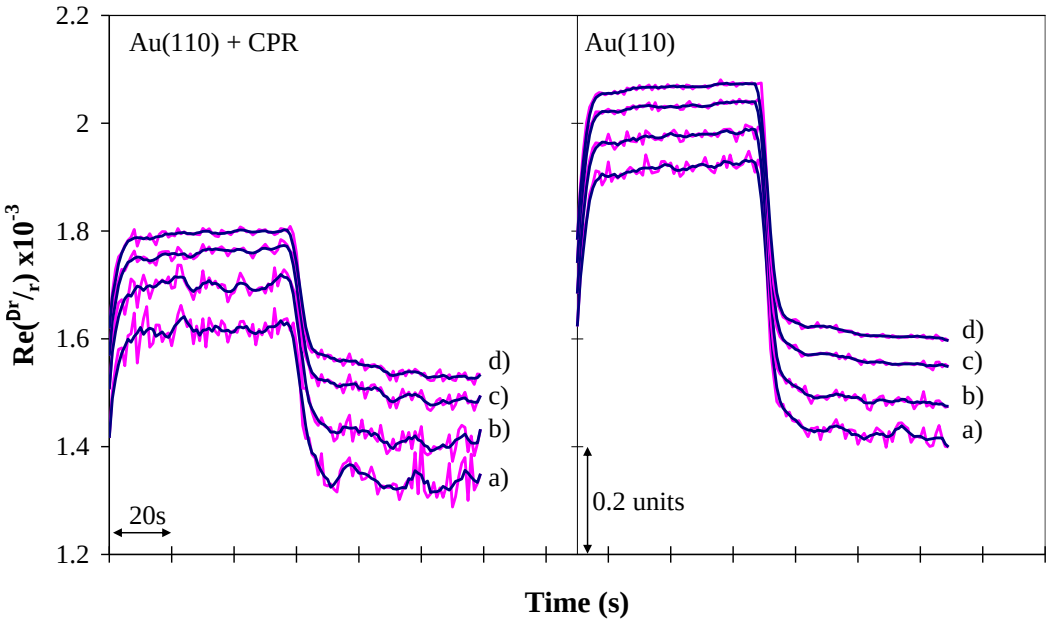

Figure 7.3: RAS intensity as a function of stepping the applied potential between -0.652 V and -0.465 V after the adsorption of a monolayer of P499C full length CPR at 2.7 eV (left side of chart) and for the clean Au(110) surface at 2.7 eV (right side of chart).The RAS intensity profiles have been shifted on the *y*-axis allowing the data to be presented in stacked formation for clarity. In each case the average RAS intensity was obtained after a) 5 b) 10 c) 25 and d) 50 potential steps and is shown with the corresponding 5 point smoothing average. The arrow on the *x*-axis corresponds to 20 seconds.

After the applied potential was changed to -0.465 V the RAS intensity at 2.7 eV of clean Au(110) shifts in the negative direction by ~ 0.5 units, which occurs over ~ 10 seconds after the potential was changed. This change in RAS intensity in the clean Au(110) data is greater than that observed after the adsorption of CPR at both 2.7 eV as shown in figure 7.3 left side of chart and at 2.54 eV as shown in figure 7.2 right side of chart. However the intensity does change over a similar timescale. After this initial change in RAS intensity of clean Au(110), shown in figure 7.3 right hand side of chart, two possible features were observed after ~ 15 and ~ 43 seconds of changing the applied potential to -0.465 V. These features are similar in shape to the ones observed in the RAS data after the adsorption of CPR

but only have an intensity of ~ 0.02 units significantly smaller than the intensity, ~ 0.04 units, of the features observed after the adsorption of full length CPR (figure 7.3). The features in the RAS intensity of clean Au(110) also reduce significantly in intensity as the number of potential steps averaged was increased. The change in RAS intensity of clean Au(110), as the potential was changed to -0.465 V is not associated with a large surface reconstruction and could be attributed to slight changes in arrangement of Au atoms on the Au(110) surface.

The comparison of the RAS intensity of clean Au(110) and Au(110) + CPR at 2.7 eV as a function of the same change in applied potential, might suggest that the features observed in both data sets may be due to a contribution from instrumental noise. However the features are more intense after the adsorption of a monolayer of full length CPR and appear to reduce in intensity at a slower rate than for Au(110) as the RAS response is averaged over an increasing number of potential steps, as shown in figures 7.2 and 7.3.

There are some similarities between the RAS response of clean Au(110) and after the addition of CPR, including the direction of the intensity change and the time scale of the initial change in intensity. These changes are now examined in detail using the rapid RAS instrument.

7.2.3 Monitoring the RAS Intensity of Clean Au(110) and After the Adsorption of a Monolayer of Full Length CPR as a Function of Applied Potential Using the Rapid RAS Instrument

The rapid RAS instrument employs a 32 channel UV enhanced photodiode array which allows the RAS intensity to be monitored over a range of wavelengths in very short time scales simultaneously. This instrument was described in detail earlier [21] and in chapter 2 and was used to monitor the RAS intensity of both the clean Au(110) and Au(110) + CPR as a function of changing the applied electrode potential.

The RAS intensity of clean Au(110) in 0.1 M NaH_2PO_4/K_2HPO_4 pH 7.2 was monitored as the potential was stepped every 60 seconds in sequence through the redox potentials of full length CPR from -0.652 V through to 0.056 V and then in reverse order back to -0.652 V. After the RAS intensity of the clean Au(110) had been monitored a monolayer of P499C full length CPR was adsorbed onto the Au(110) surface and the RAS intensity was again monitored as a function of the same potential steps. This allowed a direct comparison of the RAS response of clean Au(110) and Au(110) + CPR uncompromised by any slight variations in the RAS induced by differences in specimen preparation and the flame annealing and crystal preparation process.

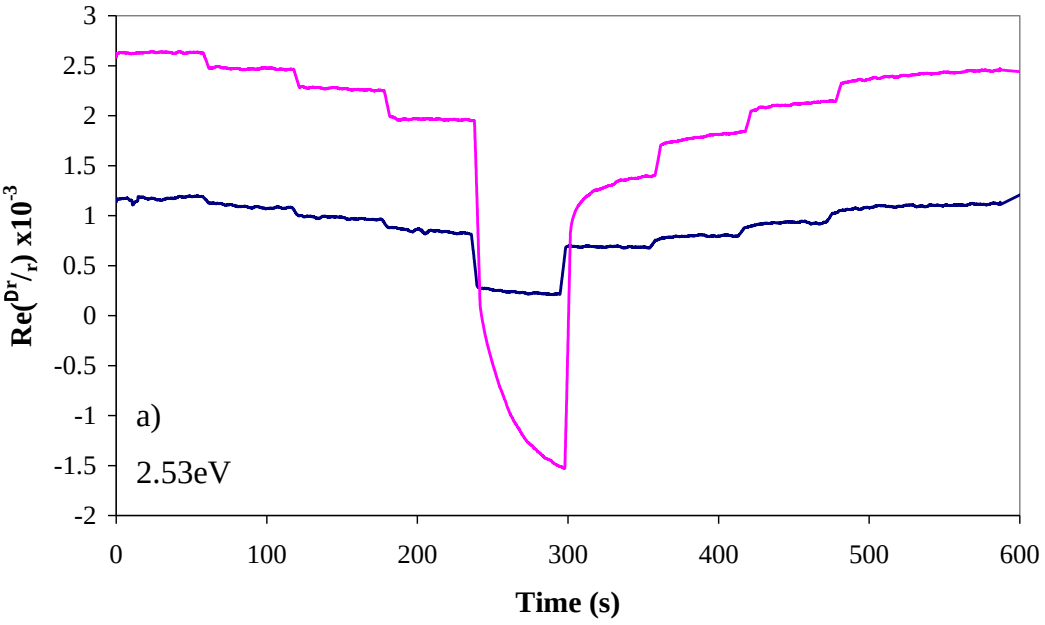

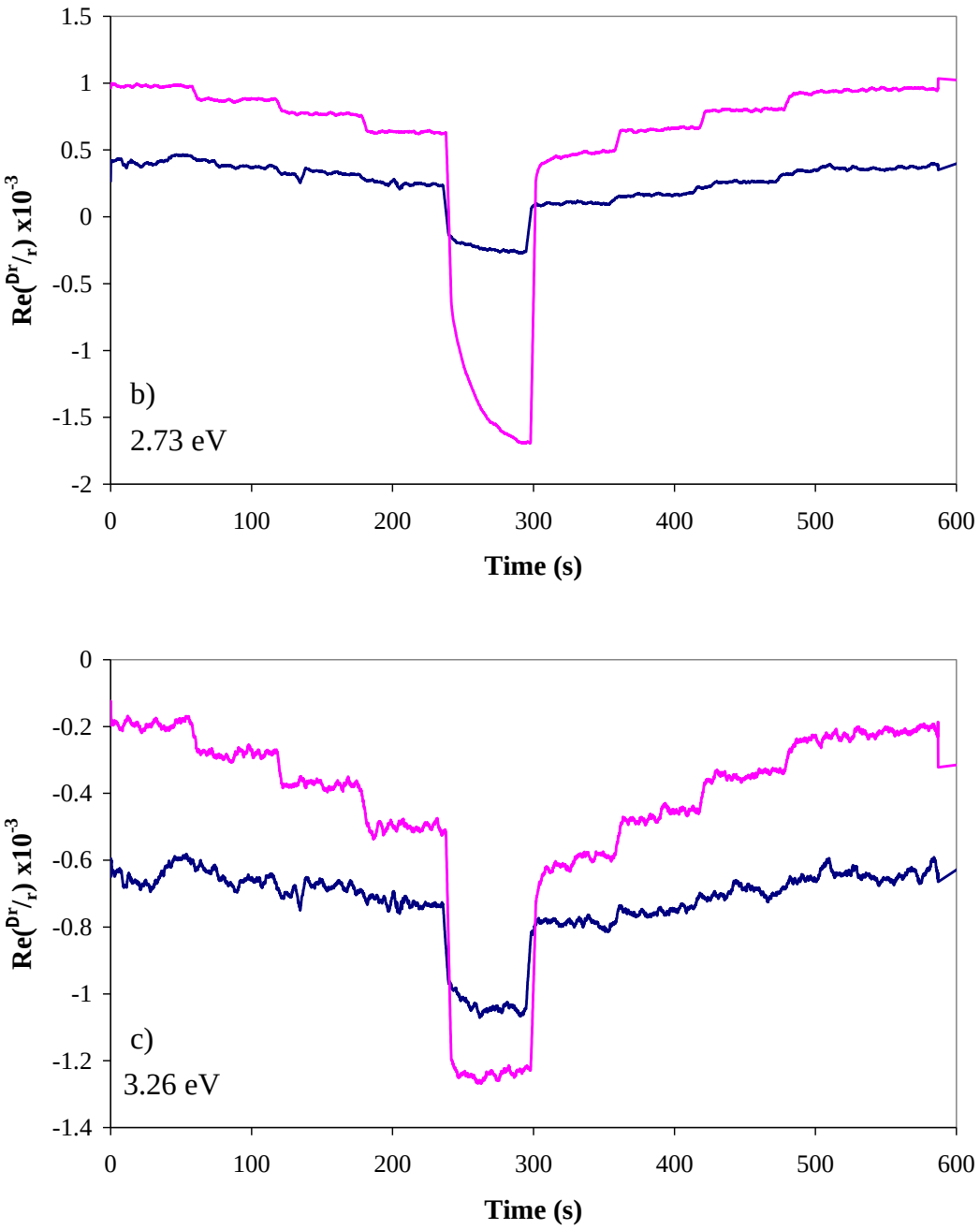

Figure 7.4: Rapid RAS intensity of clean Au(110) (pink line) and Au(110) + full length CPR (blue line) recorded as a function of stepping the applied potential between -0.652 V, -0.557 V, -0.465 V, -0.376 V and 0.056 V in sequence every 60 seconds starting and finishing at -0.652 V. The RAS intensity is shown at a) 2.53 eV b) 2.73 eV and c) 3.26 eV.

The RAS intensity of both clean Au(110) and Au(110) + CPR at 3 energies across the RA spectral range are shown in figure 7.5. The change in RAS intensity of clean Au(110) is greater than that of Au(110) + CPR, with the largest change in RAS intensity of both the clean Au(110) and Au(110) + CPR observed between 240 seconds and 300 seconds, as the applied potential was changed from -0.376 V to 0.056 V. The change in RAS as the potential is changed from -0.376 V to 0.056 V is associated with the surface reconstruction from a (1×3) to the anion induced (1×1) surface structure for clean Au(110) [10] as shown in figure 7.5 a). However the RA spectral signature of the anion induced (1×1) surface structure is not observed at 0.056 V after the adsorption of a monolayer of P499C full length CPR, as shown in figure 7.5 b). These results establish that the RAS response of the Au(110) surface as a function of the applied potential is significantly modified by the adsorption of CPR. Both the RAS intensity of clean Au(110) and Au(110) + CPR demonstrate a slight irreversibility in the RAS intensity at corresponding changes in the applied potential. In both cases the RAS intensity observed at -0.376 V does not return to the same intensity at -0.376 V after the potential was stepped to 0.056 V (figure 7.4). This may be the result of a slightly mixed surface structure after the potential is changed from 0.056 V to -0.376 V.

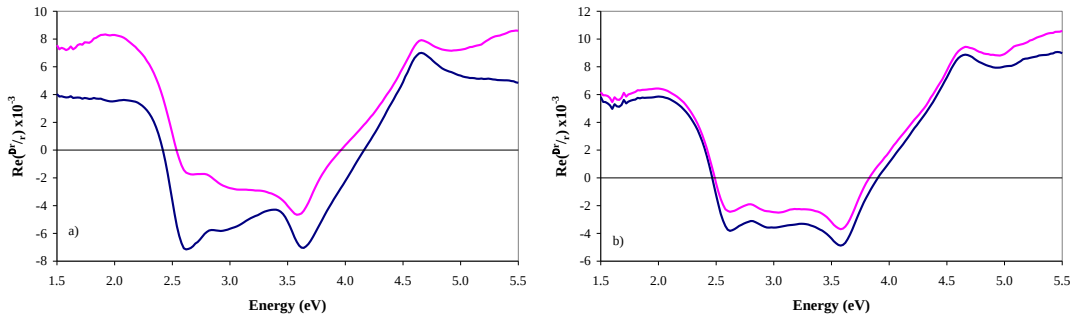

Figure 7.5: RA spectra produced at -0.376 V (pink line) and 0.056 V (blue line) of a) the clean Au(110) surface and b) Au(110) + full length CPR, produced approximately 90 minutes after the clean Au(110) spectra were produced.

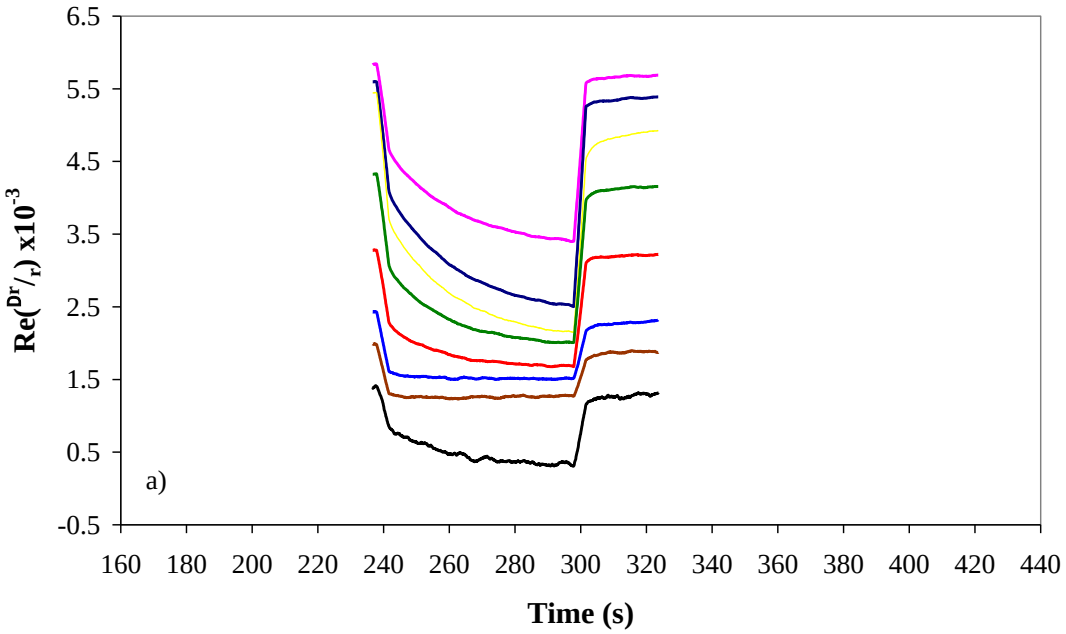

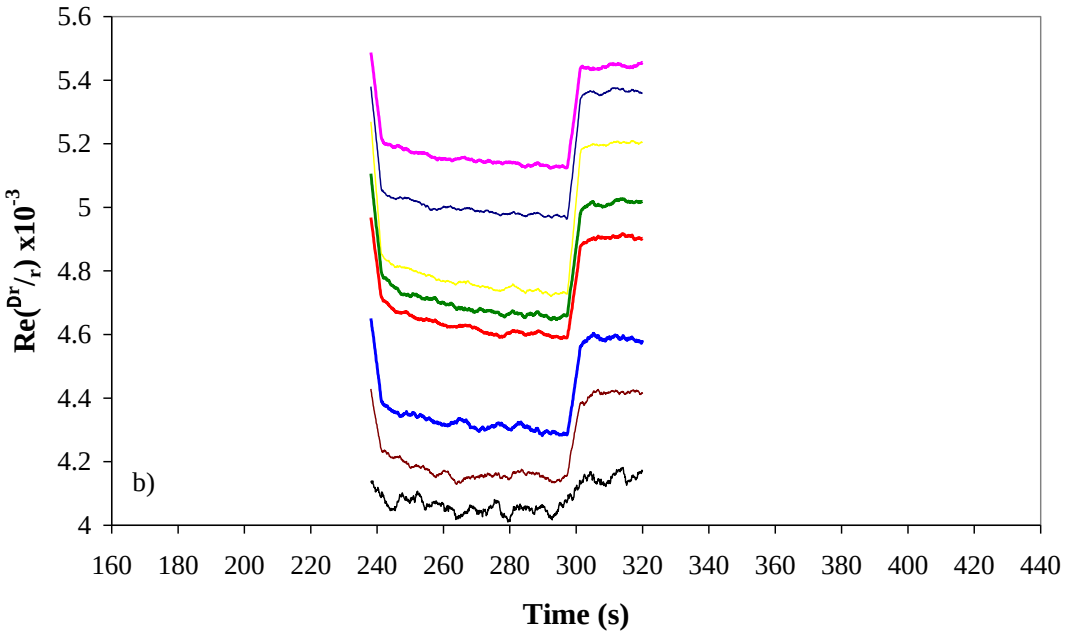

Figure 7.6: The RAS intensity of a) clean Au(110) and b) Au(110) + CPR as the applied potential is changed from -0.376 V to 0.056 V at 240 s and back to -0.376 V at 300 s monitored at 1.84 eV (pink line), 2.07 eV (dark blue line), 2.59 eV (yellow line), 2.73 eV (green line), 2.89 eV (red line), 3.16 eV (blue line), 3.26 eV (brown line), 3.74 eV (black line).

The effect of changing the applied potential between the negative redox potentials of -0.652 V, -0.557 V, -0.465 V and -0.376 V induces only a small change in the RAS intensity of both the clean Au(110) and after the adsorption of CPR, as observed in figure 7.5 as the potential was stepped between the negative potentials between 0 to 240 seconds and 300 to 600 seconds. The influence of the adsorption of CPR can be more clearly observed by comparing the RAS intensity as the potential is changed from -0.376 V to 0.056 V and back to -0.376 V after 60 seconds for both clean Au(110) and Au(110) + CPR, as shown in figure 7.6.

The RAS intensity of clean Au(110) increases in the negative direction by a greater amount than the intensity of Au(110) + CPR as the potential is changed from -0.376 V to 0.056 V. The dynamics of this change in RAS intensity of the clean Au(110) appears to involve two stages with a quick initial change followed by a slower change. The RAS intensity changes very quickly over approximately the first 5 seconds and then follows a slower steady negative increase in intensity which continues until the potential is switched from 0.056 V to -0.376 V. This secondary change in intensity is clearly observed at 1.84 eV, 2.07 eV, 2.59 eV and 2.73 eV as shown in figure 7.6 a). This apparent two stage change in RAS intensity does not occur across the full spectral range. At higher energies, between 3.16 eV and 3.26 eV the RAS intensity appears to change quickly and then reach a maximum after ~ 5 seconds, as shown in figure 7.6 a).

The changes in RAS intensity as a function of the corresponding applied potential changes after the adsorption of a monolayer of CPR are shown in figure 7.6 b). The adsorption of full length CPR reduces the overall change in RAS intensity observed and also appears to affect the dynamics of the intensity change. The two stage change in RAS intensity clearly observed in the RAS of clean Au(110) (figure 7.6 a)) is much more subtle after the addition of CPR and the RAS intensity appears to follow the same dynamics across the full spectral range. These differences in the dynamic behaviour of the RAS intensity as the potential was changed from -0.376 V to 0.056 V suggest that the adsorption of CPR molecules influences the RAS response as a function of applied potential. The slower secondary negative drift in RAS intensity observed after the initial rapid change in intensity as the potential is changed from -0.376 V to 0.056 V has been measured

across the full spectral range for both clean Au(110) and Au(110) + CPR and is shown in figure 7.7. The RAS intensity of the clean Au(110) surface drifts by approximately 1.0 units following the initial rapid change in intensity as the potential is changed from -0.376 V to 0.056 V. This secondary negative drift in RAS intensity is shown to decrease drastically between 3.0 eV and 3.5 eV for clean Au(110) in figure 7.7. The RAS intensity after the adsorption of a monolayer of CPR only drifts by ~ 0.08 units following the initial intensity increase after the potential was changed from -0.376 V to 0.056 V. This drift in intensity after the adsorption of a monolayer of CPR is shown to remain almost constant across the full spectral range in figure 7.7. The data in figure 7.7 clearly demonstrates that the adsorption of CPR influences the RAS intensity dynamics of the Au(110) surface. The two stage change in RAS intensity observed for clean Au(110) could be associated with the surface reconstruction from the (1×3) to the anion induced (1×1) surface structure induced by change the applied potential to the 0.056 V. The secondary slower change in RAS intensity could be associated with a slower ordering process which may involve the ordering of the adsorbed anions on the Au surface, which is not expected to occur after the adsorption of CPR.

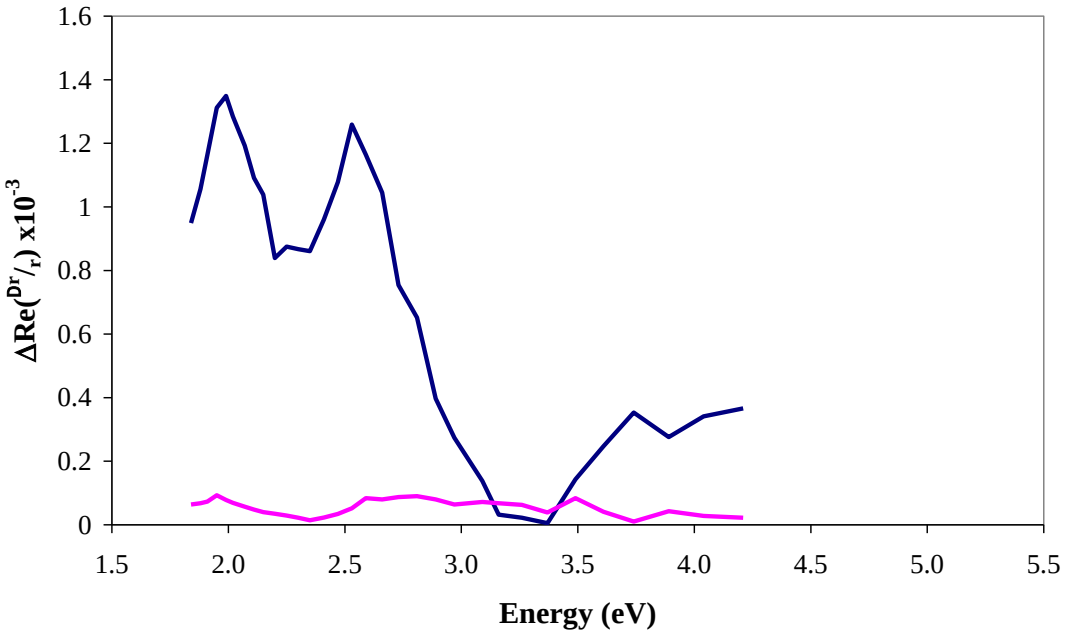

Figure 7.7: Difference in RAS intensity 10 seconds after the potential was changed to 0.056 V and again 40 seconds later for clean Au(110) (blue line) and Au(110) + CPR (pink line).

The rapid RAS data clearly demonstrates that the adsorption of CPR influences the RAS response of the Au(110) surface as a function of applied potential, with a significant reduction in the overall change in intensity as well as changes in the dynamics of the intensity shift. However similarities between the RAS response of Au(110) and Au(110) + CPR were also observed, such as the observed irreversible behaviour of the RAS intensity after the 0.056 V potential step and the fact that the largest change in RAS intensity was observed in both the clean Au(110) and Au(110) + CPR data as the potential was changed from -0.376 V to 0.056 V. These similarities suggest that the Au(110) substrate could also influence the RAS Au(110) + CPR but it is difficult to accurately determine the extent of this.

7.3 Summary

This chapter has demonstrated the effect of changing the applied electrode potential on the RAS response of both clean Au(110) and Au(110) + CPR. This potential step

induces a 2 electron transfer in CPR which is expected to be accompanied by extensive domain motion [1-4]. The data discussed in this chapter demonstrate how this change in potential induces a shift in the RAS intensity of Au(110) + CPR after which small features were observed in the RAS intensity at 2.7 eV and 2.54 eV. These features are of a similar intensity and occurred on a similar time scale to the ones observed in the preliminary data in chapter 4. The features could be associated with conformational events in CPR induced by the electron transfer process. However as the RAS intensity was averaged over an increasing number of potential steps the intensity of these features decreased. It is possible that as a result of repeated potential steps the CPR molecules denature, if this was to happen then it would affect the function of the adsorbed CPR molecules, which could prevent or restrict conformation events in CPR. This would account for the decrease in intensity of the features observed in the average RAS intensity of multiple potential steps. However the decrease in intensity of the features could also indicate that they are caused by a contribution from instrumental noise. The same potential steps induced a similar but greater shift in RAS intensity of clean Au(110). Small features were also observed in the RAS intensity of clean Au(110), which could be associated with the features observed in the RAS intensity after the adsorption of CPR. However the rapid RAS data has demonstrated that the adsorption of CPR influences the RAS response to the applied potential and highlighted clear differences in the RAS response of clean Au(110) and Au(110) + CPR. Despite these differences it is very difficult to accurately pin down a signal produced by a change in conformation of the adsorbed CPR molecules.

Although the data discussed in this chapter have highlighted some differences in the RAS response as a result of the adsorption of CPR, some similarities between the RAS intensity of clean Au(110) and Au(110) + CPR as a function of applied potential were also observed. In order to extract accurate information on conformational events in the adsorbed CPR molecules it is necessary to separate as much of the RAS signal of the Au(110) substrate from that of the adsorbed CPR molecules as possible. The following chapter of this thesis explores techniques that achieve this aim.

7.4 References

[1] J. Ellis, A. Gutierrez, I. L. Barsukov, W. C. Huang, J. G. Grossmann, and G. C. Roberts, *J. Biol. Chem*. **284**, 36628 (2010)

[2] A. Gutierrez, M. Paine, C. R. Wolf , N. S. Scrutton, and G. C. Roberts. *Biochemistry* **41**, 4626 (2002)

[3] A. Grunau, K. Geraki, J. G. Grossmann, and A. Gutierrez, *Biochemistry* **46**, 8244 (2007)

[4] S. Hay, S. Brenner, B. Khara, A. M. Quinn, S. E. Rigby, and N. S. Scrutton. *J. Am. Chem. Soc.* **132**, 9738 (2010)

[5] Image analysis carried out using Image SXM, S. D. Barrett, [http://www.ImageSXM.org.uk] (2011)

[6] P. Weightman, G. J. Dolan, C. I. Smith, M. C. Cuquerella, N. J. Almond, T. Farrell, D. G. Fernig, C. Edwards and D. S. Martin, *Phys. Rev. Lett.* **96**, 086102 (2006)

[7] C. I. Smith, A. Bowfield, G. J. Dolan, M. C. Cuquerella, C. P. Mansley, D. G. Fernig, C. Edwards and P. Weightman, *J. Chem. Phys.* **130**, 044702 (2009)

[8] C. P. Mansley, C. I. Smith, A. Bowfield, D. G. Fernig, C. Edwards and P. Weightman, *J. Chem. Phys.* **132**, 214708 (2010)

[9] A. Bowfield, C. I. Smith, G. J. Dolan, M. C. Cuquerella, C. P. Mansley and P. Weightman, *e-J. Surf. Sci. Nanotech.* **7**, 225 (2009)

[10] C. I. Smith, A. Bowfield, N. J. Almond, C. P. Mansley, J. H. Convery and P. Weightman, *J. Phys.: Condens. Matter* **22**, 392001 (2010)

[11] M Sun, T. A. Moore and P. –S. Song, *J. Am. Chem. Soc*. **94**, 1730 (1972)

[12] W. A. Eaton, J, Hofrichter, M. W. Makinen, R. D. Andersen and M. L. Ludwig, *Biochemistry* **14**, 2146 (1975)

[13] L. B. -A. Johansson, A. Davidson, G. Lindblom and K. R. Naqvi, *Biochemistry* **18**, 4249 (1979)

[14] T. Climent, R. González-Luque, M. Merchán and L. Serrano-Andrés, *J. Phys. Chem. A* **110**, 13584 (2006)

[15] M. Salim, U. Siddiqui, G. Kodali and R. J. Stanley, *J. Phys. Chem. B* **112**, 119 (2008)

[16] R. LeParc, C. I. Smith, M. C. Cuquerella, R. L. Williams, D. G. Fernig, C. Edwards, D. S. Martin and P. Weightman, *Langmuir* **22**, 3413 (2006)

[17] A. Bowfield, C. I. Smith, M. C. Cuquerella, T. Farrell, D. G. Fernig, C. Edwards and P. Weightman, *Phys. Status Solidi C* **5**, 2600 (2008).

[18] B. M. della Rocca, C. I. Smith, C. Tesauro, A. Desideri and P. Weightman, *Surf. Sci.* **604**, 2170 (2010).

[19] D. Hamdane, C. Xia, S. C. Im, H. Zhang, J. J. P. Kim and L. Waskell, *J. Biol. Chem*. **284**, 11374 (2009)

[20] S. Brenner, S. Hay, A. W. Munro and N. S. Scrutton, *FEBS J*. **275**, 4540 (2008)

[21] P. Harrison, T. Farrell, A. Maunder, C. I. Smith and P. Weightman, *Meas. Sci. Technol*. **12**, 2185 (2001)

Chapter 8

Further Investigation and Analysis of Protein Adsorbed at the Au(110)/Electrolyte Interface

This chapter discusses the RAS data of P499C full length CPR adsorbed onto the Au(110)/electrode as a function of applied potential in detail and attempts to separate the RAS signal of the adsorbed CPR molecules from that of the Au(110) substrate through further analysis.

8.1 Introduction

The effect of stepping the applied electrode potential between the redox potentials of the P499C full length cytochrome P450 reductase (CPR) has been shown to induce changes in the RAS intensity. Small features have been observed in the RAS intensity following changes to the potential applied to the Au(110) substrate when monitored at key energies. These small features may be associated with conformational events in the adsorbed CPR molecules as discussed in chapter 7. However the work discussed in chapter 7 also demonstrated that the same potential step also induces changes in the RAS intensity of the clean Au(110) surface and despite clear differences in the dynamics and overall intensity of these changes it is very difficult to separate the RAS contribution from the adsorbed CPR molecules and the Au(110) substrate.

The work presented in this chapter seeks to establish the extent to which the Au(110) surface contributes to the RAS of Au(110) + CPR at various redox potentials, and explores possible techniques of reducing the RAS contribution from the Au(110) substrate.

8.2 Does the Adsorption of P499C Full Length CPR Prevent the Au(110) Surface from Reconstructing?

The potential range in which the CPR molecules are expected to change conformation is known to induce a surface reconstruction of the clean Au(110) surface which reconstructs from a (1×3) structure to the anion induced (1×1) structure as the potential is changed from the negative redox potentials to 0.056 V [1]. This change in surface structure induces a large change in the RAS of clean Au(110) and the dynamics of the intensity change have been monitored in the rapid RAS data in chapter 7. However it is difficult to determine the interactions between the adsorbed molecules and the Au(110) substrate and to separate their contributions to the RAS profile. It has been established that in some circumstances the adsorption of molecules can restrict the reconstructions of the Au(110) surface [2]. Mansley *et*

al. [2] showed that the adsorption of cytosine onto the (1×1) Au(110) surface prevented the Au(110) surface from reconstructing to the (1×3) surface structure as a function of applied potential. It is therefore important to establish to what extent the adsorption of P499C full length CPR restricts the Au(110) surface from reconstructing as a function of applied potential.

The RA spectra of the clean Au(110) at applied electrode potentials of -0.652 V, -0.557 V, -0.465 V, -0.376 V and 0.056 V, has been shown and discussed in detail in chapter 4.2 and are shown in figure 8.1 a). The RA spectra of Au(110) after the adsorption of a monolayer of P499C full length CPR produced at the potentials -0.652 V, -0.557 V, -0.465 V, -0.376 V and 0.056 V are shown in figure 8.1 b). The RA spectra all follow a very similar shape with a negative increase in intensity observed as the potential is changed to increasingly more positive redox potentials (figure 8.1 b)). The largest change in intensity was observed as the potential is changed to 0.056 V. The RA spectral shape at 0.056 V however remained very similar to the spectra produced at the negative redox potentials as shown in figure 8.1 b). The similarity of the RA spectra produced at all the applied potentials after the adsorption of CPR and the lack of any large changes in the RA spectral shape suggests that that the Au(110) surface does not undergo a large surface reconstruction at 0.056 V after the adsorption of a monolayer of CPR.

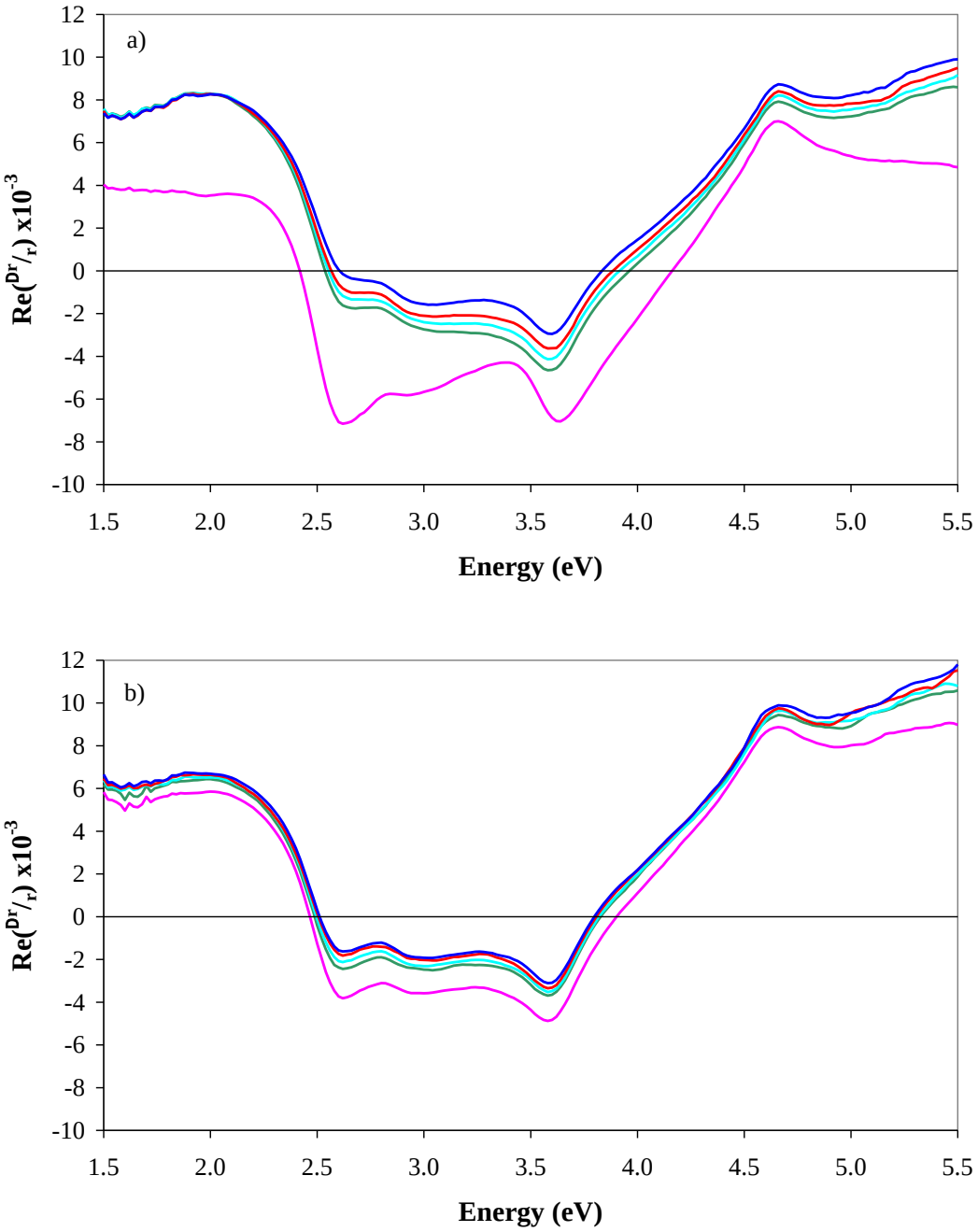

Figure 8.1: RA spectra of a) Au(110) and b) Au(110) + CPR in 0.1 M NaH_2PO_4/K_2HPO_4 pH 7.2 recorded at 0.056 V (pink line), -0.376 V (green line), -0.465 V (turquoise line), -0.557 V (red line) and -0.652V (blue line) vs SCE.

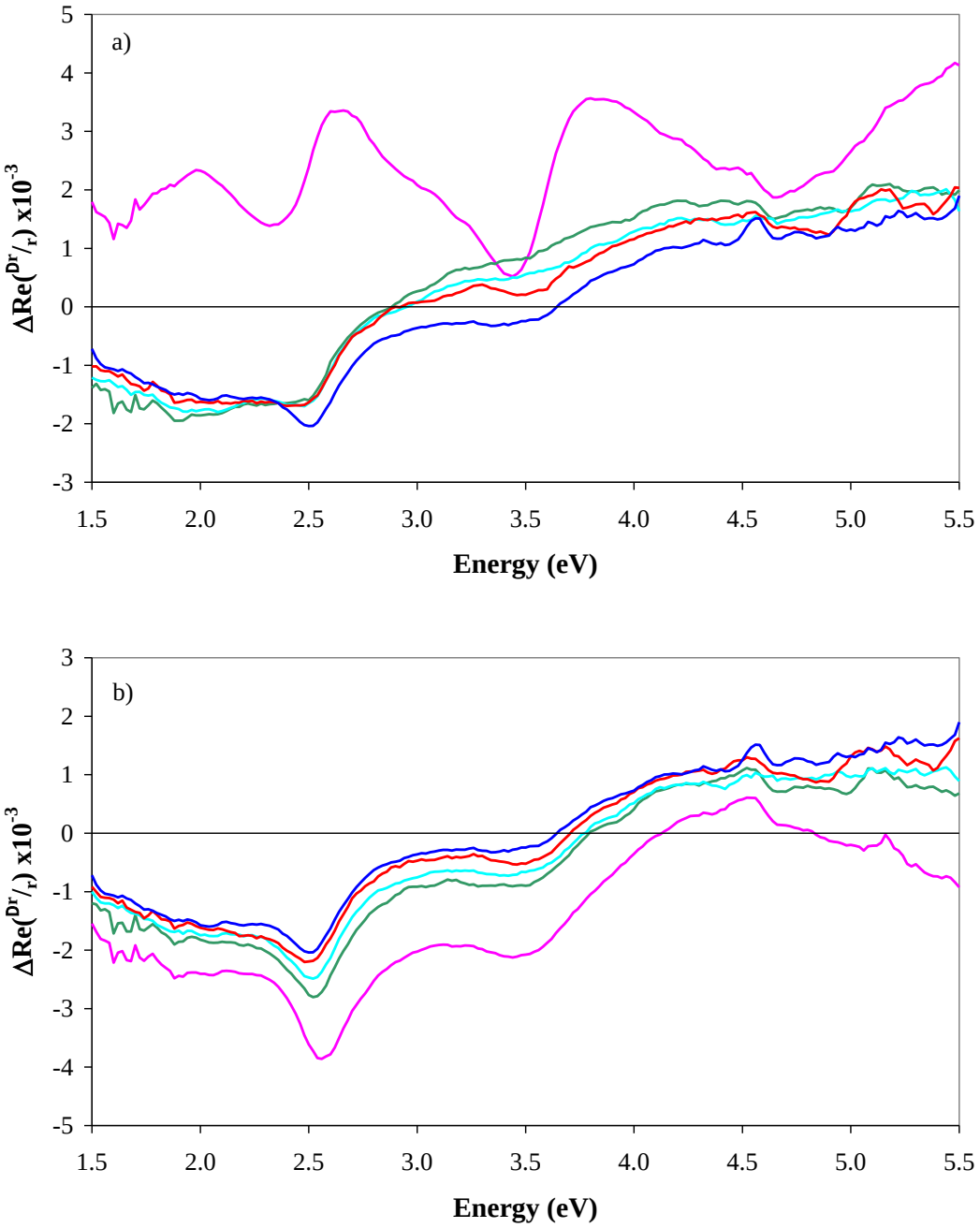

Figure 8.2: RA spectra of P499C full length CPR at 0.056 V (pink line), -0.376 V (green line), -0.465 V (turquoise line), -0.557 V (red line) and -0.652V (blue line) vs SCE, produced after a) the subtraction of the RAS of Au(110) from the RAS of Au(110) at corresponding potentials and b) the subtraction of the RAS of Au(110) at -0.652 V from the RAS of Au(110) + CPR at all potentials.

The RA spectra attributed to the adsorbed CPR molecules have been obtained using the methodology used both in previous work [2-5] and explained in chapter 4. Figure 8.2 a) shows the results of subtracting the RAS of Au(110) from the RAS of Au(110) + CPR produced at the corresponding applied potentials. The RA spectra in figure 8.2 b) were produced by subtracting the RAS of Au(110) at -0.652 V, the potential at which the CPR molecules adsorbed onto the Au(110) surface, from the RAS of Au(110) + CPR obtained at all the redox potentials. The RA spectra in figure 8.2 a) produced at negative redox potentials follow a similar spectral shape, however the RA spectrum of CPR at 0.056 V in figure 8.2 a) is very different, both in spectral shape and intensity. This large change in RA spectral shape at 0.056 V was not expected due to the observation of very similar RA spectra of Au(110) + CPR at all redox potentials, as shown in figure 8.1 suggesting that it arises from the large changes observed in the RAS of the Au(110) as the applied potential is varied. The RA spectra in figure 8.2 b) which have been produced by subtracting the RAS of Au(110) at -0.652 V from all the spectra in figure 8.1 all the resultant spectra have a very similar spectral shape, with only a variation in intensity observed as the potential is changed. The largest change in intensity was observed at 0.056 V. This variation between the RA spectra produced at each potential is consistent with the spectral variation observed in figure 8.1 and suggests that the adsorption of P499C full length CPR freezes the Au(110) surface in the (1×3) surface structure.

8.2.1 Simulation of RA Spectra of Au(110) + P499C Full Length CPR

An alternative way of exploring whether the Au(110) surface is frozen in a (1×3) structure at all potentials after the adsorption of CPR can be achieved by simulating the RA spectra using the approach of Mansley *et al.* [2]. It is assumed that the spectra of Au(110) + CPR is a the sum of RAS contribution from the Au(110) surface and the adsorbed CPR molecules and a simulated RA spectrum is produced by adding different weighted combinations of these two contributions.

The simulation assumes:

RAS Au(110)/full length CPR at redox potential = X*(RAS of Au(110) at redox potential) + Y*(RAS of full length CPR/Au at -0.652 V) (Equation 8.1)

where X and Y are percentages and the RAS of Au(110) at each potential is taken from figure 8.1 a) and the RAS of full length CPR/Au(110) at -0.652 V is taken from figure 8.1 b).

Simulated RA spectra were produced at each redox potential by varying the values of X and Y in equation 8.1, where $\chi 2$ minimisation was used to produce the best possible simulation. This procedure assumes that the RAS contribution from CPR does not change as a function of the applied potential. The simulated RA spectra are shown in figure 8.3 along with the corresponding experimental RA spectra at each potential.

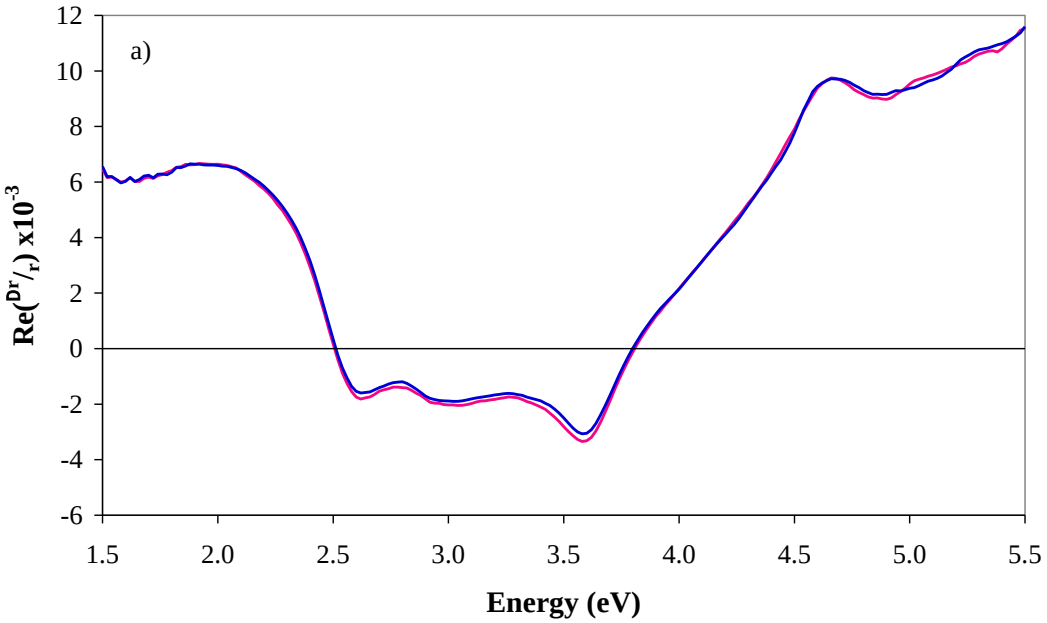
a)
12
10
8
6
4
2
0
-2
-4
-6
1.5
2.0
2.5
3.0
3.5
4.0
4.5
5.0
5.5
Energy (eV)

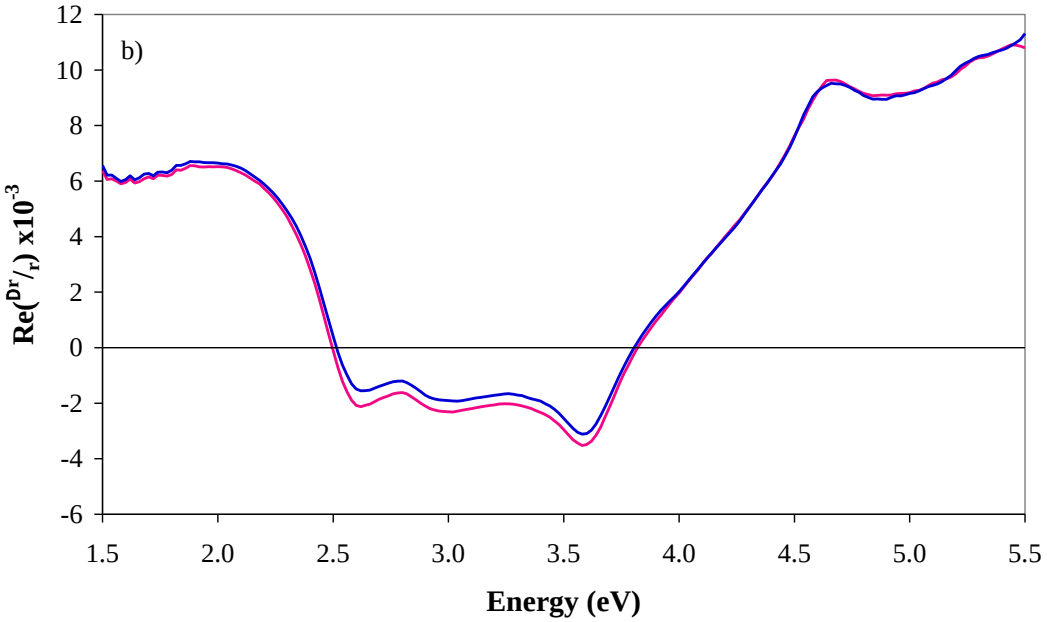
b)
12
10
8
6
4
2
0
-2
-4
-6
1.5
2.0
2.5
3.0
3.5
4.0
4.5
5.0
5.5
Energy (eV)

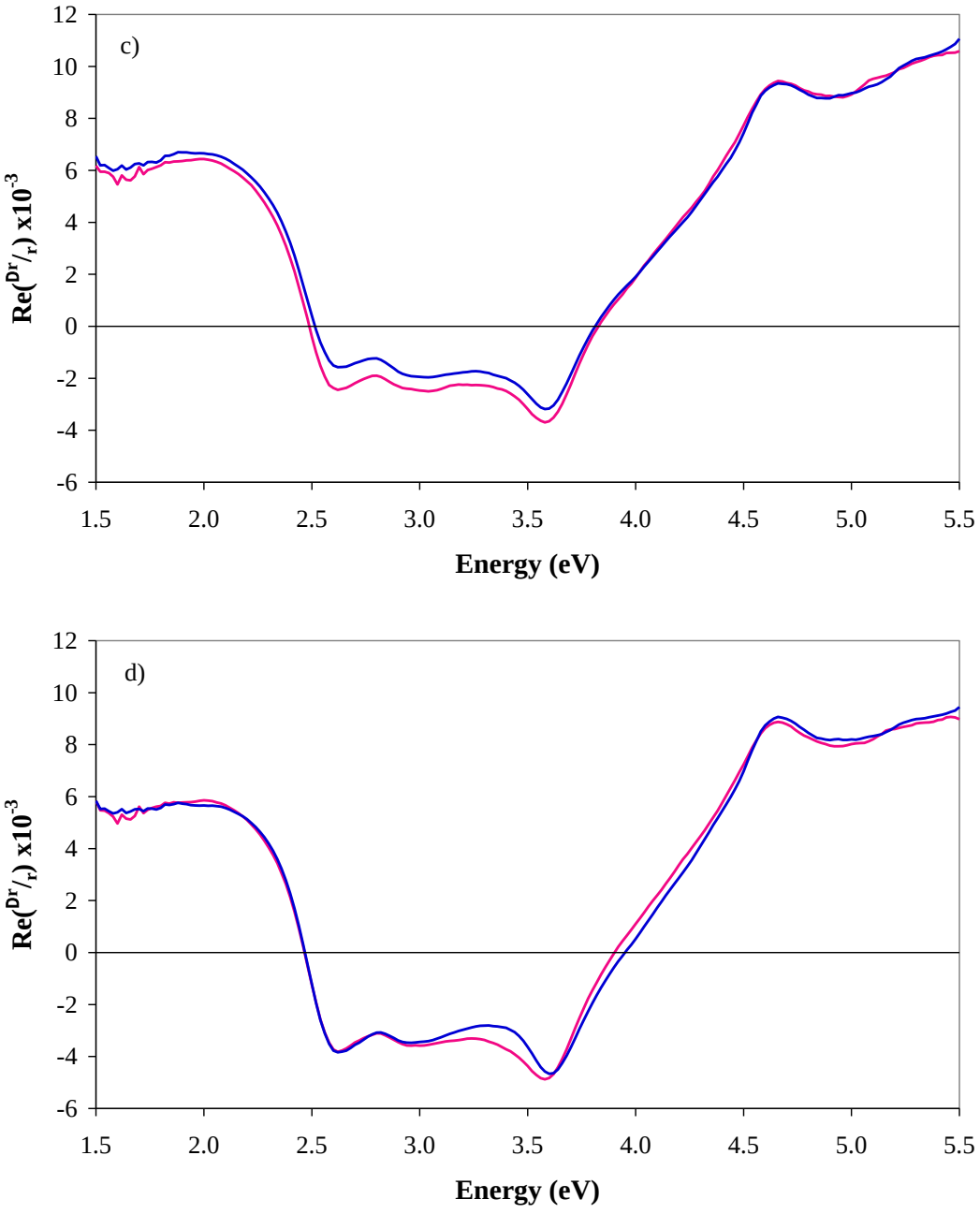

Figure 8.3: Experimental RA spectra of Au(110) + full length CPR (red line) and simulated RA spectra of Au(110) + full length CPR (blue line) at a) -0.557 V, b) -0.465 V, c) -0.376 V and d) 0.056 V vs SCE.

The simulated spectra in figure 8.3 are very close to the experimental RA spectra produced at each potential, so the values of X and Y used to simulate each spectrum can provide an idea of the how much the Au(110) substrate and the CPR

RAS contributions change as a function of applied potential. The X and Y values for each of the simulated spectra are shown in table 8.1. If the value of Y remained unchanged in each of the simulated spectra then it would indicate that the RAS contribution from the Au(110) substrate and the adsorbed CPR does not change as a function of applied potential. However the values of X and Y, shown in table 8.1, demonstrate that at more positive potentials the simulated spectra were produced by increasing the value of X and decreasing the value of Y. This indicates that as the potential is made more positive the RAS contribution from the Au(110) substrate changes however it could also indicate that the RAS of the adsorbed CPR changes. Whilst the simulated spectra are in good agreement with the recorded RA spectra (figure 8.3) and the values of X and Y can provide some insight into the Au reconstructions after the adsorption of CPR it is difficult to separate changes in the RAS contributions of the Au(110) substrate and the adsorbed CPR.

	Percentage	
Potential	X	Y
-0.652 V	0	100
-0.557 V	1	99
-0.465 V	8	92
-0.376 V	12	88
0.056 V	33	67

Table 8.1: X and Y percentage values used in equation 8.1 to simulate RA spectra at each potential.

8.2.2 Adsorption of CPR Impedes the Potential Induced (1×3) to (1×1) Reconstruction of Au(110)

As the simulated data in the previous section did not provide conclusive evidence that the adsorption of CPR impedes the Au(110) surface reconstruction from the (1×3) to the anion induced (1×1) surface structure, the work presented in this

section aims to confirm that the adsorption of CPR prevents the surface reconstruction of the Au(110) surface. Figure 8.3 shows the RA spectra of the Au(110) surface at -0.652 V and 0.056 V in the buffer solution used in this work and compares these spectra to the RA spectral signatures of the Au(110) (1×3) and anion induced (1×1) surface structures. The RA spectrum observed at -0.652 V is very similar to the spectral signature of the (1×3) surface structure, as shown in figure 8.3. The data in figure 8.3 also shows the similarity between the RA spectrum of the Au(110) anion induced (1×1) and the RA spectrum produced at 0.056 V.

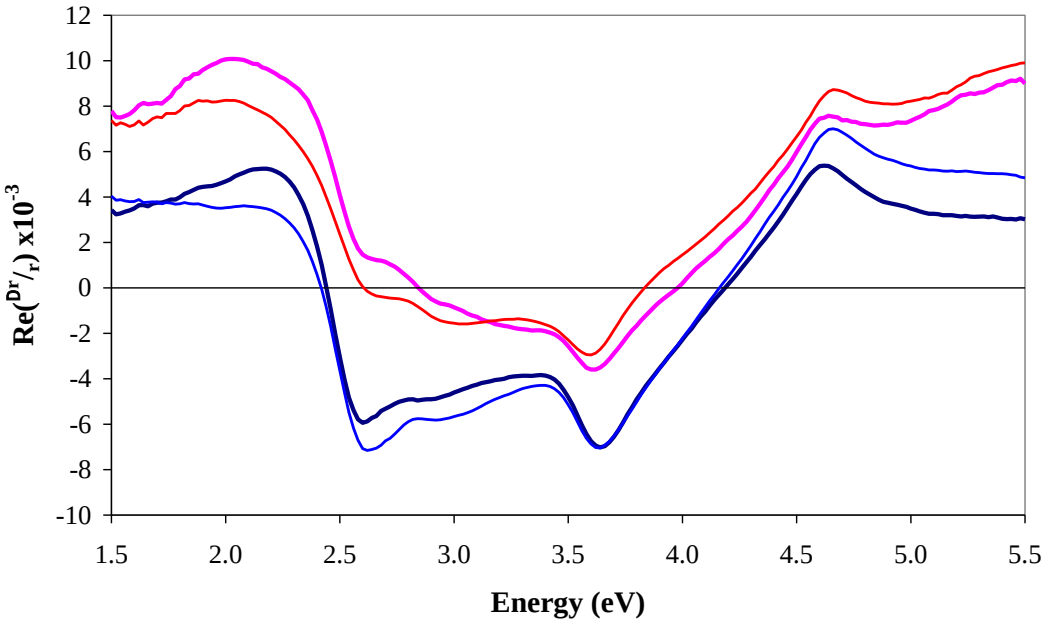

Figure 8.3: RA spectra of Au(110) in 0.1M NaH_2PO_4/K_2HPO_4 pH 7.2 at -0.652 V (red line) and 0.056 V (blue line) along with the RA spectral signatures of the anion induced (1×1) (dark blue line) and (1×3) (pink line) Au(110) surface reconstructions [1].

Following the adsorption of full length CPR onto the Au(110) surface at -0.652 V the applied potential was changed to 0.056 V. The result of subtracting the RAS of Au(110) surface at 0.056 V from the RAS of Au(110) + CPR at 0.056 V is shown in figure 8.4. This spectral difference is remarkably similar to the difference between the RAS of Au(110) at -0.652 V and 0.056 V. This similarity demonstrates

that when the applied potential changes from -0.652 V to 0.056 V the Au(110) surface is unable to change to the (1×1) anion induced structure when it is covered by a monolayer of adsorbed CPR. This result is expected as the adsorption of CPR should prevent the adsorption of anions.

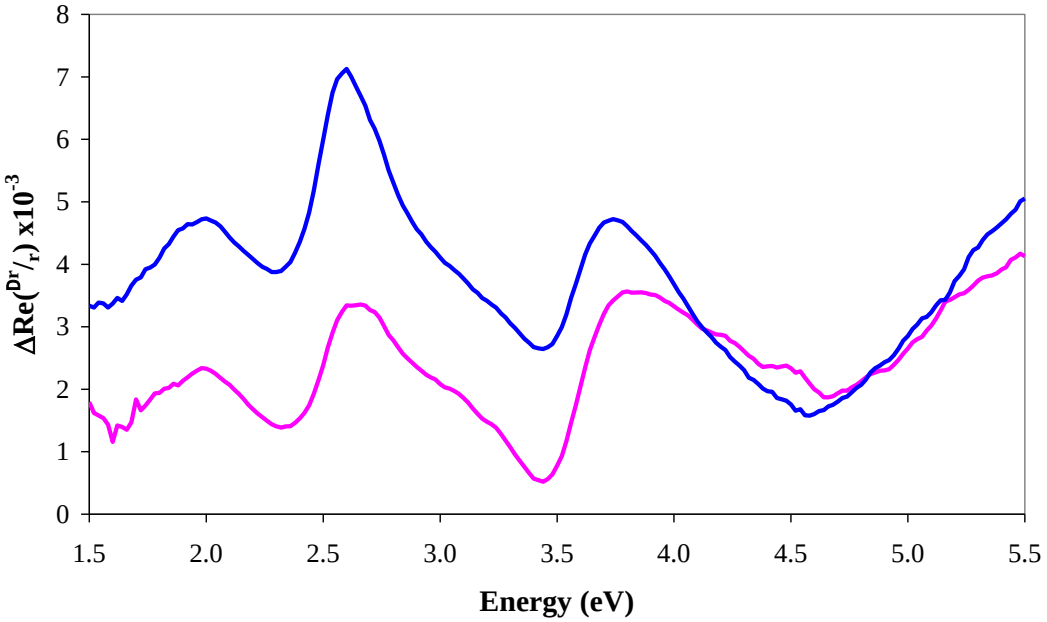

Figure 8.4: RA spectral differences produced following the subtraction of the RAS of clean Au(110) at 0.056 V from the RAS of clean Au(110) at -0.652 V (blue line) and the subtraction of the RAS of clean Au(110) at 0.056 V from the RAS of CPR/Au at 0.056 V (pink line).

The difference between the two subtractions in figure 8.4 should correspond to the RAS of CPR adsorbed on the Au(110) surface in an oxidised state. This difference is shown in figure 8.5 where it is compared to the RAS of adsorbed CPR in a reduced state at -0.652 V produced following the subtraction of Au(110) at -0.652 V from the RAS of Au(110) + CPR at -0.652 V. The spectra in figure 8.5 are similar in shape but differ in intensity, specifically the negative intensity of two features at ~ 2.6 eV and ~ 3.5 eV are increased in the RA spectrum of CPR at 0.056 V, as shown in figure 8.5. Since the intensity of a RAS signal depends on the degree of order on the surface the differences in intensity between the two RAS

profiles in figure 8.5 could be explained by noting that the spectrum of CPR produced at 0.056 V is associated with oxidised CPR, which is expected to adopt a more compact 'closed' structure, whereas the spectrum produced at -0.652 V corresponds to reduced CPR which is expected to adopt a more open structure [6-9]. This difference in conformation of the adsorbed CPR molecules may result in a reduction in the degree of order on the surface at -0.652 V.

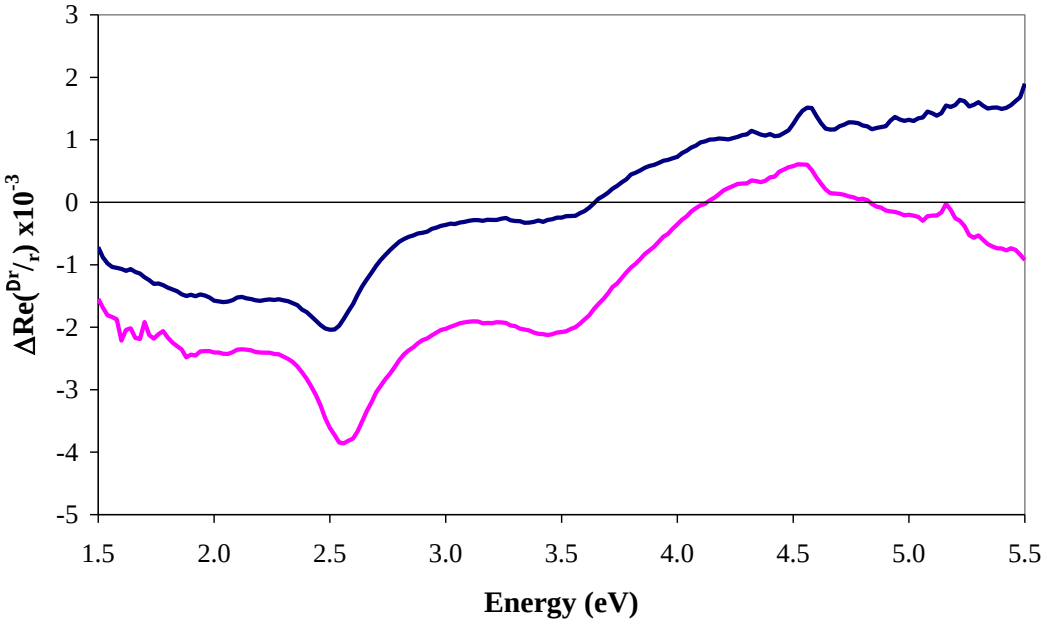

Figure 8.5: RA spectra of reduced CPR at -0.652 V (blue line) produced following the subtraction of the RAS of clean Au(110) at -0.652 V from the RAS of Au(110) + CPR at -0.652 V, and RA spectral difference between the spectra in figure 8.4 (pink line), which can be attributed to the RAS of oxidised CPR at 0.056 V.

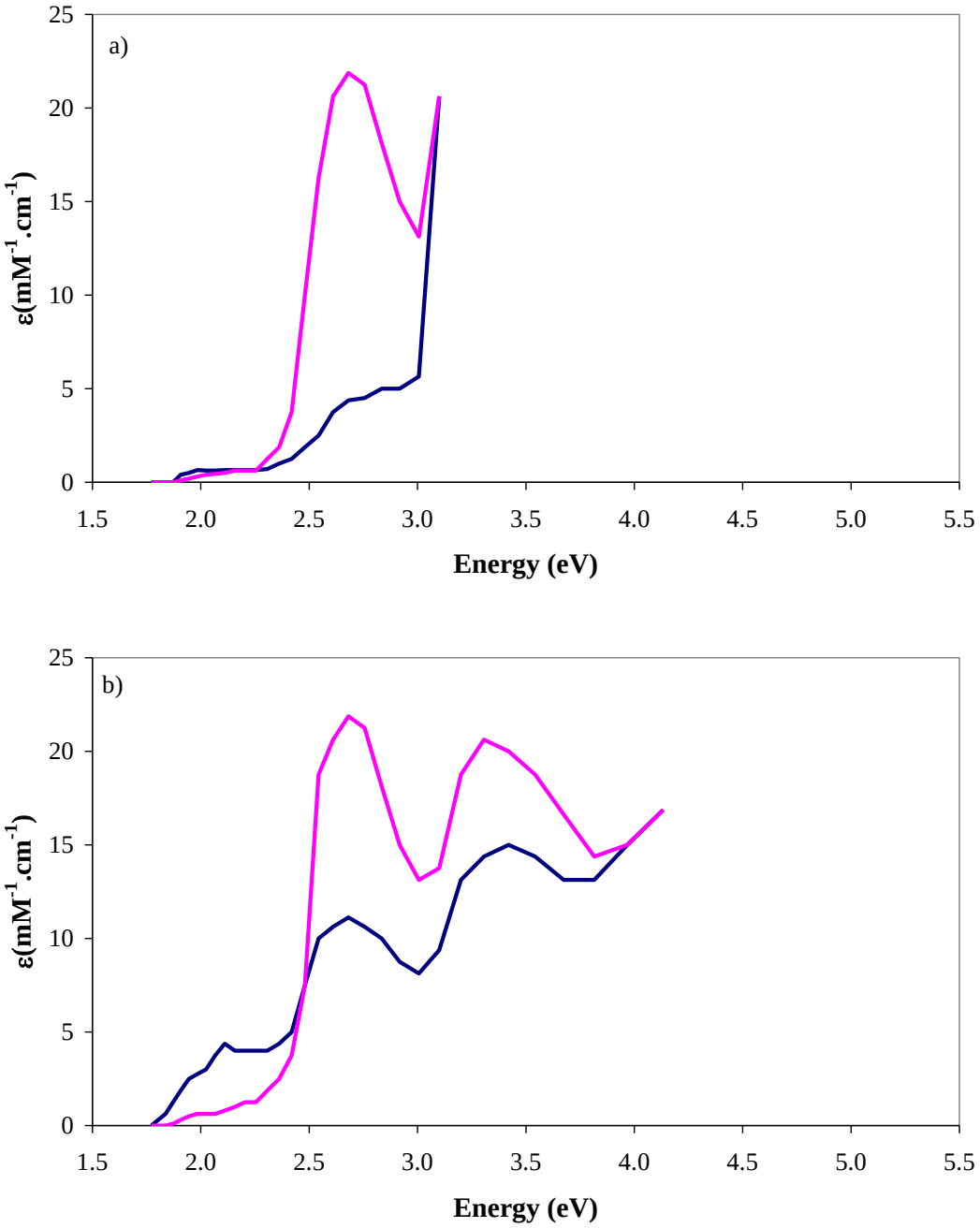

Figure 8.6 Absorbance spectra produced after mixing a) 20-fold excess and b) stoichiometric amounts of NADPH with oxidised CPR in solution. In each case the oxidised spectrum refers to the pink line whilst the reduced CPR spectrum refers to the blue line. Data reproduced from [10].

The data in figure 8.5 can be compared to the difference between absorbance spectra of oxidised and reduced CPR produced in earlier stopped-flow experiments

by S. Brenner *et al.* [10], where oxidised CPR in solution was reduced by mixing with either a 20-fold excess or stochiometric amounts of NADPH at pH 7.0 as shown in figure 8.6. The absorbance spectra shown in figure 8.6 both show a feature at ~ 2.7 eV and the data produced by mixing stoichiometric amounts of NADPH also shows a feature at ~ 3.5 eV. The intensity of these features is increased in the oxidised CPR, which is similar to the increase in the intensities of the negative peaks shown at these energies in figure 8.5. This suggests that the changes in RA spectral intensity observed in figure 8.5 are the result of the oxidation and reduction of the adsorbed CPR molecules.

In chapter 4 it was shown how stepping the applied potential between the redox potentials of the fully reduced (-0.652 V) and fully oxidised (0.056 V) states of what is now known to be a multilayer of CPR induced long term changes in the RAS. A similar but less prominent effect has been observed in the data produced after the adsorption of a monolayer of CPR. Figure 8.7 shows the RAS of the adsorbed CPR immediately after the adsorption on the Au(110) (1×3) surface at -0.652 V. This is compared with the RAS of CPR at the same potential but following the oxidation of the protein by changing the potential to 0.056 V.

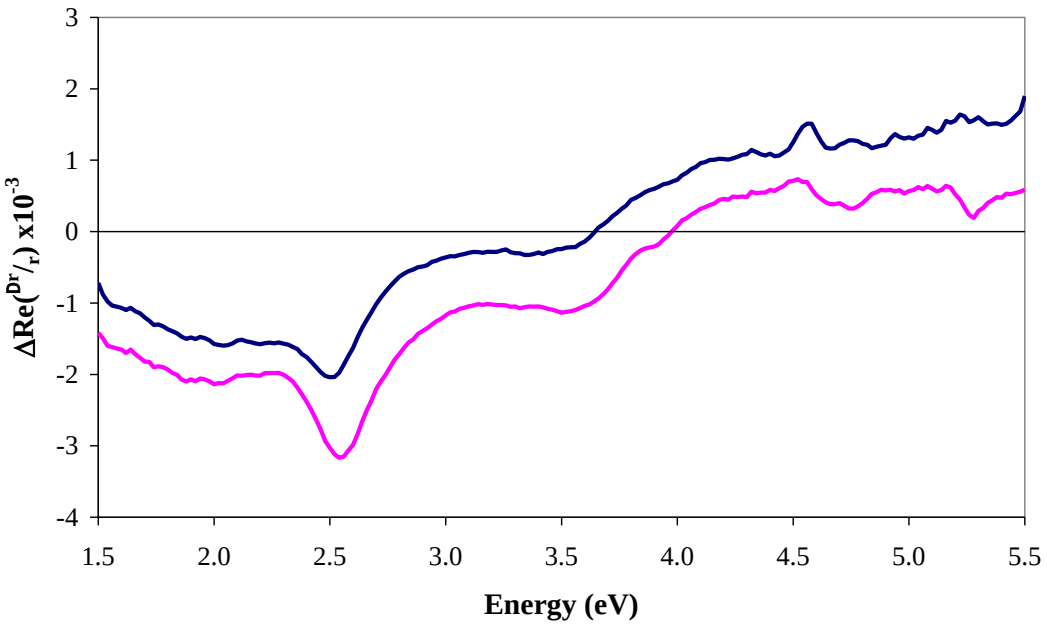

Figure 8.7: RA spectra of CPR at -0.652 V produced following the subtraction of the RAS of Au(110) at -0.652 V from the RAS of CPR/Au at -0.652 V recorded immediately after adsorption on the (1×3) surface at -0.652 V (blue line) and after changing to 0.056 V and back to -0.652 V (pink line).

The effect oxidising the protein and then reducing it has increased the intensity of the RAS profile but has not changed its shape. This difference could arise from the formation of a more ordered monolayer on the surface resulting from the conformational changes expected on going from a reduced to an oxidised to a reduced form. Alternatively once the CPR has been oxidised on the surface and adopted a more closed structure it may not be possible for the structure to receive electrons from the Au substrate when the potential is changed to -0.652 V. If this is the case then the difference between the two profiles shown in figure 8.7 should correspond to the difference in the absorption spectrum of the oxidised and reduced form of CPR in solution shown in figure 8.6 a) and b) . The RA spectra in figure 8.7 shows an increase in features at ~ 2.6 eV and ~ 3.5 eV upon oxidation and reduction, which is in good agreement with the absorbance spectra of oxidised and reduced CPR produced in stopped-flow experiments [10]. However at the lower energy range the stopped-flow data [10] shows a clear increase in intensity in the reduced

spectrum between 2.0 eV and 2.5 eV (figure 8.6). This increase in intensity is not observed in the RA spectra shown in figure 8.7. This difference between the RA spectra and the stopped-flow data may be attributed to a weaker contribution from the adsorbed CPR molecules in the 2.0- 2.5 eV region of the spectrum. The association of the spectral difference with the oxidised and reduced forms of CPR is supported further by noting that a similar spectral difference was observed between the spectra in figure 8.5. The difference between the intensity of the features is greater in figure 8.5 which could be associated with the fact that the spectra in figure 8.5 were produced at -0.652 V and 0.056 V so it would be expected that more adsorbed CPR molecules would be in the oxidised state at 0.056 V, whereas the spectra in figure 8.7 were both produced at -0.652 V and with an RAS contribution from oxidised CPR molecules expected to arise from an irreversibility in the oxidation and reduction of CPR adsorbed on the Au(110) surface which may not effect all the adsorbed CPR molecules.

8.2.3 Interaction Between CPR and the Anion Induced (1×1) Reconstruction of Au(110)

The previous section suggests that the adsorption of CPR at -0.652 V freezes the Au(110) surface in the (1×3) reconstruction. The results of a corresponding study in which CPR was adsorbed on the Au(110) surface in the anion induced (1×1) surface structure at 0.056 V, is now presented. Following the adsorption of CPR at 0.056 V the applied potential was changed to -0.652 V, the RAS of Au(110) at -0.652 V was then subtracted from the RAS of Au(110) + CPR at -0.652 V. This spectral difference is compared with the difference between the RAS of Au(110) at 0.056 V and -0.652 V as shown in figure 8.8.

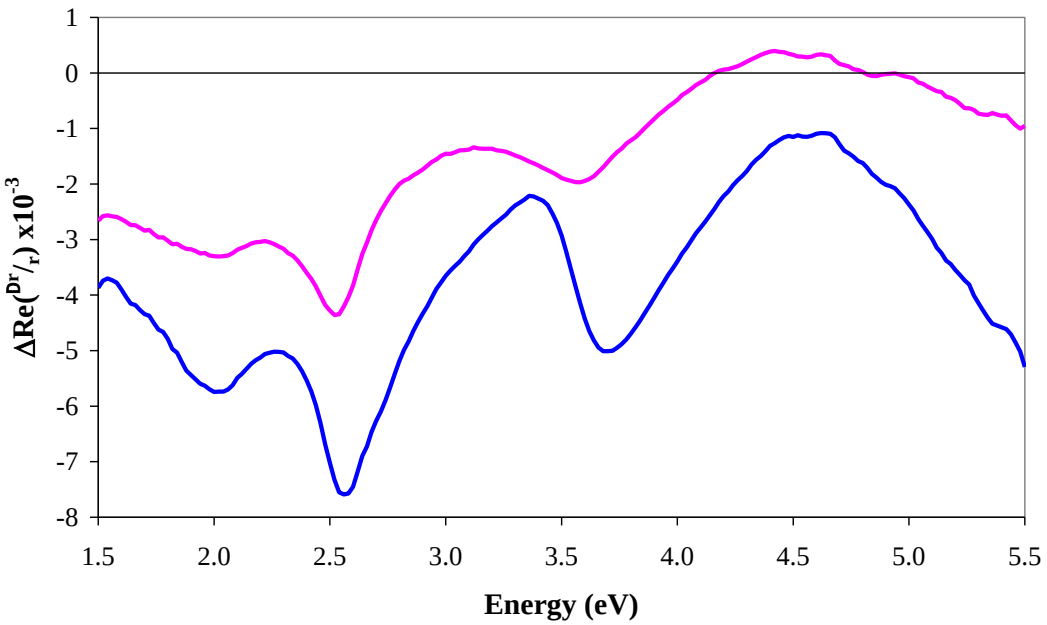

Figure 8.8: RA spectral differences produced following the subtraction of the RAS of clean Au(110) at -0.652 V from the RAS of clean Au(110) at 0.056 V (blue line) and the subtraction of the RAS of clean Au(110) at -0.652 V from the RAS of CPR/Au adsorbed at 0.056 V and measured at -0.652V (pink line).

The two spectra in figure 8.8 show strong similarities but they do not agree with each other as well as the comparison shown in figure 8.4 after the adsorption of CPR onto the Au(110) surface at -0.652 V. This suggests that the adsorption of CPR at 0.056 V may not prevent the Au(110) surface from reconstructing to the (1×3) structure as the potential is changed to -0.652 V possibly because the presence of anions on the surface at 0.056 V prevents or impedes the formation of an ordered monolayer of CPR. Following the same methodology used previously the difference between the spectra in figure 8.8 should be associated with the reduced CPR. This difference is shown in figure 8.9 and is compared to the RA spectrum of oxidised CPR produced following the subtraction of the RAS of Au(110) at 0.056 V from the RAS of Au(110) + CPR at 0.056 V.

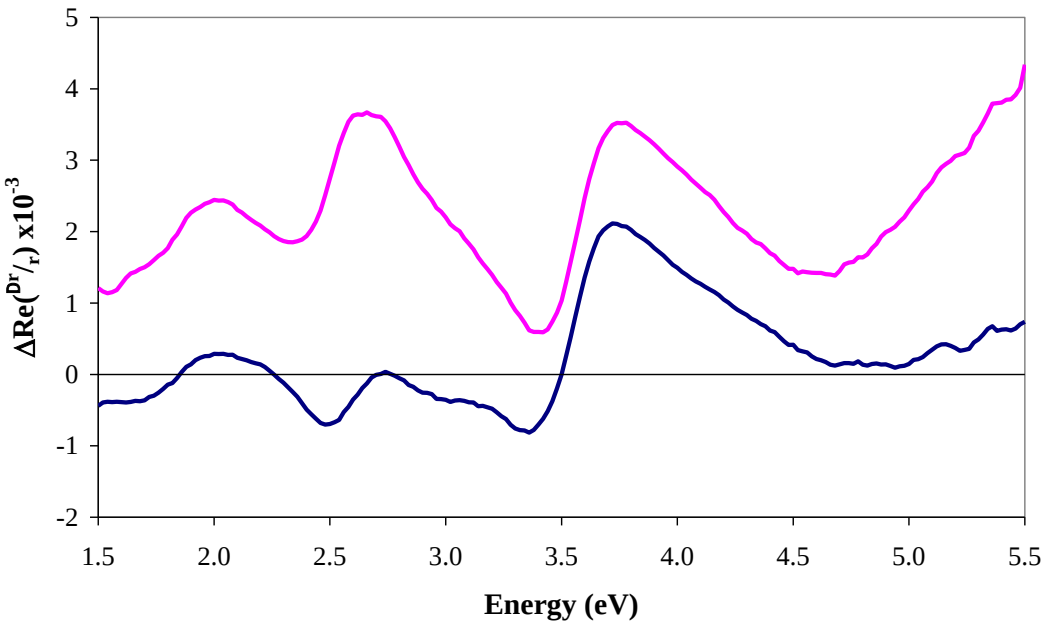

Figure 8.9: RA spectral differences of CPR at 0.056 V (blue line) produced following the subtraction of the RAS of clean Au(110) at 0.056 V from the RAS of Au(110) + CPR at 0.056 V and the RA spectral difference between the spectra in figure 8.8 (pink line) which can be attributed to the RAS of CPR at -0.652 V.

The RA spectra shown in figure 8.9 can be considered the RA spectra of oxidised and reduced CPR adsorbed on the anion induced (1×1) Au(110) surface. The RA spectral profiles are fairly similar. However there are clear differences in the intensities of the two spectra and the intensity of the feature at ~ 2.8 eV, which decreases significantly upon oxidation. This change is not in agreement with the absorption spectra of the oxidised and reduced forms of CPR in solution, shown in figure 8.6 [10]. The absorbance spectra produced by Brenner *et al.* [10] showed an increase in intensity in this region following the oxidation of CPR, opposite to that observed in the data in figure 8.9

The difference between the RAS data produced after the adsorption of CPR at -0.652 V and at 0.056 V may be associated with the extent to which the adsorption of CPR prevents the Au(110) substrate from reconstructing. There is strong evidence to suggest that the adsorption of CPR at -0.652 V freezes the Au(110) surface in the (1×3) reconstruction. However this effect is not as strong

when observed following the adsorption of CPR at 0.056 V. It is possible that the differences between the interaction of CPR molecules with the Au(110) surface at the two potentials of -0.652 V and 0.056 V revealed by RAS arise from the presence of anions on the Au(110) surface at 0.056 V. This could impede the adsorption of CPR and disrupt the formation of an ordered monolayer of CPR at 0.056 V. The difference in the Au(110) surface structures at the two potentials may also cause the CPR molecules to adsorb in a different order or orientation. It is also the case that since CPR is expected to adopt a more compact structure upon oxidation at 0.056 V, this may also effect the adsorption of CPR onto the Au(110) surface at 0.056 V. It is possible to conclude that the difference in surface structure, the adsorption of anions and the change in redox state of CPR molecules have a significant influence on the adsorption of CPR.

8.3 P499C Full Length CPR Adsorbed onto the Roughened Au(110) Surface

This section reports the results obtained by the adsorption of a monolayer of P499C full length CPR on to a roughened Au(110) surface. The roughening of the Au(110) surface is expected to prevent the surface from reconstructing as the potential is varied.

It has been shown in earlier work by Martin *et al* [11] that a clean ordered Au(110) (1×2) surface can be roughened by increasing sequences of Ar ion bombardment. This roughening of the Au(110) surface saw the loss of (1×2) surface structure and the long range periodic order. The resultant Au(110) surface was considered to consist of a mixed surface structure. It is expected that continually stepping the applied potential between -0.652 V and 0.056 V over a long time scale would result in the formation of a mixed Au(110) surface structure. This mixed surface structure is not expected to reconstruct as a function of the applied potential, therefore minimising the changes in RAS contribution of Au(110) as a function of applied potential.

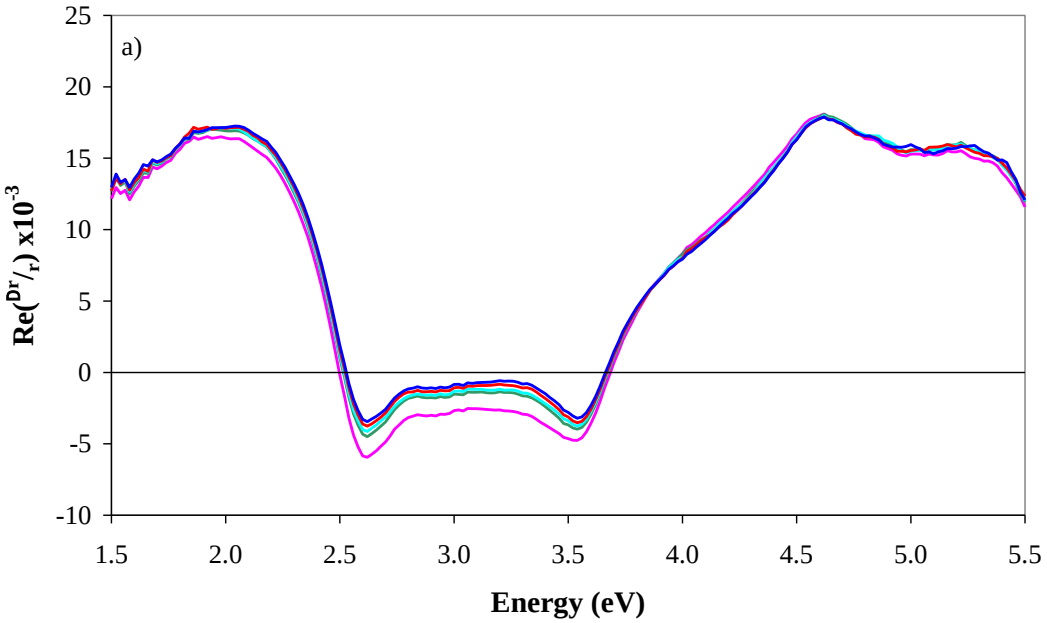
a)
25
20
15
10
5
0
-5
-10
1.5
2.0
2.5
3.0
3.5
4.0
4.5
5.0
5.5
Re(Δr/r) x10-3
Energy (eV)

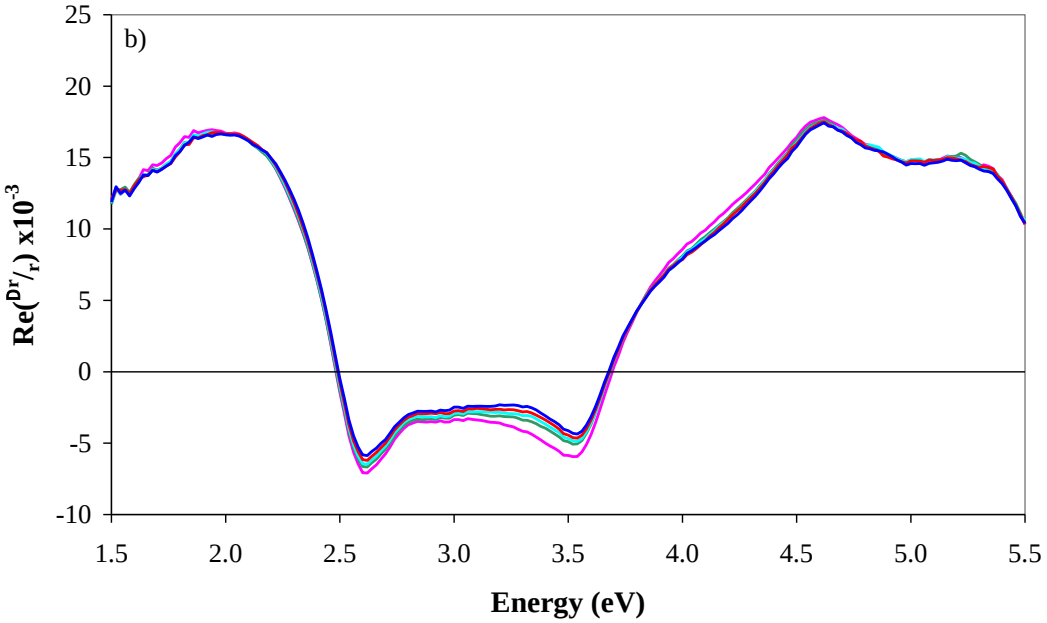
b)
25
20
15
10
5
0
-5
-10
1.5
2.0
2.5
3.0
3.5
4.0
4.5
5.0
5.5
Re(Δr/r) x10-3
Energy (eV)

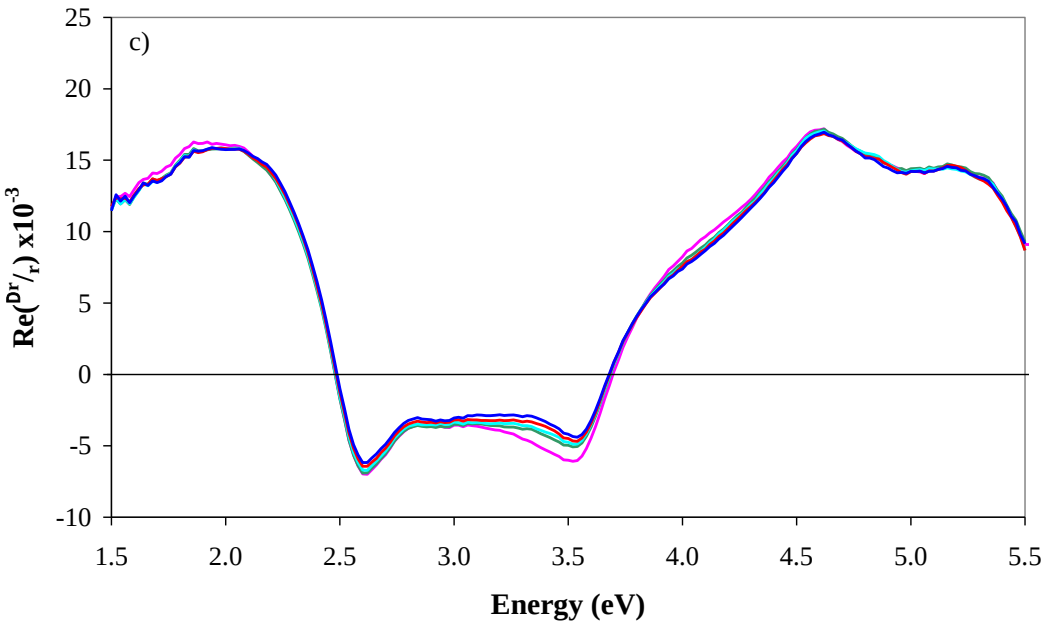

Figure 8.10: RA spectra of Au(110) 0.1 M NaH_2PO_4/K_2HPO_4 pH 7.2 produced at 0.056 V (pink line), -0.376 V (green line), -0.465 V (turquoise line), -0.557 V (red line) and -0.652V (blue line) vs SCE after stepping between 0.056 V and -0.652 V repeatedly for a) 24 hours b) 48 hours and c) 72 hours.

The RA spectra in figure 8.10 demonstrate how repeatedly stepping the applied potential between -0.652 V and 0.056 V changes the RA spectra of clean Au(110) as a function of the applied potential. The differences between the RA spectra of Au(110) at each potential were reduced significantly as a function of stepping the applied potential. The RA spectra in figure 8.10 c) shows that changing the applied potential had very little effect on the RA spectral shape, and the RA spectra of Au(110) produced at 0.056 V and -0.652 V have an almost identical shape. This suggests that changing the applied potential does not induce a surface reconstruction of the roughened Au(110) surface.

After the surface was roughened and almost identical RA spectra of the Au(110) surface were produced at each potential, P499C full length CPR was added to the electrochemical cell under the conditions established for the adsorption of a monolayer of CPR onto the Au(110) surface. The RA spectra produced after the addition of CPR are almost identical to the RA spectra of the clean roughened

Au(110) as shown in figure 8.11. The characteristic 2.54 eV peak associated with the Au-S bond and other spectral features associated with the adsorption of a monolayer of CPR were not observed. This indicates that CPR does not adsorb onto the roughened Au(110) surface, which would suggest that an ordered substrate is required for the adsorption of an ordered monolayer of CPR.

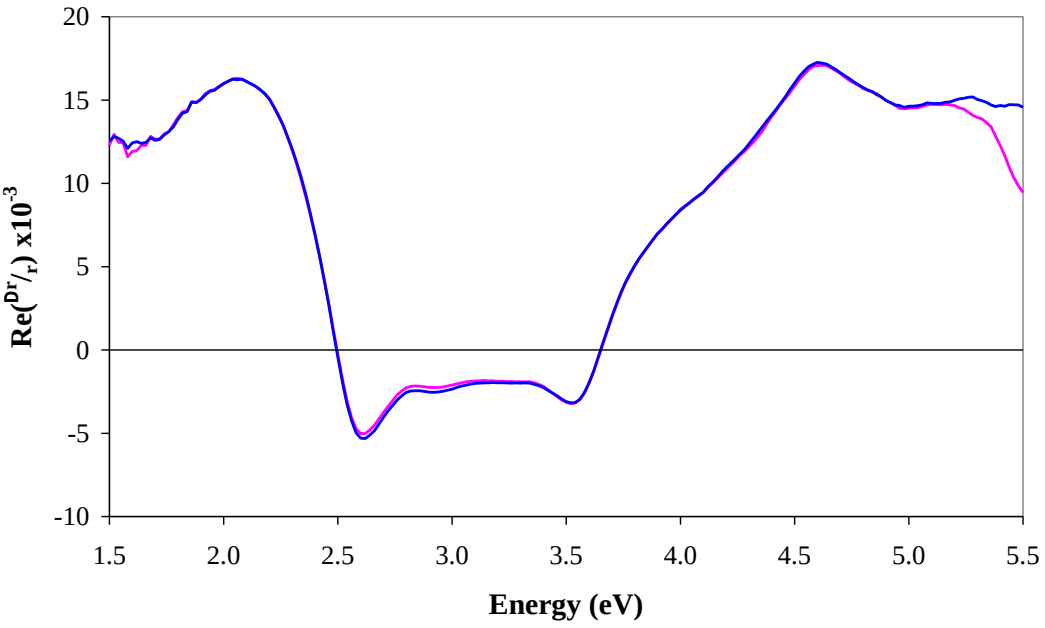

Figure 8.11: RA spectra of clean roughened Au(110) surface at -0.652 V (pink line) and after the addition of P499C full length CPR at -0.652 V (blue line).

It has been shown that by stepping the applied potential it is possible to produce a Au(110) surface that does not reconstruct as a function of the applied potential. The variant P499C full length CPR does not adsorb in an ordered monolayer on the roughened surface. These results confirm that the substrate influences the adsorption of an ordered monolayer and are consistent with the autocorrelation analysis [12] of the AFM images of CPR adsorbed on polycrystalline Au discussed in chapter 5.

8.3.1 Preliminary Investigation of the Oxidation of Full Length CPR with $NADP^+$

The function of CPR is to transfer electrons from electron donors onto cytochrome P450 enzymes via the FAD and FMN domains [13]. CPR catalyses the oxidation of nicotinamide adenine phosphate dinucleotide (NADPH), a natural 2 electron donor, to form $NADP^+$. The reversibility of this process was demonstrated by a recent stopped-flow kinetic study [14] where the reverse electron transfer from the isolated two electron reduced FAD domain to $NADP^+$ was studied. The oxidation of the isolated FAD domain by $NADP^+$ provides a technique which is expected to induce a conformational change in adsorbed CPR molecules without the need to change the applied electrode potential. Therefore oxidation of reduced CPR by the addition of $NADP^+$ offers a possible solution to the interference of the Au(110) surface reconstructions observed in potential induced electron transfer processes in CPR adsorbed on the Au(110) surface. The work discussed in this section explores the use of $NADP^+$ to induce conformational change in reduced CPR molecules adsorbed on the Au(110) surface.

Prior to the addition of $NADP^+$, a monolayer of P499C full length CPR was adsorbed onto the Au(110) surface at -0.652 V. The resultant RA spectrum after the adsorption of a monolayer of P499C full length CPR is shown in figure 8.12 and is consistent with the RA spectral signature of a monolayer of CPR on Au(110) at -0.652 V.

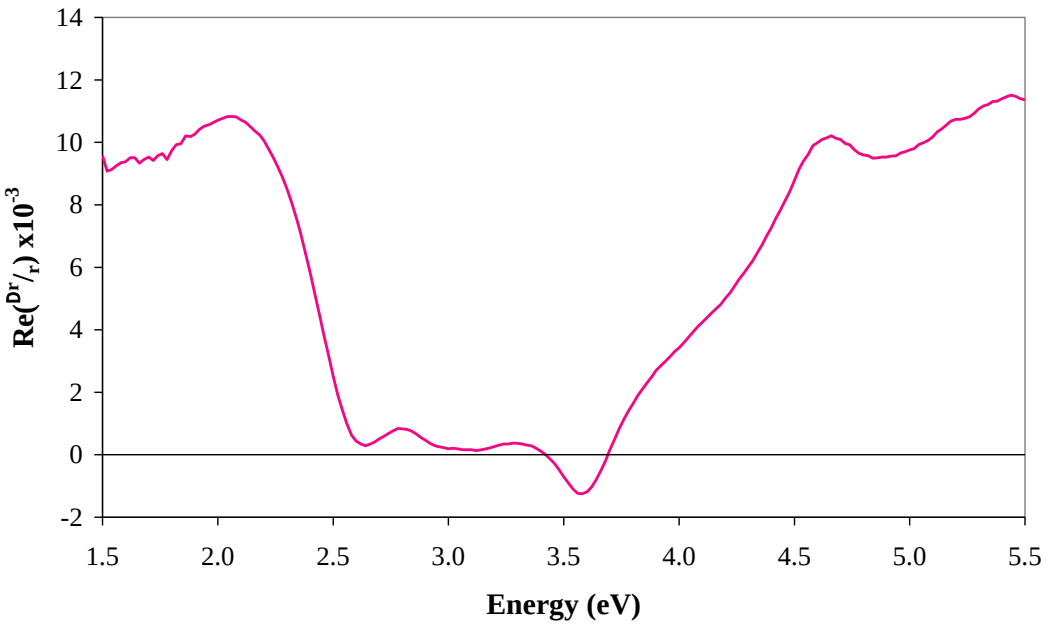

Figure 8.12: RA spectrum of Au(110) + a monolayer of P499C full length CPR at -0.652 V vs SCE.

The adsorption of P499C full length CPR molecules at -0.652 V is expected to induce a fully reduced state in the adsorbed CPR molecules. In this state CPR is expected to adopt an open conformation. The applied electrode potential was held at -0.652 V while $NADP^+$ solution was added to the electrochemical cell. The ratio of CPR to $NADP^+$ concentration was 1:3, which was expected to be sufficient for the oxidation of the adsorbed CPR molecules. The RAS intensity was monitored at 2.7 eV as a function of time after the addition of $NADP^+$ to the electrochemical cell, which is shown in figure 8.13.

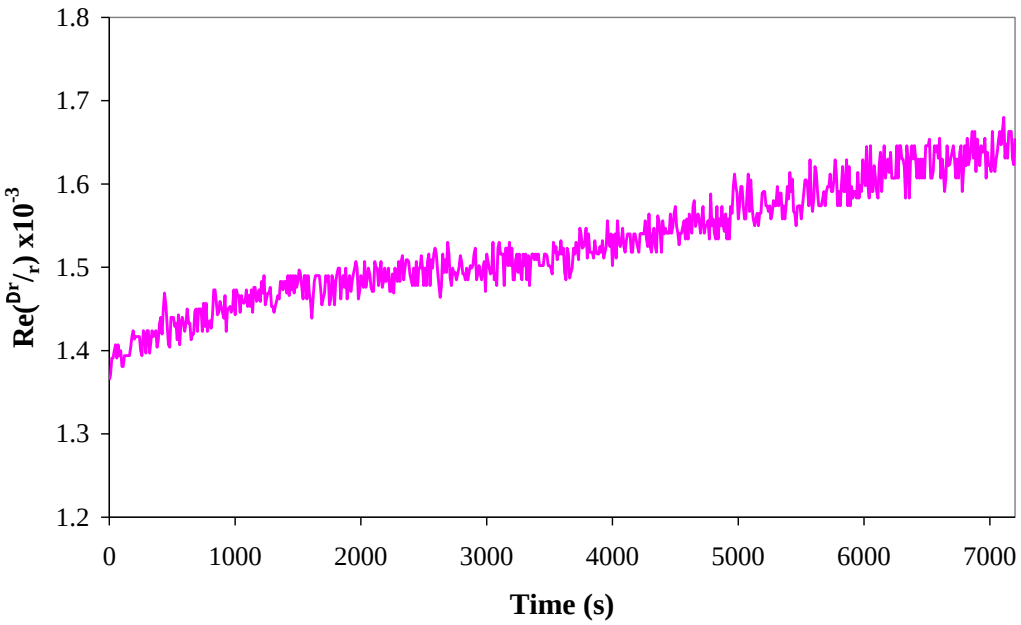

Figure 8.13: RAS intensity at 2.7 eV of Au(110) + a monolayer of P499C full length CPR monitored as a function of time after the addition of $NADP^+$ at -0.652 V.

The addition of $NADP^+$ caused a steady positive increase in the RAS intensity at 2.7 eV over a 2 hour period, as shown in figure 8.13. This slow steady change in RAS intensity could be associated with the oxidation of the adsorbed CPR molecules. The oxidation of the adsorbed CPR molecules is expected to induce a change in conformation of CPR [6-9], so monitoring the change in RAS intensity at 2.7 eV as a function of time after the addition of $NADP^+$ may reveal information on conformational events in CPR involving the isoalloxazine rings [15-19]. The slow steady change in RAS intensity observed at 2.7 eV (figure 8.13) could be a signal of a change in conformation in the adsorbed CPR molecules.

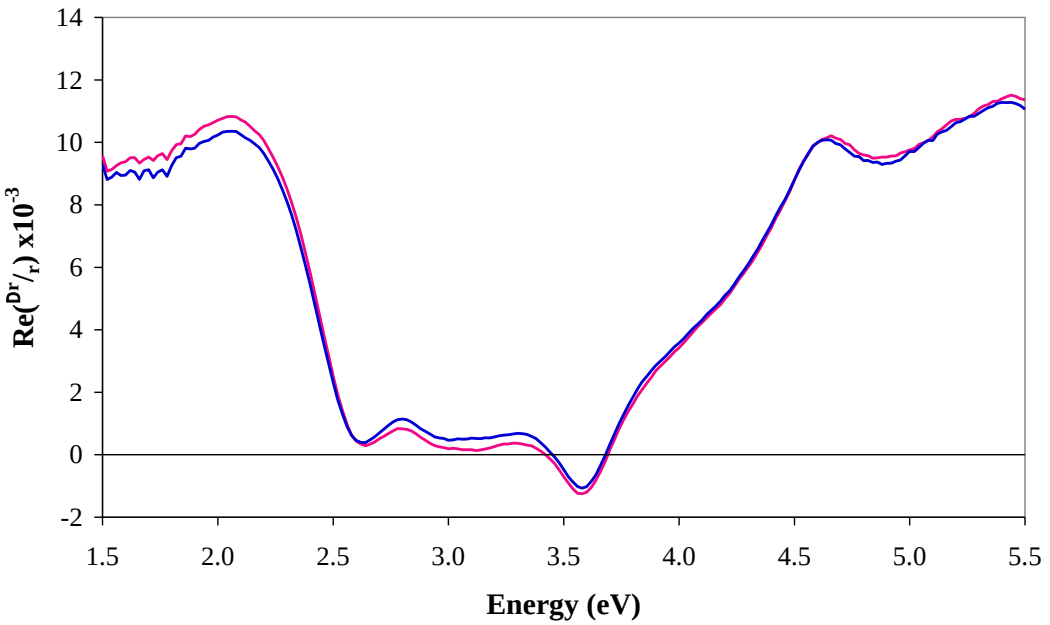

Figure 8.14: RA spectra of Au(110) + P499C full length CPR before the addition of $NADP^+$ (red line) and after the addition of $NADP^+$ (blue line) all recorded at -0.652 V vs SCE.

RA spectra produced before and after the addition of $NADP^+$ at -0.652 V are shown in figure 8.14, both spectra follow a very similar shape however a slight change in intensity at certain energies was observed. Below 2.5 eV the intensity shifted in the negative direction, whereas between 2.5 eV and 4.0 eV the intensity increased in the positive direction after the addition of $NADP^+$. These shifts in intensity can be more clearly observed by subtracting the RAS of Au(110) + CPR (red line figure 8.14) from the RAS of Au(110) + CPR produced after the addition of $NADP^+$ (blue line figure 8.14) This subtraction is shown in figure 8.15. If the addition of $NADP^+$ causes the oxidation of the adsorbed CPR molecules then the difference spectrum in figure 8.15 could be attributed to the different RAS response between the reduced and oxidised adsorbed CPR.

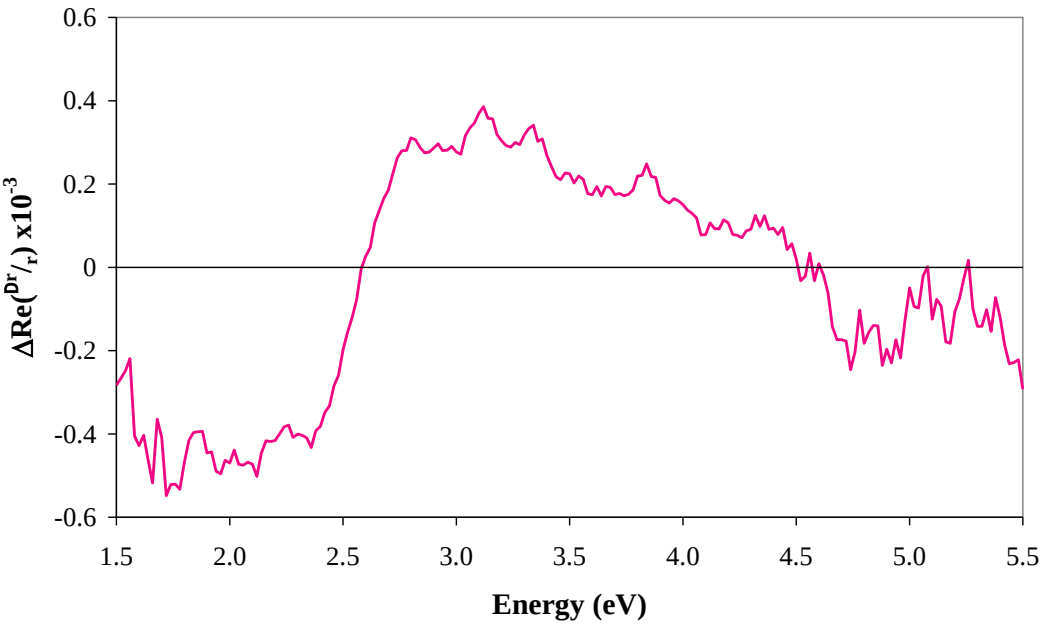

Figure 8.15: RA spectrum produced following the subtraction of the RAS Au(110) + full length CPR from the RAS of Au(110) + full length CPR after the addition of $NADP^+$ at -0.652 V.

The results of the subtraction shown in figure 8.15 show the effect of NADP+ on the RAS of Au(110) + CPR at -0.652 V. The changes in intensity are expected to illustrate how the oxidation of adsorbed CPR molecules induces changes in the RA spectrum. A similar change in intensity was observed between absorption spectra produced from reduced and oxidised CPR in solution in earlier stopped-flow experiments [10], the results of which have been described earlier in this thesis. The absorption spectra produced in these stopped-flow experiments [10] are shown in figure 8.16 along with the difference between the oxidised and reduced absorption spectra in each case. These differences are compared directly with the RAS difference spectrum from figure 8.15 (figure 8.17).

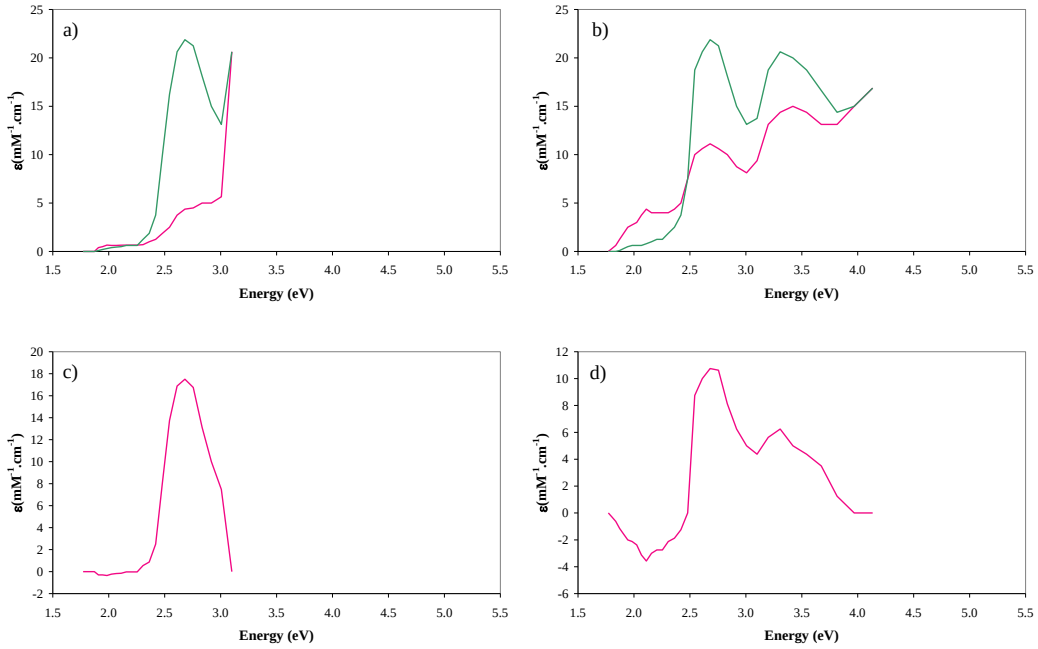

Figure 8.16: Anaerobic stopped-flow diode array data produced by a) mixing a 20-fold excess of NADPH and b) stoichiometric amounts of NADPH with oxidised CPR in pH 7.0 showing the Oxidised CPR (green line) and reduced CPR (red line) spectra. The differences between oxidised CPR and reduced CPR produced after c) mixing a 20-fold excess of NADPH and d) stoichiometric amounts of NADPH with oxidised CPR in pH 7.0. Reproduced from [10]

The spectra in figure 8.17 are plotted as a function of energy with the RAS data plotted against the left *y*-axis and the absorbance spectra reproduced from the stopped-flow experiments by Brenner *et al.* [10] plotted against the right *y* axis. All three spectra are relatively flat below ~ 2.3 eV with a large positive peak observed at ~ 2.7 eV in both absorption spectra, with a second smaller positive peak observed at ~ 3.3 eV in the absorption difference produced after mixing stoichiometric amounts of NADPH with oxidised CPR. These positive features in the absorption spectra are in a similar region to the wide positive peak observed in the RAS difference spectrum, which is observed between ~ 2.7 eV and ~ 3.4 eV before it slowly decreases in intensity at higher energies as shown in figure 8.17.

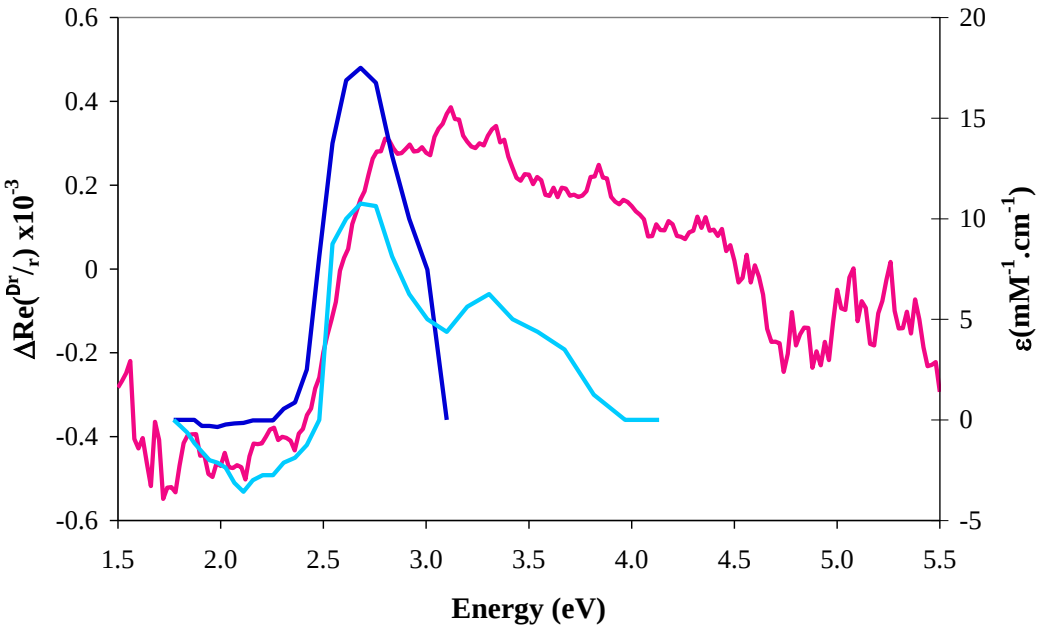

Figure 8.17: Comparison of the difference in absorbance spectra produced from oxidised and reduced CPR (dark blue and turquoise line) right *y*-axis, reproduced from [10] and changes in RA spectral shape as a result of mixing $NADP^+$ with reduced CPR (red line) left *y*-axis.

The observed similarities between the spectral features in figure 8.17 suggests that the RA spectral changes observed after the addition of $NADP^+$ may be attributed to the oxidation of the adsorbed CPR molecules on the Au(110) surface. This indicates that the adsorbed CPR molecules are in a functional state and changes in their redox state are detectable in the RAS. The difference between the two spectra in figure 8.14 could demonstrate that the oxidation of the adsorbed CPR molecules only induces a very small change in the RA spectrum, which is consistent with the adsorbed CPR having only a weak contribution in the RAS of Au(110) + CPR, which was discussed in chapter 6. The relative size of this difference in spectral shape (figure 8.13 and 8.14) highlights the difficulty in observing this as function of applied potential, as the work in this chapter has also shown that the interaction between the adsorbed CPR and Au(110) surface as a function of applied potential is complicated and changes in the Au(110) surface structure after the

adsorption of CPR may contribute to the observed change in RAS intensity as a function of applied potential.

Further experimental work is needed before these features can be attributed to the change in redox state of the adsorbed CPR molecules. Firstly it is not clear whether the addition of $NADP^+$ induces changes in the RAS as a result of $NADP^+$ adsorbing onto areas of the exposed Au(110) surface, and secondly the work of Gutierrez [14] used $NADP^+$ to oxidise reduced isolated FAD in stopped-flow experiments, not the full length version of CPR.

8.4 Summary

The idea that the adsorption of P499C full length CPR onto the Au(110) surface impedes the Au(110) surface reconstructions from the (1×3) to the anion induced (1×1) has been explored in this chapter. RA spectra of the Au(110) surface at redox potentials of -0.652 V, -0.557 V, -0.465 V, -0.376 V and 0.056 V after the adsorption of full length CPR, suggests that the Au(110) substrate may not full reconstruct from the (1×3) to the anion induced (1×1) over this potential range. Further analysis allowed the RA spectra which may be associated with the oxidised and reduced form of the adsorbed CPR molecules to be produced. These spectra were in some agreement with the oxidised and reduced absorption spectra of CPR in solution, produced in earlier stopped-flow experiments [10].

The work in this chapter also demonstrated that the adsorption of CPR onto the Au(110) in an anion induced (1×1) structure produced different results. The adsorbed anions, the change in surface structure or the change in oxidation state of the adsorbed CPR molecules may all be associated with the difference in behaviour observed after the adsorption of CPR onto the Au(110) anion induced (1×1) surface.

The addition of $NADP^+$ induced a small change in the RAS of Au(110) + CPR between 2.5 eV and 3.5 eV. The change in RA spectral shape as a result of the addition of $NADP^+$ was compared to the difference between absorbance spectra of oxidised and reduced CPR in solution. There were some similarities in this

comparison which suggests that the change in the RA spectral shape is associated with the oxidation of the adsorbed CPR molecules, however these similarities did not provide conclusive evidence of a change in conformation in the adsorbed molecules.

8.5 References

[1] C. I. Smith, A. Bowfield, N. J. Almond, C. P. Mansley, J. H. Convery and P. Weightman, *J. Phys.: Condens. Matter* **22**, 392001 (2010)

[2] C. P. Mansley, C. I. Smith, A. Bowfield, D. G. Fernig, C. Edwards and P. Weightman, *J. Chem. Phys*. **132**, 214708 (2010)

[3] P. Weightman, G. J. Dolan, C. I. Smith, M. C. Cuquerella, N. J. Almond, T. Farrell, D. G. Fernig, C. Edwards and D. S. Martin, *Phys. Rev. Lett.* **96**, 086102 (2006)

[4] C. I. Smith, A. Bowfield, G. J. Dolan, M. C. Cuquerella, C. P. Mansley, D. G. Fernig, C. Edwards and P. Weightman, *J. Chem. Phys.* **130**, 044702 (2009)

[5] A. Bowfield, C. I. Smith, G. J. Dolan, M. C. Cuquerella, C. P. Mansley and P. Weightman, *e-J. Surf. Sci. Nanotech.* **7**, 225 (2009)

[6] A. Gutierrez, M. Paine, C. R. Wolf, N. S. Scrutton and G. C. Roberts, *Biochemistry* **41**, 4626 (2002)

[7] A. Grunau, K. Geraki, J. G. Grossmann, and A. Gutierrez, *Biochemistry* **46**, 8244 (2007)

[8] J.Ellis, A. Gutierrez, I. L. Barsukov, W. C. Huang, J. G. Grossmann and G. C. Roberts, *J. Biol. Chem*. **284**, 36628 (2010)

[9] S. Hay, S. Brenner, B. Khara, A. M. Quinn, S. E. Rigby and N. S. Scrutton, *J. Am. Chem. Soc*. **132**, 9738 (2010)

[10] S. Brenner, S. Hay, A. W. Munro and N. S. Scrutton, *FEBS J*. **275**, 4540 (2008)

[11] D. S. Martin, N. P. Blanchard and P. Weightman, *Surf. Sci*. **532,** 1 (2003)

[12] Image analysis carried out using Image SXM, S. D. Barrett, [http://www.ImageSXM.org.uk] (2011)

[13] A. Gutierrez, A. Grunau, M. Paine, A. W. Munro, C. R. Wolf, G. C. K. Roberts and N. S. Scrutton, *Biochem. Soc. T*. **31**, 497 (2003)

[14] A. Gutierrez, L. Y. Lian, C. R. Wolf, N. S. Scrutton and G. C. K. Roberts, *Biochemistry* **40**, 1964 (2001)

[15] M Sun, T. A. Moore and P. –S. Song, *J. Am. Chem. Soc*. **94**, 1730 (1972)

[16] W. A. Eaton, J, Hofrichter, M. W. Makinen, R. D. Andersen and M. L. Ludwig, *Biochemistry* **14**, 2146 (1975)

[17] L. B. -A. Johansson, A. Davidson, G. Lindblom and K. R. Naqvi, *Biochemistry* **18**, 4249 (1979)

[18] T. Climent, R. González-Luque, M. Merchán and L. Serrano-Andrés, *J. Phys. Chem. A* **110**, 13584 (2006)

[19] M. Salim, U. Siddiqui, G. Kodali and R. J. Stanley, *J. Phys. Chem. B* **112**, 119 (2008)

Chapter 9

Conclusions

This chapter aims to bring together the work carried out in this thesis and conclude on the findings. The chapter will also discuss possible future work which could continue this research.

9.1 Conclusions

There are very few ways of investigating conformational change in cytochrome P50 reductase (CPR) as a function of electron transfer processes. In the work reported in this thesis I explored the possibility of adsorbing an important protein in an ordered arrangement on the Au(110)/liquid interface with a view to exploit the established potential of RAS to monitor conformational change of molecules adsorbed at this interface in real time.

The major impediment to the objectives of the research programme was the difficulty of establishing the conditions under which an ordered monolayer of protein formed on the surface. As a result of this difficulty a considerable number of experiments were performed on what was eventually discovered to be multilayers of adsorbed protein. This considerably delayed the project. However once this problem was clarified it was possible to establish the conditions necessary to produce a monolayer of protein adsorbed at the Au(110)/liquid interface: these conditions were found to be quite precise. This is a significant achievement reported in this thesis.

Once the monolayer was established it was possible to make a number of important observations. Monitoring the RAS intensity and the azimuthal angle between the plane of polarisation of the incident light and the crystal axis of the surface allowed the orientation of the adsorbed protein molecules to be established. As found in similar studies of small molecules, the relationship between the behaviour of the adsorbed protein and the Au(110) substrate as the applied potential was varied showed that the presence of the adsorbed molecules significantly impedes the kinetic freedom of the substrate.

In conclusion it is still an open question as to whether the results of the experiments discussed in this thesis demonstrate the observation of conformational change in the protein in real time using RAS. However what has been established in this thesis are the conditions in which this important question can be resolved in further work.

9.2 Future Work

As far as I am aware the work reported in this thesis is the first RAS investigation of its kind where a large protein has been adsorbed on the Au(110) surface with the goal of monitoring conformational events associated with electron transfer processes. Although the work has made significant progress in understanding the adsorption of CPR onto the Au surface, it has been difficult to observe conformational events in the CPR as a result of electron transfer processes. One possible reason for this difficulty is due to the weak RAS contribution from the adsorbed CPR, especially in the region in which the isoalloxazine rings are expected to contribute. It has been discussed that this weak contribution may be associated with the orientation of the adsorbed CPR molecules on the surface. Therefore it maybe necessary to change the orientation of the adsorbed molecules on the Au surface in order to increase the RAS signal from CPR.

The position of the engineered mutant cysteine molecules which are expected to be involved in the adsorption process may influence the orientation of the adsorbed CPR molecules on the Au(110) surface. Thus by changing the position of the mutant cysteine it could be expected that the protein will be adsorbed in a different orientation. Several other potential positions for the mutant cysteine molecule have been identified. Some of these positions are only slightly different to the position used throughout the work described in this thesis. However they may increase the RAS signal arising from dipole transitions in the isoalloxazine rings. The various possible positions of the mutant cysteine molecules are shown below in figure 9.1. As well as a change in the position of the cysteine it is also possible that the introduction of 3 separate cysteine molecules in various positions could result in the formation of a tripod of Au-S bonds. This is not only expected to provide a more stable platform for the adsorbed molecules but may further impede Au(110) surface reconstructions as a function of the applied electrode potential.

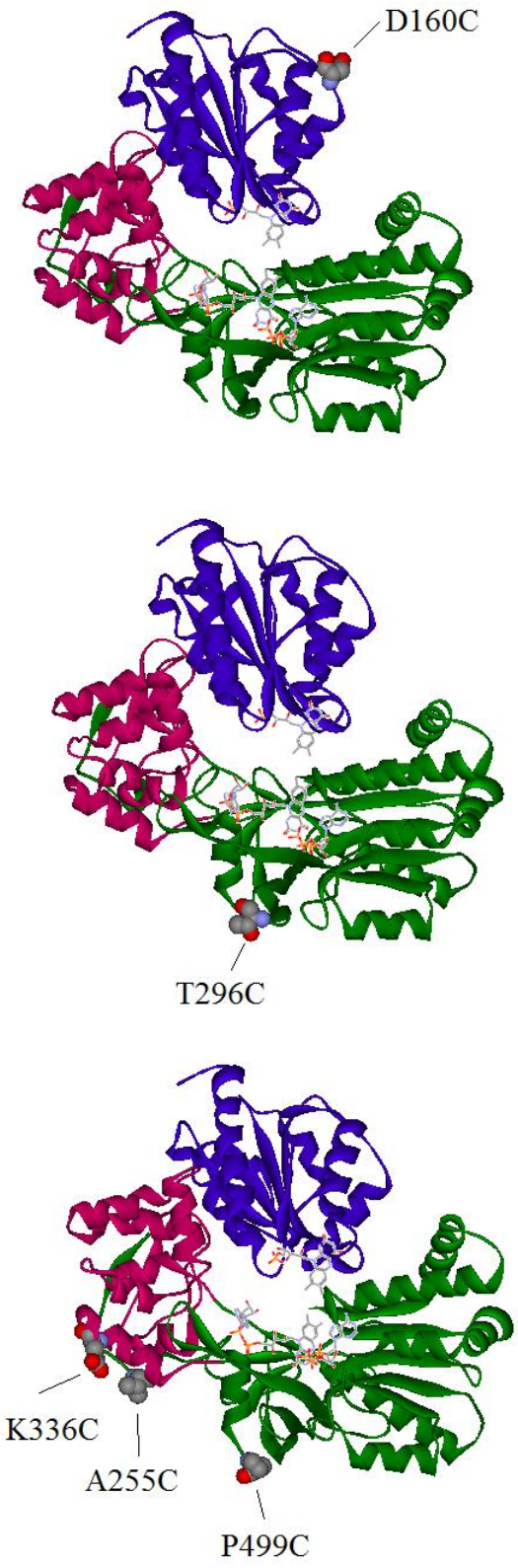

Figure 9.1: Molecular graphics ribbon diagram representation for the structure of cytochrome P450 reductase with possible positions of mutant cysteine molecules.

Another area of research which may add information is electrochemical QCM-D. This would allow potential control of the Au substrate and therefore allow electron transfer processes to be induced whilst monitoring the frequency and dissipation of the crystal using the QCM-D instrument. QCM-D proved to be very useful in determining the layer thickness of the adsorbed CPR molecules in the work presented in this thesis. The sensitivity and accuracy of QCM-D could be exploited to monitor changes in CPR conformation, specifically it would be expected that a conformational change from an open flexible CPR structure to a more compact one would be observed in the measured dissipation. The change in conformation could also be induced with the addition of $NADP^+$, which, as well as the dissipative changes, may also induce a change in the measured resonant frequency due to change in mass of the adsorbed CPR as a result of the binding of $NADP^+$.

CPR is naturally reduced by the electron transfer from NADPH, however this was not analysed with RAS in this work as it requires an anaerobic enviroment. This maybe possible to achieve but would require a glove box to be assembled around the RAS kit, which must not obscure the path of the light onto the Au(110) surface. This is likely to be difficult to assemble and may not provide further information on the dynamic behaviour of CPR, unless the RAS signal from CPR can also be increased.

The thesis reports some analysis of the orientation of the adsorbed CPR molecules on the Au(110) surface. It may be advantageous to support this analysis with AFM images of the Au(110) surface after the adsorption of a monolayer of CPR.

Publications

Spectral Signatures of the Surface Reconstructions of Au(110)/Electrolyte Interfaces

C. I. Smith, A. Bowfield, N. J. Almond, C. P. Mansley, J. H. Convery and P. Weightman, *J. Phys.: Condens. Matter* **22**, 392001 (2010)

Controlling the Formation of a Monolayer of Cytochrome P450 Reductase onto Au Surfaces

J. H. Convery, C. I. Smith, B. Khara, N. S. Scrutton, P. Harrison, T. Farrell, D. S. Martin and P. Weightman, *Phys. Rev. E* **86**, 011903 (2012)